

REPORT NO. GDCA-DBG73-001  
CONTRACT NAS8-27806

(GDCA-DB-12-172) PREPARATION OF COMPOSITE MATERIALS IN SPACE VOLUME II: TECHNICAL REPORT Final Report (General Dynamics/Convair) . . . . . 11.75

173-20009  
170110  
170110

COPIES 11 33/11 170110

# PREPARATION OF COMPOSITE MATERIALS IN SPACE

## VOLUME II - TECHNICAL REPORT



FINAL REPORT

**GENERAL DYNAMICS**  
*Convair Aerospace Division*

REPORT NO. GDCA-DBG73-001  
CONTRACT NAS 8-27806

**PREPARATION OF COMPOSITE MATERIALS IN SPACE**  
VOLUME II - TECHNICAL REPORT

FINAL REPORT

January 1973

W. H. Steurer and S. Kaye

Submitted to  
National Aeronautics and Space Administration  
GEORGE C. MARSHALL SPACE FLIGHT CENTER  
Process Engineering Laboratory  
Huntsville, Alabama

Prepared by  
CONVAIR AEROSPACE DIVISION OF GENERAL DYNAMICS  
San Diego California

## FOREWORD

This report was prepared by General Dynamics-Convair Aerospace Division under Contract NAS8-27806, "Preparation of Composite Materials in Space" for the George C. Marshall Space Flight Center of the National Aeronautics and Space Administration. The work was administered under the technical direction of the Process Engineering Laboratory and monitored by Messrs. I. C. Yates, Jr. (S&E-PE-A) and F. J. Beyerle (S&E-PE-MXC).

The report was prepared jointly by Dr. W. H. Steurer and Dr. S. Kaye. Major contributions were further made by D. J. Gorham (processes and techniques), Dr. Jan Raat (fluid mechanics), and Dr. M. Featherby (materials and metallurgy). Laboratory experimentation and equipment design were carried out by J. A. Pardubsky and T. L. Hursman.

PRECEDING PAGE BLANK NOT FILMED

## TABLE OF CONTENTS

<u>Section</u>	<u>Page</u>
1 OBJECTIVES AND SCOPE	1-1
2 STUDY APPROACH	2-1
2.1 UNIQUE PROCESSING CHARACTERISTICS	2-1
2.2 DEVELOPMENT REQUIREMENTS	2-2
2.3 INDICATED DEVELOPMENT PROGRAM	2-2
2.4 DEVELOPMENTAL ROLE OF THIS STUDY	2-3
3 INVESTIGATIONS AND RESULTS	3-1
3.1 THEORETICAL INVESTIGATIONS	3-1
3.1.1 Summary	3-1
3.1.2 Fundamental Studies on the Motion of Liquids, and Suspended Solids	3-1
3.1.3 Numerical Analysis of Solidification Around a Stationary Gas Bubble	3-12
3.1.4 Surface-Tension Induced Flow Phenomena Near a Liquid-gas Interface	3-13
3.1.5 The Motion of Solidification Fronts	3-16
3.2 FIBER-AND PARTICLE-REINFORCED METAL COMPOSITES	3-18
3.2.1 Process and Product Definition	3-18
3.2.2 Summary of Results	3-20
3.2.3 Method of Approach	3-21
3.2.4 Criteria for Particle/Fiber Dispersion	3-24
3.2.5 Criteria for Mixture Stability and Segregation	3-38
3.2.6 Geometric Reinforcement Content Limitations	3-51
3.2.7 Prediction of Composite Properties	3-54
3.2.8 Materials Investigations	3-61
3.2.9 Composite Experiments	3-64
3.3 CONTROLLED DENSITY MATERIALS	3-77
3.3.1 Definition of Products and Processes	3-77
3.3.2 Summary of Results	3-78
3.3.4 Dispersion Criteria for Reinforced Foams	3-82
3.3.5 Methods of Foam Generation	3-84
3.3.6 Microsphere Foam	3-87
3.3.7 Foams Produced for Foaming Agents	3-90
3.3.8 Gas Injection Foaming Experiments and Results	3-121

**PRECEDING PAGE BLANK NOT FILMED**

## TABLE OF CONTENTS

<u>Section</u>		<u>Page</u>
3.4	UNIDIRECTIONAL EUTECTICS	3-121
3.4.1	Process and Product Definition	3-121
3.4.2	Summary of Results	3-122
3.4.3	Materials and Predicted Properties	3-123
3.4.4	Solidification Experiments	3-123
3.4.5	Zero-G Experiments	3-124
3.5	COMPILATION OF MATERIALS DATA	3-125
3.5.1	Apparatus Description	3-125
3.5.2	Properties of Simulated Matrices	3-131
3.5.3	Properties of Molten Metals	3-131
3.5.4	Properties of Reinforcement Materials	3-134
3.5.5	Wetting Data	3-134
4	ZERO-G EXPERIMENT REQUIREMENTS	4-1
4.1	PROCESSING METHODS	4-1
4.2	SUBORBITAL EXPERIMENT REQUIREMENTS	4-1
4.3	ORBITAL EXPERIMENT REQUIREMENTS	4-3
4.3.1	Mission Definition	4-3
4.3.2	Experiment Apparatus	4-3
4.3.3	Support Systems	4-4
4.3.4	Experiment Performance	4-5
4.3.5	Operational Requirements	4-5
5	CONCLUSIONS	5-1
5.1	GENERAL CONCLUSIONS	5-1
5.2	FIBER AND PARTICLE COMPOSITES	5-1
5.3	CONTROLLED DENSITY MATERIALS	5-3
5.4	UNIDIRECTIONAL EUTECTICS	5-4
6	RECOMMENDATIONS	6-1
6.1	GENERAL RECOMMENDATIONS	6-1
6.2	SPECIFIC RECOMMENDATIONS	6-1
6.3	RECOMMENDED SUPPORTING EFFORTS	6-2
6.4	RECOMMENDED EXPERIMENTAL PROGRAM	6-3
6.4.1	Laboratory Experiments	6-3
6.4.2	Drop Tower and KC-135 Experiments	6-4
6.4.3	Research Rocket Experiments	6-4
6.4.4	Automated Satellites	6-5
6.4.5	Shuttle-Based Laboratories	6-5

## TABLE OF CONTENTS

<u>APPENDIX</u>		<u>Page</u>
A	RELAXATION OF VISCOUS FLUID MOTION IN A CYLINDRICAL CONTAINER	A-1
B	RELAXATION OF VISCOUS FLUID MOTION IN A SPHERICAL CONTAINER	B-1
C	OSCILLATORY FLUID MOTION IN CYLINDRICAL CONTAINER	C-1
D	OSCILLATORY FLUID MOTION IN SPHERICAL CONTAINER	D-1

## SUMMARY

This document is the final technical report on the "Preparation of Composite Materials in Space" under Contract NAS8-27806. It gives an account of the performed investigations and their results. The report is presented in two volumes.

The objective of the study was to define promising materials, significant processing criteria and the related processing techniques and apparatus for the preparation of composites in space, and to establish a program for zero-g experiments and the required developmental efforts.

The study was directed at the preparation of the following composite types: 1) metal-base fiber and particle composites, including cemented compacts, 2) controlled density metals, comprising plain and reinforced metal foams, and 3) unidirectionally solidified eutectic alloys.

The materials and processing requirements for these composite types were defined by theoretical studies and laboratory investigations, comprising the evaluation of materials, processing techniques and individual processing parameters. These efforts included the establishment of the basic criteria for liquid-state processing by fluid mechanics studies and experiments, the compilation of applicable materials data, the definition of sample preparation techniques for zero-g experiments and the construction of special laboratory facilities.

A program of suborbital and orbital experiments for the 1972 to 1978 time period was established, identifying materials, processes and the required experiment equipment.

Some of the more significant conclusions reached in the study are:

1. The zero-g environment of orbital operations offers the capability to produce metal-base composite materials and castings which exhibit properties and, particularly, unique combinations of properties that cannot be achieved in terrestrial production.
2. The primary criterion for effective fiber/particle composites and controlled density materials is the achievement of perfect random dispersion. Due to the complexity of interactions between molten metals and solid or gaseous dispersions, material treatments and processing techniques have to be developed specifically for each material combination.

3. The behavior of mixtures of liquid metals and properly treated fibers or particles can be accurately predicted for zero-g conditions or specific low-g levels. Relationships and data for such predictions have been established theoretically and experimentally.
4. Controlled density materials can be produced either by the dispersion of gas in the molten metal or by decomposition of pre-dispersed solid particles. The latter method, for which specific materials have been defined experimentally, is most adaptable to initial zero-g experiments.
5. The primary requirements for the preparation of unidirectional eutectics are highest material purity and extremely low solidification rates.
6. Since the concerned composites are unique to zero-g processing, conclusive property data can only be obtained from zero-g experiments. With the exception of unidirectional eutectics, which call for sustained zero-g conditions, adequate data can be generated in suborbital experiments. For highest experiment return at minimum cost, efforts should be concentrated on one base material for each composite type, and the evaluation of all significant variables.

## SECTION 1

### OBJECTIVES AND SCOPE

The general objective of this study was to evaluate the potential of producing new composite materials by liquid-state processing in space, unfeasible in the terrestrial environment due to segregation. The specific objectives were:

- a. To define the most promising metal-base composite materials for processing in zero-g.
- b. To define the materials and processing parameters for the preparation of typical composites in zero-g.
- c. To identify major problem areas and to investigate them in sufficient depth to outline an approach for the solution of these problems.
- d. To define experimental programs required for the solution of problems identified in (c) in ground-based studies and experiments, and in zero-g experiments.
- e. To define process techniques, peculiar apparatus concepts, and operational requirements for experimental investigations in orbital facilities.

The composite classes investigated in this study comprise: 1) Fiber- and Particle-Reinforced Metal- Base Composites, 2) Controlled Density Metals (plain and reinforced metal foams), and 3) Unidirectional eutectics. Main emphasis has been placed on composite classes (1) and (2) in view of the wide variety of individual composite types, the high applications potential and the uniqueness of the processes to zero-g.

Originally, the scope identified two other classes: Cemented Compacts and Supersaturated Alloys. However, Cemented Compacts can be considered as a specific type of particle composites and have, therefore, been included in class (1); the investigation of supersaturated alloys was deleted in view of a separate study of this subject under another contract.

To accomplish the stated objectives, the following scope of major subject areas was adopted for the study.

- a. Conceptual evaluation of composites and preliminary definition of processes, materials, and their predominant criteria for the purpose of identifying the subjects for detailed study.

- b. Establishment of relationships and numerical data for the behavior of liquids and mixtures by theoretical studies and laboratory experiments.
- c. Experimental investigation of processing parameters that govern the dispersion of solids and gases in liquid metals.
- d. Experimental investigation of surface requirements and treatments to achieve high wettability of reinforcements.
- e. Analysis of the compatibility of reinforcements with liquid metals and definition of compatible material combinations.
- f. Assessment of attainable composite properties, as related to materials, reinforcement configuration, and reinforcement content.
- g. Experimental determination of reinforcement content limitations as related to reinforcement configuration and mold size.
- h. Evaluation of methods for the generation of metal foams and experimental investigation of the most promising methods.
- i. Theoretical analysis and laboratory experiments on the unidirectional solidification of eutectic alloys.
- j. Compilation of applicable materials data and measurement of properties not reported in the literature.
- k. Experimental preparation and evaluation of composite samples and definition of techniques for the preparation of zero-g experiment samples.
- l. Definition of the most effective materials and processing methods for initial zero-g experiments.
- m. Study of process and apparatus requirements for experiments in suborbital and orbital facilities.

Laboratory investigations further necessitated the development of special experimental facilities. Major facilities constructed in the course of the study include several apparatus for the measurement of liquid-metal properties, an apparatus for the measurement of segregation rate and dispersion phenomena, an apparatus for the melting and solidification profiles of specific sample configurations, an induction furnace for processing of eutectic alloys, and a high-purity argon chamber for material preparation and sample assembly, equipped with all necessary tooling.

## SECTION 2

### STUDY APPROACH

The broad objectives of this study necessitated a limitation of the depth to which individual subjects could be investigated, commensurate with their significance or with the required efforts. The following discussion of the basic approach is presented as a rationale for the study scope (Section 1) and for the extent to which each subject was evaluated.

#### 2.1 UNIQUE PROCESSING CHARACTERISTICS

The absence of segregation in liquid/solid and liquid/gas mixtures in the weightless environment of orbital vehicles offers the opportunity of producing metal-base composites by processing in the liquid-matrix state. In the terrestrial environment, liquid-state production of composites is limited to matrices of high viscosity, such as polymers; in view of the low viscosity of liquid metals, metal-base composites can be produced only by solid-state techniques, with extreme limitations as to materials, product shapes, and anisotropy of properties. The preparation of metal-base composites by liquid-state processing in the segregation-free space environment permits random orientation of reinforcements for complete anisotropy of properties, the dispersion of gases for density control, and castability of end-products in final configuration. The segregation-free environment further eliminates thermal convection and permits a high degree of nucleation and solidification control.

The preparation of composites in space introduces a number of new areas of materials and process technology, such as:

- a. Liquid-state processing in zero-g.
- b. The dispersion of solids and gases in liquid metals.
- c. Physical and chemical interface phenomena between molten metals, solids, and gases.

As in any new technology, this, in turn, introduces a multitude of problems, such as the high oxidation sensitivity of liquid metals, degradation of the reinforcement properties at the involved high temperatures, chemical reactions between solids or gases and the molten metal, wetting characteristics of the solid dispersions, physical interactions between solids in the process of dispersion, or the laws of fluid mechanics in zero-g that govern the establishment of a stable dispersion.

## 2.2 DEVELOPMENTAL REQUIREMENTS

The ideal conditions for the preparation of a perfect metal composite by liquid state processing are:

- a. Absolute zero-g.
- b. No oxidation of the molten matrix.
- c. Perfect wettability of reinforcements.
- d. No chemical reaction between reinforcements and molten matrix.
- e. No degradation of mechanical reinforcement properties at the liquid-metal temperature.
- f. No coalescence of gas bubbles for controlled density metals.
- g. Uniform dispersion of reinforcements and/or gases.
- h. High bond strength between matrix and reinforcements after solidification.

The achievement of these conditions involves a multitude of problems that have to be solved and techniques that have to be developed. As will be shown in the subsequent discussion of investigations, most problems differ for each material combination; specific material treatments and techniques have to be developed for each specific case. Furthermore, even in space operations absolute zero-g is not achieved and the sensitivity of the liquid mixture to small-g forces has to be defined. Finally, since by definition the concerned composites cannot be prepared in the terrestrial gravity environment, the determination of the composite capabilities can be obtained only in low-g experiments.

## 2.3 INDICATED DEVELOPMENT PROGRAM

The first goal of developmental efforts is the early preparation of prototype composite materials that permit the measurement of properties and provide a reliable basis for the definition of advanced composite types, product applications, and the requirements of orbital facilities. On the basis of both technical and economical considerations, this goal is achieved most effectively by the following stepwise program:

**Phase 1: Definition of processing parameters, processing requirements, and promising materials.**

- Phase 2: For each composite class, development of detailed processing specifications and techniques for one specific base metal and determination of composite capabilities in suborbital low-g experiments.
- Phase 3: On the basis of the results of Phase 2, definition, development, and testing of composites with other base metals, oriented toward specific product applications.
- Phase 4: Experiments in pre-shuttle orbital facilities (Skylab, automated satellites) with larger quantities of the most effective materials from Phase 2 and 3, including the casting of shapes representative of specific products.
- Phase 5: Definition of full-scale experiments in shuttle-based orbital laboratories in terms of materials or products, processing facilities, support requirements, and operations.

#### 2.4 DEVELOPMENTAL ROLE OF THIS STUDY

The scope of the study documented in this report represents Phase 1 of the suggested program. Primary emphasis has, therefore, been placed on the identification of processing parameters, fundamental requirements of zero-g liquid-state processing, promising materials and processing methods, and the related problems. Subjects considered to be of basic significance have been treated in reasonable depth; subjects that either were considered less significant - at least at this time - or involved prohibitive efforts or facilities, were assessed in exploratory studies and experiments. The ultimate objective of all investigations was to generate a reliable basis for an effective performance of Phase 2.

## SECTION 3

### INVESTIGATIONS AND RESULTS

#### 3.1 THEORETICAL INVESTIGATIONS

3.1.1 SUMMARY. Detailed analyses have been made of the decay of rotary motions of a liquid matrix as well as the characteristics of oscillatory motions. The fundamental solutions permit quantitative analyses of centrifugal drifting and rotational relaxation of suspended particles.

A discussion is given of the transition from laminar to turbulent flow of the liquid matrix. The utilization of turbulent mixing for obtaining uniform particle dispersion is discussed for a number of simple configurations.

A new model for surface-tension induced flow phenomena is advanced involving the Prandtl boundary layer concept. This approach will permit a quantitative analysis of the transport of momentum, energy or mass near a liquid-gas interface.

Available solutions for one-dimensional solidification problems offer practical guidance in such processes as crystal growth and the solidification of castings.

3.1.2 FUNDAMENTAL STUDIES ON THE MOTION OF LIQUIDS AND SUSPENDED SOLIDS. Theoretical analyses of mixing processes involving the dispersion of solids in a liquid matrix necessitate a fundamental assessment of the motion of the liquid.

The following sections deal with a number of quantitative estimates. Container shapes are assumed cylindrical or spherical and the suspended solids are treated as spherical particles. As first approximations, the results are of course still useful when applied to more general configurations. There are no restrictions on the physical properties other than the assumptions that the liquid is incompressible and Newtonian.

In Appendices A and B, a detailed investigation is made of the decay of viscous fluid motion, whereas oscillatory flow fields are analyzed in Appendices C and D. The solutions to these various problems can be found in the applied mathematics literature of the 19th and early 20th century although the derivations often are a bit unwieldy from the viewpoint of present-day fluid mechanics.

The characteristic decay time for the rotating motion in a suddenly stopped cylinder is found to be  $\tau = 0.16 a^2/\nu$  (where  $a$  is the cylinder radius and  $\nu$  is the liquid kinematic viscosity), whereas the corresponding problem for a spherical container yields  $\tau = 0.11 a^2/\nu$  ( $a$  being the radius of the sphere). It appears that for a finite cylinder the relaxation time is not significantly reduced by the presence of the endplates unless the cylinder is very short. For a cylinder with a slenderness ratio of unity the reduction amounts to 15%. The foregoing results indicate that the shape of the container does not have an important effect on the liquid decay.

The flow field in oscillating cylinders or spheres is determined by the parameter

$$M = \sqrt{\frac{\omega_0 a^2}{2\nu}}$$

where  $\omega_0$  is the angular oscillation frequency. For small values of  $M$  (e. g., large liquid viscosity) the fluid tends to rotate as a solid with the container. For large values of  $M$ , on the other hand, the oscillating fluid motion remains confined to a thin layer adjacent to the wall, the inner core being practically at rest.

In Section 3.1.2.1 an investigation is made of the centrifugal drifting of suspended particles. The first (and most important) mode of the solution for the rotating flow field in a cylinder is used as a representative motion of the liquid matrix. A characteristic drift time  $\tau_d$  (time required for a particle to drift from the center to the cylinder wall) is found to be

$$\tau_d = 3.7 \frac{\nu}{R^2} \frac{\rho_1}{\rho_s - \rho_1} \frac{a^2}{q_{\max}^2}$$

where  $R$  is the particle radius,  $\rho_s$  and  $\rho_1$  are the material densities of the solid and the liquid, and  $q_{\max}$  is the maximum liquid velocity. Whether or not particle drifting is important depends on the particular experimental conditions.

A simple criterion for drifting to be unimportant on the time scale of the decay of the liquid motion is found to be

$$\frac{q_{\max} R}{\nu} \leq 1$$

This criterion is independent (!) of the size of the container (because both  $\tau$  and  $\tau_d$  depend on the square of the cylinder radius so that this dependence cancels out upon forming their ratio).

In Section 3. 1. 2. 2 the rotational relaxation of suspended particles is investigated. The rotational relaxation time is found as

$$\tau_r = 0.15 \frac{\rho_s R^2}{\rho_1 \nu}$$

It is shown that the time required by suspended particles to adjust themselves to the decreasing liquid vorticity is always small compared to the time required by the liquid to come to rest. Finally, in Section 3. 1. 2. 3, transition from laminar to turbulent flow is discussed. The macroscopic mixing, associated with turbulent motion, offers attractive possibilities for obtaining uniform particle dispersion. The following simple configurations are suggested for further experimental work on the dispersion of solids:

- a. Turbulent flow between two concentric cylinders with the inner cylinder rotating and the outer one at rest (Taylor instability).
- b. Turbulent flow in rotating cylinder with eccentric axis of rotation.
- c. Turbulent flow in oscillating cylinder (possibly with eccentric axis of rotation).

Only in the first arrangement is it possible to make precise a priori predictions about the laminar instability and the breakdown to fully turbulent flow.

3. 1. 2. 1 Centrifugal Drifting of Suspended Particles. In this section we study the effect of centrifugal drifting of suspended particles in a rotating fluid, the relative motion being caused by the difference in density between the particles and the fluid (gravity is assumed absent). For the sake of simplicity we assume the particles to be spherical. The first mode of the solution for cylindrical flow (Appendix A) is taken as a representative fluid motion, i. e. ,

$$q(r,t) = A_1 e^{-\alpha_1^2 \frac{\nu t}{a^2}} J_1\left(\alpha_1 \frac{r}{a}\right) \quad (1)$$

Particle size and relative velocity are considered to be sufficiently small so that we may assume that the basic fluid motion remains essentially unaffected by the presence of the particles.

The centrifugal force on a particle is  $F_1 = m q^2/r$  where  $m$  is the particle mass. The particle also experiences a Coriolis force of magnitude  $F_2 = 2 m V q/r$  where  $V$  is the velocity of the particle relative to the fluid ( $F_2$  and  $V$ , being perpendicular to each other, are both lying in a plane normal to the axis of rotation). However, we find  $F_2/F_1 \sim V/q$  so that the Coriolis force may be disregarded in view of our assumption that the relative motion is slight compared to the basic motion. It is not difficult to show that the particle inertia effect due to the spatial variation of the angular velocity

of the fluid (about the axis of rotation) may then also be neglected. Furthermore, the particle inertia force due to the temporal variation of angular velocity will be small compared to the centrifugal force if the time required for one rotation is small compared to the relaxation time of the fluid.

Thus the principal driving force is the centrifugal force and the motion of the particle will be essentially radial. In the following we assume that the relative motion may, with good approximation, be treated in quasi-steady fashion with the viscous resistance set equal to the instantaneous value of the Stokes solution for a sphere:  $6\pi\mu VR$ , where  $R$  is the radius of the sphere and  $\mu$  is the dynamic viscosity. The use of the Stokes formula is permitted as long as the Reynolds number of the relative motion  $VR/\nu$  is smaller than unity.

The pressure gradient in the fluid is such that it precisely balances the centrifugal force experienced by the fluid particles. Because the suspended sphere is assumed to be small compared to the cylinder radius, the outward force on the particle due to the combined action of pressure gradient and centrifugal effect may be written as

$$\frac{4}{3} \pi R^3 (\rho_s - \rho_l) \frac{q^2}{r}$$

where  $\rho_s$  and  $\rho_l$  are the material densities of the sphere and the liquid respectively;  $q$  and  $r$  are "local" quantities (taken at the center of the sphere).

According to our quasi-steady treatment this outward force is at all times balanced by the viscous Stokes drag, which gives the following result for the instantaneous relative velocity of the sphere

$$V = \frac{2}{9} \frac{R^2}{\nu} \frac{\rho_s - \rho_l}{\rho_l} \frac{q^2}{r} \quad (2)$$

It follows from Equations 1 and 2 for the average drift velocity along the cylinder radius at time zero

$$\bar{V} = \frac{2}{9} \frac{R^2}{\nu} \frac{\rho_s - \rho_l}{\rho_l} \frac{A_1^2}{a} \int_0^{\alpha_1} \frac{J_1^2(Z)}{Z} dZ$$

The value of the integral being 0.42, we find,

$$\bar{V} = 0.093 \frac{R^2}{\nu} \frac{\rho_s - \rho_l}{\rho_l} \frac{A_1^2}{a}$$

or, expressing the coefficient  $A_1$  in terms of the maximum flow velocity ( $q_{\max} = 0.58 A_1$ ),

$$\bar{V} = 0.27 \frac{R^2}{\nu} \frac{\rho_s - \rho_1}{\rho_1} \frac{q_{\max}^2}{a} \quad (3)$$

Using Equation 2, it is readily shown that the maximum drift velocity occurs at about one-third of the cylinder radius, its value being given by,

$$V_{\max} = 0.5 \frac{R^2}{\nu} \frac{\rho_s - \rho_1}{\rho_1} \frac{q_{\max}^2}{a} \quad (4)$$

We may define a characteristic drift time  $\tau_d$  as the time required for a particle to travel from the center to the cylinder wall with the average velocity defined by Equation 3, i. e.,

$$\tau_d = 3.7 \frac{\nu}{R^2} \frac{\rho_1}{\rho_s - \rho_1} \frac{a^2}{q_{\max}^2} \quad (5)$$

The importance of particle drifting can now be estimated through a comparison of  $\tau_d$  with the relaxation time  $\tau$  of the fluid motion (Appendix A, Equation A7). We find,

$$\frac{\tau}{\tau_d} = 0.043 \frac{\rho_s - \rho_1}{\rho_1} \text{Re}^2 \quad (6)$$

Where  $\text{Re}$  is the Reynolds number  $q_{\max} R/\nu$ . This ratio must be small compared to unity for particle drifting to be unimportant. If, on the other hand,  $\tau/\tau_d$  is of the order of unity, then particle distributions will certainly be nonuniform with a pronounced concentration near the container wall. Because the ratio  $(\rho_s - \rho_1)/\rho_1$  will generally be of the order of unity, Equation 6 suggests the simpler criterion

$$\frac{q_{\max} R}{\nu} \leq 1$$

for particle drifting to be negligible. Note that this criterion is independent of the size of the container (both  $\tau$  and  $\tau_d$  being proportional to the square of the cylinder radius).

It is of interest to check the validity of our quasi-steady treatment a posteriori by calculating the start-up time of the particle from the approximate (we are neglecting the acceleration reaction of the fluid) equation of motion,

$$m \frac{dV}{dt} = -6\pi\mu VR + F \quad (7)$$

where, to first approximation, the driving force  $F$  is considered a constant.

The solution of Equation 7 is

$$V = \frac{F}{6\pi\mu R} \left[ 1 - e^{-\frac{6\pi\mu R t}{m}} \right]$$

so that the start-up time  $\tau_s$  is found to be of order

$$\tau_s \sim \frac{m}{6\pi\mu R} = \frac{2}{9} \frac{\rho_s R^2}{\rho_l \nu}$$

Comparing  $\tau_s$  with the characteristic drift time  $\tau_d$ , defined by Equation 5, we find, in view of Equation 4

$$\frac{\tau_s}{\tau_d} = 0.12 \frac{\rho_s}{\rho_l} \frac{R}{a} (\text{Re}_p)_{\max}$$

where  $(\text{Re}_p)_{\max} = V_{\max} R/\nu$  is the maximum Reynolds number of the relative motion of the particle. Because  $(\text{Re}_p)_{\max} < 1$  (for the Stokes approximation to be valid) and  $R/a \ll 1$ , the start-up time is clearly negligible compared with the drift time so that a quasi-steady treatment is permitted.

The foregoing conclusions are expected to remain valid for particles and containers of a more general shape.

**3.1.2.2 Rotational Relaxation of Suspended Particles.** In the foregoing analysis of centrifugal drift we have neglected the rotation of the particles. In this section we study the rotational relaxation of particles neglecting drift. To obtain quantitative information about the relaxation time, we investigate the motion of a spherical particle that, at time zero, is given an angular velocity  $\omega_0$  in an infinite liquid at rest.

The equation of rotational motion of the sphere is

$$T = I \frac{d\omega}{dt} \quad (1)$$

where  $T$  is the torque exerted by the fluid on the sphere,  $I$  is the moment of inertia of the sphere about its axis of rotation and  $\omega(t)$  is the instantaneous angular velocity of the sphere. For a spherical body,

$$I = \frac{2}{5} MR^2 \quad (2)$$

where  $M = \frac{4}{3} \pi R^3 \rho_s$  is the mass of the sphere. The torque represents the integrated moment of the shear stress along the surface of the sphere. The fluid motion is governed by Equation B1 of Appendix B and the surface shear stress is found to be

$$\tau(R, \theta, t) = \mu R \sin \theta \left[ \frac{\partial}{\partial r} \left( \frac{q_1}{r} \right) \right]_R$$

the torque can then be expressed as

$$\begin{aligned} T &= 2 \pi R^3 \int_0^\pi \sin^2 \theta \tau(R, \theta, t) d\theta \\ &= \frac{8}{3} \pi \mu R^4 \left[ \frac{\partial}{\partial r} \left( \frac{q_1}{r} \right) \right]_R \end{aligned} \quad (3)$$

After substitution of Equations 2 and 3, the equation of motion, Equation 1, becomes

$$\frac{d\omega}{dt} = \frac{5\nu}{R} \frac{\rho_1}{\rho_s} \left[ \frac{\partial}{\partial r} \left( \frac{q_1}{r} \right) \right]_R \quad (4)$$

The right-hand side of Equation 4 contains the unknown velocity distribution  $q_1(r, t)$ , which must be solved from Equation B1 with boundary conditions  $q_1(r, 0) = 0$ ,  $q_1(\infty, t) = 0$  and  $q_1(R, t) = R\omega(t)$ .

Applying the Laplace transform

$$\bar{q}_1(r, p) = \int_0^\infty e^{-pt} q_1(r, t) dt$$

to Equation B1, we find

$$r^2 \frac{\partial^2 \bar{q}_1}{\partial r^2} + 2r \frac{\partial \bar{q}_1}{\partial r} - \left( \frac{p}{\nu} r^2 + 2 \right) \bar{q}_1 = 0 \quad (5)$$

with boundary conditions

$$\bar{q}_1(\infty, p) = 0 \quad (6a)$$

$$\bar{q}_1(R, p) = R \int_0^{\infty} e^{-pt} \omega(t) dt \quad (6b)$$

The solutions of Equation 5 are the modified spherical Bessel functions of the first and second kind of order unity (Appendix D),

$$i_1\left(\sqrt{\frac{p}{\nu}} r\right), \quad k_1\left(\sqrt{\frac{p}{\nu}} r\right)$$

The first solution tends to infinity as  $r$  tends to infinity and must be rejected in view of Equation 6a. The solution in the Laplace-transformed plane, satisfying Equations 6a and 6b then becomes,

$$\bar{q}_1(r, p) = R \frac{k_1\left(\sqrt{\frac{p}{\nu}} r\right)}{k_1\left(\sqrt{\frac{p}{\nu}} R\right)} \int_0^{\infty} e^{-pt} \omega(t) dt \quad (7)$$

Attempts to transform the complete solution back to the physical plane would lead to considerable difficulty in view of the fact that the time dependence of the angular velocity  $\omega$  is a priori unknown (Equation 4). However, for the purposes of the present analysis it suffices to consider large time values only. In the plane of the Laplace transform this amounts to considering small values of  $p$ . For small values of the argument of the function  $k_1(Z)$ , we may write

$$k_1(Z) = \frac{\pi}{2Z} \left(1 + \frac{1}{Z}\right) e^{-Z} = \frac{\pi}{2Z^2} \left[1 + O(Z^2)\right]$$

so that, for small values of  $p$ , Equation 7 simplifies into

$$\bar{q}_1(r, p) \sim \frac{R^3}{r^2} \int_0^{\infty} e^{-pt} \omega(t) dt$$

which immediately yields the following solution in the physical plane for large values of the time,

$$q_1(r, t) \sim \frac{R^3}{r^2} \omega(t)$$

The equation of rotational motion (Equation 4) then takes the form

$$\frac{d\omega}{dt} = - \frac{15\nu}{R^2} \frac{\rho_1}{\rho_s} \omega$$

with solution

$$\omega(t) = \omega_0 e^{-15 \frac{\rho_1}{\rho_s} \frac{\nu t}{R^2}} \quad (8)$$

Equation 8 describes the rotational behavior of the particle at large values of the time. We define the rotational relaxation time  $\tau_r$  as the time required for the angular velocity to drop off to 10% of its initial value. We then find,

$$\tau_r = 0.15 \frac{\rho_s}{\rho_1} \frac{R^2}{\nu} \quad (9)$$

It is interesting to compare  $\tau_r$  with the relaxation time  $\tau$  of the fluid motion in a circular cylinder (Equation A7 of Appendix A). We find,

$$\frac{\tau_r}{\tau} \approx \frac{\rho_s}{\rho_1} \left(\frac{R}{a}\right)^2$$

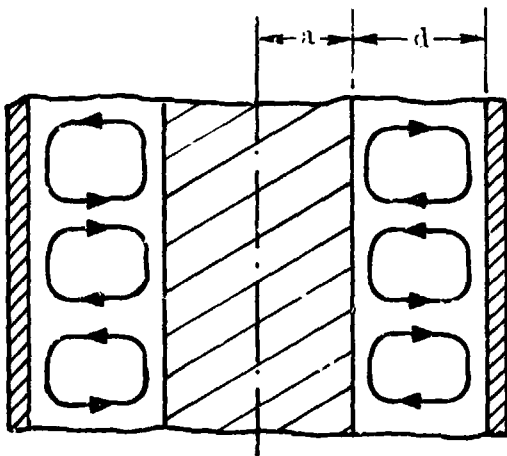
Clearly, when the particle radius is very small compared to the container radius, this ratio will be very small compared to unity. We conclude that any difference between the local angular velocity of the liquid and the angular velocity of a suspended particle is rapidly damped out through the action of viscosity. In other words, the time required by suspended particles to adjust themselves to the decreasing liquid vorticity is small compared to the time required by the fluid to come to rest. This will of course remain true for particles and containers of a more general shape.

**3.1.2.3 Turbulent Transition.** When fluids are sufficiently agitated, laminar motions may become unstable, i. e., small disturbances due to geometrical imperfections, surface roughness, mechanical vibrations, etc. tend to be amplified into large random fluctuations. The resulting turbulent motion is characterized by a pronounced macroscopic mixing and such flow configurations are naturally of great interest from the standpoint of obtaining uniform mixtures.

Transition in Accelerated Containers. It has been established<sup>1,2</sup> that the flow in suddenly accelerated cylinders may become turbulent during the starting process. However, the flow will revert to the laminar pattern when the steady state is reached due to the stabilizing influence of the centrifugal forces. The latter effect is readily understood if, in the steady state, we consider a fluid particle with velocity  $q_1$  at radius  $r_1$  and suppose it to be displaced to a larger radius  $r_2$ . Conservation of angular momentum requires that the new velocity be  $q_2 = q_1 r_1 / r_2 < q_1$ . In the steady state the fluid rotates as a solid with the cylinder so that the velocity increases linearly between the center and the wall. Thus in the new position the velocity of the displaced fluid particle is smaller than that of the neighboring particles. As a consequence, the local pressure gradient will be larger than that required to balance the centrifugal force on the displaced particle. It follows that the particle will be forced back to its original position. Thus the laminar flow is stable in the steady state.

It has been established, however, that turbulence may persist under conditions of steady rotation if a slight amount of eccentricity is built into the arrangement. Such an arrangement might therefore be of some interest for macroscopic mixing.

Taylor Instability. In the case of a liquid contained between two concentric cylinders, arguments similar to that of the previous section indicate that the laminar flow is stable if the outer cylinder rotates and the inner is at rest but unstable if the inner cylinder rotates and the outer is at rest.



The latter case has been theoretically and experimentally investigated in detail by Taylor.<sup>3,4,5</sup> When the fluid is only slightly agitated, the flow is rendered stable by the "damping" effect of viscosity. However, with increasing speed of the inner cylinder, a system of ring-shaped flow vortices (with axes along the streamlines of the basic flow) will appear, which rotate in alternately opposite directions (Figure 3-1).

The onset of the vortex formation is determined by the critical value of the Taylor number, i.e.,

$$Ta = \frac{Ud}{\nu} \sqrt{a} \gtrsim 40$$

Figure 3-1. Taylor Vortices Between Concentric Cylinders

<sup>1</sup> Schlichting, H. "Ueber die Entstehung der Turbulenz in einem rotierenden Zylinder," *Nachr. Ges. Wiss. Goettingen, Math. Phys. Klasse.* p. 160, 1932.

<sup>2</sup> Schultz-Grunow, F. "Zur Stabilität der Couetteströmung," *ZAMM*, Vol. 39, p. 101, 1959.

<sup>3</sup> *Phil. Trans.* A233, pp. 289-293 (1923).

<sup>4</sup> *Proc. Roy. Soc.* A151, pp. 494-512 (1935).

<sup>5</sup> *Proc. Roy. Soc.* A157, pp. 523-546, 565 (1936).

where  $U$  and  $a$  denote the peripheral velocity and radius of the inner cylinder;  $d$  is the width of the annulus and  $\nu$  is the kinematic viscosity of the fluid.

When the Taylor number exceeds its critical value by an increasingly large margin, the secondary flow pattern will become more pronounced through the absorption of additional energy in the vortices. The entire flow field remains laminar, however, for values of  $Ta$  up to approximately 400 beyond which the cellular flow breaks down into a turbulent pattern characterized by random macroscopic mixing.

Turbulent Transition in Oscillating Containers. When the oscillatory flow in a cylindrical or spherical container (Appendices C and D) is governed by increasingly large values of the parameter  $M$ , the regular laminar motion eventually will break down into a turbulent flow pattern. The laminar instability is expected to initially occur in that part of the fluid where the velocities are greatest, i. e., near the entire wall of the cylinder and near the wall of the sphere in the plane  $\theta = \pi/2$ . Unfortunately, very little is known, either experimentally or theoretically, about the mechanism of instability and turbulent transition in this type of flow.

Because for large values of  $M$  the fluid motion near the wall becomes identical with that generated by an oscillating infinite flat plate, we may expect to obtain useful information by reviewing available results pertaining to the latter configuration. However, even in this relatively simpler flow problem, our understanding of the instability mechanism is rather limited. Although the solution to "Stokes' second problem" has been known since 1851<sup>6</sup>, it apparently took more than a century before this solution was experimentally verified and the conditions for the breakdown of the laminar motion were investigated. The first quantitative measurements were carried out by O'Brien and Logan<sup>7</sup> in 1964. These investigators, using water as the test medium, observed deviations from the regular flow pattern at Reynolds numbers of about 300, the latter being defined as

$$Re = \frac{q_0 \lambda}{\nu}$$

where  $q_0$  is the maximum wall velocity and  $\lambda$  is the viscous wave length (Appendices C and D). Substituting  $\lambda = 2\pi a/M$  and  $q_0 = \alpha_0 a \omega_0$  ( $\alpha_0$  being the angular amplitude of the container oscillations), the critical condition can be expressed as

$$\pi \alpha_0 M \gtrsim 75 \quad \left( M = \sqrt{\frac{\omega_0 a^2}{2\nu}} \right)$$

<sup>6</sup> Stokes, G. G. "On the effect of the internal friction of fluids on the motion of pendulums," *Cambr. Phil. Trans.*, Vol. 9, NR. 8, 1851.

<sup>7</sup> O'Brien, V. and Logan, F. E. "Periodic boundary layer flows over a flat plate," the Johns Hopkins Univ. APL Rep. CM-1045, May 1964.

It is not quite clear from the results of O'Brien and Logan's work how far one would have to go beyond their critical Reynolds number before the flow would cease to appear laminar and well-ordered. Presumably the Reynolds number would have to be increased substantially before a complete breakdown into turbulent flow would occur.

The wall curvature of cylindrical or spherical containers is not expected to influence the foregoing results to any great extent (the thickness of the viscous layer being small compared to the container size). However, an entirely different type of flow instability becomes possible for these oscillating containers. As indicated in Figure C-1 of Appendix C, there exists a phase lag of the various fluid layers with respect to the motion of the wall. As a result, the fluid layers adjacent to the wall will be moving slower than those at some distance away from the wall during part of each oscillation cycle. It is therefore conceivable that centrifugal instabilities would cause a Taylor-type circumferential vortex pattern. This type of instability could be more important than the one observed in the previously discussed case of the oscillating flat plate. In the absence of experimental evidence, the precise details of the transition mechanism of the flow in oscillating containers remains therefore somewhat speculative. It might furthermore be of interest to investigate eccentric arrangements. However, once turbulent flow is obtained throughout the container, a simple arrangement for macroscopic mixing would become available.

3.1.3 NUMERICAL ANALYSIS OF SOLIDIFICATION AROUND A STATIONARY GAS BUBBLE. The feasibility has been investigated of a numerical analysis of the solidification process around a stationary gas bubble. In view of the rotational symmetry, the temperature distribution and position of the solidification front will depend on two spatial variables and the time so that finite-difference schemes are in principle applicable.

It appears that such schemes would be capable of global engineering estimates of the temperature field and the progression of the solidification front. At the same time it appears that further (and highly desirable) refinements of the calculations would constitute a major task. Considerable complications are caused by the singularity that occurs as the solidification front touches the most forward point of the bubble. Using the simplest boundary condition of an insulating bubble, the solidification front must be perpendicular to the bubble surface whenever the two surfaces intersect. For symmetry reasons, however, the approaching front will be tangent to the frontal bubble surface, causing a singularity at the moment of first contact. For rough engineering calculations the problem could be circumvented by considering a spherical cavity with a small frontal cusp, thereby assuming that such a modification would not significantly affect the global behavior of the solidification front. A more refined treatment would of course entail a detailed analytical investigation of the area around the singular point. As mentioned before, preliminary investigations have shown this to be an extensive and difficult task.

### 3.1.4 SURFACE-TENSION INDUCED FLOW PHENOMENA NEAR A LIQUID-GAS INTERFACE

3.1.4.1 Discussion of Marangoni Effect. Longitudinal variations of surface tension (caused by differences in temperature or composition) in a fluid interface produce fluid motion in and near the interface. This phenomenon is called the Marangoni effect, after the Italian physicist Carlo Marangoni, who, in 1871, gave a correct qualitative explanation (although the phenomenon had been explained earlier, in 1855, by the British engineer James Thomson).

In more recent years the Marangoni effect has been connected with a number of important processes such as bubble motion, boiling heat transfer, the spreading of lubricants or paints, crystal growth, the motion of protoplasm, the motility of bacteria, and foam stability. Although a significant body of experimental observations has led to a qualitative understanding of a number of surface-tension induced flow phenomena, adequate theories are often lacking. With very few exceptions, the available theoretical approaches are confined to low-Reynolds number considerations, which amount to a linearization of the flow field. Experimental observations or simple order of magnitude estimates, on the other hand, indicate that in reality nonlinear effects often play a significant or even essential role in determining the flow characteristics.

It is for this reason that the following discussion is concerned with a high-Reynolds number approximation of surface-tension induced flow. More particularly, we assume that large velocity-, thermal-, or concentration gradients remain confined to the immediate vicinity of the interface so that we may introduce the Prandtl boundary layer concept.

3.1.4.2 A New Model for Surface-Tension Induced Flow Phenomena. We consider a spherical gas- or vapor bubble, held stationary in a liquid with nonuniform temperature or nonuniform distribution of a contaminant. In either case the surface tension will vary along the liquid-gas interface so that the liquid will experience a nonvanishing shear stress at the interface. Such a state of stress requires the fluid in and near the interface to be in motion. For simplicity we assume that the imposed gradients in temperature or composition depend on one coordinate only so that the resulting fluid motion along the bubble will be symmetric with respect to the axis through the center of the bubble and parallel with the gradient vector.

If we postulate that the motion remains confined to a thin layer adjacent to the interface, then the governing equations are (Prandtl boundary layer approximation):

$$\frac{\partial}{\partial x} (r u) + \frac{\partial}{\partial y} (r v) = 0 \quad (1)$$

$$u \frac{\partial u}{\partial x} + v \frac{\partial u}{\partial y} = \nu \frac{\partial^2 u}{\partial y^2} \quad (2)$$

$$u \frac{\partial T}{\partial x} + v \frac{\partial T}{\partial y} = \frac{\nu}{Pr} \frac{\partial^2 T}{\partial y^2} \quad (3a)$$

$$u \frac{\partial C}{\partial x} + v \frac{\partial C}{\partial y} = \frac{\nu}{Sc} \frac{\partial^2 C}{\partial y^2} \quad (3b)$$

where  $x$  and  $y$  are measured along and perpendicular to the interface, respectively, and  $u$  and  $v$  are the corresponding velocity components;  $r(x)$  is the distance from the interface to the axis of symmetry,  $T$  is the temperature and  $C$  is the concentration (density) of the contaminant;  $\nu$ ,  $Pr$ , and  $Sc$  are the liquid kinematic viscosity, Prandtl number, and Schmidt number, respectively.

The boundary layer concept leading to the foregoing simplified equations has two important features, viz. 1) lengthwise gradients are small compared to normal gradients, and 2) the external pressure is impressed upon the boundary layer. Thus, in the present problem the pressure is constant throughout.

The boundary conditions at the outer edge of the boundary layer are:

$$u \rightarrow 0 \quad (4a)$$

$$T \rightarrow T_e(x) \quad (4b)$$

$$C \rightarrow C_e(x) \quad (4c)$$

At the interface we have

$$v = 0 \quad (5a)$$

and furthermore, assuming that neither heat nor contaminant is transported into the gas,

$$\frac{\partial T}{\partial y} = 0 \quad (5b)$$

$$\frac{\partial C}{\partial y} = 0 \quad (5c)$$

A consideration of the state of stress at the interface yields (neglecting the motion of the gas):

$$\tau = \mu \frac{\partial u}{\partial y} = - \frac{\partial \sigma}{\partial x}$$

where  $\tau$  is the shear stress,  $\mu$  is the liquid dynamic viscosity, and  $\sigma$  is the surface tension.

We may express the surface tension as a linear function of temperature and composition, i. e.

$$\frac{\partial \sigma}{\partial T} = -\alpha, \quad \frac{\partial \sigma}{\partial C} = -\beta$$

The stress boundary condition then becomes:

$$\mu \frac{\partial u}{\partial y} = \alpha \frac{\partial T}{\partial x} + \beta \frac{\partial C}{\partial x} \quad (5d)$$

We now have a consistent set of differential equations and boundary conditions. In order to investigate the validity of the boundary layer model, we can now make some rough estimates of the various flow quantities. For this purpose we limit ourselves to temperature-driven flow. In that case Equation 5d yields the following estimate near the top (or the bottom) of the bubble:

$$\frac{\mu u}{\delta} \sim \alpha \frac{dT_e}{dx} \quad (6)$$

where  $\delta$  is a measure for the thickness of the boundary layer and where, as a first approximation, we have set  $\partial T/\partial x$  equal to the imposed external temperature gradient  $dT_e/dx$ .

Furthermore, the boundary layer approximation implies that the inertia terms in the equation of motion, Equation 2, are of the same magnitude as the viscous term so that

$$\frac{u^2}{R} \sim \frac{\nu u}{\delta^2} \quad (7)$$

where  $R$  is the bubble radius. Eliminating  $u$  from Equations 6 and 7, we find,

$$\frac{\delta}{R} \sim \left( \frac{\mu \nu}{\alpha R^2 dT_e/dx} \right)^{1/3} \quad (8)$$

We must have  $\delta/R \ll 1$  for the boundary layer approximation to be valid. If we consider for example an air bubble in water at room temperature, with  $\mu = 10^{-3}$  kgm/msec,  $\nu = 10^{-6}$  m<sup>2</sup>/sec,  $\alpha = 0.25 \times 10^{-3}$  kgm/sec<sup>2</sup> °K,  $R = 0.01$  m and  $dT_e/dx = 100^\circ\text{K/m}$ , then Equation 8 yields  $\delta/R \sim 0.07$ , which is small enough to provide a posteriori justification of the boundary layer approximation.

Clearly, it is attractive to extract solutions from the aforementioned set of differential equations and boundary conditions, which appear to be valid over a wide range of practical conditions. Such solutions would generate important numerical information

regarding velocity-, temperature-, and concentration distributions, which in turn would provide a much improved understanding of the Marangoni effect. The present system can be solved at least approximately, for instance by using the Von Karman-Pohlhausen technique, which reduces the problem to a set of ordinary differential equations along the interface by assuming reasonable distributions of the dependent variables across the boundary layer.

However, preliminary studies indicate the existence of an exact solution near the forward stagnation point (for small values of  $x$ ). This solution can be derived by expanding the dependent variables in Taylor-series in  $x$ . This procedure reduces the partial differential equations to successive sets of (coupled) ordinary differential equations for the coefficients of the Taylor-expansions. It appears that to lowest order the energy equation and its boundary conditions are identically satisfied by a constant temperature, i. e., at  $x \rightarrow 0$  the temperature is constant (regardless the Prandtl number) across the boundary layer and equal to the prescribed temperature at the outer edge.

3.1.5 THE MOTION OF SOLIDIFICATION FRONTS. Exact solutions<sup>3</sup> exist for one-dimensional melting and solidification problems under a variety of initial conditions. These results find important practical application in processes such as crystal growth and the solidification of castings.

A typical feature of such problems is the existence of a moving surface of separation between the two phases. This feature renders the problems nonlinear so that the principle of superposition of elementary solutions (a powerful tool in a great variety of conduction problems) must be abandoned. As a consequence only one-dimensional configurations have been analyzed in depth.

A typical example is the solution for the penetration of a solidification front into a liquid initially at uniform temperature  $T_0$  with a solid surface (at  $x=0$ ) maintained at constant temperature  $T_w$  for time  $t > 0$  (Neumann's problem).

If it is assumed that the change of volume upon solidification may be neglected so that the solid and liquid phases have equal density (this restriction can be removed if necessary), the temperature distributions on either side of the solidification front are found to be,

$$T_s(x, t) = T_w + (T_m - T_w) \frac{\operatorname{erf}(x/2 \sqrt{\alpha_s t})}{\operatorname{erf}(\lambda)}$$

$$T_l(x, t) = T_0 - (T_0 - T_m) \frac{\operatorname{erfc}(x/2 \sqrt{\alpha_l t})}{\operatorname{erfc}(\lambda \sqrt{\alpha_s/\alpha_l})}$$

<sup>3</sup> Carslaw, H. S. and Jaeger, J. C. "Conduction of Heat in Solids," Chapter 11, Oxford, Clarendon Press, Second Edition, 1959.

where

$T_s$  = solid temperature

$T_l$  = liquid temperature

$T_m$  = melting temperature

$\alpha_s$  = solid thermal diffusivity

$\alpha_l$  = liquid thermal diffusivity

erf = error function

erfc = complementary error function.

The parameter  $\lambda$  is a known function of the material properties. The temperature distributions at time  $t > 0$  are depicted in Figure 3-2.

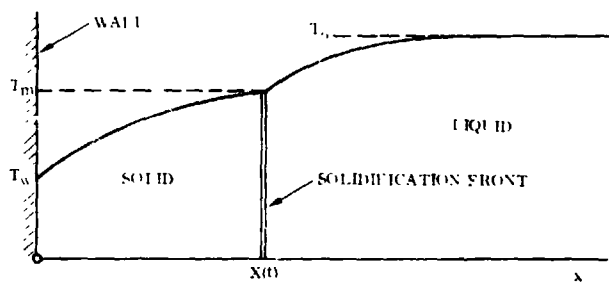


Figure 3-2. Temperature Distributions on Either Side of Solidification Front (One-Dimensional Solidification)

At the solidification front (which always has the melting temperature  $T_m$ ) the liberated heat of solidification is continually transported into the solid by conduction as the front moves into the liquid. The position of the front as a function of time is found to be

$$X(t) = 2 \lambda \sqrt{\alpha_s t}$$

Thus the velocity of the front is non-uniform, tending to zero for large times as the temperature gradients

in the solid become too small to transport any significant amount of heat.

If the densities of the solid and liquid phases are no longer assumed equal, the motion of the liquid must be taken into account. This does not materially complicate the analysis. In particular, the solution for the position of the solidification front remains the same (with a slightly modified expression for the parameter  $\lambda$ ).

The foregoing solution is useful for obtaining estimates of solidification times of liquids brought into large moulds where the latter may be assumed to act as heat sinks with nearly constant temperature.

Other useful solutions exist for the motion of one-dimensional melting fronts moving into solids, the case of melting ranges with gradual liberation of solidification heat (rather than a fixed melting temperature), and multiphase problems (with successive transition temperatures or transition ranges).

## 3.2 FIBER- AND PARTICLE-REINFORCED METAL COMPOSITES

**3.2.1 PROCESS AND PRODUCT DEFINITION.** The objective of this composite class is to produce high-strength material ingots or finished components by casting of a mixture of molten metal and solid reinforcements, followed by solidification. An effective end product calls for uniform fiber dispersion. This can only be achieved by processing under zero-g, since in the gravity environment segregation of the reinforcements will occur during the matrix-melting cycle. Laboratory experiments have shown that density differences as small as  $0.1 \text{ g/cm}^3$  lead to immediate segregation. The process comprises three types of composites: 1) random-oriented fiber composites, 2) composites with controlled fiber orientation, and 3) particle composites.

Consideration of Type 2) is deferred, since it requires the establishment of techniques for, and solution of all problems of, Type 1). From the viewpoint of liquid-state processing, Types 1) and 3) are identical since the distinction between "fibers" and "particles" can be identified by the L/D ratio (particles  $L/D = 1$ ; fibers  $L/D > 1$ ). They differ, however, with regard to the metallurgical effects required to obtain specific end-product characteristics: for Type 1) the prime criterion is an intimate bond between fibers and matrix, necessary to obtain high composite strength. For Type 3) it has to be considered that particles per se have no strengthening effect. They may, however, act as stabilizers for a cold worked microstructure, as in the case of dispersion-strengthened alloys for high temperature applications. Or they may act as nuclei for crystallization and grain-size control. Particles in the form of flakes may have a strengthening effect, which is, however, expected to be inferior to fibers (Type 1).

**3.2.1.1 Materials Selection.** The basic criteria for selection and matrix/reinforcement compatibility are:

### a. Fiber-Reinforced Composites

1. High fiber strength.
2. Chemical compatibility of matrix and fibers in the liquid and solidified matrix state.
3. High wettability.
4. High adhesion after solidification and/or diffusion at the matrix-fiber interface.
5. High fiber-matrix bond strength.

### b. Dispersion-Strengthened Alloys

1. Effectiveness of particles in increasing critical shear stress in individual matrix crystals.
2. Dispersability of non-wetting particles or precipitation of particles from the matrix alloy by an additional thermal treatment after melting.

c. Fine-Grain Castings

1. Nucleation effectiveness of particles for a specific matrix.
2. High wettability.

3.2.1.2 Processes. Fiber and particle composite may be produced by either of two processes, characterized by method of mixture preparation: 1) "dry" mixing of matrix powder and reinforcements at room temperature, and 2) "wet" mixing of molten matrix and reinforcements. They involve the following steps:

a. "Dry" Mixing

1. Cleaning of components (de-oxidation)
2. Dry mixing
3. Compaction (optional)
4. Matrix-melt cycle
5. Solidification

b. "Wet" Mixing

1. Melting of matrix
2. Addition of reinforcements
3. Wet mixing (agitation) and dispersion control
4. Solidification

In the first process, the dispersion is established in dry-mixing phase, so that no agitation is necessary during the melt cycle ("re-melting"). It is, therefore, ideally suited for initial experiments. It has, further, the advantage that it is adaptable to nonwetting reinforcements, such as fine oxide particles. The drawback of this process is the presence of voids, which are difficult to remove under zero-g, even in a perfectly evacuated mold.

In the "wet" mixing process, the reinforcements can either be precast into the matrix, without regard for distribution, or added to the matrix after liquification. The advantage of the wet process is the absence of voids, and the disadvantage the necessity of mixture agitation for the establishment of uniform dispersion.

3.2.1.3 Processing Criteria. Cleaning, mixing, and compacting of powders and reinforcements for the preparation of the pre-mix should present no major problems. However, during the melt cycle various interactions may occur between the reinforcements, such as agglomeration due to interface energies, which are directly related to the surface tension of the liquid matrix or, more accurately, the interfacial tension.

It is apparent that any interactions between reinforcements are more pronounced in the wet mixing process, where the reinforcements will necessarily come in contact with each other.

In view of the significance of the behavior of liquid/solid mixtures for the processing of composites, and in view of the complete lack of applicable data, high emphasis was placed on the theoretical and experimental investigation of the criteria and material characteristics that govern the behavior of still and agitated mixtures.

### 3.2.2 SUMMARY OF RESULTS

1. Three methods for composite preparation have been defined: a) compact method, in which the dispersion is established in 1-g while the zero-g process consists of a melt cycle; b) premixed ingot method, in which joining is accomplished in 1-g and mixing in zero-g; c) space method, in which all operations are carried out in zero-g.
2. For suborbital zero-g experiments, methods a) and b) are proposed.
3. Effective matrix materials are Al, Mg, Ni, Co, and Fe. Aluminum is proposed as base metal for in-depth development of techniques and for initial zero-g experiments.
4. Promising reinforcement materials are graphite, boron, tungsten, and whiskers of  $\text{Al}_2\text{O}_3$ , SiC,  $\text{Si}_3\text{N}_4$ , and BN.
5. For high strength composites, high L/D fibers (over 50) are required; they are readily available.
6. Mixtures of short fibers and particles with a total content in the order of 1% are most promising for composites with high creep strength.
7. The maximum reinforcement content is geometrically limited to 14% for fiber composites with high L/D and to 60% for particle composites.
8. The ratio of mold diameter to fiber length should be over 4 to minimize geometric wall effects and to obtain data representative of random dispersion.
9. For perfect reinforcement dispersion, high wettability and freedom from adhering gases are of equal importance.
10. Wetting characteristics are sensitive to minute surface contaminations; all reinforcements have to be cleaned and stored in an inert fluid.
11. All promising reinforcement materials are nonwetting with regard to the candidate matrix metals; coating materials and techniques have to be devised individually for specific material combinations.
12. Coating of the prepared reinforcements with matrix material has been found effective for surface preservation and for joining with the molten matrix.

13. Prewetting of the reinforcements prior to joining with the molten matrix enhances the elimination of adhering gases.
14. Material preparation and composite processing have to be carried out in either a high-purity inert gas or in high vacuum.
15. Reinforcement treatment requirements and techniques have to be developed individually for each matrix metal.
16. Positive wetting characteristics do not assure high bond strength. Bond strength characteristics have to be determined experimentally for each material combination and reinforcement surface treatment.
17. Detailed fluid mechanics relationships for the behavior of liquid/solid mixtures in zero-g have been established. They serve as a basis for the development of mixing techniques and the prediction of the time required to obtain stable dispersion (zero-motion).
18. The mobility of reinforcements in the liquid matrix depends on matrix viscosity, reinforcement diameter, and L/D.
19. Numerical data have been generated for the relationship of segregation rate to g-level. Even at density differences of  $0.1 \text{ g/cm}^3$  the segregation rate in 1-g is prohibitive and liquid-state processing of composites is unique to zero- or low-g environment.

**3.2.3 METHOD OF APPROACH.** The evaluation of fiber- and particle-composites is carried out in five major phases:

- a. Identification of the mixture variables.
- b. Determination of the effects of these variables on the mixture characteristics and the establishment of generally applicable relationships by means of experiments with transparent-matrix mixtures.
- c. Application of the results of (b) to, and verification with, metal-matrix mixtures.
- d. Delineation of the effective regimes with regard to composite types and zero-g processing; definition of promising composite materials and the applicable processing parameters and techniques.
- e. Definition of specific materials and processes for zero-g experiments and identification of problems for in-depth investigations.

The approach is illustrated in more detail in Figure 3-3. The top section identifies the mixture variables, which serve as the basic input for the subsequent evaluations (phase 1). They consist of three groups:

- a. Liquid matrix properties.

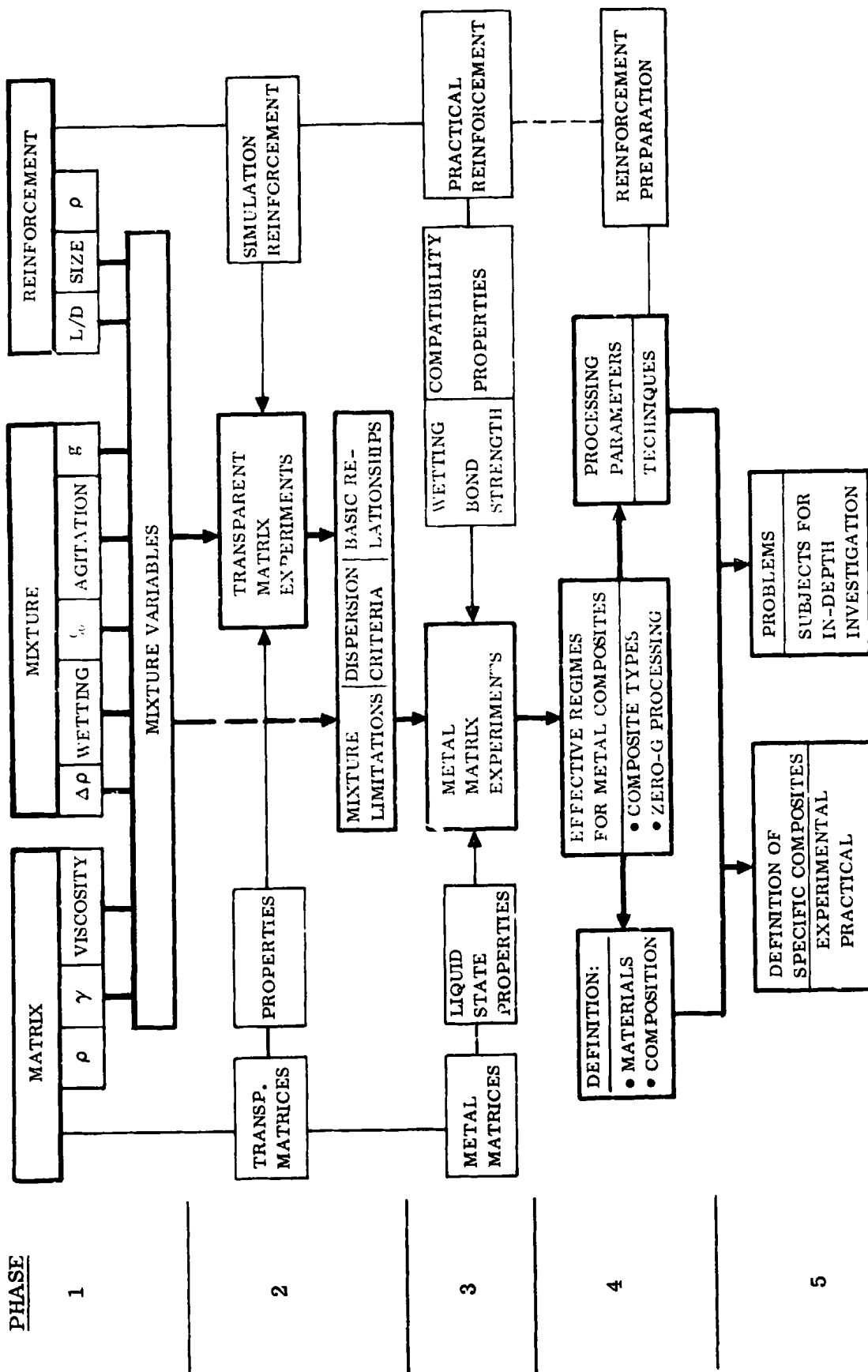


Figure 3-3. Fiber and Particle Composites - Approach and Sequence of Tasks

1. Density ( $\rho$ ).
  2. Surface tension ( $\gamma$ ).
  3. Viscosity ( $\mu$ ).
- b. Solid reinforcement characteristics.
1. Density ( $\rho$ ).
  2. Configuration (L/D).
  3. Absolute size (represented by ratio of container diameter to length of fiber C/L).
- c. Combined matrix/reinforcement characteristics.
1. Density difference ( $\Delta \rho$ ).
  2. Wetting characteristics.
  3. Reinforcement content (volume percent).
  4. Degree and mode of agitation.
  5. g-level.

Secondary variables, such as mixture temperature or particle surface finish are, at this point, not taken in consideration since they are not of a basic nature.

The effects of these variables on the behavior of mixtures and the resulting dispersion (phase 2) were evaluated in extensive experiment series with transparent matrices. The preparation of mixtures deals with dynamic phenomena whose observation in metals is extremely difficult and costly, if not impossible. With transparent matrices, such observation is simple and reliable. Moreover, all liquid-metal properties, with the exception of surface tension, can be accurately reproduced in transparent matrices so that the results are directly applicable to metals.

Beside the effects of various material characteristics upon dispersion and dispersion stability, the transparent matrix experiments of phase 2 included the evaluation of mixing techniques and the determination of reinforcement content limitations.

A prerequisite of these experiments was the experimental measurement of the applicable properties (viscosity, surface tension, density) of the selected transparent matrices.

Concurrently with the experimental investigations, theoretical fluid-mechanics studies were carried out on the effect of the primary variables on the behavior of liquid/solid mixtures and, particularly, the mobility of reinforcements. An excellent correlation between experimental and theoretical data was achieved for large L/D reinforcements. A dimensionless relationship has been established between Reynolds number and a

suitably defined group of relevant parameters, which permits the calculation of reinforcement mobility and segregation rate for a wide range of matrix-fiber combinations and g-levels with adequate accuracy.

The so obtained generally applicable relationships and data on liquid/solid mixtures provide a reliable basis for mixture and mixing experiments with liquid metals and the selection of effective variables (phase 3). A prerequisite of these experiments is, again, the availability of data on the relevant matrix and reinforcement properties, obtained in the following supporting investigations:

- a. Liquid-state metal properties (density, viscosity, surface tension).
- b. Mechanical properties of reinforcements.
- c. Temperature stability of reinforcements.
- d. Chemical compatibility of various matrices and reinforcements.
- e. Wetting characteristics between various matrix and reinforcement materials.
- f. Bond strength between matrices and reinforcements after solidification.

In phase 4, the results of phases 2 and 3 are further evaluated with the objective to arrive at specific conclusions and definitions with regard to:

- a. The effective regimes of fiber- and particle-composites; the effective regime is characterized by limitations as to composition, effective materials, and zero-g processing (g-sensitive or useful range).
- b. Promising composite types in terms of materials, composition, and applications.
- c. Significant processing parameters, specific processing techniques, and the pertinent criteria.

From the so established envelope of effective materials and processes, specific composites were defined in phase 5: 1) for early zero-g experiments, and 2) for the potential space production of practical materials. The final phase further included the identification of unresolved problem areas and research tasks as they evolved from the investigation.

**3.2.4 CRITERIA FOR PARTICLE/FIBER DISPERSION.** The most basic requirement of metal-base particle or fiber composites is a uniform random dispersion of the solids in the liquid matrix during the high-temperature processing cycle. An absolute and mandatory prerequisite for the development of such composites is the establishment of criteria that govern the dispersion of solids in liquids. The first-order criteria for the dispersion of solids in liquids are:

- a. Effects of the material-dependent interface characteristics between solids and liquids.
- b. Mobility of reinforcements in the liquid matrix as related to acceleration (g-) forces.
- c. Physical (mechanical-dimensional) effects and limitations.

The material-property related criteria for the dispersion of solids in liquids are developed in two steps:

- a. Criteria for the dispersion of solids in two or more fluids.
- b. Criteria for the dispersion of solids in a single fluid.

Some of the following discussion involves subjects of common knowledge. The important aspect is their interpretation as to their significance upon dispersion characteristics. The resulting conclusions, together with the evidence obtained in laboratory experiments, convey a clear picture of the factors which govern the dispersion of solids in liquid metals.

**3.2.4.1 Solids in Two or More Fluids.** The following discussion is limited to a two-fluid system. It is completely adequate for the definition of criteria that apply equally to a system of more than two fluids.

The most common two-fluid system is a liquid and a gas in contact with a solid, as it is used for the classic definition of wetting characteristics. However, the use of the term "fluids" implies that conditions apply equally to two liquids; they would even apply to two gases, even though practically unfeasible.

The behavior of two-fluid systems has been evaluated in equal-density experiments, in which solids (fibers, particles) are neutrally buoyant in two immiscible liquids, one of which may represent a gas.

Let us first consider a fiber, perpendicularly crossing the interface between fluid G, representing a gas, and fluid L, representing a liquid matrix, as illustrated in Figure 3-4. If the liquid contact angle  $\beta$  is high (A = nonwetting), the surface tension at the curvature draws the fiber into the gas; it is rejected by the liquid. If the contact angle is low (B = wetting), the fiber is pulled into the liquid.

Let us now consider a solid sphere at the interface. If the contact angle is again high, the sphere is pulled into the gas; however, it comes to rest at an equilibrium position at which the contact angle is satisfied by the curvature of the sphere and the liquid surface has become flat (Figure 3-4, C). The same equilibrium position is obtained at low contact angles (D = "wetting"), except that the major part of the sphere is now in the liquid. Consequently, at any finite contact angle, a sphere, once coming in contact with the interface, will be "trapped" at the interface.

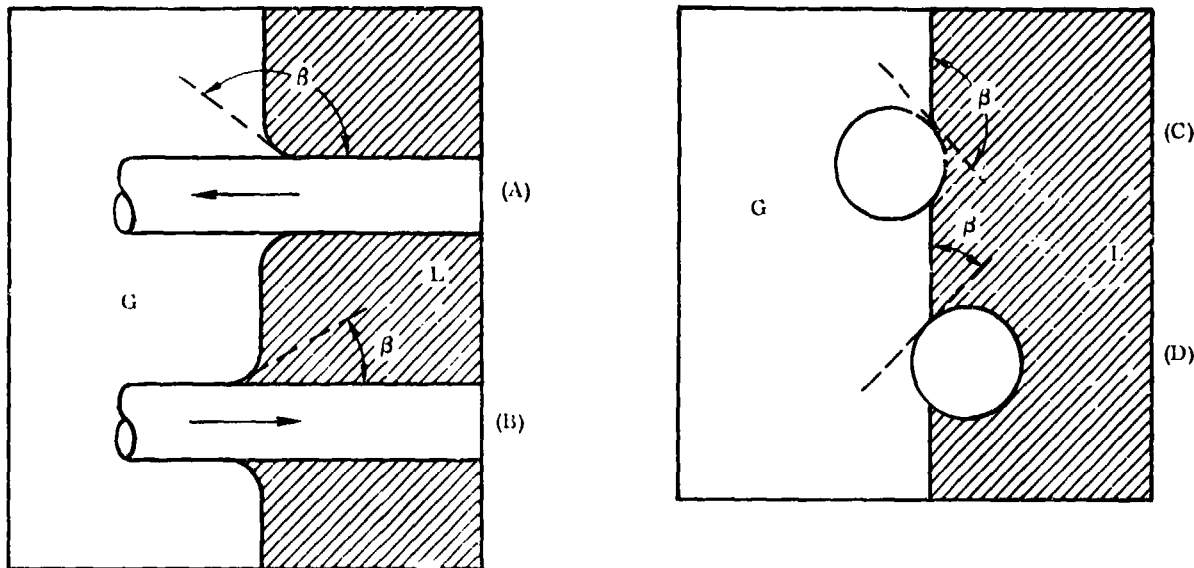


Figure 3-4. Effect of Wetting Characteristics on Positions of Fibers and Spheres at a Two-Fluid Interface

Let us finally apply the considerations of a sphere to a cylindrical fiber that enters the interface at any angle other than the 90 degrees assumed in (A) and (B), representing the practical condition of a random-fiber mixture. In view of the near-circular configuration, it will—like the sphere—be pulled to the equilibrium position; i.e., it will be tilted forward, and aligned in the interface plane as in (C) and (D). In other words, fibers entering the interface will be trapped along the interface. Experiments have further shown beyond any doubt that at higher fiber contents, where fibers are in close contact, groups of fibers will align themselves parallel to each other at the liquid/gas interface (Figure 3-5).

Since any two-fluid system exhibits a finite contact angle, the conditions previously discussed apply to two-fluid systems in general.

**Conclusion 1:** In two-fluid systems (liquid/liquid, liquid/gas), solids in contact with the interface will agglomerate there. Straight fibers will agglomerate in parallel patterns. This effect will be particularly pronounced under dynamic mixing, since there is a high chance for the fibers to come in contact with the interface.

**Conclusion 2:** Perfect random dispersion can only be achieved in a single-fluid system.

**Conclusion 3:** In reinforced foams, which always represent a two-fluid system, fibers will agglomerate at the gas bubbles; the fraction of fibers agglomerating depends on the ratio of fiber length to bubble diameter, on the means of dispersion (compact foaming or dynamic mixing), and on the presence and nature of a third phase (bubble surface stabilizer).

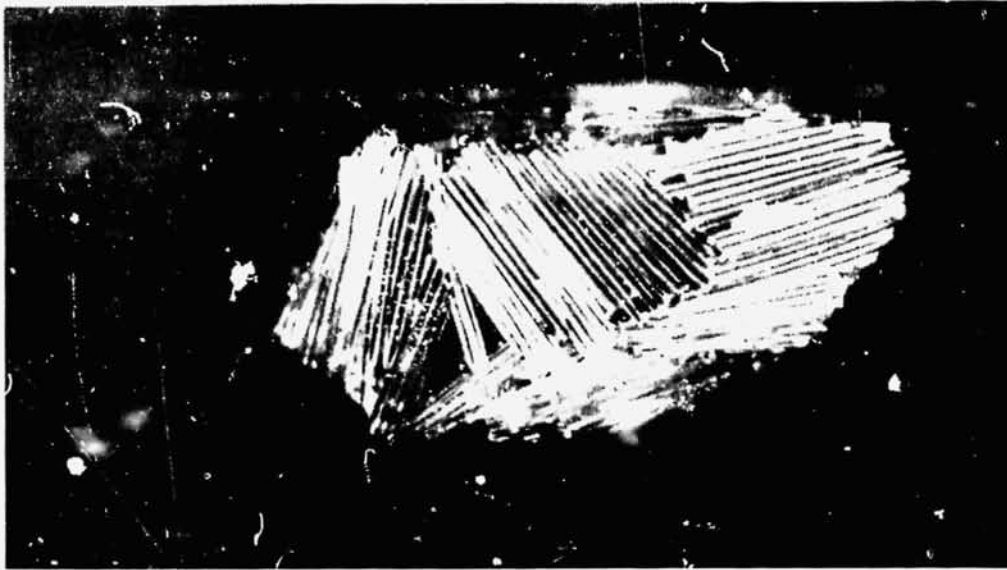


Figure 3-5. Agglomeration and Alignment of Fibers Around a Gas Bubble

**3.2.4.2 Single-Fluid Systems.** According to conclusion 2, above, dispersion of solids in a perfect single-fluid system is free from interface disturbances. The only forces that may interfere with the free mobility of solids are surface energies and mass attraction forces. In a preliminary and cursory assessment of surface energies it has been found that the potential forces between solid particles or fibers are by several orders of magnitude smaller than those encountered at two-fluid interfaces. For the purposes of the present study, they can, therefore, be neglected. However, an accurate evaluation of the nature and magnitude of surface energies and their interaction in a separate research program is indicated. The mass attraction (gravitational) forces between solid particles are, in turn, many magnitudes smaller than surface energy forces; they can be definitely neglected.

For all practical purposes, therefore, a one-fluid system should permit free dispersion and application of the laws of fluid mechanics. At first glance, this appears to be a simple solution. The problem is, that the fluid or liquid has to be perfect and free from even traces of a second fluid. In metals, such perfection is not readily achieved, and many unexplainable phenomena encountered in the past in metal/solid mixtures can be related to the presence of a second fluid.

Such traces of a second fluid are invariably concentrated at the surface of the solids, creating a localized two-fluid system that exhibits all typical characteristics of the two-fluid system as defined in Section 3.2.4.1. Since these characteristics are unfavorable with regard to free dispersion, the sources for the concealed second fluid in an apparent one-fluid system and the means for their elimination have to be found.

Experimental Evidence. Figure 3-6 shows the effect of various degrees of localized two-fluid condition on the dispersion of fibers in a fully wetting liquid. The fibers of Figure 3-6A were prewetted; while the gas-free fibers disperse freely, others are still tied together by small gas bubbles resulting from unfavorable angles of immersion. The fibers of Figure 3-6B were immersed without prewetting; the substantial amount of trapped gas inhibits dispersion. Disruption of the agglomeration can be achieved by stirring; this effect is, however, only temporary. As soon as the mixture is allowed to come to rest, the agglomerations of Figures 3-6A and B are re-established.

The causes for the existence of a localized two-fluid condition are quite complex. They are not only related to surface properties, but also to chemical interactions between matrix and solid surfaces and to minute procedural details during the preparation of the mixture. Due to this complexity, attempts to establish a logical system of the sequence of causes and effects were unsuccessful.

Conclusion 4. The prime problem in the achievement of perfect dispersion of solids in liquids is the presence of localized two-fluid conditions due to minute amounts of gases adhering to the solids. Perfect dispersion calls for the elimination of such gases, which can be accomplished by proper material selection, reinforcement preparation, and mixing techniques.

3.2.4.3 Dispersion Criteria for Various Types of Mixtures. In the approach used in the following discussion, each cause and effect is discussed individually. The three objectives of this approach are:

- a. To identify the conditions and processing parameters most favorable to uniform dispersion.
- b. To provide a tool for tracing the causes for negative phenomena in the evaluation of laboratory and flight experiments.
- c. To identify fundamental problems for further research.

The discussion is presented in the form of statements that are results of extensive studies, laboratory investigations, and experiments. The reference to these supporting activities and to experimental evidence is kept at a minimum for the sake of clarity and continuity.

The subject matter arrangement is: first order, surface characteristics; second order, single fiber versus bulk; third order, processing and other details. To facilitate reference and cross-reference, the individual statements are identified by a letter-code system.

Qualifying remark: "wetting" and "nonwetting" are practical terms. From the viewpoint of physics, they are inaccurate, yet an accurate distinction does not exist.

REPRODUCIBILITY OF THE ORIGINAL PAGE IS POOR.



A. PREWETTED

B. DRY IMMERSION

Figure 3-6. Effect of Adhering Gases (Localized Two-Fluid System) on Dispersion of Wetting Fibers After Agitation

Generally, "wetting" refers to low contact angles, and "nonwetting" to large contact angles. Experience has shown that the contact angle alone provides no comparable measurement of the wetting characteristics. It is beyond the scope of this study to resolve this dilemma, which represents a topic for a separate fundamental investigation. Absolute nonwetting condition, or a contact angle of 180 degrees, is unfeasible. The term "nonwetting" is used here in its practical interpretation and refers to large contact angles.

#### A. Wetting Fibers/Particles

Aa. Clean Surface. An individual "clean" particle or fiber that is highly wetted by the liquid is expected to disperse freely in the liquid, i.e., retain full mobility independent of other identical particles, unless mechanical crowding is encountered. This ideal one-fluid condition is, however, only achieved if the following conditions are met:

- (1) Absolute surface cleanliness.
- (2) High surface smoothness.
- (3) Immersion perpendicular to the liquid surface.
- (4) Slow immersion rate.

Let us first assume that these conditions are met. During the perpendicular, gradual immersion, the liquid will establish the low contact angle typical for high wettability and gradually shift adhering gases off the surface; after completed immersion, a perfect one-fluid condition, i.e., free mobility of the particles, is achieved. A practical application of this ideal process is the continuous immersion-coating of filaments or wires (see Ac, below).

If the particles are not clean (1), the situation of Ab, below, applies. On rough surfaces (2), gases may remain trapped, in spite of otherwise perfect conditions. Potential trapping of gases may also result from immersion at low angles (3) or at too high speed (4) due to local turbulence and cavitation effects. However, even in such cases the amount of trapped gases is small, resulting only in very localized two-fluid conditions that may interfere with free dispersion only under continued agitation.

Ab. Contaminated Surface. There is a wide variety of potential contaminations, ranging from a completely oxidized surface to dirt particles. Oxidized metal surfaces are in most cases nonwetting, and the conditions of C apply. Other contaminants (grease, dirt, etc.) are too numerous to be classified and lead to varied degrees of gas adsorption and localized two-fluid conditions. A careful surface de-oxidation and/or cleaning is a prerequisite of any dispersion of solids in liquids. The use of fluxes immediately before immersion is most effective (see Ad below). Of further importance is the storage of particles between the time of cleaning and composite preparation; storage in an inert liquid is simple and reliable.

Ac. Matrix-coated particles and fibers have been found to produce a virtually gas-free immersion and perfect dispersion, provided that there are no gases trapped at the particle-coating interface. Such gases are effectively eliminated by prewetting of the particle or fiber with an appropriate flux. In the continuous coating of filaments this is easily achieved in a two-bath system or, if feasible, by placing the flux on top of the molten coating material.

Ad. Prewetted Particles. Prewetting of the particles with an appropriate and highly wetting flux has proven to be most effective for the removal of all gases from the surface, even in the presence of a reasonable surface roughness. The prewetting liquid may at the same time serve for surface cleaning and de-oxidation. Perfect dispersion was, for instance, obtained by dropping oxidized fibers through a flux into the molten matrix.

Experimental Evidence. The free movement of fibers after dispersion under ideal conditions (fibers wetted by the liquid and prewetted) can be observed in Figure 3-7, which represents four consecutive motion picture frames of bulk fibers moving downward under 1-g after mixing. Even local entanglements are only of a temporary nature, as the involved fibers free themselves and show no evidence of any connecting force. (For observation in Figure 3-7, select a specific spot and compare from left to right.)

#### B. Bulk Immersion of Wetted Particles

In all cases of bulk immersion, gases may be trapped in the particle or fiber network, even of high wettability, leading to localized two-fluid systems and imperfect dispersion. The amount of trapped gases depends on the bulk density and the condition of the individual fibers, as discussed in A, above. In view of the multitude of possible conditions, only two basic cases are identified: 1) dry immersion, and 2) prewetted immersion.



Figure 3-7. Free Mobility of Fibers in a Perfectly Dispersed Mixture

- Ba. Dry Bulk Immersion. In a bulk, a certain amount of trapped gases cannot be avoided, which leads to incomplete dispersion. In some experiments, where dry batches of wetting fibers were immersed, partial batches—apparently clinging to a gas bubble—could not be further dispersed. The effect is less pronounced if the fibers are matrix-coated; particularly at slow immersion, some of the gas trapped in the batch is forced out, as the coating melts and joins with the liquid matrix surface.
- Bb. Immersion of Prewetted Bulk. A thorough prewetting of the bulk immediately prior to immersion has been found as the most effective means for achieving perfect one-fluid condition and dispersion.

It is important to realize that the effectiveness of prewetting is brought about solely by the physical removal of gas from the surface in the prewetting process. During subsequent immersion the two liquids—the matrix and the prewetting agent—establish contact and shield the fiber from any new gas exposure. Chemical functions of the prewetting liquid, such as de-oxidation, are entirely separate.

Experimental Evidence 1. Figures 3-8 and 3-9 illustrate the effect of prewetting of bulk fibers on dispersion. Both experiments were carried out with the same fiber material (highly wetted by the liquid) and under otherwise identical conditions. The dry immersed bulk batch (Figure 3-8) stays together; stirring causes it only to break up into smaller batches. The prewetted bulk batch (Figure 3-9) dispersed instantly.

Experimental Evidence 2. A beaker was half filled with liquid In-Bi (bottom) and half with a flux (top). Bulk batches of copper fibers were dropped through the flux into the metal, where they exhibited 100% dispersion. The experiment was repeated several times with gradual dilution of the flux. The effect remained the same, even after the flux was replaced by plain water.

Conclusion 5. If deployed individually, clean or matrix-coated wetting particles disperse freely. Dry immersion of bulk entails the danger of incomplete dispersion due to trapped gases. The most reliable means of achieving complete and stable dispersion is prewetting of the clean bare or matrix-coated bulk in a wetting agent. For prewetting, the use of an appropriate flux is most effective, since it also assures fiber cleanliness.

### C. Nonwetting Particles/Fibers

- Ca. Single Particle/Surface Deployed. A single nonwetting particle deployed at the liquid surface is "rejected" by the liquid unless it is completely immersed. It is apparent that in this case we deal with a two-fluid system (liquid/gas). The particle obeys the postulations of conclusion 1 and behaves as illustrated in Figure 3-4.

REPRODUCIBILITY OF THE ORIGINAL PAGE IS POOR.

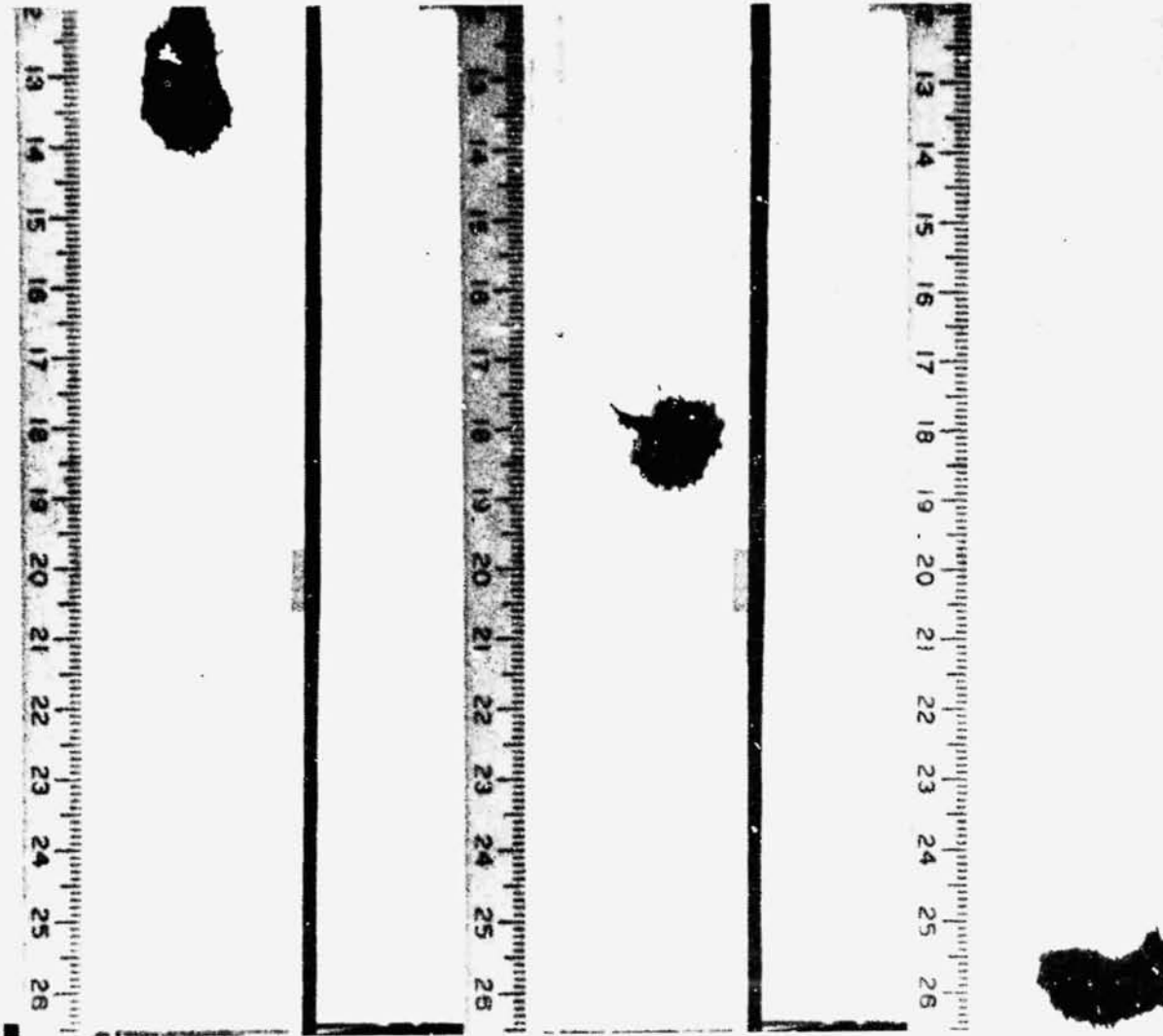


Figure 3-8. Dry Immersion of Wetting Bulk Fibers

Cb. Single Particle/Fully Immersed. If a single nonwetting particle is forced below the surface to complete immersion, it will stay in suspension as long as the liquid is at rest. At first glance it appears that we now deal with a one-fluid system. This is, however, erroneous, since during the process of immersion gases are trapped at the particle surface. The amount and distribution of these adhering gases depend on the particle surface finish. At a very smooth surface, the gases tend to form a bubble at one point, which in the case of a fiber appears at one end in  $g$  and both ends in zero- $g$ . If the surface finish is not perfectly smooth, which represents the practical condition, gases are distributed over the entire surface, regardless whether an additional bubble is formed or not. Consequently, the particle is in a localized two-fluid system and follows its laws. This means that the suspension is highly unstable:

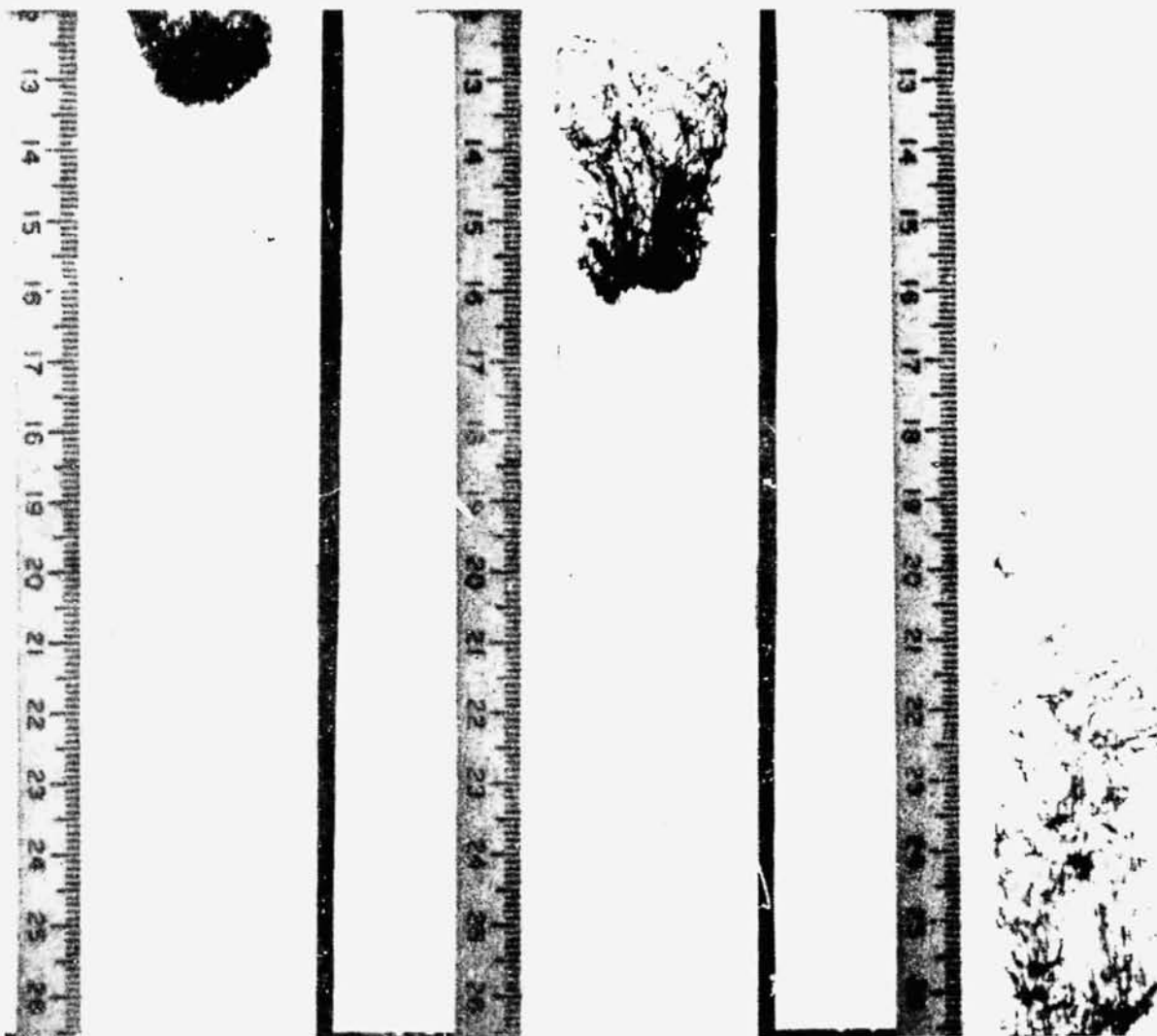


Figure 3-9. Effect of Prewetting on Dispersion (Bulk Fibers  
Otherwise Identical to Figure 3-8)

as soon as the particle comes in contact with an interface — the container wall or another particle — it will "stick" there. This occurs quickly in agitated systems; but even in still systems, the particle will — due to thermal motion — eventually come in contact with an interface. This effect is most pronounced in liquid of high surface tension, such as metals.

Cc. Several Particles/Immersed. Several particles forced into complete immersion individually will in accordance with Cb, above, agglomerate, as demonstrated in Figure 3-10 with teflon strips in water (nonwetting). The time to agglomeration depends on the degree of agitation, and the interparticle bond strength on the surface tension of the matrix. In low surface tension liquids, such as water (73 dyne/cm) or Fluorolube (20 dyne/cm), the bond will resist agitation, but may be broken by mechanical means. In high surface tension liquids (metals) the particles will not separate even by mechanical action.

Cd. Wettability Control Coatings.

Particles treated for wettability with chemically stable coatings will behave like wetting particles (A/B). However, most thin coatings are unstable and dissolve. The behavior of particles with unstable coatings has not yet been conclusively explored. It can be assumed that the amount of gas trapped at the surface during immersion is minimized, since at this point the coating is still intact. During the subsequent complete immersion and dissolution of the coating, there should be a substantially reduced tendency for agglomeration. The behavior will further be affected by the method of coating and the potential of gases trapped between the coating and the nonwetting substrate.



Figure 3-10. Agglomeration of Nonwetting Fibers After Agitation

Ce. Additional Matrix Coating. The purpose of a matrix coating in addition to the wetting coating Cd is to further minimize or eliminate the trapping of gases during immersion and to facilitate initial dispersion. Once the coating is molten and has become part of the matrix, the particles will behave as stated in Cd, except for a further minimized effect of adhering gases. Whether the presence of gases can be completely eliminated by this method, and how essentially gas-free, nonwetting particles behave, has not yet been evaluated experimentally.

Cf. Prewetted Particles. According to experimental evidence, the most effective means to reduce the amount of surface-adhering gases is the prewetting of the particle prior to immersion. This presumes that a liquid or flux can be found that wets the otherwise nonwetting particle. This process is, however, only effective by individual fiber immersion.

D. Bulk Immersion of Nonwetting Particles

Da. No Surface Treatment. If several nonwetting particles/fibers are immersed together (interparticle contact), they will not separate in the liquid in view of substantial amounts of gases trapped in the particle network in addition to the gas adhering to the surface of each particle (Ca, Cb). At each particle contact point and at interparticle spaces, localized two-fluid systems are in existence, which attempt to pull the particles to the minimum energy position. These tension forces remain active, since mechanical interlocking and gas bubbles prevent particle motion. The resultant of the multitude of tension points is

a strong bond in the batch of particles. The bond strength increases with the surface tension of the liquid and with number of particles deployed together. The bulk batches form strongly bonded units in the liquid, which cannot be dispersed by any means.

- Db. Coated Particles/Fibers. For nonwetting particles or fibers coated for high wettability, the effect of gases trapped during bulk immersion is similar to wetting particles, condition Ba. After immersion the behavior of the immersed bulk depends on the chemical stability of the coating. Bulk batches with stable coatings behave like bulks of particles of high wettability (Ba). If the coating is unstable, the bulk batch will usually separate into smaller batches, which may or may not further disperse depending on the rate of coating dissolution. In the case of fast dissolving coatings, the gas trapped initially in the bulk will concentrate in some of these smaller batches and hold them firmly together, so that they cannot be further separated even under violent agitation. If the rate of coating dissolution is low, the particles may disperse. After loss of the coating they will generally behave like Da above, even though the tendency for coagulation is somewhat reduced.
- Dc. Matrix-Coated. Bulk batches of nonwetting fibers coated as described in Ce behave during immersion exactly as matrix-coated wetting bulk particles (Ba). After immersion, the gases not removed during immersion will hold partial batches firmly together and complete dispersion cannot be achieved.
- Dd. Prewetted Nonwetting Bulk. In this case, the first question is whether the prewetting agent wets the particles. Obviously, a nonwetting agent is ineffective and offers no improvement of the behavior at dry immersion, as discussed in Dabc, above. If the agent is wetting, the effects during immersion are identical to those defined in Bb (prewetted wetting particles). After immersion, however, the dispersion depends on the wetting characteristics of the individual particles. Uncoated particles or those with dissolving coatings will agglomerate in stable batches. Prewetted matrix-coated particles behave like Bb during immersion, and after immersion as described in Dc, above. Prewetted batches with stable wettability coatings behave like wetting particles (Bb) and disperse freely if the coating is absolutely clean (de-oxidized).

Conclusion 6. Under dry immersion, nonwetting particles exhibit various degrees of agglomeration depending on the type and stability of surface treatments. The only condition under which complete dispersion of nonwetting particles is achieved is the combination of 1) a stable, clean wettability coating, and 2) prewetting of the bulk with a wetting agent.

#### E. Pre-cast Metal - Particle Mixtures

The essential zero-g processing phase in the preparation of composites is the establishment of dispersion. It has, therefore, been proposed to combine the component materials in terrestrial operation into an ingot consisting of a segregated mixture and to confine zero-g processing to remixing during a melt cycle. In

this case, the attainable dispersion depends entirely on the materials and procedures used in the terrestrial ingot preparation and is defined by the applicable conditions A through D, above.

#### F. Compacted Mixtures

In the case of compacts, the dispersion is prepared by dry-mixing of solid components. The purpose of zero-g processing is to transform the compact into a composite casting without disturbing the dispersion. Here the problem is not, as in the preceding cases, the establishment of dispersion in a liquid, but the preservation of an existing dispersion through a matrix-melt cycle. The interparticle wetting characteristics affect primarily the strength of the re-solidified compact and have little effect upon dispersion.

It may be remarked that this discussion is confined to compacts that are g-sensitive during the melt cycle and, therefore, represent a case for zero-g processing. This eliminates 1) compacts in which the volumetric content of nonwetting particles is so high that movement during the melt cycle is mechanically prohibited, and 2) compacts with oxidized particles, maintaining an oxide framework through the melt cycle which likewise prohibits free movement. Both compact types can be processed in the one-g environment; type (1) is quite common (cutting tool materials); type (2) is of little use since it exhibits little fusion and, therefore, poor strength. The g-sensitive compacts are classified in three categories in accordance with the fluid systems resulting from their preparation.

Fa. Preparation in Air. If dry mixing and compaction is carried out in air or another oxidizing gas, either or both of the following effects may be encountered: 1) generation of an oxide network which renders the compact unfit for zero-g processing, and 2) local agglomeration of particles due to two-fluid interface conditions. Agglomeration is enhanced by poor interparticle wetting.

Fb. Preparation in Inert Gas. If the entire preparation, from the cleaning and de-oxidation of particles to compacting is carried out in an inert gas environment, internal oxidation is eliminated. The still existing two-fluid condition may lead to localized agglomeration of particles, which is, again, enhanced by poor interparticle wetting. In fiber compacts, a disturbance of the dispersion is only encountered if the gas pockets are substantial and/or the absolute fiber length is of the same order of magnitude as the matrix particles. Even though not verified experimentally, it can be expected that an essentially stable dispersion is obtained at low gas contents and ratios of fiber length to matrix particle size over 3. Fiber wetting characteristics affect primarily the end product strength and appear to be of little significance upon dispersion.

Fc. Preparation in Vacuum. If the entire preparation is carried out in vacuum (pressure  $10^{-4}$  mm Hg or less), a perfectly stable dispersion should be obtained, even though the vapor pressure of the matrix at melting temperature

will still represent a two-fluid system. The two-fluid effect may, however, become significant at poor interparticle wetting characteristics. Wetting characteristics further affect the end product strength, particularly in the case of fiber compacts.

Conclusion 7. The prime requirements for effective cemented compacts are 1) high wettability between particles/fibers and matrix, and 2) compact preparation, from particle cleaning to compacting, in an inert gas or in vacuum.

3.2.5 CRITERIA FOR MIXTURE STABILITY AND SEGREGATION. The two basic methods considered in this study for establishing fiber- or particle-dispersion are:

- a. Mixing of the solids with the liquid (molten) matrix under zero-g conditions.
- b. Predispersion by "dry" mixing and compaction of powdered matrix and reinforcements.

The assessment of the fluid dynamics of the mixing process (a) and of various mixing techniques requires numerical data on the mobility of the solids as related to their configuration, the properties of the liquid matrix, and the accelerating force (g). Upon achieving dispersion by deceleration to zero-motion in (a) and by matrix-melting in (b), the dispersion stability is determined by the sensitivity of the solids to g-forces and, to a lesser degree, to thermal gradients. The g-sensitivity of a mixture serves as a measurement for the effectiveness of zero- or low-g processing. Mixtures essentially insensitive to g may be processed terrestrially; mixtures that exhibit a substantial g-sensitivity, and consequently segregation (sedimentation) under 1-g, can be processed only in zero-g. It is of basic importance to define more accurately the conditions under which the segregation rate reaches a critical value, beyond which terrestrial processing is unfeasible.

Both segregation rate and mobility of particles are primarily dependent on the following variables:

- a. Density difference ( $\Delta \rho$ ) of particles and matrix.
- b. Matrix viscosity ( $\mu$ ).
- c. Particle size and configuration (L/D).
- d. g-level and superimposed g-forces during mixing.

The effect of these variables on mobility and segregation rate was evaluated by theoretical analysis and by extensive experimentation as discussed in the following sections.

3.2.5.1 Experimental Investigation of Particle Mobility and g-Sensitivity. In view of the extreme difficulty — if not impossibility — of observing particle motion in liquid metals, all experiments were carried out in transparent liquids and the particle motion recorded by motion picture photography. Transparent matrices provided the additional advantage of a wide range of viscosities that can be easily adjusted to desired values by the concentration of a solution. The selected viscosity range from 1 to 110 centipoise included the range of liquid metal viscosities (1 to 7), providing an exact simulation of the effect of viscosity on liquid metal mixtures. The only liquid metal property that cannot be perfectly simulated with transparent liquids is surface tension. However, according to theoretical evaluations, surface tension plays a subordinate role in the motion of solids, particularly in the case of microspheres or fibers of high L/D ratios as they are of prime interest for practical applications. Surface tension may become more significant only in nonspherical particles and short fibers with an L/D close to unity. For all other parameters, such as matrix viscosity, density difference, and composite geometry, an exact simulation was obtained.

The use of transparent fluids necessitated the exact determination of their significant properties (density, viscosity, surface tension).

For all experiments, 1-g was used as an accelerating force for the following reasons: 1) the use of terrestrial g is convenient and accurate, 2) 1-g is the criterion for the definition of mixture conditions that are not compatible with terrestrial processing, and 3) numerical data for particle mobility at other g-levels can be accurately calculated with the relationships derived from the 1-g experiments and described in Section 3.2.5.1.

As a well-comparable value for mobility and segregation rate the terminal velocity was determined for the following reasons: 1) it is the decisive value for the behavior of mixtures, 2) it can be directly correlated with established fluid dynamics relationships, and 3) it can be measured accurately.

Apparatus. The apparatus used for the transparent matrix experiments is shown schematically in Figure 3-11. It consists of a square lucite sample tube A containing a particle in a constant temperature bath B. The rate of fall is measured by using stopwatch C to determine how long it takes the particle to fall a finite distance measured along millimeter scale D. The thermistor sensor E operating through controller F regulates the bath temperature by activating or deactivating the heater in bath G. The camera H is operated in the single frame mode at specified intervals or continuously to 32 frames per second by means of the power supply I and timer J.

Experimental Materials. Transparent liquids for metal-matrix simulation were selected to provide a wide range of viscosities, densities, and surface tension. The selected liquids and their properties, in the order of increasing viscosity, were:

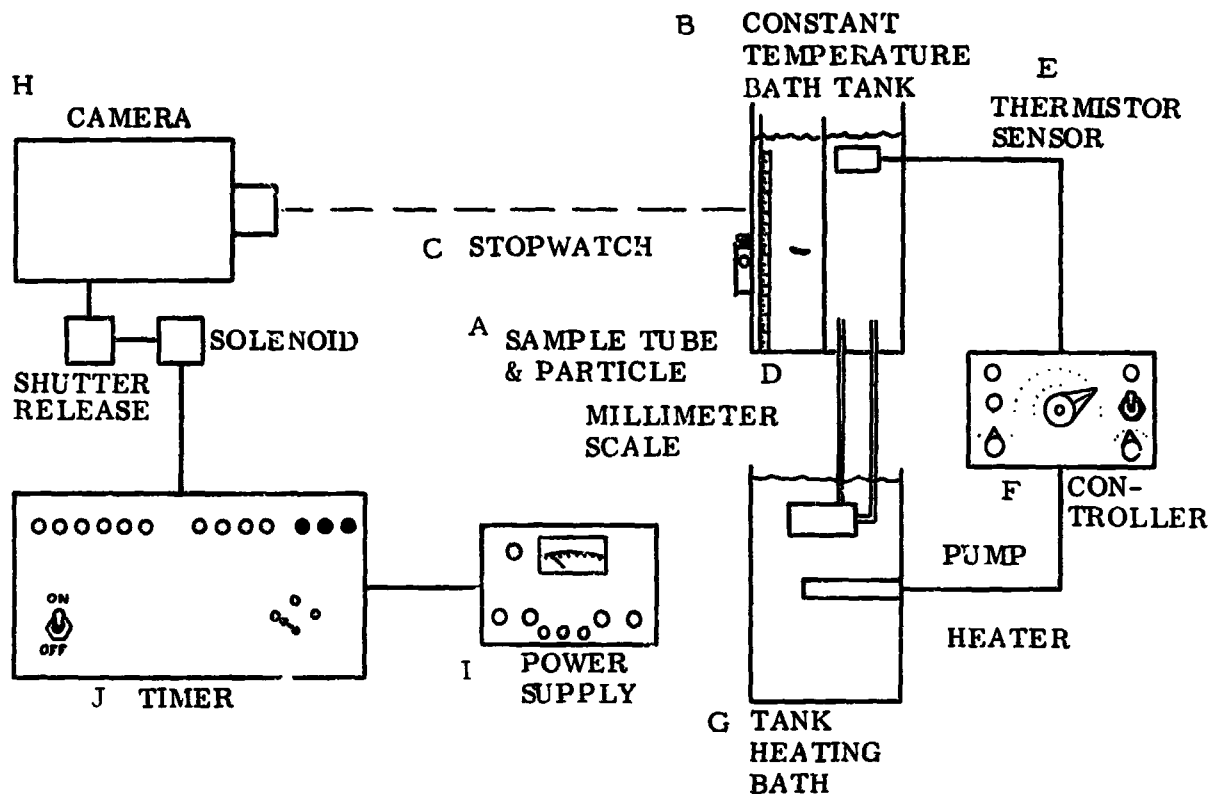


Figure 3-11. Apparatus for Experiment with Transparent Mixtures

	Density (gm/cc)	Viscosity (centipoise)	Surface Tension (dyne/cm)
Distilled Water	1.0	1.0	71.0
Water/25% glycerine	1.07	1.9	69
Water/75% glycerine	1.2	27.5	67
Fluorolube	1.3	37	28
Silicone 200	0.971	110	24

Fibers were selected to provide a wide range of densities. Since practical composites will preferably involve thin fibers, diameters from 0.125 to 0.625 mm were chosen. The slenderness ratio  $L/D$  was varied in increments from 5 to 100. The fiber materials, their densities, and the density difference  $\Delta\rho$  with the experimental liquids were:

Fiber Material	Density (gm/cc)	Density Difference, $\Delta\rho$				
		Water	Glyc. 25%	Glyc. 75%	Fluoro-lube	Silic. 200
Nylon	1.12	0.12	0.05	(-)	(-)	0.15
Boron	2.65	1.65	1.58	1.45	1.35	1.68
Copper	8.9	7.9	7.83	7.7	7.6	7.93
Tungsten	19.3	18.3	18.23	18.1	18.0	18.33

Experiment Performance. Individual experiments were carried out under an accelerating force of 1-g with single fibers of 0.125, 0.250, and 0.625 mm diameter, varying fiber L/D, fiber material, and the liquid matrix. Each experiment represented a discrete combination of fiber configuration, matrix viscosity, and solid/liquid density difference.

Each fiber was carefully released in a horizontal position just below the surface of the liquid matrix. The position of the fiber as it was falling was recorded on 16 mm motion picture film. The films were evaluated in a 16 mm data analyzer and the measurements of position and elapsed time tabulated. From these data, the velocities at small fall increments were calculated and the terminal velocity determined.

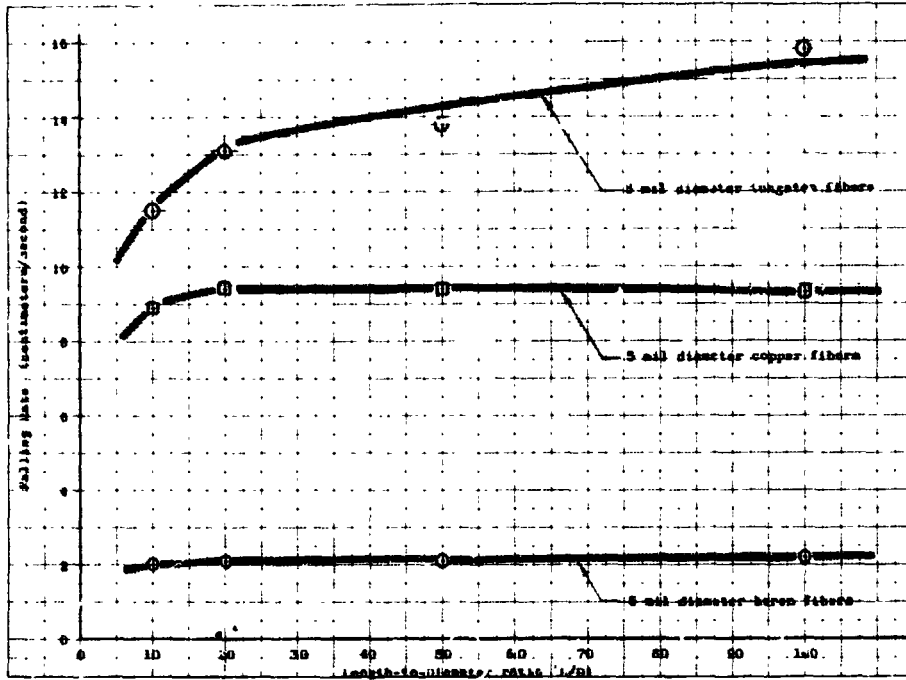
Experiment Results. In Figures 3-12 through 3-14 the measured terminal velocities are plotted against fiber L/D for various fiber materials (levels of  $\Delta\rho$ ). Each plot represents one matrix liquid (one viscosity). It is significant that, in all cases, the terminal velocity levels off at an L/D = 10 and is, for all practical purposes, constant for L/D ratios over 20. Since for random fiber composites only the high L/D regime is of practical interest, the fiber mobility in terms of terminal velocity can be defined by a single value for a given  $\Delta\rho$ , matrix viscosity, and fiber diameter. The experimental data for the large L/D terminal velocities (U) are listed in Table 3-1.

The decline of the terminal velocity in the regime below an L/D of 10 can be readily explained by the increasing significance of the flow conditions at the fiber ends. The lowest value should be encountered with irregular shaped particles. The experiments with the 0.125 mm diameter fibers were, however, not continued in the low L/D regime due to experimental difficulties in preparing, handling and observing such small samples. However, the experiment series with the 0.625 mm diameter fibers permitted coverage of the entire L/D range from 1 to 80. The results, Figure 3-12B, show a decrease from the large L/D value of approximately 50% toward L/D = 1. If particles of L/D = 1 are spherical instead of cylindrical, the flow situation is entirely different and the terminal velocity is expected to be in the order of the large L/D fibers.

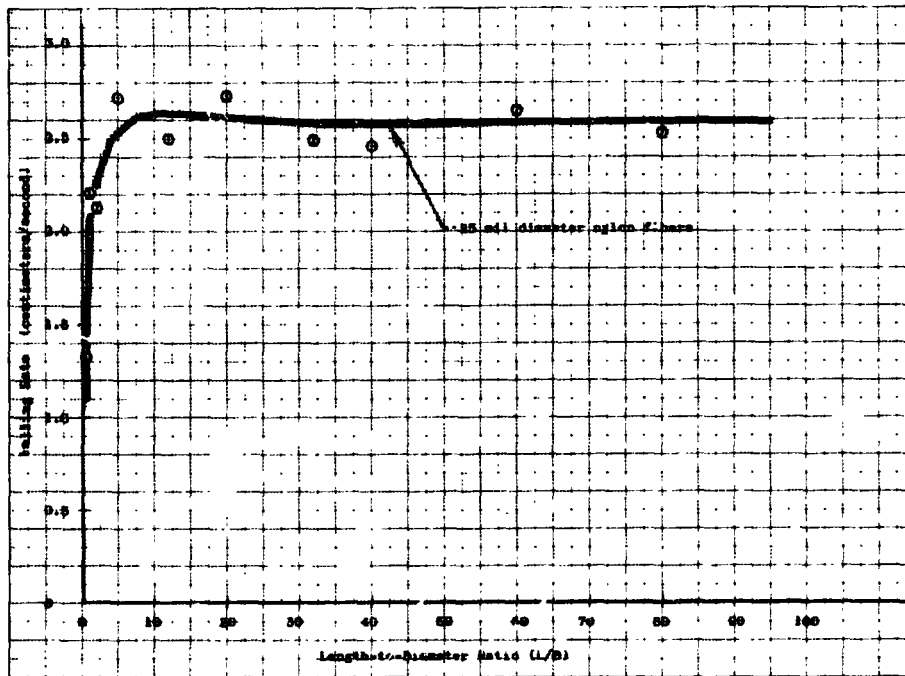
Figure 3-15 shows the relationship between  $\Delta\rho$  and the terminal velocity or segregation rate for various matrix viscosities, as measured on 0.125 mm diameter fibers. The  $\Delta\rho$  range extends from 1 to 20. If we examine the low  $\Delta\rho$  regime in Figure 3-15, it appears that the curves do not point toward zero, as to be expected for  $\Delta\rho = 0$ . Either, there is a change in the characteristic between  $\Delta\rho$  of 0 and 1, or the velocity zero is reached at  $\Delta\rho$  values  $> 0$  for high matrix viscosities.

The effect of matrix viscosity on segregation rate is plotted in Figure 3-16. Of primary interest is the viscosity-range between 1 and 7 (metals) in which the relationship appears to be essentially linear in the log-log plot. However, higher viscosities may be encountered with non-eutectic alloys in which melting covers a certain temperature range with varying viscosity.

REPRODUCIBILITY OF THE ORIGINAL PAGE IS POOR.

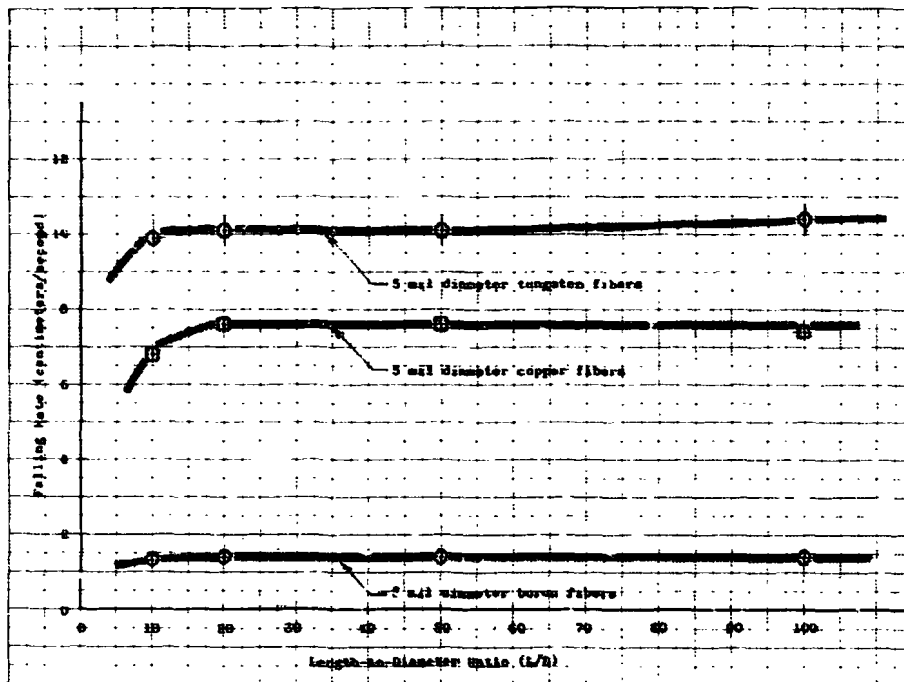


A. Fiber Diameter 0.125 mm

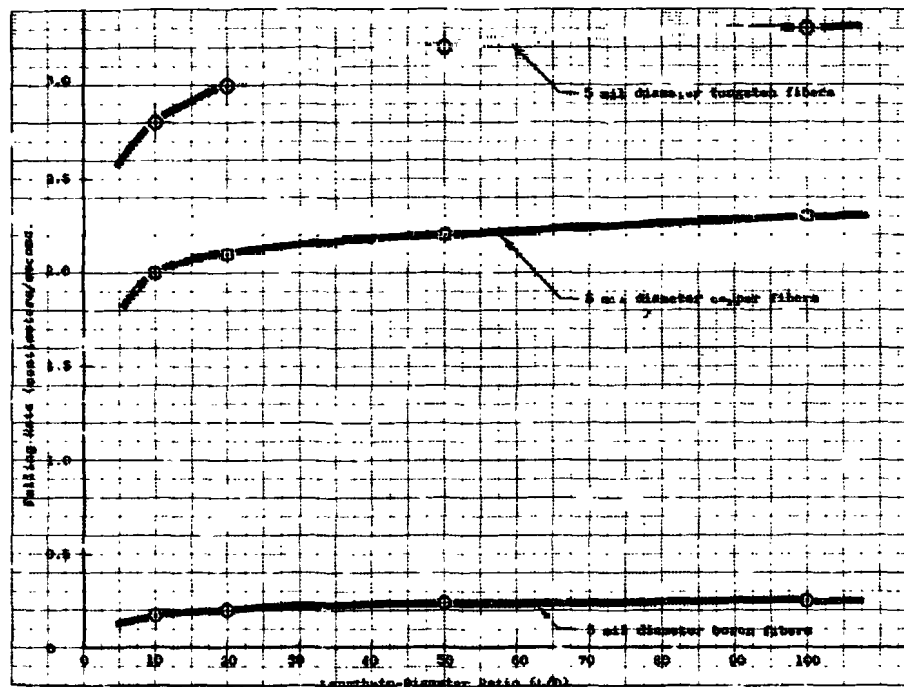


B. Fiber Diameter 0.625 mm

Figure 3-12. Terminal Velocities of Fibers in Distilled Water ( $\mu = 1$ ) Under 1-g

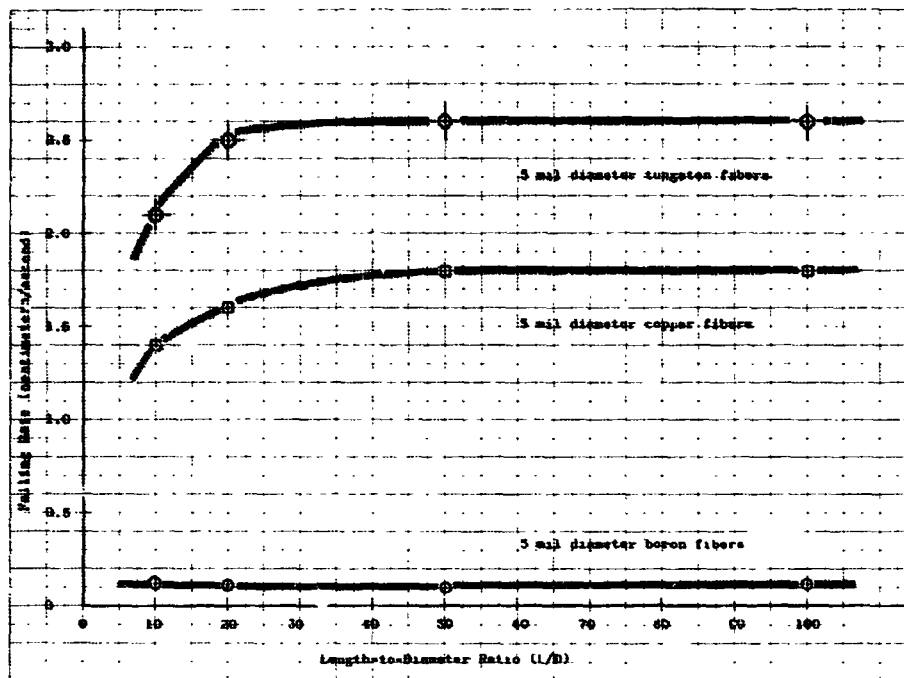


A. 25% Glycerine ( $\mu = 1.3$ )

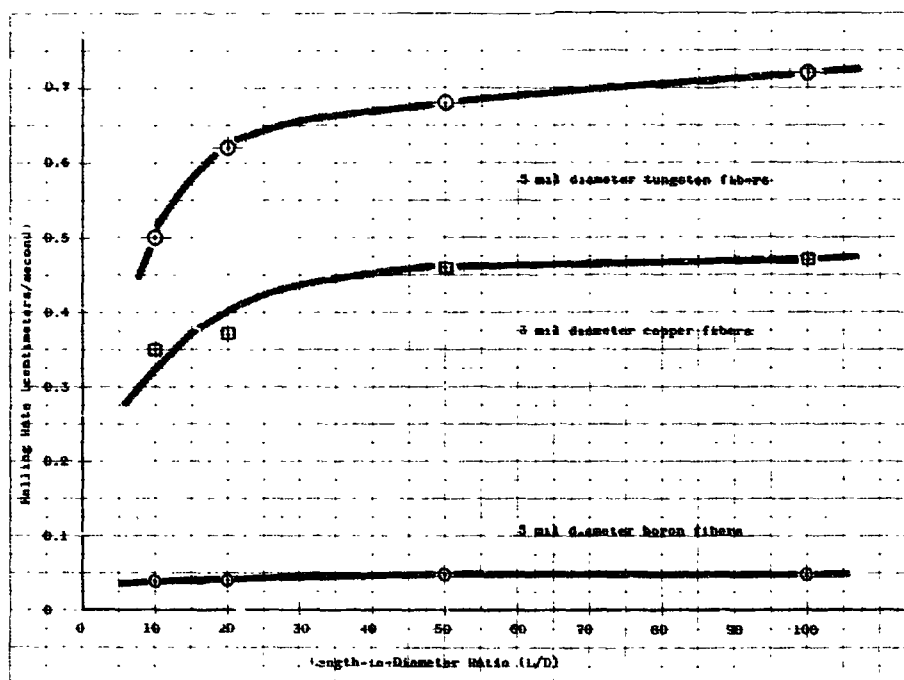


B. 75% Glycerine ( $\mu = 27.5$ )

Figure 3-13. Terminal Velocities of Fibers in Water/Glycerine Solutions Under 1-g



A. Fluorolube ( $\mu = 37$ )



B. Silicone 200 ( $\mu = 110$ )

Figure 3-14. Terminal Velocities of Fibers in High-Viscosity Liquids Under 1-g

Table 3-1. Correlation of Terminal Fiber Sedimentation Rates in Terms of Reynolds Number (Re) and Sedimentation Parameter (N)

Liquid	Fiber	$\rho_s$	$\frac{\rho_s - \rho_l}{\rho_l}$	U, L/D > 10 (cm/sec)	Re	N
Water $\rho_l = 1$ $\mu = 1$	Boron	2.65	1.65	2.1	2.67	31.2
	Copper	8.9	7.9	9.4	12.0	155
	Tungsten	19.3	18.3	13.8	17.5	359
	Nylon	1.12	0.12	0.92	2.34	19.3
Water + 25% Glyc. $\rho_l = 1.07$ $\mu = 1.9$	Boron	2.65	1.48	1.4	1.0	7.53
	Copper	8.9	7.32	7.6	6.0	52.8
	Tungsten	19.3	17.1	10	7.2	103
Water + 75% Glyc. $\rho_l = 1.2$ $\mu = 27.5$	Boron	2.65	1.21	0.24	0.0133	0.0452
	Copper	8.9	5.9	2.2	0.122	0.22
	Tungsten	19.3	15.1	3.2	0.177	0.565
Fluorlube $\rho_l = 1.3$ $\mu = 37$	Boron	2.65	1.04	0.12	0.00535	0.0252
	Copper	8.9	5.85	1.8	0.080	0.141
	Tungsten	19.3	13.9	2.6	0.116	0.335
Silicone Oil $\rho_l = 1$ $\mu = 110$	Boron	2.65	1.65	0.047	0.000543	0.00258
	Copper	8.9	7.9	0.47	0.00543	0.0128
	Tungsten	19.3	18.3	0.72	0.0083	0.0196

All fibers have a diameter of 0.125 mm, except nylon 0.250 mm.

The liquid density  $\rho_l$ , solid density  $\rho_s$ , and liquid dynamic viscosity  $\mu$  are all relative to water.

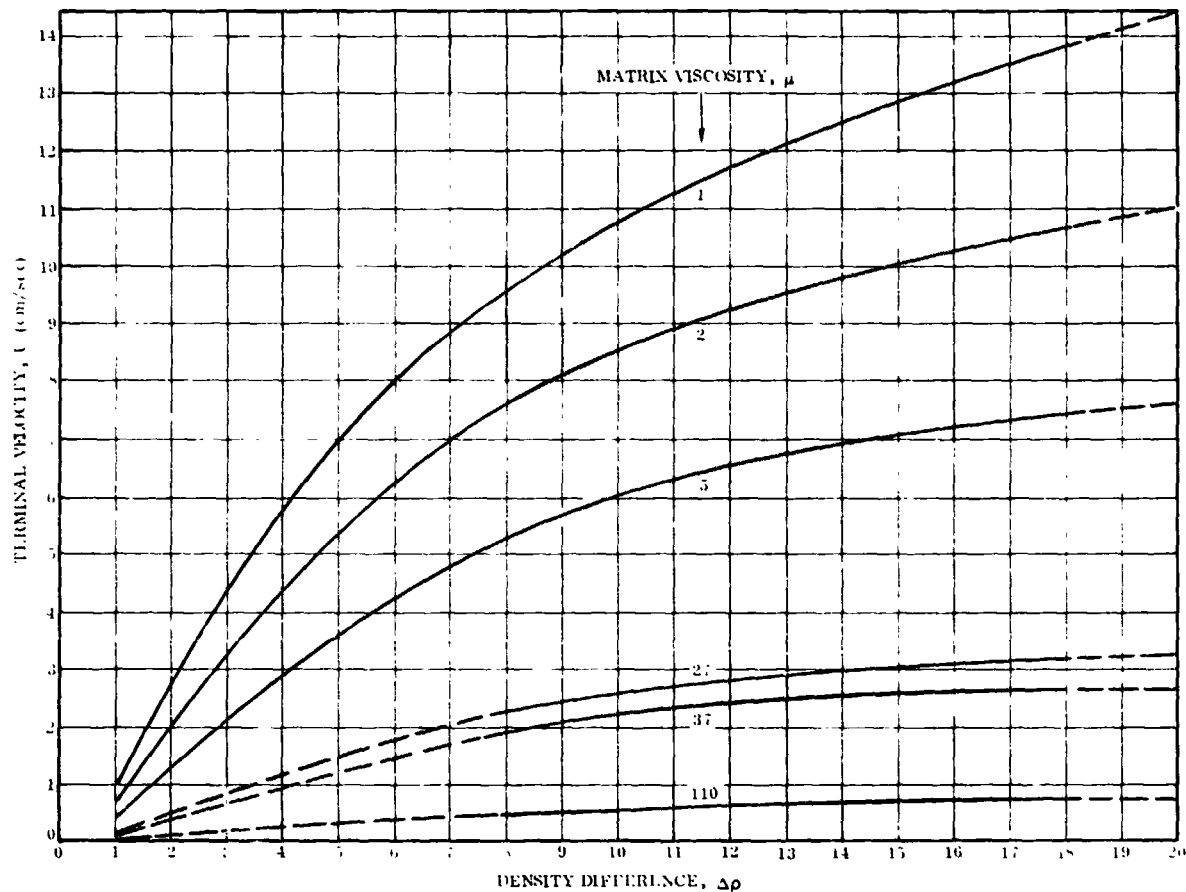


Figure 3-15. Effect of Density Difference,  $\Delta\rho$ , on 1-g Terminal Velocity for Various Matrix Viscosities (large L/D fibers, 0.125 mm diameter)

**3.2.5.2 Theoretical Interpretation of Segregation Experiments.** The experiments indicate that for slenderness ratios larger than approximately 10, the terminal velocity becomes independent of the slenderness ratio (unless the viscosity is very large). In that case the effect of the free end faces on the drag becomes negligible so that the cylinders behave as if they were infinitely long.

The highest Reynolds number,  $Re = UD/\nu$ , observed in the experiments was about 20 so that we are dealing with low-Reynolds number flow. However, in most experiments the Reynolds number was not low enough to justify the use of the Oseen drag relation

$$C_D = \frac{F}{\frac{1}{2} \rho_l U^2 D} = \frac{8\pi}{Re \ln(7.4/Re)}$$

which gives accurate results for Reynolds numbers up to about 0.5 (the formula is exact in the limit  $Re = 0$ ). For those experiments in which  $Re < 0.5$  almost exact results can be obtained for the terminal velocity, using this formula. For higher

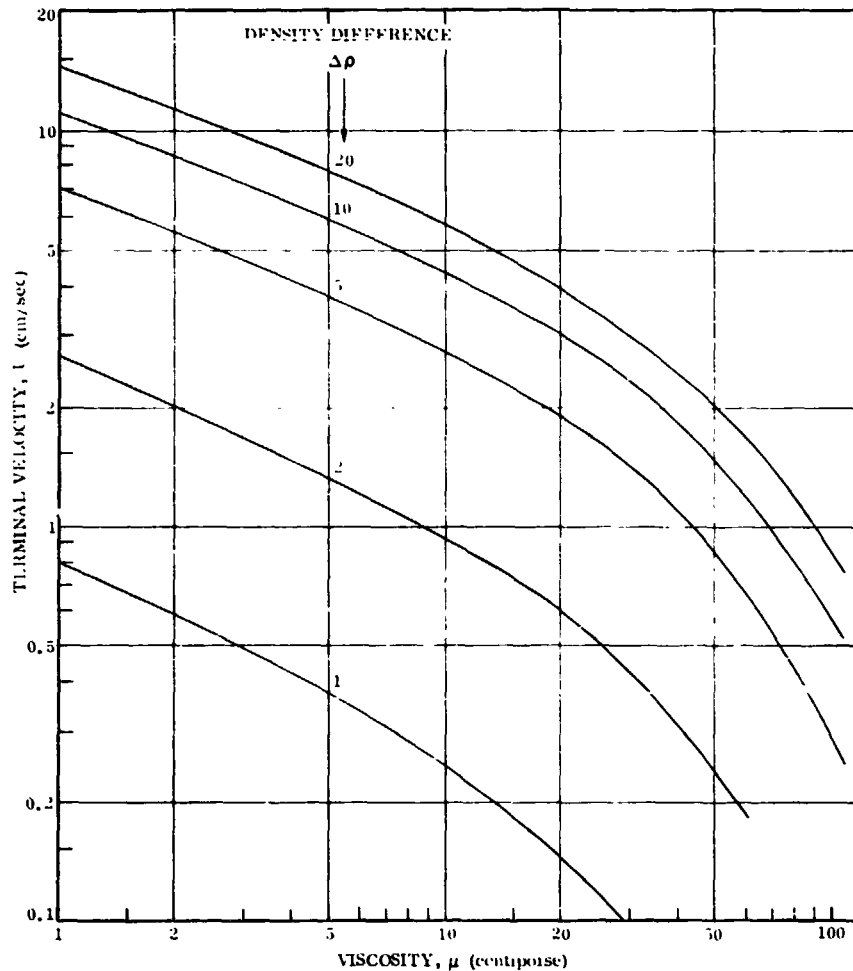


Figure 3-16. Effect of Matrix Viscosity on 1-g Terminal Velocity for Various Levels of  $\rho$  (large  $L/D$  fibers, 0.125 mm diameter)

Reynolds numbers we have developed an empirical formula for the terminal velocity as follows. Experimental drag data for circular cylinders (e. g., G. K. Batchelor, "An Introduction to Fluid Mechanics." Cambr. Univ. Press 1967) indicate that over the range  $0.1 < Re < 30$ , we may write, with good approximation,

$${}^{10}\log C_D = -0.6 {}^{10}\log Re + 1.1$$

or,

$$C_D = 12.6 Re^{-0.6}$$

which yields for the drag force per unit length of the cylinder,

$$F = 6.3 \rho_l U^2 D \left(\frac{UD}{\nu}\right)^{-0.6}$$

Equating the drag force with the difference between weight and buoyancy force, we find

$$\frac{\pi D^2}{4} g (\rho_s - \rho_l) = 6.3 \rho_l U^2 D \left(\frac{UD}{\nu}\right)^{-0.6}$$

so that

$$Re = 0.23 N^{5/7} \quad (1)$$

where

$$N = \frac{\rho_s - \rho_l}{\rho_l} \frac{gD^3}{\nu^2}$$

Thus, all sedimentation experiments in the range  $0.1 < Re < 30$  can be correlated in terms of Eq. 1. This relation is plotted in Figure 3-17 and compared with the experimentally determined sedimentation rates. The agreement is generally satisfactory. The discrepancies are at least partly due to inaccuracies in the viscosity data. In Table 3-1 the experimental data are converted into nondimensional form. The experiments in the highly viscous Fluorolube and Silicone oil have Reynolds numbers below 0.5 and under these conditions nearly exact predictions can be made by means of the Oseen drag relation. The range of Reynolds number presented in Figure 3-17 is the most interesting one from the standpoint of predicting the sedimentation rates in liquid metals. In principle, the functional relationship between  $Re$  and  $N$  could be derived over an arbitrary range of Reynolds numbers, providing a priori information about sedimentation rates of (slender) fibers in all Newtonian liquids. Also, the similarity law

$$Re = \text{function } (N)$$

provides the proper scaling law for the simulation of low-gravity sedimentation on earth. Clearly, the same sedimentation rate is obtained if the ratios

$$\frac{D}{\nu}, \quad \frac{\rho_s - \rho_l}{\rho_l} gD$$

are kept the same.

The correlation also defines the role played by the various relevant parameters in the sedimentation process. For instance, if we double the diameter of the boron fibers in water, the sedimentation parameter  $N$  increases by a factor 8 to 250. According to Figure 3-17, the corresponding Reynolds number is 12, which yields a sedimentation rate 2.25 times as large as the original one.

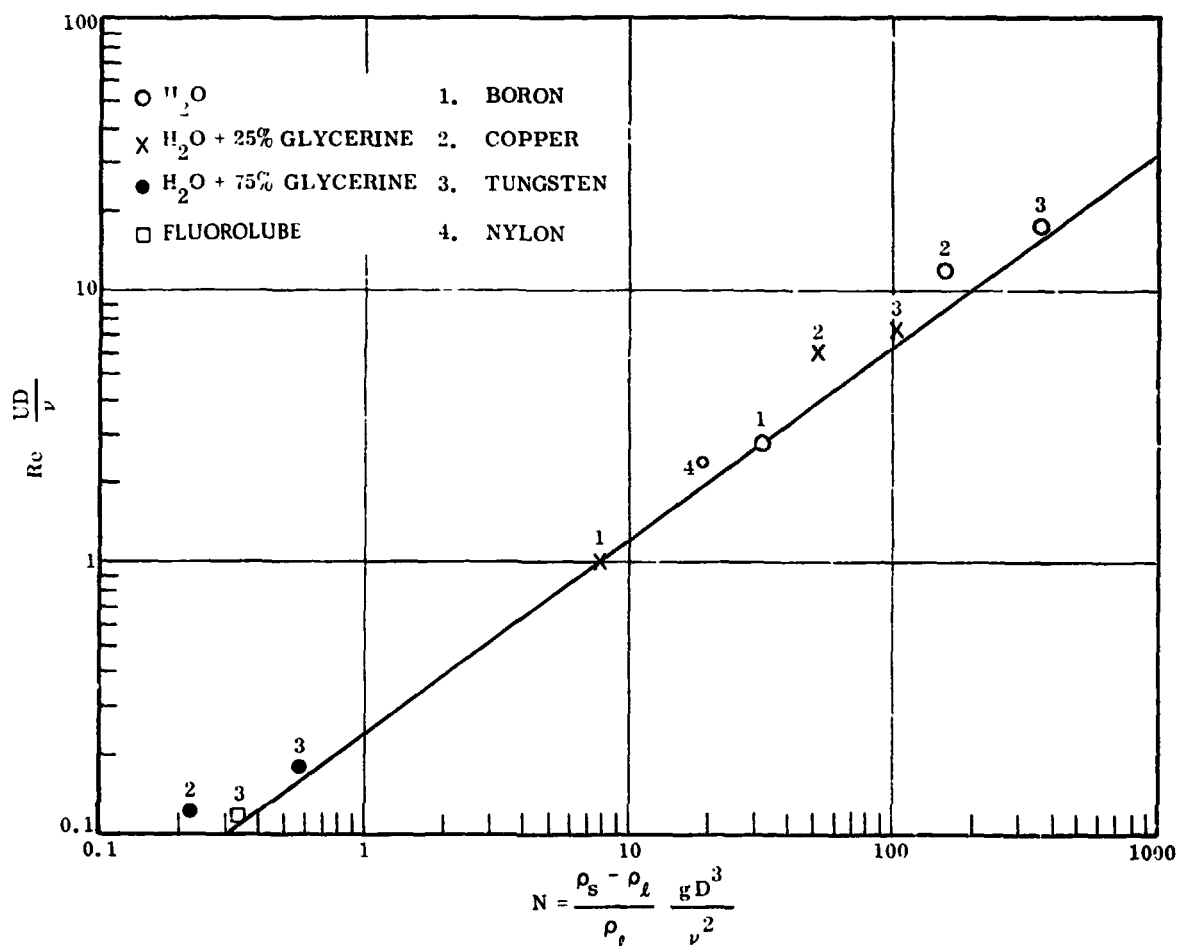


Figure 3-17. Sedimentation Reynolds Number Versus Sedimentation Parameter N

The relationship of Eq. 1 and Figure 3-17 further permits a translation of the terminal velocities obtained experimentally for 1g to other g-levels. In Figure 3-18 the correlation between g and segregation rate is plotted in dimensionless terms, using the parameter  $U/U_{1-g}$  (ratio of velocity at any given g-level to the velocity at 1g) for the g-range of 1.0 to  $10^{-4}$ .

By means of this relationship, numerical values for lower g-levels were calculated for the experimental data of Section 3.2.5.1. A final summary chart is presented in Figure 3-19, correlating terminal velocity,  $\Delta\rho$ , matrix viscosity, and g-level. As all data discussed in this section, the summary chart applies only to large L/D fibers of 0.125 mm diameter. However, by means of the established relationships, data for other fiber diameters can be calculated with adequate accuracy.

The correlation of experimental data on short fibers would bring in the slenderness ratio as a new variable. For the time being, we have not attempted such a correlation since at present the primary practical interest is in fibers with slenderness ratio roughly between 20 and 50.

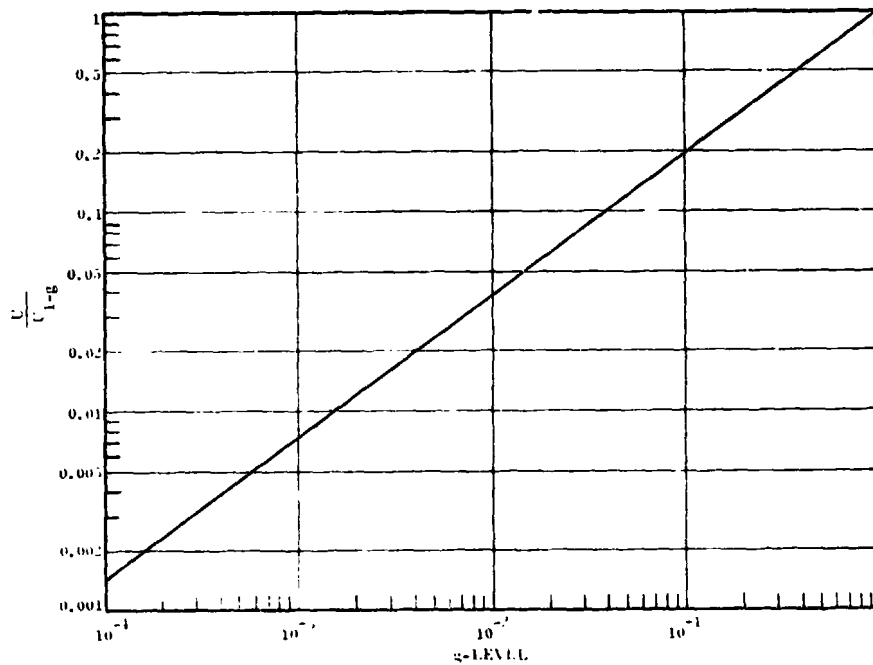


Figure 3-18. Dimensionless Correlation of g-Level and Terminal Velocity for Large L/D Cylindrical Reinforcements (terminal velocity at 1-g = 1.0)

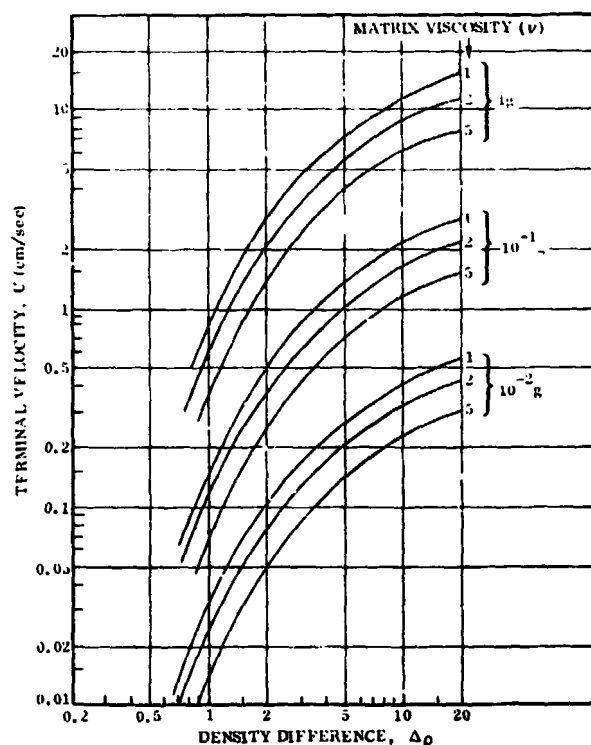


Figure 3-19. Relationship of Terminal Velocity to Density Difference for the Viscosity Regime of Liquid Metals and Various g-Levels (large L/D fibers, 0.125 mm diameter)

**3.2.6 GEOMETRIC REINFORCEMENT CONTENT LIMITATIONS.** Another important parameter of random composites is the maximum possible reinforcement content. The maximum content is defined by a distribution geometry at which all particles are in mutual contact. It depends primarily on the configuration of the individual reinforcement particle and the resulting geometry of the reinforcement distribution. It depends further on the container size and configuration. The variety of possible container sizes and configurations has, for the purpose of this investigation, been reduced to two basic conditions: 1) a semi-infinite container where the wall effects can be neglected, and 2) a finite cylindrical container. For 1) it was attempted to obtain dimensionless values by introducing the parameter  $C/L$  of container diameter to maximum reinforcement length.

**3.2.6.1 Semi-Infinite Container.** For the semi-infinite container the distribution geometry is defined by the reinforcement configuration only, while the absolute reinforcement size is of no significance. The maximum content for spherical particles at maximum-density packing is well known to be 74%, representing the ideal geometry that is never reached in practical mixtures. The maximum content is further reduced if the particles are nonspherical, even though they may also be classified as  $L/D = 1$ . As to be expected, the maximum particle contents depend extensively on the particle configuration. The following content maxima were measured for spherical and odd-shaped particles:

<u>Particle Type</u>	<u>Maximum Particle Content (Vol %)</u>	
	<u>As-Mixed</u>	<u>Densified</u>
Spherical	60	67
Polyhedral	52	60
Granules	49	57

As-mixed refers to "soft settling" of particles under 1-g from an agitated mixture in a container at rest (minimum, yet complete interparticle contact). The densified condition was obtained by vibrating the container after settling.

For cylindrical reinforcements (fibers), the content maxima are related to the  $L/D$ . For the experimental determination of maximum fiber content, the following procedure was adopted. Fibers of a given  $L/D$  were thoroughly mixed with a low-viscosity liquid in containers with a  $C/L$  between 5 and 25, which can, for all practical purposes, be considered as semi-infinite. The cylindrical container was then put at rest in a vertical position, allowing the fibers to settle under 1-g. The height of the settled mixture was measured and the volumetric fiber content determined. The following variables were applied:

- a. Fiber  $L/D$ .

- b. Fiber material density.
- c. Original mixture content (loading factor).

The original percentage of fibers added to the liquid (c) was varied to obtain various degrees of fiber mobility or crowding during mixing. Two fiber materials (b) were used: copper and nylon, representing a  $\Delta\rho$  of 7.9 and 0.12. The purpose of this variation was to obtain different degrees of random orientation. It is apparent that under the test condition of the unidirectional 1-g the random orientation, typical to zero-g, is not achieved. The heavier copper fibers attempt to orient themselves perpendicular to the g-force, resulting in higher bulk densities. The small  $\Delta\rho$  of the nylon fibers, representing almost neutral buoyancy, produces a much higher degree of randomness. According to the relationships established in Section 3.2.5.2, the behavior of the nylon fibers at 1-g is equivalent to copper fibers at approximately  $10^{-4}$  g. The distribution obtained with the nylon fibers represents, therefore, a close approximation to the zero-g condition.

The results of the fiber and particle experiments for the semi-infinite container are presented in Figure 3-20. As to be expected, there is a sharp increase of bulk density below an L/D of 20, approaching at L/D below 5 the values for spherical and odd-shaped particles. At L/D values over 30, of prime interest for fiber-reinforced composites, the bulk density is essentially constant.

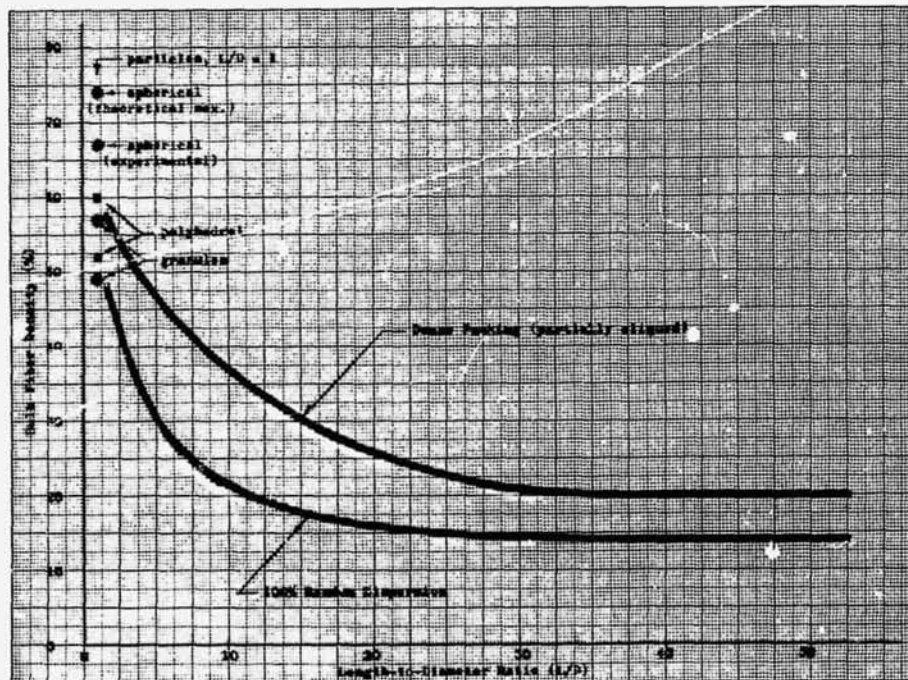


Figure 3-20. Maximum Volume Fraction of Random Dispersed Fibers and Particles (semi-infinite container,  $C/L \approx \infty$ )

On the basis of these experimental data, the maximum possible contents for random-fiber-reinforced composites can be defined as:

Fiber L/D	5	10	20	30	
a. Partially aligned	47	37	26	20	vol %
b. Random orientation	30	21	16	14	vol %
c. Mixing mobility	26	16	12	10	vol %

The maximum contents at which there is sufficient fiber mobility for mixing (c) are estimated values.

**3.2.6.2 Effect of Container Size.** For most random composites, the maxima for the semi-infinite container are valid, since emphasis is on small fiber diameters and fiber lengths below 5 mm. There are, however, three cases where container size constraints have to be taken in consideration: 1) small sample capsules, as they may be necessary in early zero-g experiments, 2) thin-wall castings, and 3) fibers over 5 mm length.

In view of the expected container size limitations in early zero-g experiments in the drop tower, KC-135, and in research rockets, the problem was considered important enough to be explored experimentally. Experiments were carried out as described in the foregoing Section 3.2.6.1, except that the container size was varied over a C/L range from 1 to 5. It was expected that a clear relationship between fiber L/D, C/L, and the resulting maximum contents would evolve. Unexpectedly, this was not the case. Extensive discrepancies between experiments with various fiber materials ( $\Delta\rho$ ) and matrix viscosities were encountered some of which are, at this point, still unresolved. Such discrepancies were expected in approaching a C/L of 1 where random distribution is no longer possible. However, irregular values were also obtained at higher values of C/L, and extensive efforts were expended to find an explanation for these discrepancies in the attempt to arrive at a fair correlation.

The best results to date are shown in Figure 3-21, obtained with copper fibers, representing a high  $\Delta\rho$  and 1-g conditions, and with nylon fibers whose low  $\Delta\rho(0.1)$  can be considered a close simulation of low-g conditions. As to be expected, the maximum content decreases at low values of C/L. For fiber L/D values over 10, the conditions of the semi-infinite container are reached at a C/L of 4. This is not the case with fibers of lower L/D, where the content continues to increase at C/L values beyond 4.

In the C/L region below 2, conditions are unpredictable due to the strong wall effect. As indicated by the values obtained in another experiment series (dotted curves), the maximum content at C/L of 1 may either be a minimum, or suddenly rise to very

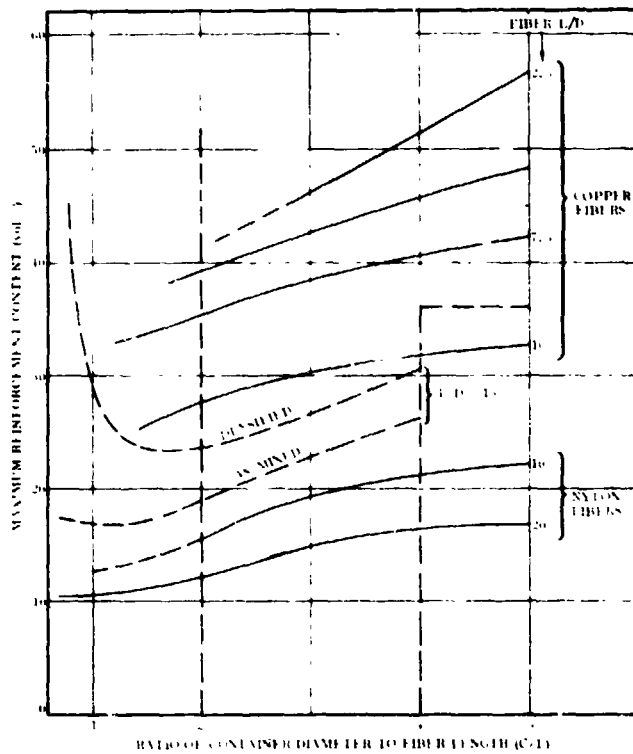


Figure 3-21. Effect of Container Size on Maximum Fiber Content

high values, resulting from extensive fiber alignment parallel with the container wall. The widely varying data obtained in this regime can be explained by the fact that the wall-alignment is not solely of a mechanical nature, but also the result of interface effects, which, in turn, vary with the matrix-fiber material combination as discussed in Section 3.2.4.1.

The almost linear, but extended dependency of the content upon  $C/L$  for the fibers with a  $L/D$  of 2.5 can be explained, in part, by the reduced alignment effect, approaching the conditions of  $L/D = 1$  particles where alignment effects are negligible.

In Figure 3-21 we may delineate two regimes of usefulness: 1) a fairly reliable regime, comprising  $L/D$ 's of 10 and more for  $C/L$  above 3, and 2) all other data above  $C/L = 2$ , which may be tentatively adopted as guide values for composite experiments. The extensive efforts required for further exploration of the regime below  $C/L = 2$  appear unjustified, since they are of little practical value. Most zero-g experiment conditions fall into the reliable regime 1).

**3.2.7 PREDICTION OF COMPOSITE PROPERTIES.** In view of the preclusive reinforcement segregation encountered in terrestrial casting of composites, they are presently fabricated by hot pressing, cold pressing, and sintering, or by infiltration. These methods permit alignment of the fibrous reinforcements to increase the packing density and orient them for the maximum strengthening and stiffening effect in one direction (at the expense of strengthening in the other directions).

Alignment of fibers in zero-g casting is not feasible due to turbulence in the mold. Magnetic or electrostatic alignment techniques would be ineffective in a metal matrix. The cast reinforcements would therefore be randomly dispersed and the strength of the composite would be far less than the "aligned" strength and elastic modulus would be in the 0° direction, but the properties would be isotropic and property increases could be attained in all directions.

3.2.7.1 Properties Attainable with High L/D Fibers. The amount of strengthening and stiffening attained in unidirectional composites depends on the volume of fibers or whiskers added and may approximate to a rule of mixtures (Figure 3-22).

Factors having a strong influence on the composite strengthening include:

- a. Strength of the fibers.
- b. Volume and distribution of fibers.
- c. Orientation of fibers.
- d. L/D ratio of fibers.
- e. Bond strength with solidified matrix.
- f. Strength and ductility of solidified matrix.

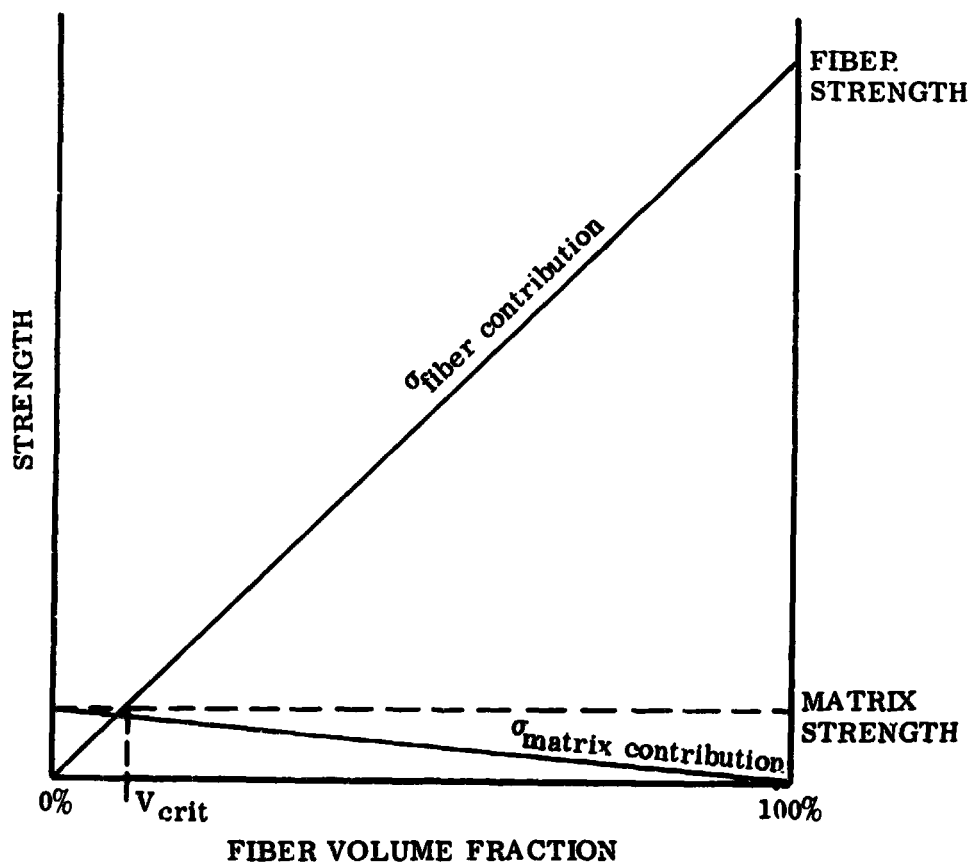
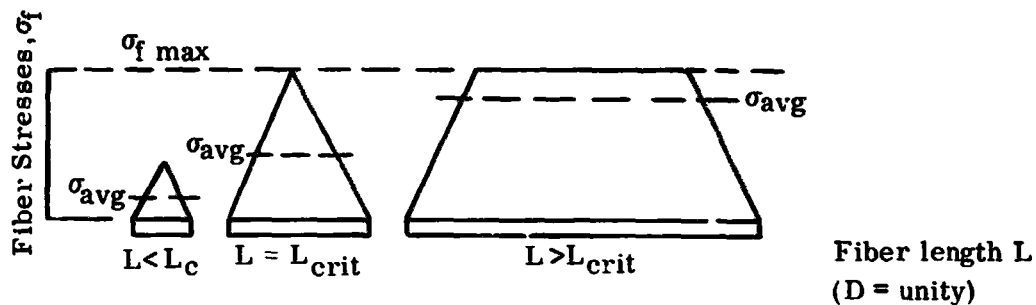


Figure 3-22. Strengthening in Unidirectional Composites

A number of these factors are dependent on other phenomena such as compatibility, preparation techniques, use of coatings, and test temperatures. Figure 3-22 assumes good alignment and bonding and is intended primarily for the large continuous reinforcements such as boron or silica where the filaments are well spaced and little interaction in the form of dispersion strengthening takes place. The initial decline in strength does apply both to filaments and fibers because the few fibers added are insufficient to sustain the loads transferred; consequently, they break prematurely and the remaining matrix is left with the equivalent of a hole. Eventually sufficient fibers can be added (above  $V_{crit}$ ) to take their share of the load and produce a strengthening effect on the matrix. For  $\text{SiO}_2$  reinforced Al,  $V_{crit}$  is of the order of 4 vol %, and about 0.7 vol % for  $\text{Al}_2\text{O}_3$  whisker reinforced aluminum, and can be determined both experimentally and by analysis. Aligning the filaments all in one direction ( $0^\circ$ ) provides a manyfold increase in strength in that direction at high volume fractions, but the strength in other directions can be as low or maybe lower than the bulk matrix strength. Reorienting some of the aligned filaments to improve for instance the transverse strength lowers the strength in the  $0^\circ$  direction until at a completely random orientation the strength of the composite is about 18% (in all directions) of the  $0^\circ$  UD strength for a given filament volume fraction. Discontinuous fibers behave similarly to the continuous filaments but for any given volume fraction the amount of strengthening is less. Stress concentrations at the end of each fiber reduce the strength of the composite. Using fibers with L/D ratios much greater than the critical L/D (see Figure 3-23) for the system will improve the situation (strength increases with increasing L/D up to a limiting point) but will still remain less than for comparable continuous reinforcements. The limiting point is proportional to the ratio of the fiber and matrix moduli. For B/Al this ratio is 6 and the maximum strength of long discontinuous boron filaments is about 80% of the continuously reinforced composite. When the ratio increases to 120 as with boron/epoxy the limiting factor is about 0.55 (5%).

The results of Section 3.2.6 show that the amount of reinforcement that can be added to a molten alloy and still remain sufficiently fluid for casting is dependent primarily on the L/D ratio of the reinforcement. The practical limit for particles (L/D = 1) of 52 vol % falls rapidly to 16 vol % at an L/D of 20 and to 14% at L/D's of 40 or more. (See Figure 3-20.) Above these limits, 'log-jamming' of the fibers occurs. For effective reinforcing by whiskers, L/D's of 100 or more are required and L/D's of over 1000 are commonly available with some materials.  $L/D_{crit}$  increases as the strength of the fiber increases or as the bond strength or matrix shear strength is reduced — perhaps as the temperature is increased.

**3.2.7.2 Properties Attainable with Short Fibers and/or Particles.** Because of the severely limited volume fractions and random orientation of the discontinuous fibers, only modest increases in ultimate tensile strengthening can be expected in large-L/D fiber composites. Although ultimate tensile strength (UTS) is usually the inferred property of consequence where whisker reinforcements are discussed, there are other properties that could benefit significantly from whisker reinforcement. An even more



$$L/D_{crit} = \frac{\sigma_{\text{fiber (max)}}}{2\tau} \quad \tau = \text{matrix shear strength / bond strength at failure strain}$$

For SiC whisker  $\sigma = 2 \text{ mpsi}$  in Al  $\tau = 2 \times 10^3 \text{ psi}$

for  $[\sigma = 1 \text{ mpsi} \quad \tau = 5 \times 10^3 \text{ psi}]$

$$L/D_{crit} = 500 \quad [100]$$

Figure 3-23. Calculation of  $L/D_{crit}$  (Minimum  $L/D$  for Strengthening)

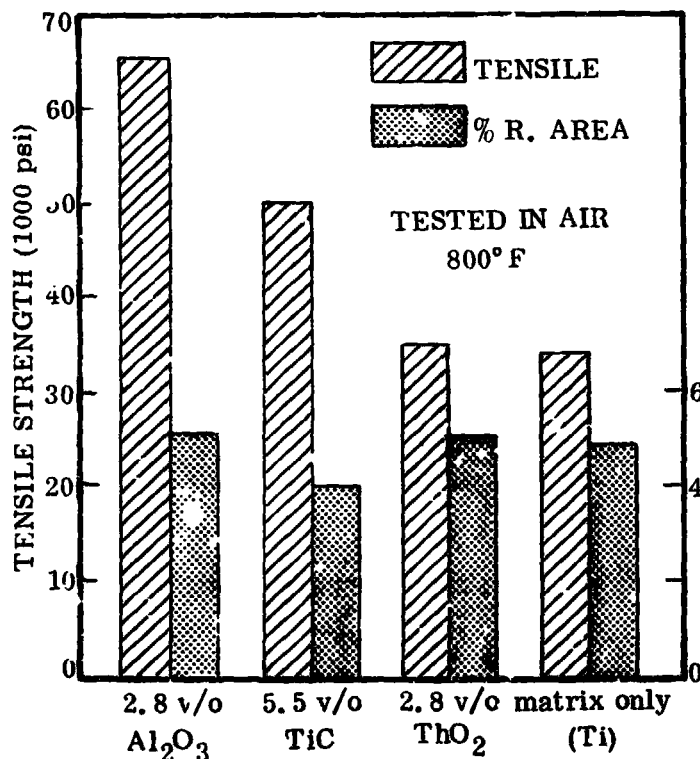
promising aspect is that these properties need not depend on the very high  $L/D$  whiskers normally acquired to increase the UTS. By using shorter and perhaps cheaper whiskers, higher volume fractions could be incorporated. Properties that are likely to be improved by a larger volume of shorter whiskers rather than a few long, high-strength whiskers are yield strength, the elastic moduli, shear strength, stress rupture, and fatigue and creep resistance.

The effect of short whiskers on some properties has been demonstrated by Mitron R&D Corp, which showed strengthening of Al castings with as little as 0.043% of whisker reinforcements. The most significant increase is the doubling of the as-cast yield strength; the UTS is improved by 25 to 30% and the elongation increased in some cases, decreased in others. An analysis of the available data shows that most of the fibers are below the critical  $L/D$  ratio. Some  $L/D$ 's are 10 or lower; consequently, the observed strengthening is almost certainly not solely due to the high strength of the whiskers. Calculations of peak loads in the centers of typical whiskers are of the order of 150 ksi compared to their ultimate strengths of 2 to 5 mpsi. The property improvements are typical of grain refinement and dispersion strengthening.

Micrographs of the control samples were not available for comparison, but the presence of fibers as nuclei tends to reduce the grain size. The resulting improvement of mechanical properties is further amplified by a bridging effect of the whiskers across two or more grains which is quite pronounced in random dispersion. This "zippering" effect is very likely also responsible for the increased ductility, observed in some cases.

During loading, dislocations pile-up at the grain boundaries, leading to microcracks. In non-reinforced alloys, these microcracks propagate to cause failure; in random reinforced metals, the whiskers act as crack stoppers and transfer the load to adjacent grains which, in turn, deform and cause other microcracks. Since more grains are involved, the load as well as the microcracks are more evenly distributed and the plastic deformation capability of the bulk material is increased, resulting in higher elongation.

Although more particles can be added to a melt than whiskers, the relative or combined strengthening efficiencies of whiskers and particles are not known, and smaller quantities of whiskers may be as effective and more desirable. A case in point is whisker-reinforced aluminum. The microstructures of whisker-reinforced Al castings show a tendency of whisker agglomeration at the grain boundaries and segregation into the intergranular matrix. This result is to be expected, particularly for nonwetting whiskers in view of the presumably different wetting contact angles of the grain and the intergranular material, representing the condition of a two-fluid system (Section 3.2.4). This condition would prevent grain boundary sliding and would lead to a significant improvement of creep strength at elevated temperatures. The properties are expected to be further improved by the simultaneous dispersion of particles. Increases in strength from particle dispersions are usually accompanied by reductions in ductility. There are however, exceptions and Figure 3-24 shows that some improvements in ductility due to the addition of particles can be achieved in favorable cases. (Reduction of area values are used as measure of ductility.) Thus the property improvements of the Mitron alloys, which contain a certain amount of particle-like short whiskers, are not unique to whisker reinforcements, nor are they solely attributable to the high strength of the whiskers. They do show, however, that significant improvements can be attained with very small quantities of whiskers, regardless of the strengthening effect. These properties can be expected to improve further as the reinforcement additions are increased (up to 20 vol. % for L/D = 10 whiskers or up to 60 vol. % for particles).



Ref.: Jech, R. W., Schwoppe, A. D. and Weber, E. P., "The Development of SAP-Type Structures in Titanium" in "High Temperature Materials" edited by Hehemann, E. and Ault, M., 1957, pp. 332-341.

Figure 3-24. Dispersion Strengthening of Titanium

Attempts to modify the microstructure could lead to widening the applications of random composites and tailoring the properties to specific needs. Concurrently, the development of coatings to improve whisker stability in high-melting-point matrices should proceed to extend the range of materials for selection.

Stress-rupture properties have been found to increase significantly with fiber reinforcements of higher L/D ratios. In the case of unidirectional fibers, an increase of life up to 20% has been obtained with 20 vol. % and an L/D of only 8. At random fiber distribution the improvement is undoubtedly less, yet isotropic; this may, at least in part, be offset by the simultaneous dispersion of particles whose favorable effect on rupture life is well established.

To further define the capabilities of whisker/particle reinforced metals especially at elevated temperatures, which is the most promising regime of these zero-g fabricated materials, additional work should be performed.

If whiskers are proved superior to particles as reinforcements then improved versions of materials such as thoria-dispersed nickel appear possible as illustrated. Unfortunately the incorporation of whiskers in most useful molten matrices presents severe problems. Only Al castings have been successfully reinforced so far. The other structurally useful metals are Fe, Ni, Co, Ti, Cr, and they all have melting points over 1450° C. Candidate whisker reinforcements are SiC, Si<sub>3</sub>N<sub>4</sub>, Al<sub>2</sub>O<sub>3</sub>, C, BN (and B). A literature survey shows that these materials react and may be destroyed at temperatures as low as 900 to 1000° C, well below the melting points of the matrices. Coatings would provide an answer to this problem but no suitable coatings are known. Duplex coatings would undoubtedly be necessary, one as a barrier, the other to provide wetting. The potential for strengthening or stabilization is there, but the exploitation of these composites must await the development of these coatings. Work can proceed, however, on model systems and on matrices with melting points up to those of Al and Mg. The elevated temperature properties of Al have been improved in the form of sintered aluminum powder (S. A. P.). If it can be demonstrated that limited quantities of whiskers are significantly superior to the flake Al<sub>2</sub>O<sub>3</sub> presently used, and that casting is superior to the powder metallurgy techniques used with S. A. P., then this is one of the applications for zero-g composite fabrication that should be actively pursued. Extending the high-temperature capability of aluminum a few hundred degrees would enable it to replace titanium in many areas, and space processing would be economically justifiable.

Areas of interest are 1) the relative reinforcing efficiencies of whiskers (or fibers) and particles, 2) the extent of the zippering effect, characteristic of fibers, and 3) the relative changes in properties as the volume fractions are increased to their practical limits. Mixtures of whiskers and particles may prove to be complementary and help overcome the volume fraction limitations of random dispersion.

The expected combinations of properties attainable in various fiber, whisker and particle reinforced composites are summarized in Table 3-2. The purpose of this chart is to convey an overview of the expected property improvements and to identify the most promising composite types for specific property combinations as required for specific applications. It indicates that the most attractive overall combination of properties can be expected in a mixture of whiskers and particles.

In all efficiency assessments, one should not lose sight of the advantages of the isotropy of properties and the product castability which can be achieved only in zero-g processing.

**Conclusions.** The prime advantage of random fiber and whisker reinforced composites is the resulting isotropy of properties. The absolute gain in ultimate tensile strength is, according to the present state of knowledge, modest. Conclusive data can only be obtained in zero-g processing experiments, which require a minimum zero- or low-g time in the order of 5 minutes.

Table 3-2. Expected Improvements Over Matrix Properties of Fiber and Particle Composites

Composite Property	Type of Random Reinforcement						
	High L/D Whiskers (L/D ~ 1000)	Low L/D Whiskers (L/D ~ 10)	High L/D Filaments (L/D ~ 300)	Low L/D Filaments (L/D ~ 10)	Particles (L/D ~ 1)	Mixture of High Low L/D Whiskers	Mixture of Particles and Whiskers
Ultimate Tensile Strength*							
Yield Strength							
Elastic Modulus							
Creep/Stress Rupture							
Fatigue Resistance							
Ductility							
Priority	5	3	5	4	2	2	1

\*Torsion, compression and bending strength should follow similar trend.

Legend: The black fraction of each circle identifies the expected degree of property improvement, except for ductility where it represents the absolute magnitude. "Priority": 1 = most, 5 = least effective overall combination of properties.

3.2.8 MATERIALS INVESTIGATIONS. Matrix materials for this study were selected on the basis of their practical applications potential. They comprise Al, Mg, Ni, Co, Fe, Cr, Ti, and some of their alloys. The selection of reinforcement materials was governed by their mechanical properties and their availability. The most attractive reinforcements are whiskers of  $Al_2O_3$ , SiC,  $Si_3N_4$  and BN, graphite fibers, chopped boron filaments, and chopped tungsten wire.

The definition of promising composite systems is a matter of compatibility between matrix and reinforcement materials that has to be assessed individually for each material combination. For a given matrix metal, the effectiveness and usefulness of each reinforcement material has to be evaluated step-wise as illustrated in Figure 3-25.

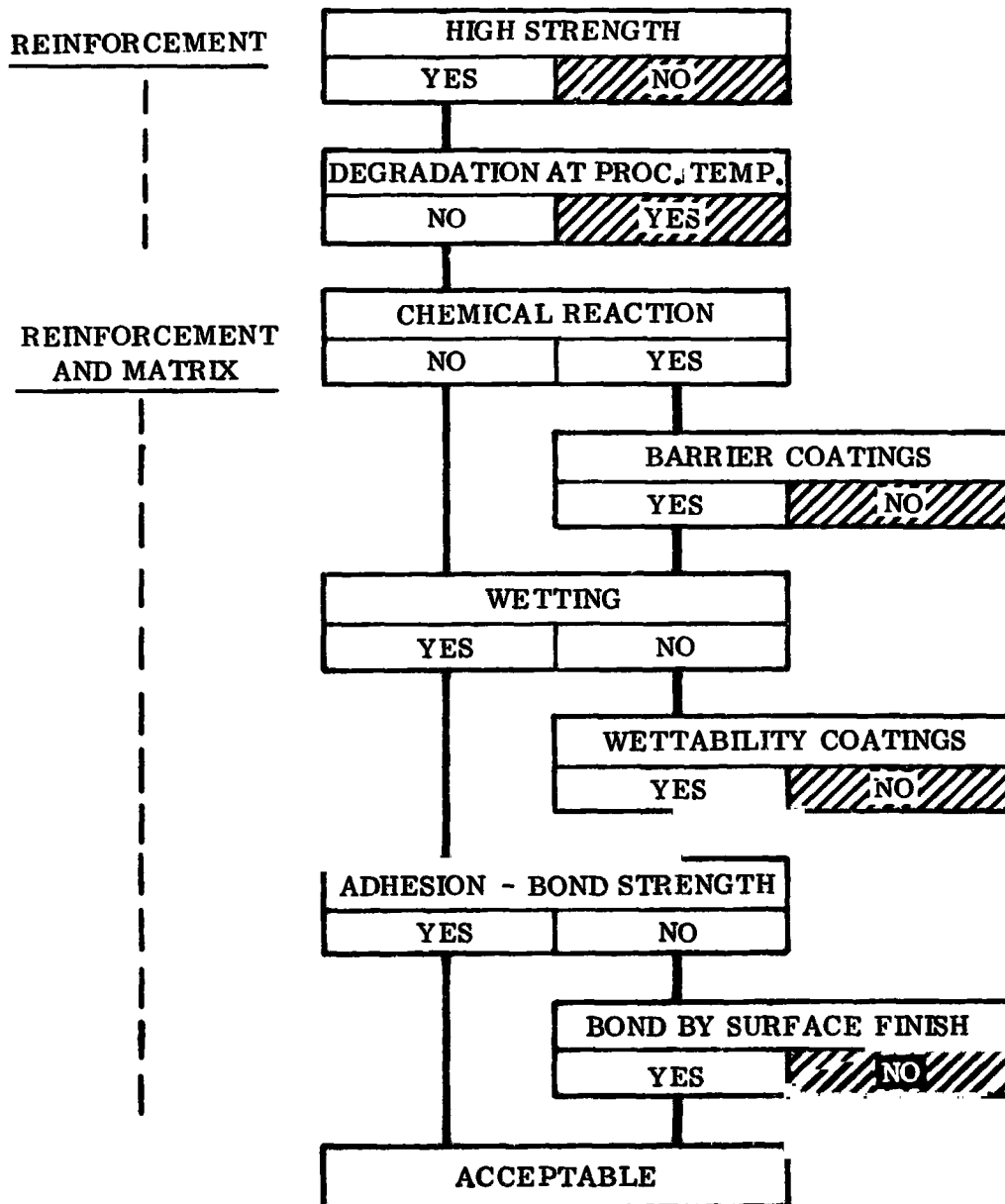


Figure 3-25. Evaluation Sequence for Reinforcements

The primary criteria for reinforcement selection, in order of stepwise evaluation, are:

1. High strength.
2. Temperature stability, i. e. , no appreciable degradation of the strength at the melting temperature of the concerned matrix.
3. Chemical compatibility or the feasibility of barrier coatings to suppress chemical reaction.
4. Wettability, in the feasibility of coatings to activate wettability.
5. High adhesion and bond strength after solidification.

For a specific matrix only those reinforcements are promising that meet all these requirements.

The conclusive evaluation of each of these parameters for each combination of matrix and reinforcement materials represents theoretical studies and laboratory investigations of substantial magnitude. The wide scope and the limited efforts of this study permitted, therefore, only exploratory studies and laboratory experiments. The results of these exploratory investigations are summarized in Table 3-3, which identifies the degree of compatibility between the selected candidate materials as well as the compatibility problems to be resolved.

The net result of all materials studies and laboratory investigations may be summarized as follows:

- a. All mechanically effective reinforcement materials are nonwetting with regard to all candidate matrix metals. Coatings to achieve wettability have to be developed for each specific material combination.
- b. Al reinforcement materials are compatible with molten Al and Mg with regard to physical (strength) as well as chemical stability.
- c. Only  $\text{Al}_2\text{O}_3$  is physically and chemically compatible with molten Ni, Co, and Fe.
- d. B and BN are unacceptable for higher temperature base metals in view of strength degradation.
- e. SiC,  $\text{Si}_3\text{N}_4$ , graphite, and tungsten are physically stable at higher temperatures, yet react with all high-temperature matrices; their usefulness depends on the successful development of protective coatings.

On the basis of these results and in view of the efforts involved in the development of specific coatings it is recommended to concentrate near-term efforts on aluminum-base composites. They combine a high assurance of success with practical usefulness and adaptability to the time limitations of suborbital low-g experiments.

Table 3-3. Compatibility of Reinforcements With Liquid Matrices

Reinforcements	Matrices						
	Al	Mg	Fe	Ni	Co	Cr	Ti
SiC	●	●	C	C	C	C	C
Si <sub>3</sub> N <sub>4</sub>	●	●	C	C	C	C	C
Al <sub>2</sub> O <sub>3</sub>	●	●	●	●	●	C	C
C	●	●	C	C	C	C	C
BN	●	●	X	X	X	X	X
B	●	●	X	X	X	X	X

● Compatible, yet nonwetting; coating required.

C Not compatible due to chemical reactivity.

X Not compatible; reinforcement degradation due to temperature.

The development of Al-base composites will consist of the following major tasks:

- a. Development of coatings and coating techniques to activate wettability for graphite fibers, chopped boron filaments, chopped tungsten wire, and whiskers of Al<sub>2</sub>O<sub>3</sub> and SiC.
- b. Testing of bond strength and development of methods to increase bond strength, such as mechanical surface treatments or heat treatments to produce a diffusion interface.
- c. On the basis of laboratory experiments, selection of specific Al-alloys for specific reinforcements or reinforcement coatings.
- d. Development of exact specifications for the preparation of component materials for sample preparation and for process performance.
- e. Preparation of samples for zero-g experiments, with various reinforcement types and contents, including mixtures of fibers or whiskers and particles.
- f. Evaluation of zero-g experiments and integration of the results in composite optimization and in the definition of compositions for specific product applications.

The experiences and data obtained with aluminum composites may then provide a reliable basis for the development of composites with high-temperature base metals.

3.2.9 COMPOSITE EXPERIMENTS. The composite experiments described in the following sections comprise, for the most part, work whose objective was to characterize qualities of a product rather than to understand the properties of the dispersed phase. In addition to the problems of fiber alignment, fiber length selection, optimum volume fraction, and response to wetting, which have already been discussed, there are questions of bonding and reactivity or compatibility. Experiments and results with aluminum will be treated first because of its potential for a practical composite, because it has a reasonably low melting point at which to work, and because it exhibits most of the important problems that may be encountered during processing of typical composites.

#### 3.2.9.1 Aluminum-Graphite Dispersion Tests

Material. The Al-graphite composite was an aluminum infiltrated specially treated Thorn 1 fiber prepared by Aerospace Corporation. Figure 3-26 shows the well wetted and bonded fibers in the aluminum matrix. The Al is a high silicon alloy to enhance the flow properties. The material configuration is circular strands about 0.062-inch diameter.

Alloys A-356, 2024, and soft wire were the compositions used in the test as matrix material.

Procedure. A strand of composite pickled in dilute  $H_2SO_4$  was mixed with the pickled matrix and heated in a 0.25-inch stainless steel tube capped at one end. Metallurgical



Figure 3-26. Graphite Fiber in Aluminum Matrix

mounts were made after the melt was cooled to determine the dispersion of the fibers. The material was used in the virgin and the pickled state, in air, vacuum, and argon, and with and without stirring.

**Results.** Aluminum wires pickled in dilute  $H_2SO_4$  fused when heated to the melting point but did not disperse the composite when the experiment was performed under a blanket of argon and the mixture was stirred. The graphite composite remained intact (Figure 3-27). Impurities in argon seem capable of reacting with Al to make it brittle, which is a reason for the void. In Figure 3-28, the interface gap is shown for comparison with the good dispersion obtained.

When the experiment was repeated in a vacuum of  $1 \times 10^{-5}$ , overheating caused the Al to evaporate rapidly and coat the vacuum chamber. The aluminum matrix fused into a good melt but the composite strand remained intact.

A successful dispersion of composite in matrix was obtained by using A-356 alloy in a vacuum environment with stirring for a very short time at a temperature about  $100^\circ C$  above the melting point. (See Figure 3-29.) No interface is visible in the transition zone.

#### 3.2.9.2 Graphite Wetting Tests

**Materials.** Strands of Al-graphite composite, A-356 alloy, Alcoa No. 30 flux, KF,  $MgCl_2$ ,  $CaCl_2$ ,  $SnCl_2$ , a bow made of tungsten wire.

**Procedure.** The aluminum alloy was melted in a ceramic crucible with a layer of flux on top. Graphite yarn was strung on the tungsten bow wire and immersed with agitation through the layer of melted flux into the molten Al.

**Results.** The graphite was not wetted by the aluminum.  $SnCl_2$  especially, wet both the fibers and the aluminum but did not cause the Al to wet the carbon.

#### 3.2.9.3 Zinc-Glass Dispersion and Wetting Tests

**Materials.** Zn-coated fiberglass tape, which is a composite manufactured by Aerospace Corp., Zn-Sn alloy, fluxes.

**Procedure.** Same as with graphite-aluminum previously described. Some chopped composite fibers were also used.

**Results.** The composite could not be dispersed into the zinc. If heating were persistent and excessive, the zinc dewetted and balled up. More extensive testing is required if dispersion is to be obtained.

REPRODUCIBILITY OF THE ORIGINAL PAGE IS POOR.

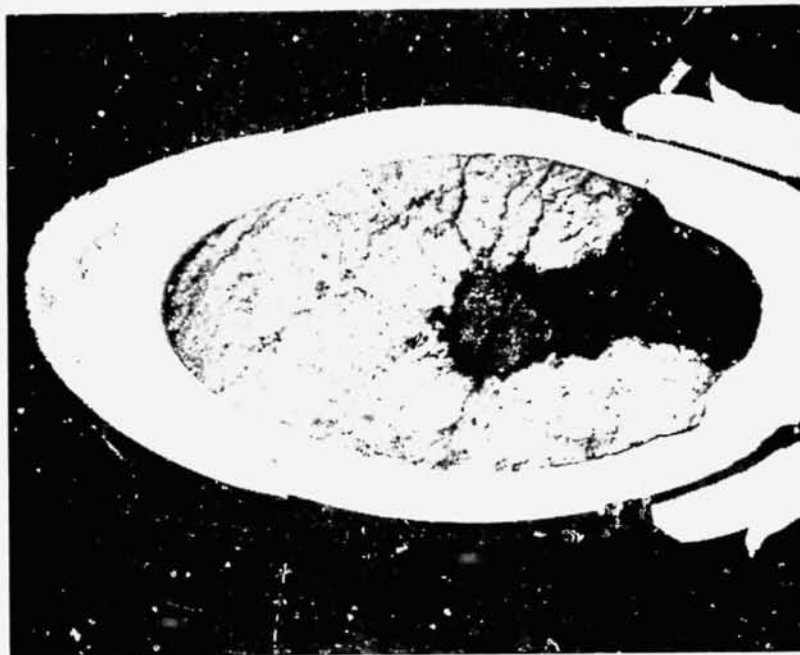
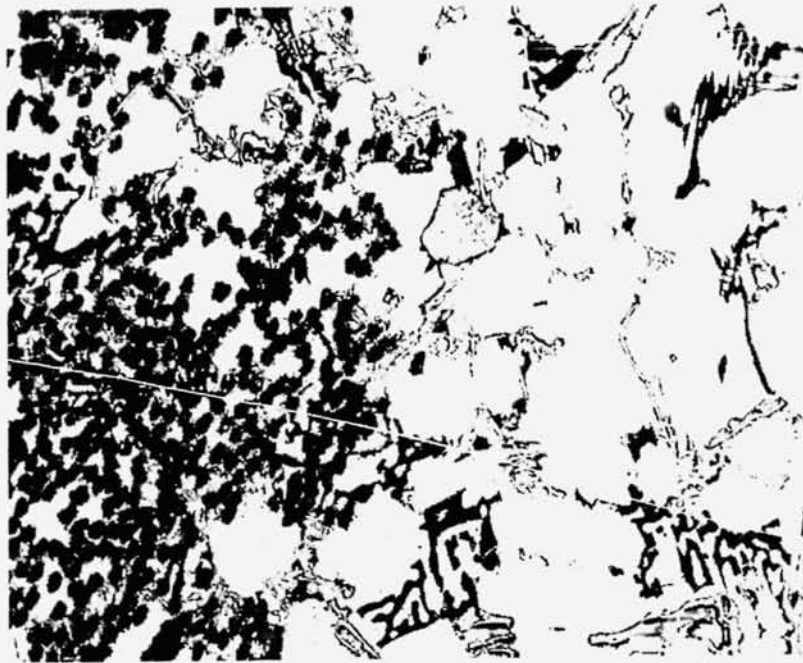


Figure 3-27. Undispersed Al-Graphite Composite Strand in Aluminum Alloy



250X

Figure 3-28. Interface Gap Between Unbonded Al-Graphite Composite and Al Alloy from Figure 3-27



250X

Figure 3-29. Graphite Fibers Dispersed in Aluminum A-356 Alloy

#### 3.2.9.4 Reinforcement Experiments

##### Test for Influence of Oxide on In/Bi

Materials. Two In/Bi cylinders 8 mm tall and 4 mm in diameter.

Procedure. Clean one cylinder in 20% HCl for melting in boiled oxygen-free water. Melt uncleaned piece in tap water.

Results. The cleaned rod fused into a round globule at 73°C (melting point of alloy). The second rod slumped over at 77°C but retained its elongated shape.

Conclusion. An oxide skin held the configuration together as confirmed by the next experiment.

##### Test for influence of Oxide on In/Bi Compacts

Materials. In/Bi filings and 20 vol % spherical tungsten powder; In/Bi filings only.

Procedure. Mix filings and powder, then press in a die to produce a sample. Make duplicate sample with filings only. Heat to 82°C.

Results. Both specimens retained their shape up to 82°C in water but slumped over when they were then vibrated. The tungsten powder sank unwetted to the bottom of the sample. This showed that the oxide skin and the resulting internal oxide network held the samples together because a fluxed and clean sample collapsed into a globule at the melting point. The work with Al-graphite described previously showed that stirring, pickling, and vacuum manipulations can eliminate oxide problems.

3.2.9.5 In/Bi-Copper Composite Fluxless Wetting Tests. Apollo 14 tests showed that Cu fibers must be wetted in order to disperse in In/Bi alloy. Flux is a contaminant and is therefore undesirable. A test was therefore made to determine whether ultrasonic techniques would be useful for effecting the wetting and dispersal of Cu fibers in In/Bi alloy.

Materials. In/Bi alloy, chopped Cu wire cleaned with sandpaper.

Procedure. Immerse wires in In/Bi alloy contained in the tank of an ultrasonic cleaner.

Results. The alloy could be scraped off the fibers that were merely dipped in the melt. But there was complete wetting of the wires so that the coating could not be mechanically removed from the fibers immersed with ultrasonic power applied.

3.2.9.6 In/Bi-Copper Composite Dispersion Tests. Tests were made to determine the dispersion properties of Cu fibers in In/Bi alloy.

Procedure. Copper has a similar density to the indium-bismuth matrix (8.9 gm/cc versus 8.3 gm/cc, respectively) and the system is "partially wetting." A 0.05 volume fraction of copper wires, 5 mils in diameter with an L/D ratio of 20, was used as the fiber reinforcement. The sequence of operations to introduce the wires into the center of an In-Bi ingot is shown diagrammatically in Figure 3-30. Both tungsten and copper wire filaments were cut to length (0.100 ± 0.010 inch). Twenty grams of both materials were made for the bulk fiber experiments.

First the Cu wires were cleaned in alcohol and HCl, then were introduced slowly, while still wetted with HCl, into a glass vial containing molten In-Bi under a layer of dilute HCl (Figure 3-30a). The HCl kept the fibers and matrix clean and therefore acted as a flux. The fibers were thoroughly wetted with In-Bi by this technique. The sample was allowed to solidify and was inverted inside the vial and covered with dilute HCl (b). Superheated In-Bi at 95°C was poured into the vial through the acid flux onto the sample. Thus the surface of the sample was slightly melted so that a single specimen was formed (c). The sample was re-inverted (d) then melted in the vial for a total of three minutes (e), to assure that the sample was completely molten. After solidification the sample was sectioned for examination (Figure 3-31).

REPRODUCIBILITY OF THE ORIGINAL PAGE IS POOR.

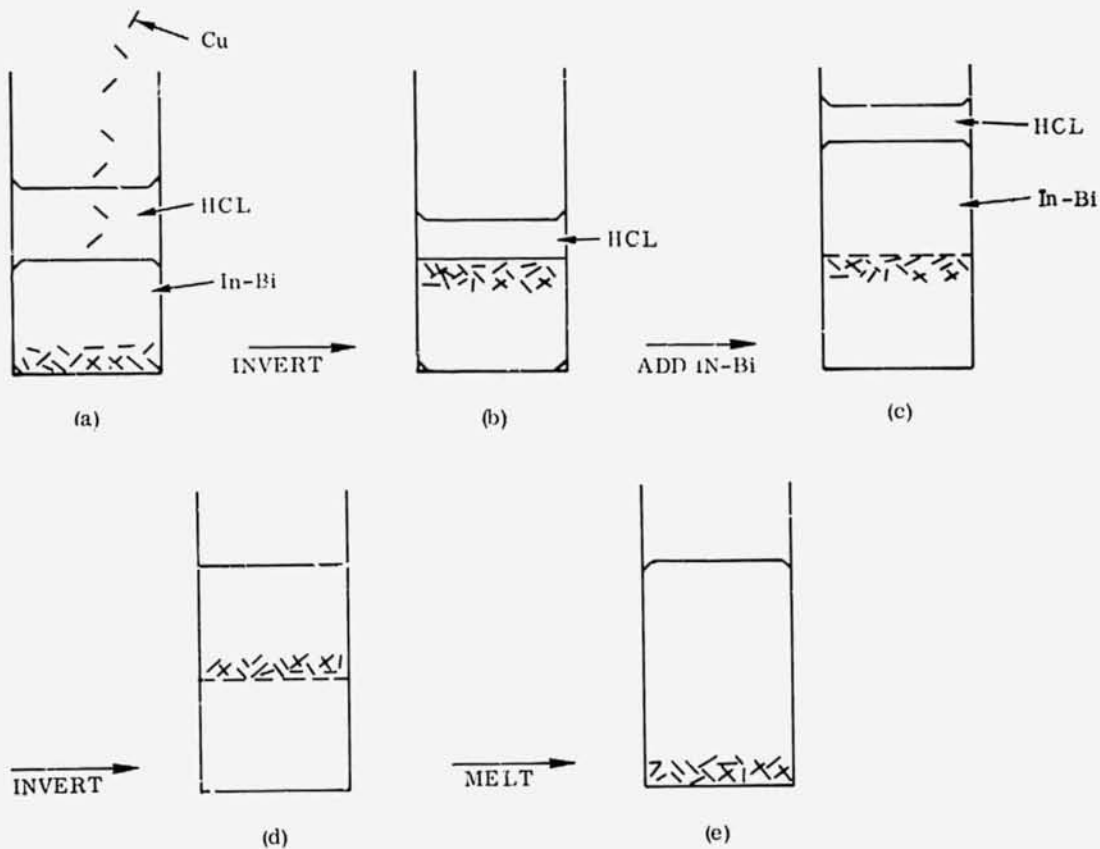


Figure 3-30. Sequence of Operations for In-Bi/Cu Dispersion Experiment



4X

Figure 3-31. In-Bi With Cu Fibers

Results. The macrostructure shows that the copper fibers had sunk to the bottom of the sample and that "log jamming" is evident. Since "log jamming" occurs at volume fractions as low as 0.05 and for L/D ratios as low as 20, this problem is expected to be even more severe with more useful reinforcements, i. e. , higher L/D ratios and higher fiber contents. Also, copper fibers were found agglomerated around the internal surfaces of the void. This agrees with the data observations made on Apollo 14 samples.

3.2.9.7 Wetting Experiments. Normally, the reinforcing material in a composite is the load carrying medium in the material, and the matrix serves as a carrier, protector, and load splicing medium around the reinforcement. However the interfacial bonding between the two elements of the composite must be effectual if these functions are to serve their purpose. The bonding is determined by the wetting and adhesion properties of the materials.

Materials. All investigations and experiments were based on seven matrices and eight reinforcements.

<u>Matrices</u>	<u>Reinforcements</u>
Copper	Al <sub>2</sub> O <sub>3</sub>
Indium-Bismuth	Boron
Lead	Copper
Inotype	Iron
Silver	Nickel
Tin	Silicon Carbide
Zinc	AM 350 Steel
	Tungsten

#### Procedure

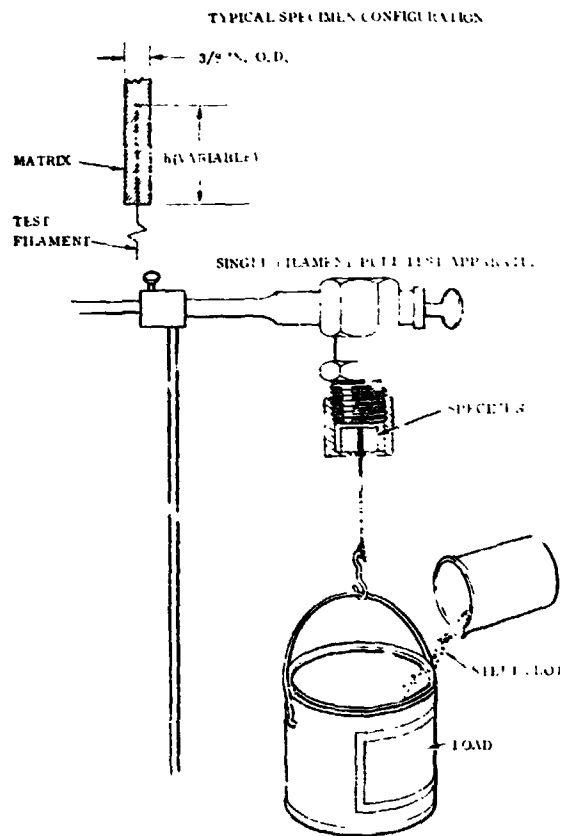
Chemical Compatibility. The chemical compatibility of candidate metals was assessed by judgement. Evidence of interactions were evaluated visually and supplemented by metallography.

Wetting and Adherence. Wetting characteristics were determined by dipping of wires or sheet strips with various surface conditions in the liquid matrix and observation of the behavior of the liquid film after removal. Wettability was expressed as nonwetting, partially wetting, and fully wetting.

Samples that showed adequate wetting characteristics were slowly cooled; after solidification of the matrix film, adherence was tested by scraping with a cutting tool. Adhesion was expressed by ● = fully-wetting or (-) = peeling-off.

Results. The results of the wetting were arranged in the form of a table given in the physical properties discussion, Section 3.5.5. A discussion of results of wetting and bonding is also given in Section 3.5.5.

**3.2.9.8 Single-Fiber Bond Strength Test.** In ground experiments (1-g) the effectiveness of reinforcements in a composite system cannot be determined since gravity precludes the maintenance of dispersion. However, theoretical predictions can be made on the basis of laboratory shear strength tests between filaments and the solidified matrix.



**Procedure.** For the single-fiber bond test, filaments were cast into the matrix, using a 0.35-inch-diameter cylindrical glass mold. The shear strength tests were carried out at room temperature. The shear strength was determined from the cylindrical contact area of the filaments and the maximum load according to:

$$F_s = \frac{\text{LOAD}}{\pi Dh} \text{ (psi)}$$

where

D = filament diameter

h = depth in matrix or contact height

The test apparatus is illustrated in Figure 3-32. The load was applied gradually by dispensing steel shot in the loading bucket. The maximum load was obtained from the weight of the filled bucket at the moment when the first movement of the filament was observed.

Figure 3-32. Apparatus for Single-Fiber Bond Strength Tests

**Results.** The test results for copper and tungsten with various surface treatments are summarized in Table 3-4. The data represent averages of several tests carried out with each material and surface condition.

Table 3-4. Single Filament Bond (Pull) Tests, In-Bi Matrix

Filament Material	Dia. (Thick) (mil)	Treatment						Cast Depth, h (mil)	Test Temp. (°C)	Shear Strength (g/cm <sup>2</sup> )
		Pcgrease	Deoxidize	Fluxcoat	Electroless Coating (Copper)	Graphite Coating	Coat (In-Bi)			
Copper	5	x	x		x		x	84	22	6.73 × 10 <sup>5</sup>
Copper	5	x		x	x		x	80	22	6.6 × 10 <sup>5</sup>
Tungsten	10	x					x	204	22	0.36 × 10 <sup>5</sup>
Tungsten	10	x				x	x	193	22	0.51 × 10 <sup>5</sup>
Tungsten	10	x			x		x	185	22	0.54 × 10 <sup>5</sup>

3.2.9.9 Coating Tungsten Filaments. While tungsten presented no problems of chemical compatibility, the wetting and bonding characteristics were negative. This indicated the necessity of coating. Copper was applied successfully by chemical deposition (electroless). All coatings showed good adherence. Successful coating with copper by electroless plating was achieved with the following process. This procedure is effective for all metals except those which react with strong acids, such as Al. The first step is used only for tungsten.

a. Clean

Solution: 50% distilled water  
50% NaOH  
for 30 minutes

Purpose: To remove graphite coating left on tungsten from processing.

b. Rinse in distilled water.

c. Activate

Solution: 25% activator 9070 ( $\text{SnCl}_2 + \text{PdCl}_2$ )  
20% HCl  
55% distilled water

Immerse and agitate for 8 minutes at room temperature.

d. Rinse in distilled water.

e. Accelerate

Solution: 10% solution 9071  
90% distilled water

Immerse and agitate for 2 minutes at room temperature.

f. Rinse in distilled water.

g. Coating

Solution: 10% solution 22A  
10% solution 22B  
80% distilled water

h. Rinse in distilled water.

i. Store in an argon filled bag to prevent an oxide layer from forming on the surface of the filaments.

Under the microscope, small samples of tungsten filaments ( $L/D = 10$ ) coated by the described process showed 100% coating with a shiny copper surface. The copper coating on the single fiber tungsten wires caused an average increase in shear strength of 6%. Graphite fibers can also be coated with copper by the same process.

3.2.9.10 Directionally Solidified Eutectics. A series of experiments was performed to obtain a baseline product for further studies

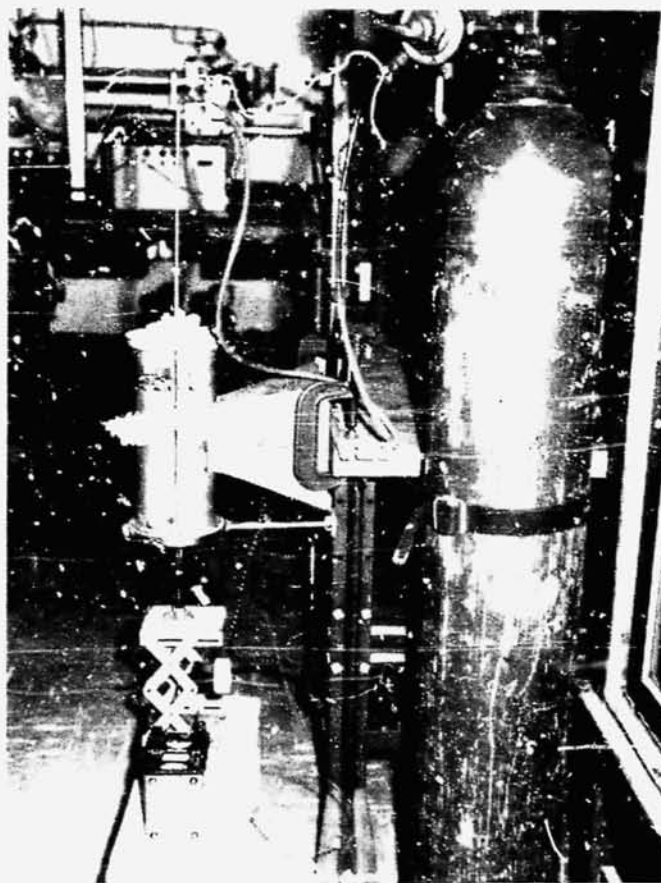


Figure 3-33. Directional Solidification Apparatus

The apparatus shown in Figure 3-33 consisting of a clamshell furnace with power control and a temperature monitor was not sophisticated enough to enable a good product to be obtained. Better heating and cooling control was desirable as well as better atmospheric control.

Materials. Sn, Cu; Al, Ni powders.

Procedure. Mix the metal powders and melt. Cool by initiating nucleation or by passive methods, progressively from one end to the opposite end.

Results. The Sn -3% Cu melt was cooled in an uncovered tube at an uncontrolled rate. No evidence of oriented crystals was present.

The remaining experiments were performed with Al and Ni powders using about 5.7% Ni. Initial experiments did not yield oriented material because of oxide coatings on the Al. The Al sintered instead of melting

under the prevailing conditions. When great precautions were taken to prevent the access of oxygen a good melt was obtained. The solidified product then exhibited partly oriented material. This partial result was probably caused by end effects from heat leakage of the furnace and because the Al was only 99.5% pure.

More experiments were performed with 99.999% Al powder but this also undoubtedly was oxidized on the surface. In some cases the Ni powder adhered to an oxide skin adhering to the aluminum and did not dissolve, even though the experimental compact was prepared in argon or helium.

Induced nucleation with constant controlled cooling was tried using a stainless steel cold finger as a heat sink. Inadequate atmospheric control as well as pressure and temperature surges in the water supplied upset the equilibrium conditions required for a good product. Future experiments require more precise regulation of temperature, purer starting materials, and greater precision in controls of the atmosphere and processing parameters.

**3.2.9.11 Cemented Compacts.** Two systems were examined for cemented carbide studies, tungsten carbide-cobalt and titanium carbide-cobalt to check their suitability for future zero-g experiments.

**Procedure.** The powders (1 gram samples) were mixed, pressed, set in loose  $\text{Al}_2\text{O}_3$  powder, and sintered at  $1350^\circ\text{C}$  in about 20 mmHg  $\text{H}_2$  atmosphere; also in a vacuum.

**Results.** The WC-Co sample sintered in vacuum showed no evidence of segregation. The TiC-Co mixes did not fuse; consequently, more Co was added up to 45 weight %. The liquid phase of the mix should constitute 85% liquid at  $1340^\circ\text{C}$ . Macrographs showed no evidence of segregation. Oxide layers on the surfaces interfere with the preparation.

**3.2.9.12 Study of Wetted Particle Motion in a Solidifying System.** It is known that nonwetted particles that are suspended in a solidifying mixture are sometimes not occluded in an advancing solidification front but are driven ahead and increase in concentration in the suspending medium. This is known to occur with thoria in nickel, for example, and indeed, one takes advantage of the phenomenon in commercial ice making by skimming off the concentrated impurities as they collect. An experiment was made to study the phenomenon as it applied to cemented compacts.

**Materials.** Fuller's earth, water.

**Procedure.** The fuller's earth, which appeared to be wetting, was suspended in the water, which was then partly frozen with liquid nitrogen. The liquid was decanted.

**Results.** The concentration of solid in each portion was essentially the same. This suggests that wettable suspensoids are not excluded from the solid as a solidification front advances. Hence these may be quite appropriate for application in zero-g. However, impurities can influence the crystal and grain structure of an alloy.

**3.2.9.13 Wetting and Bonding Phenomena.** A metallic matrix containing strong fibers or wires serves to transfer stress from the matrix to the fiber by means of plastic flow. This transfer of stress can occur only if a bond exists between the metal and the fiber. The strength of the composite material will depend on the strength of the interfacial bond. Whether any bonding occurs at all depends on the surface properties (wettability) of the reinforcement. Thus, one problem with graphite is poor fiber matrix adhesion.

**Wetting and Compatibility.** The phenomenon of wetting is very closely associated with chemical compatibility. Experiments have been described wherein copper fibers immersed in molten aluminum did not wet. When wetting was caused to take place, solubility phenomena became predominant so that the Cu wire reinforcements dissolved completely. The ideal composite system will therefore consist of reinforcements that will be wetted by the matrix material but will not dissolve in it. This is a function of high surface energy and low chemical reactivity such as is exhibited by water on glass and by copper on tungsten. The problem in composite casting is how to accomplish this satisfactorily.

**Wetting Methods and Techniques.** Various strategies may be used to produce wetting systems. However the final system must also be chemically compatible. The following sections discuss the approach.

**General Properties of Solid Surfaces.** The molecules in a solid lack the mobility of a liquid. Consequently the surfaces do not contract spontaneously as a liquid although the surface energy may be higher. Thus a liquid, like a hydrocarbon, will spread much faster on water than on a solid even though once formed, the film is very stable, e. g. , lubrication.

The immobility is only partial, however, for the diffusion of metals into metals is a well-known phenomenon. Metals frequently exhibit mobility below their melting points when corners and edges become rounded, e. g. , sintering. The essential difference from liquids is mobility.

**Cleanliness and Condition of Solid Surfaces.** In consequence of the surface energy of a solid, it will nearly always be contaminated with a thin layer of foreign matter. Freshly cleaved crystal surfaces usually become coated with a film of greasy material if left unprotected for a short time in air. Freshly split mica, for example, sticks so tightly on contact that the layers cannot even slide without considerable tearing and scratching. A layer of adsorbent only one molecule thick alters the properties of a surface intensely.

Oxygen is probably adsorbed on most solid surfaces. Usually the first layer on a metal is combined by covalent forces. On continuous exposure, especially at high temperatures, thick oxide films will form. With aluminum, the film forms so readily and is held so tenaciously that it becomes very difficult to wet the surface with another molten metal.

**Wetting Methods.** The brief background given above suggests many approaches to accomplishing wetting, many of which are well known or obvious.

- a. **Heat.** Since the chief barrier to wetting is a film of more or less strongly adsorbed contaminant it should be able to be removed by heat. In the extreme, even the

matrix metal will be volatilized and the gaseous metal molecules will mix with any other gaseous metal molecule. Only on lowering the temperature will phase separations appear and even these may be mutually wettable.

- b. Vaporization. Instead of removing adsorbed gas by heat, it may be removed by restricting molecules from reaching the surface. Thus if a metal is placed in a high vacuum (or on the moon) the sticking phenomenon of cleaved crystals is evident. Vacua of  $1 \times 10^{-5}$  or better are required before this wetting aid becomes useful.
- c. Ultrasonics. Ultrasonic vibration or friction is an aid that includes a heat effect when it is vigorous. Otherwise it is simply a mechanical motion of such frequency that the adsorbed material is removed kinetically or by vibratory motions that mechanically decouple the adsorbed contaminants. Ultrasonic soldering machines are manufactured and ultrasonic wetting of Cu by In/Bi is described in this report.
- d. Chemical Removal. Besides such heating, shaking, or scraping the barrier film, it may be conveniently removed by a chemical reaction. The reactants or "fluxes" that accomplish the cleaning may also protect the surface. For example, dilute hydrochloric acid dissolves the copper oxide film from Cu fibers, which are then wet by In/Bi. Solder does not melt until the temperature is much higher, however, so that oxidation is encouraged, not prevented. This tendency is opposed by materials such as resins and salts that wet the metal, are resistant to oxidation, and thus prevent oxygen from reaching the bare metal surface.
- e. Immersion. Immersion methods are closely related to fluxing or chemical methods but apply to systems that become active when the adsorbed gas only is removed. Liquid fluxes, for example, may not only dissolve away an oxide film but may displace adsorbed gases and create a more active interface. Two glass slides may not stick together, for example, until the layer of air between them is displaced by water. Two pieces of glass are then quite firmly attached indeed and will break in many cases before they can be separated unless the water layer is sheared by sliding.
- f. Stirring and Friction. There are two other strictly mechanical processes that aid in producing wetting. The mechanism, depending on the system to which it is applied, consists of dissolving away the surface and exposing fresh bare metal, or abraiding the surface layer. This removes any gases and oxide coat and exposes virgin metal. Friction is particularly effective in breaking up the surface of aluminum and allowing wetting, but the freshly exposed active surface must be wetted or protected immediately.

Compatibility Considerations. Although the components of a composite must wet, the reaction may proceed beyond mere coating phenomena until solution is attained. If the reinforcements are of small diameter, and the best ones are small, they may be completely taken up into solution, in which case they don't reinforce at all. On the other hand, if they are made thicker the portion that does dissolve may produce an interface of a third phase consisting of a compound or alloy that has little or no bonding strength at all. There may be such marked differences in thermal expansion and modulus that severe residual stresses appear.

Time, Thickness. If the interfacial bond is physically and mechanically satisfactory the composites may be produced by the selection of a processing mode that provides an optimum processing time for wetting and dispersing the reinforcements but not so long that excessive solution, interaction, or third phase production occurs. Associated with the time parameter is a thickness parameter for the reinforcement. If the processing time is short the reinforcements can be thin. If the processing time becomes prolonged, some compensation may be made by increasing the size of the fiber, provided the solution product is not deleterious.

The reaction zone or the diffusion zone between the matrix and the reinforcement may be desirable and actually enhance the strength of the composite or act as an intermediate for absorbing transitional stresses between the matrix and fiber. The interphase stabilization may also be achieved at times by heat treatment of the liquid mixture or by treatment of the solid. These procedures constitute separate tasks and are subjects for further study.

Coatings. In some cases the physical system is such that two components inherently do not wet because of their surface properties. This is especially true of oxides such as glass or  $Al_2O_3$  and metals. In such cases one may deposit a film of wettable metal such as copper, silver, or nickel on the surface. The problem arising here is the bonding of the coat to the substrate. Also, the coatings are usually very thin so that they are easily absorbed, dissolved, or reacted. Then there is no bond at all and the product may be much weaker than either component alone.

Another problem is agglomeration of the fibers. Their dispersion properties and effects of L/D and volume fraction loaded are discussed in Section 3.2.5.1. The point here is that even wetted fibers may agglomerate, mat, and stick to the walls of the processing equipment unless positive action is taken to assure their uniform dispersal.

### 3.3 CONTROLLED DENSITY MATERIALS

3.3.1 DEFINITION OF PRODUCTS AND PROCESSES. This section comprises plain and reinforced metal foams. The term "foam" has the connotation of a highly irregular material system. The objective of space processing is to produce high-performance materials by means of a well-controlled dispersion and size of voids and reinforcements, attainable only under zero-g conditions. Even though the term "foam" is used in this discussion for convenience, the designation "Controlled Density Materials" is more appropriate and descriptive.

Controlled density metals comprise 1) metal-gas systems (plain foams), and 2) fiber-reinforced metal-gas systems (reinforced foams). The ultimate objective is to produce bulk materials (in contrast to structural elements built up from individual parts such as honeycomb) that permit the widest range of property combinations. The composite nature of this class of materials offers the potential to utilize the optimum properties of each component: the metal matrix provides strength, ductility or oxidation resistance,

besides acting as the binder material; the reinforcements contribute strength, high elastic modulus and creep resistance, while density and specific stiffness can be controlled by the gas dispersion. An optimum end product with a well-balanced combination of properties requires a full understanding of the numerous interactions between the three basic composite components. In the following, the major problems are derived from a discussion of the most promising processing techniques.

**3.3.2 SUMMARY OF RESULTS.** The studies and laboratory experiments carried out on the materials and methods for the preparation of metal foams produced the following results:

1. Mixtures of molten metals and discrete gas bubbles are extremely sensitive to g-forces and exhibit instantaneous segregation in 1-g. The generation of stable liquid/gas mixtures necessary for the preparation of useful foams is unique to zero-g and very low-g conditions.
2. The stability of the liquid/gas mixture can be enhanced and adapted to intermediate low-g levels by the use of alloys that exhibit a high-viscosity melting range.
3. Three basic types of controlled density materials have been identified: 1) plain metal foams, 2) metal foams reinforced with long fibers (multiple of bubble diameter), 3) metal foams reinforced with short fibers (shorter than bubble diameter).
4. The compact foaming method is most effective for process development and initial zero-g experiments due to its relative simplicity, the valid representation of all essential process parameters, and the fact that the foam is generated during zero-g processing (in flight). This should be followed by gas injection foaming experiments. Nucleate and ultrasonic foaming should be deferred in view of the extensive equipment development requirements.
5. The foremost criterion during liquid-state processing is the prevention of bubble coalescence, particularly for plain foams. This can be achieved by the selection of gases that stabilize the bubble wall. In aluminum-base foams, for example, a gas with 2% oxygen has been found most effective.
6. Fundamental relationships for the mobility of gas bubbles, their interaction with fibers and the mold wall, and their sensitivity to thermal gradients have been established. They provide a basis for the development of specific techniques and for the interpretation of zero-g experiments.
7. In plain and short-fiber reinforced foams the dispersion is dictated by the bubble distribution. For the selected compact foaming method it is defined by the dry-mixing of component materials in 1-g.
8. Short fibers exhibit mobility in the liquid matrix and tend to agglomerate at the bubble interfaces. This effect may be favorable upon the mechanical composite characteristics.

9. In long-fiber reinforced foams the gas dispersion is dictated by the geometry of the fiber network in which the bubbles are trapped under low-g conditions.
10. In all cases, reinforcements have to be treated for high wettability to assure their retention in the matrix. Otherwise, all reinforcement dispersion criteria and preparation requirements defined in Section 3.2 apply.
11. For compact foaming, the choice of matrix metals is limited by temperature-compatible foaming agents. The most promising base materials for further development are aluminum alloys.
12. For gas injection foaming the choice of materials is limited only by temperature limitations of the tooling.
13. Dry-mixing of component materials and sample compacting has been accomplished successfully. All operations have to be carried out either in high-purity inert gas, or in a high vacuum.
14. Sample molds have to meet two requirements: high wettability of surfaces in contact with the matrix and provision for volume expansion.
15. The high sensitivity to segregation presents severe problems in laboratory experiments. A valid verification of processing parameters and the preparation of samples for the measurement of product characteristics and capabilities can only be obtained in low-g experiments.
16. Successful foams — within the limitations of 1-g experimentation — have been prepared with  $TiH_2$  and oxalates as foaming agents in an aluminum matrix.
17. Samples of simulated plain and reinforced In-Bi foam have been prepared for testing in sounding rocket experiments. To date, two flight experiments have been carried out by MSFC-S&E-PE; the results are documented in NASA-TM-X-64665 of April 28, 1972.
18. For further detailed process development and low-g experiments it is proposed to concentrate efforts on:
  - a. Methods:
    - 1) Compact foaming
    - 2) Gas injection foaming
  - b. Base Materials: Aluminum alloys.
  - c. Foaming Agents:  $TiH_2$  and oxalates.
  - d. Reinforcements: Chopped Cu-Be wire, treated graphite fibers, treated boron fibers, and coated whiskers of  $Al_2O_3$  and SiC.

**3.3.3 DISPERSION CRITERIA FOR PLAIN FOAMS.** This title could be rephrased as "How Bubbles Behave," or more generally as "Patterns of Interfaces Between Two Immiscible Fluids." It is pertinent at the outset, in regard to such patterns, to consider that the most important difference between gas and liquid is the density difference. For pure fluids, either bubbles or droplets will coalesce when they meet, but the droplets can coast through the gas to coalesce with each other more freely than can the bubbles.

In the random low-gravity situation, therefore, and if the interface patterns are of fine enough scale so that the container wall effects are unimportant, the general arrangement of the fluids will be predominantly bubbles in liquid. Liquid drops may also be coasting around in the bubbles, but as time accumulates their relative population should decrease. The tendency to form bubbles in liquid rather than droplets in gas is strengthened by the lower viscosity of the gas.

It should be recognized that a fine-scale liquid/gas interface can have considerable area even in a small container and by reason of its tension can store appreciable energy. When the area is decreased, as by a coalescence event, some of this energy is mechanically released to agitate the fluid mass, often leading to further coalescence.

For many liquid/gas situations, the density and viscosity of the gas are so small as to have little effect on the behavior of the fluids, and we are left with three effective fluid properties: liquid density ( $\rho$ ), liquid viscosity ( $\mu$ ), and interface tension ( $\sigma$ ). These properties can be related to the physical parameters operating on the situation by dimensionless force ratios, of which the following are pertinent in the low gravity condition.

<u>Force Ratio</u>	<u>Defining Authority</u>	<u>Physical Parameters</u>
Inertia/Viscous	Reynolds	$\rho VL/\mu$
Inertia/Surface	Weber	$\rho V^2 L/\sigma$
Surface/Viscous	Marangoni	$\sigma/\mu V$

These add size (L) and velocity (V) to the property list and directly reveal some interesting data. For large systems and/or high velocities, inertia forces predominate over surface and viscous forces (the inverse being also true). The relative effect of surface tension and viscosity is not affected by size, but the viscous forces predominate when the velocity is high.

For dynamic consideration we may postulate a chaotically disturbed volume of liquid and gas gradually coming to rest in zero-g. The kinetic fluid energy can be converted into potential energy by extension of the liquid/gas interface, and into heat energy through viscous dissipation. If the initial disturbance is rather violent ( $We \gg 1$ ) the liquid/gas interface area may be extended by the tearing of large bubbles into small

ones. The arithmetic of this situation is interesting. A thousand one-millimeter bubbles hold the same amount of gas as one one-centimeter bubble, but their surface area is a hundred times as great. The energy stored by such surface increase, however, is probably small with most of the kinetic energy being converted directly into heat as the viscous shear flows slow down the fluid velocities. During this slowing down it is to be expected that bubbles will come into contact with and coalesce with each other, releasing stored surface energy to kinetic and thence through viscosity to heat.

Bubbles do not necessarily coalesce when they are brought together. Even a very small amount of soap or detergent in water can migrate to the interface and form there a layer of molecules so oriented as to repel electrically the approach from the rear, so to speak, of another such layer. Pure liquids such as distilled water or liquid metal do not exhibit this surface stabilization effect that makes "soap bubbles" possible, but there is evidence that deposits on the interface, such as oxide films on molten metal, can provide such stabilization. Quantitative data on the strength or vigor of the surface stabilization is not immediately available, but its effects are drastic for soapy water and definitely demonstrated for liquid metal. General considerations indicate that its effect is assessable in pressure units, such as dynes/cm<sup>2</sup>. Assuming this to be correct, a force ratio to handle the scaling of the effect might be defined as:

$$\frac{\text{Surface Stabilization Force}}{\text{Surface Tension Force}} = \frac{PL^2}{\sigma L} = PL/\sigma$$

To obtain a better understanding of the dynamics of approaching gas bubbles, it is necessary to solve the equations of fluid motion (at least approximately) for the liquid between the bubbles. Such a detailed calculation has been carried out in a separate contract report (TN-72-MS/MS-001) on The Slow Viscous Motion of Solids and Gas Bubbles Toward a Plane of Symmetry. The simplifying assumption has been made that the bubbles are approaching each other sufficiently slowly to permit the neglect of inertia effects compared to viscous effects (low-Reynolds-number approximation). The main features of the flow field between the bubbles are indicated in Figure 3-34.

With good approximation the pressure and the radial velocity may be assumed constant across the fluid layer. The pressure increase  $P - P_\infty$  over the undisturbed value  $P_\infty$  at infinity has a maximum at  $r = 0$ . This maximum appears to be an order of magnitude larger than the forward pressure increase on a solid sphere moving through an infinite fluid with the same velocity as the bubbles, but an order of magnitude smaller than the pressure increase between two approaching solid spheres. The radial velocity attains a maximum a short distance away from the axis of symmetry and then falls off to zero with increasing values of  $r$ .

Another interesting result of the analysis is that the (continually changing) shape of the liquid/gas interface during the approach of the bubbles depends on the Marangoni number.

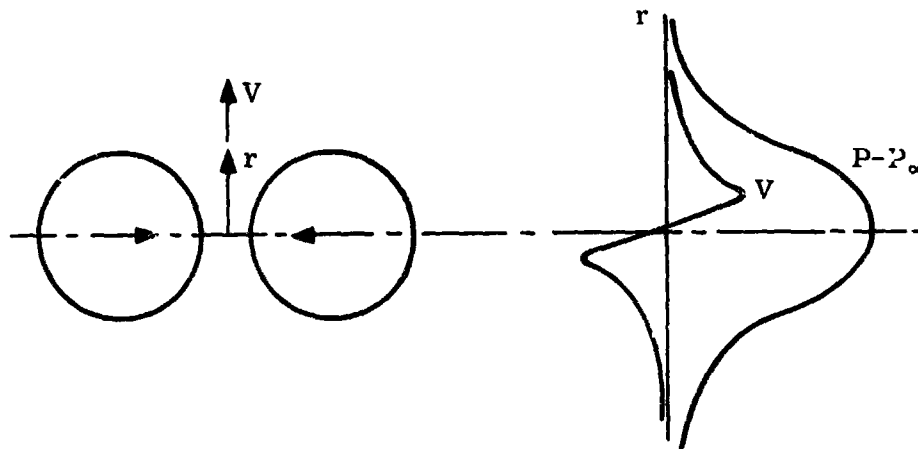


Figure 3-34. Pressure and Velocity Distribution Between Approaching Bubbles

Of course, the foregoing fluid/mechanical analysis is only applicable so long as we're dealing with a continuum. Thus, when the separation of the bubbles has become so small that we are dealing with a liquid film a few layers of molecules thick, the continuum results lose their validity. The continuum solution predicts in fact an infinite liquid pressure when the separation distance has vanished.

Considerations of stability of the liquid film between the bubbles clearly go beyond the fluid/mechanical calculations that we have thus far made. Nevertheless, our results would be required as input to a hydrodynamic stability calculation. Such a calculation might yield useful results in view of the experimental observation that fairly thick liquid films may collapse readily. A possible instability mechanism could be a slight initial rippling of the film, which in turn might be caused by a thermal gradient, a composition gradient, or the presence of a contaminant (all three causing variations in the surface tension).

Some foams are relatively long lived, and the release of potential energy stored in the multibubble configurations seems to be mainly brought about by gas diffusion through the liquid films (particularly in a foam of bubbles with a wide distribution of sizes).

**3.3.4 DISPERSION CRITERIA FOR REINFORCED FOAMS.** In line with the subject of this section, it is attempted to define the fiber dispersion criteria as they apply to reinforced foams in general. Reference to specific foaming methods is only made when necessary.

**A. Effect of Fiber Length and Bubble Diameter.** Since a foam is a two-fluid system, it follows the basic rules explained in another section:

1. In two-fluid systems (liquid/liquid, liquid/gas), solids in contact with the interface will agglomerate there. Straight fibers will agglomerate in parallel patterns. This effect will be particularly pronounced under dynamic mixing, since there is a high chance for the fibers to come in contact with the interface.

2. In reinforced foams, which always represent a two-fluid system, fibers will agglomerate at the gas bubbles; the fraction of fibers agglomerating depends on the ratio of fiber length to bubble diameter, on the means of dispersion (compact foaming or dynamic mixing), and on the presence and nature of a third phase (bubble surface stabilizer).

The first-order dispersion behavior is related to the ratio of fiber length to bubble diameter,  $L/B$ . If this ratio is in the order of 1 or less (short fibers), the dispersion of the fibers is dictated by the dispersion of the bubbles. In mixtures at rest and at large bubble spacings, only a smaller fraction of the fibers will agglomerate at the bubble walls. The fraction of fibers captured at the bubble walls increases with the degree of agitation (statistical chance of contact) and is inversely proportional to the bubble spacing.

As the ratio of fiber length to bubble diameter becomes larger than  $L/B = 1$ , the dependency of fiber distribution on bubble dispersion decreases. At  $L/B$  values of five and more, a reversal of conditions is encountered in that the bubble dispersion is dictated by the fiber distribution. In mixtures at rest and at any moment of an agitated mixture, the bubbles attempt to move to a minimum-energy position in the fiber framework.

- B. Nonwetted Fibers. The basic conditions defined in (A) are further modified by the wetting characteristics of the fibers, and all the criteria discussed in Section 3.2.4.3, A through D, apply. To obtain guiding criteria, the multitude of potential variations and combinations is reduced to a few typical or extreme conditions. If the fibers are nonwetting or become nonwetting due to dissolution of a wetting coating, the following effects are encountered: 1) Fibers in the interbubble space have the tendency to agglomerate which, in turn, depends on the bubble spacing and the relative fiber length  $L/B$ . 2) Fibers in contact with (still mixtures) or captured at (agitation) the bubble interface will be partially depleted of matrix coverage and may even protrude into the bubbles. The fundamental effect is a merging of the localized two-fluid system of the nonwetting solid with the macroscopic two-fluid system of the foam. 3) The end product has a poor overall strength.
- C. Wetted Fibers. If the fibers are well wetted by the liquid matrix, or have stable wettability coatings, the effects discussed in (B) are modified: 1) In the interbubble space agglomeration is prevented and fibers will disperse freely. 2) Fibers with low  $L/B$  will still agglomerate at the bubble wall, if they are located at, or come in contact with, the bubble interface. As spelled out in conclusion 3, Section 3.2.4.1, they will align themselves along the bubble wall and deform the bubble to an equilibrium configuration. According to Figure 3-4, they should be partially exposed (bare). Experimental evidence shows, however, that the interface fibers retain a substantial matrix coverage, resulting in smooth bubble deformations, as shown in Figure 3-35. The 100% surface bond with the matrix is important with regard to interface reinforcement



Figure 3-35. Void Shape Distortion by a Copper Fiber at the Gas/Metal Interface

strength. At large values of  $L/B$ , the dispersion is little affected by the presence of gas bubbles. The interface conditions are identical to those discussed above.

3) High overall strengthening effects can be realized, depending on the single-fiber bond (shear) strength of specific matrix and fiber materials.

Conclusion 1. The dispersion in fiber-reinforced foams is primarily dependent on the ratio of fiber length to bubble diameter:  $L/B$ . At low values of  $L/B$ , the dispersion is dictated by the bubble distribution, and at high values by the fiber dispersion.

Conclusion 2. A prerequisite of an effective reinforced foam, regardless of the foaming method, is high wetting characteristics and high fiber/matrix bond strength.

Conclusion 3. The development of effective fiber-reinforced foams calls for an understanding of the gas/matrix/fiber interface effects. It is a prerequisite for devising means of fiber arrangement control and the achievement of optimized reinforcement effects.

2.3.5 METHODS OF FOAM GENERATION. Discussions of various types of methods for producing foams are detailed in the literature.<sup>3</sup> These include the following methods of foam generation, in the order of feasibility:

<sup>3</sup> W. H. Steurer and D. H. Gorham, Processes for Space Manufacturing, Convair Aerospace Division of General Dynamics, GDC-DBG70-001, Final Report on Contract NAS 8-24979, June 1970, pp. 241 ff.

- a. Dispersion of gas-filled microspheres (predispersed by compaction with matrix).
- b. Gas generating solid additives (predispersed by compaction or mixed into liquid matrix).
- c. Gas injection (into liquid matrix).
- d. Ultrasonic foaming.
- e. Nucleate foaming.
- f. Cavitation foaming.

The following discussion applies to plain and reinforced foams; in the statement of procedures, the deployment of fibers for reinforced foams is omitted to avoid repetitions. Fibers may be introduced by "dry" mixing (pre-mix) of metal granules and fibers, or by "wet" mixing into the melt. In all cases, the mold is only partially filled; the gas pressure in the remaining expansion volume or "ullage" varies with the technique.

Laboratory investigations for the present work were confined to methods (a) and (b). These will be discussed in detail in Sections 3.3.6 and 3.3.7. Gas injection foaming, ultrasonic foaming, and nucleate foaming are discussed below. Cavitation foaming (f) is produced by rapidly lowering the pressure and thereby causing the disengagement of dissolved gas bubbles or the vaporization of a liquid matrix. The low pressure is usually initiated in the wake of a rapidly moving body such as a stirrer or propeller. No more will be stated because this development is presently in a very primitive state.

**3.3.5.1 Gas Injection Foams.** Gas injection requires the generation of discrete bubbles and dispersion of these bubbles by melt motion. The generation of discrete bubbles by pulsating gas injection is questionable, since here low inertia of the gas may simply lead to one single, growing bubble. Most promising appears continuous gas injection from a mechanically pulsating nozzle, whereby discrete bubbles will detach themselves under the effect of surface tension.

Agitation may be induced either by paddles at the pulsating nozzle or by a rotating electromagnetic field (feasibility established experimentally).

Process:     (a) Melting  
               (b) Agitation  
               (c) Gas injection and agitation  
               (d) Stilling  
               (e) Solidification

Bubble dispersion is controlled by the agitation mode, and the bubble size by the pressure differential between the gas supply pressure and the (lower) ullage pressure.

Problems: Dry mixing techniques  
Wet mixing techniques  
Gas injection techniques  
Agitation techniques and mixture behavior  
Bubble coalescence, control by surface stabilizing gases  
Bubble size control  
Foam dispersion control

3.3.5.2 Ultrasonic Foaming. The concept of ultrasonic foaming requires a metal that is rich dissolved gases. The molten matrix is moved past a transducer head where gas is driven out of solution to form discrete bubbles. It is expected that the transducer, by proper mold configuration, will also impart motion to the bulk, required for obtaining discrete bubbles and dispersion. Bubble size is controlled by the amount of dissolved gas and by ullage pressure.

Process: (a) Melting of matrix  
(b) Ultrasonic foaming  
(c) Stilling  
(d) Solidification at constant volume

Problems: Solubility of gases in metals  
Gas release by ultrasonic energy  
Transducer design to achieve liquid "pumping" action  
Stilling techniques

3.3.5.3 Nucleate Foaming. In nucleate foaming, the bubbles are generated at a temperature slightly above the matrix-melting point by gases dissolved in the matrix, or by partial vaporization of matrix material. In either case, the vapor is produced by a sudden drop of the ullage pressure over several orders of magnitude (e.g., from 1 atm to  $10^{-4}$  mm Hg). The place at which each individual bubble grows and, consequently, the dispersion is controlled by uniformly distributed micron-size particles acting as nucleation sites. The process is identical to the opening of a champagne bottle, except that the bubbles do not rise, leading to a sudden expansion of the mixture. Bubble size is controlled by the magnitude of depressurization, or, if the ullage is vented to a given space-vacuum pressure, by the initial ullage pressure. As in all foaming processes, the mold is closed after foaming and the bulk solidified at constant volume.

The feasibility of the process depends on the solubility of gases in metals. Generation of vapor from the matrix metal requires a metal of high vapor pressure (or an alloy constituent of high partial pressure). A promising candidate is magnesium, whose boiling temperature is  $1103^{\circ}\text{C}$  at 1 atm and approximately  $300^{\circ}\text{C}$  at  $10^{-4}$  mm Hg; at a processing temperature of  $675^{\circ}\text{C}$  it is expected that considerable vaporization occurs at the nucleation sites by depressurization from 1 atm to  $10^{-4}$  mm Hg. The bubble size is determined by the interaction between vapor pressure and surface tension.

Process: (a) Melting of matrix at 1 atm  
(b) Mixing with nucleation particles at 1 atm  
(c) Stilling of liquid-solid mixture  
(d) Depressurization  
(e) Solidification at constant volume

Problems: Solubility of gases in metals  
Mechanism of bubble generation at nucleation sites  
Interaction of vapor pressure and surface tension, effect on bubble growth and size  
Materials for nucleation particles  
Wet liquid/solid mixing and stilling techniques  
Criteria for bubble coalescence, discrete dispersion

3.3.6 MICROSPHERE FOAM. A simple method of foam preparation consists in dry-mixing of matrix granules with gas-filled microspheres followed by a matrix-melting cycle. Even though this method may appear primitive, it represents a valid zero-g process, since it is unfeasible under gravity conditions.

Microballoons down to micron-size are readily available in epoxy, carbon, and silica. The presence of the microballoon wall material in the final product may, in some cases, be undesirable; in most cases it appears to either make no difference, or may even be beneficial with regard to strength, bubble surface stabilization, and inhibition of coalescence. If plastic microspheres are used in high-temperature matrices, their wall material will decompose, which may again be beneficial. Carbon spheres may form carbides.

The prime advantage of the process is that it does not require agitation and dispersion control -- it falls under the category of "re-melting." Another advantage is the possibility of compacting the dry mixture into a solid sample.

It remains to be seen whether the sample preparation has to be carried out in vacuum. Otherwise the air or gas trapped between microspheres and matrix granules may be another source of predispersed foam bubbles.

During the heating cycle, the gas pressure in the microspheres will rise, resulting in a sudden bubble expansion upon melting. Again, it remains to be seen if this necessitates a controlled temperature gradient arranged so that melting starts at the side of the ullage. Bubble size is again controlled by the ullage pressure.

3.3.6.1 Materials and Processes. Presently available materials for preparing microsphere foams are microballoons of glass, of epoxy, and of carbon. The glass and epoxy spheres can be used to advantage for tests and studies with low melting metals and alloys. The disadvantages are 1) limited temperature capability for more practical materials, and 2) nonwettability. The carbon spheres are a high-temperature material. However they too do not wet.

Plating Requirements. All presently available microspheres must be coated with a wettable plating in order to be accepted into a matrix. The plating may be copper, silver, nickel, which do wet and are compatible with many metal systems.

Copper Plating. Two methods have been used to apply a wettable coat of Cu to the microspheres. Electroless copper does not coat directly on some Eccospheres<sup>®</sup> (Emerson and Cuming Co.) such as FTD-202. These are glass spheres expanded by urea in a flame and treated by ion exchange to remove sodium and reduce solubility. It is conceivable that other treatments could induce wettability also. Successful Cu plating on some beads consists of:

- a. Clean beads with solvents and acid
- b. Treat with activator (palladium chloride in HCl)
- c. Rinse
- d. Treat with accelerator; heat if necessary
- e. Rinse and dry

Another less effective technique was to use electroplating over Ag. The Ag coated beads were stirred in a beaker containing 4:1:12 ratio of  $\text{CuSO}_4:\text{H}_2\text{SO}_4:\text{H}_2\text{O}$  and a flat Cu anode at the top. Heavily coated spheres sink to the bottom. Contact with the anode must be prevented also.

Silver Plating. Silver plating has been applied to all types of glass spheres using mirror plating techniques described in the Handbook of Chemistry and Physics. This method consists of reducing an ammoniacal solution of  $\text{AgNO}_3$  with sugar to form a uniform coat of silver on the glass spheres. Vigorous stirring abrades off the silver but gentle motion is necessary to prevent welding of the spheres by a film of silver.

3.3.6.2 Plain Microsphere Foam. In-Bi foam has been prepared by the following procedure. Spheres have been plated with Ag and/or with Cu to provide a wettable surface. A flux of dilute HCl is placed over the surface of melted matrix metal to remove oxide film from the coated spheres. The spheres are put into the container holding the melt. Stirring and agitation incorporates the spheres into the matrix. The spheres tend to float on the surface of the matrix after they have been wetted. Prolonged agitation or heating causes the coating to dissolve and expose the nonwetting surface of glass or resin, which induces immediate rejection of the hollow spheres from the melt.

The phenomenon of wetting does not affect the spheres once they have been immersed below the free surface of the matrix. Although nonwetted spheres are immediately rejected and float above and outside of the metal, wetted spheres are retained by surface tension at the surface and form voids within the continuous metal phase. This condition produces a surface foam stratum above the matrix. A single cycle or two of

agitation can separate the foam into matrix and naked spheres. Figure 3-36 illustrates the two conditions.

Better bonding is achieved by heating thicker coats to about 250°C. Increasing the plating thickness increases the time before rejection occurs. However the solution time will again be more rapid at the elevated temperatures when higher melting-point matrices are used. The application of Ni-plating may serve better for such systems. The thicker less soluble plating will reduce the loss of plating by (a) flux (b) matrix metal (c) abrasion and scuffing.

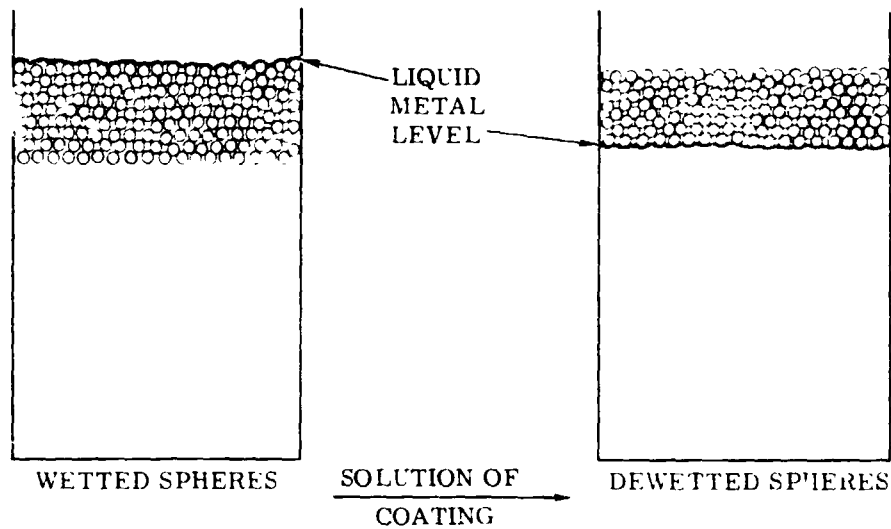


Figure 3-36. Effect of Dissolution of Metal Coatings on Glass Spheres in In-Bi Alloy

**3.3.6.3 Reinforced Microsphere Foam.** An example of In-Bi foam is shown in Figure 3-37. It consists of In-Bi matrix foam (grey areas) produced by Eccospheres<sup>®</sup> and reinforced by copper fibers. The Eccospheres<sup>®</sup> tend to cluster in aggregates, but these aggregates are dispersed throughout the melt, as are the copper fibers. The fibers and copper/silver plated spheres were stirred into molten In-Bi. The large gas voids are air entrapped during stirring. The shape of the voids is distorted by the presence of the copper fibers that tend to collect at the metal/gas interface (see Figure 3-35). The specimen showed 71% of theoretical solid density based on the weight of material used.

The best technique for use in zero-g experiments should follow the course of an infiltration experiment. Copper-plated spheres were mixed with particles of In-Bi and covered with dilute HCl. On heating the metal quickly engulfed the spheres when melting occurred. In some experiments agglomeration can produce large voids that vibration served to break up. This condition will not occur with infiltrated samples in which the spheres are close packed.

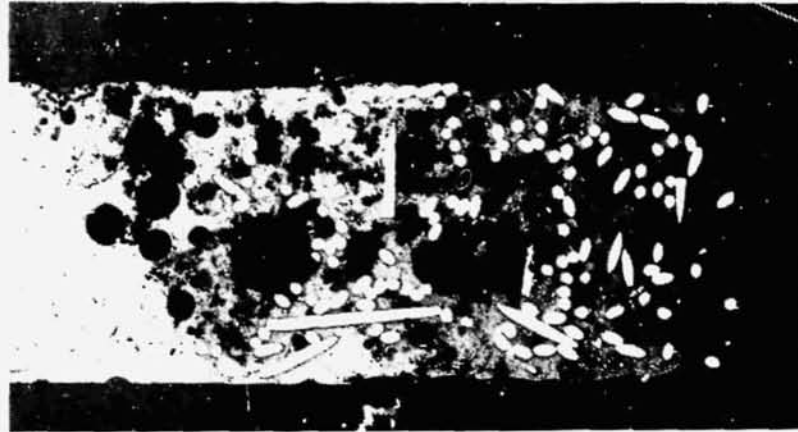


Figure 3-37. Eccospheres<sup>®</sup> (Small Dark Grey Clusters) and Gas Voids in Cu Reinforced In-Bi Alloy

**3.3.7 FOAMS PRODUCED BY FOAMING AGENTS.** This group of foams, referred to in short as "compact foams," is produced by the decomposition of solid additives during the matrix-melt cycle. The solid foaming agents are particles predispersed in the matrix metal either by solid-state compaction or by mixing into the molten matrix. Preference is given to the compaction method since it permits perfect dispersion control and lends itself well to early zero-g experiments.

#### 3.3.7.1 Materials and Process Requirements

Matrix Metals. The candidate metals selected for foaming were chosen from three groups arranged by melting point. The experiment program proceeded as a matter of convenience from foaming of low-melting-point metals such as In-Bi and Cerromatrix alloys to higher melting materials. Sn, Pb-Sn alloys, and Al alloys have been foamed; higher melting candidates of increasing melting point are Fe and Ni. Experience derived from the lower melting materials makes the investigative efforts with higher melting metals more effective.

#### Foaming Agents

Organic Foaming Agents. For low-melting-point metals, organic materials that produce gas by decomposition at relatively low temperatures have been used. These materials consisted of urea, oxalic acid, and ammonium oxalate. The gases produced by the thermal decomposition of these compounds include  $H_2$ ,  $H_2O$ ,  $NH_3$ ,  $CO$ , and  $CO_2$ . The  $H_2O$  is evolved as steam, which condenses to water as cooling occurs and allows  $NH_3$  and  $CO_2$  to dissolve in it. The resulting contraction is of no importance if the melt is cooled quickly.

The organic salts are ground to a powder before use. The presence of large crystals or nondispersed material results in the evolution of gas in bulk rather than small bubbles. Bulk gas passes rapidly to the surface and does not make foam.

Inorganic Foaming Agents. Most of the inorganic gas-producing chemicals or salts have been hydrides. The ammonium compounds  $(\text{NH}_4)_2\text{CO}_3$ ,  $\text{NH}_4\text{HCO}_3$  and  $\text{NH}_2\text{COONH}_4$  begin to decompose at about  $60^\circ\text{C}$ , which is too low for foaming metals. The hydrides used in the laboratory have been  $\text{CaH}_2$ ,  $\text{LiAlH}_4$ ,  $\text{TiH}_2$ ,  $\text{ZrH}_2$ ,  $\text{KBH}_4$ , and  $\text{NaBH}_4$ . Many other compounds produce gas, but either leave undesirable metals in the mix or give potentially corrosive gases such as  $\text{HNO}_2$ ,  $\text{HNO}_3$ ,  $\text{H}_2\text{SO}_3$  or  $\text{H}_2\text{SO}_4$ .

Of the hydride-type foaming agents,  $\text{LiAlH}_4$  contains the most gas ( $\text{H}_2$ ) per unit weight of the experimental compounds.  $\text{NaAlH}_4$  has a higher melting point and decomposes slower, and at higher temperatures. For foaming the higher melting metal, Al, which makes more practical foams,  $\text{TiH}_2$  and  $\text{ZrH}_2$  were used. These hydrides decompose at appropriate temperature for metals such as Al, Fe, and Ni.

Promoters. Promoters are materials that must be added to a metal matrix with the gas foaming agent to stabilize the foam. They probably serve to increase the viscosity of the melt and to retard drainage and thinning of the film between adjacent gas bubbles so that the collapse of the foam is prevented before the bubbles are frozen in place. The mechanism of the promoter phenomenon may also be the formation of a pasty alloy at the interface between the promoter and matrix.

The promoter must melt at a higher temperature than the matrix. It must react to a slight extent with the matrix, be slightly soluble in it, or be wetted to a sufficient extent that it will be retained in the film or bubble. High melting materials that alloy slightly with the matrix are suitable. Copper has been used with In-Bi and Pb-Sn alloys. It can also be used to make Al foam. Tungsten powder can be used with iron.

Reinforcements. The replacement of material by bubbles causes a loss of strength for a given amount of matrix although the product is less dense. Some of the strength may be recovered by adding metal fibers to the matrix to help bind the structure together. The most important use of reinforcements, however, may be to prevent the escape of bubbles from the melt. Matted fibers distributed in the matrix act to entrap the bubbles that are generated and retain them at the site.

#### Procedure

An effective procedure has been developed to obtain satisfactory foams. Improved foams will result by optimizing the variables in the following preparation, but probably not by changing the method:

- a. Powder or grind the solid matrix.
- b. Powder or grind the foaming agent.
- c. Mix the matrix and foamer intimately.
- d. Mix in reinforcements, if used.

- e. Compact the mixture.
- f. Heat compact to sintering temperature in mold.
- g. Raise temperature to form gas bubbles and foam.
- h. Program temperature rise rate and time at final temperature according to product.
- i. Quench sample and remove from mold.

Photographs of foams produced by this procedure are shown in Section 3.3.7.3.

### 3.3.7.2 Gas Evolution

#### Kinetics of Gas Evolution

The use of salts requires knowledge of the decomposition mechanism. The general form of the typical decomposition curve and the individual phases of decomposition are shown in Figure 3-38.

$\text{LiAlH}_4$  shows all the points of the typical curve, but in some salts steps may be missing. The particle size for example will greatly affect the distribution of particles in the melt and the rate of evolution of gas. It does then not proceed at a purely mathematical speed. The rate of formation of nuclei at which dissociation occurs may be zero, constant, proportional to the time, or the  $(\text{time})^2$ . Chain reactions on the decomposing surface or the effect of product accumulation may hasten or slow the reaction. The significance of these properties is that it will be difficult to select salts as foam formers on a systematic basis. The property data and chemical behavior of appropriate salts have to serve merely as guidelines in finding a suitable material by empirical methods.

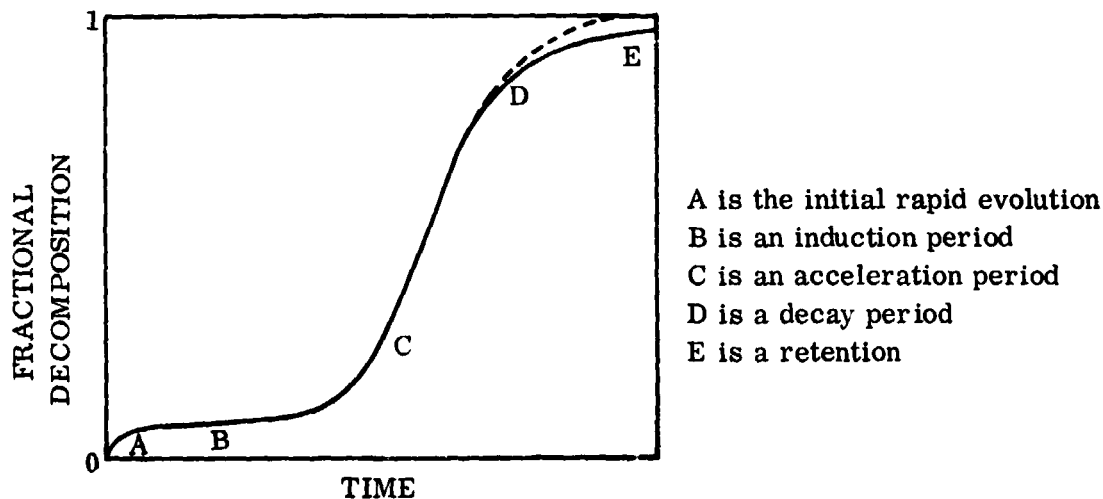


Figure 3-38. The Generalized Isothermal Decomposition Curve

## Gas Evolution Experiments

Studies were undertaken to determine the kinetics and nature of the decomposition of the gas producing agents. Among the variables investigated were:

- a. Lowest temperature at which gas evolution is beginning or is significant.
- b. Maximum volume of gas evolved.
- c. Amount of gas per unit weight of compound.
- d. Volume of gas versus time at constant temperature.
- e. Volume of gas versus time at a given heating rate.

Apparatus. The apparatus used to evaluate the decomposition kinetics of organic salts that decomposed at a low temperature is shown in Figure 3-39. It consists of:

- a. A heating pot containing lead alloy.
- b. A Fyrex reaction vessel for receiving the salt to be decomposed.
- c. An addition bulb attached to the reaction vessel at an angle through a standard taper ground glass joint. Rotation of the addition bulb causes the salt to fall into the preheated reaction vessel.
- d. A calibrated, air-jacketed gas burette to receive and measure the volume of gas evolved.
- e. A leveling bulb containing mineral oil to equalize the gas pressure inside and outside the apparatus.

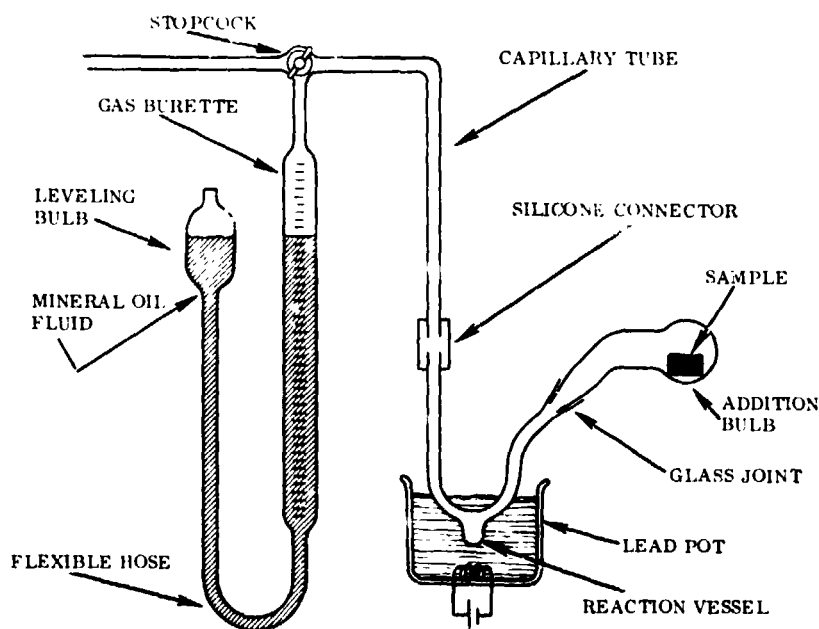


Figure 3-39. Thermal Decomposition Apparatus

Temperature control is achieved by enclosing the gas burette within a glass tube stoppered at both ends, which insulates the gas chamber from the ambient atmosphere. A heavy-wall capillary tube is used to connect the gas chamber to the reaction vessel.

Sample Preparation and Handling. The rate and amount of gas evolution were measured as follows. A sample of salt of appropriate size was weighed out accurately into a 1-mil gage tinfoil formed into the shape of a vial. The foil acts as a capsule when the ends are folded and twisted shut. This method allows the quantitative transfer of a salt sample from the addition bulb to the reaction vessel. Also, by enclosing the salt in the foil, premature sublimation or vaporization of the only partly decomposed salt from the reaction zone is suppressed. Loss of material before decomposition is complete constitutes a source of error.

The apparatus was modified for decomposing the more stable salts by making the reaction vessel shown in Figure 3-40. For materials of higher melting temperature, such as Al, it was convenient to use induction heating. The induction coil heated a carbon susceptor in which a stainless steel susceptor containing the sample salt was located. Temperature was measured with an iron-constantan thermocouple. The apparatus was purged with argon before an experiment because the decomposition gas  $H_2$  reacts with  $O_2$  above  $500^\circ C$ . The experiment was begun by dropping the sample into the apparatus which was then closed with a stopper.

Gas Evolution Measurements. There is an initial induction period during which the sample warms up, then a fast reaction period during which most of the gas is evolved. The rate of gas evolution gradually slows after the rapid reaction is over. Many organic materials decompose over a range of temperatures or at various rates depending on the temperature level of the decomposition. It is reasonable that the decomposition of such materials should be studied at constant temperature for various temperature levels. In almost all such reactions, the change is irreversible and increasing the opposing pressure does not cause the original materials to appear.

By lifting the gas leveling bulb to the height of the three-way stopcock, the liquid in the gas burette displaces all the gas and brings the pressure within the system to equilibrium with the atmosphere. The heating bath is then raised to immerse the open reaction bulb in the molten lead alloy. When the temperature of the bulb reaches that of the alloy, the addition bulb is inserted into the ground-glass joint and rotated to cause the salt sample to fall into the reaction vessel. The stopcock is turned so that the gas enters the burette and the pressure in it is equalized by lowering the bulb as gas is collected.

A different type of reaction is exhibited with many inorganic salts. The reaction in many cases is reversible. Sometimes, as with many hydrates, the specific equilibrium composition depends on the opposing partial pressure of gas evolved. With other solids, such as metal hydrides, a series of definite degraded products is formed or a mixture

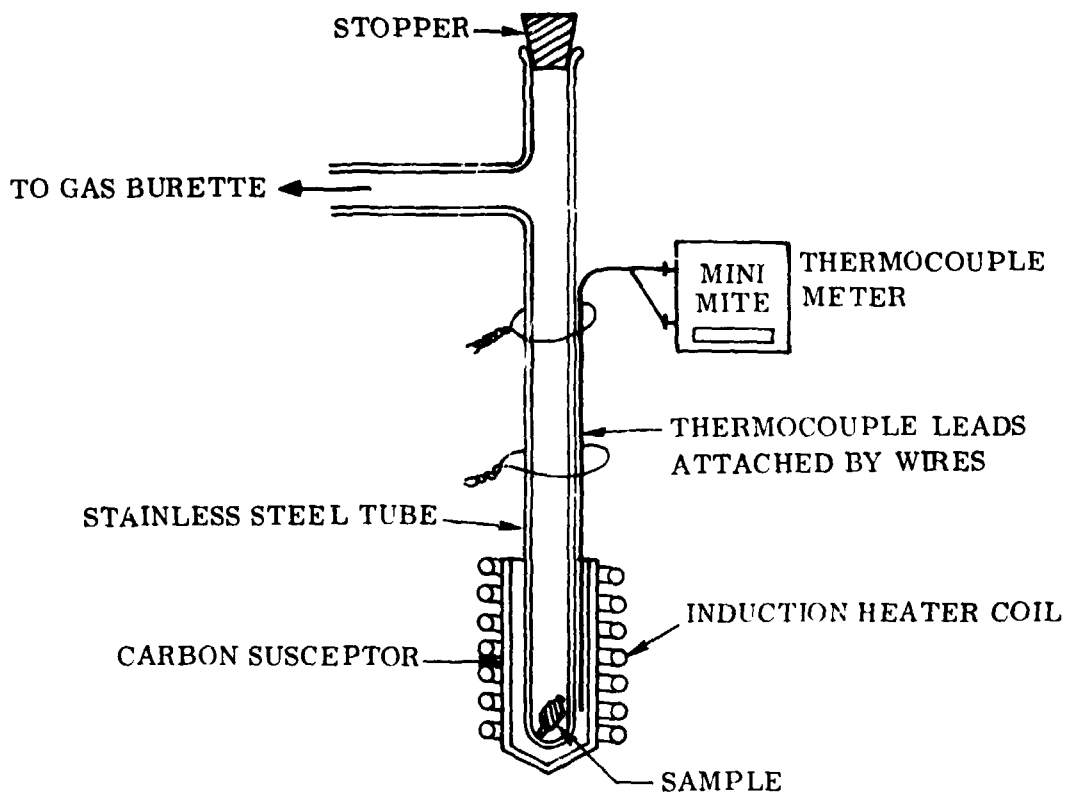


Figure 3-40. High-Temperature Salt Decomposition Tube

of intermediates of indefinite composition is produced. An appropriate way to study the latter materials is to subject them to programmed heating rates and measure the amount of gas evolved as the temperature rises. At atmospheric pressure, the evolved gas leaves the site of reaction so that the salt undergoes decomposition until none is left. In our experiments, the gas was collected in the same apparatus as before. The heating was performed crudely, but in a consistent way with a Meker burner. The amount of gas that had been evolved at various temperatures was then measured.

Three to eight determinations were averaged to obtain any given result. No special precautions were taken to purify the salts. Indeed it was found that samples of borohydrides from different zones in the container gave varying results as well as exhibiting varying activity with water. At least the surface must therefore have deteriorated. Tubes of copper first used as sample containers because of its thermal conductivity had to be replaced because of its reactivity with  $H_2$ . Copper oxide was always present.

The tinfoil used to contain and transfer the sample was not entirely inactive and undoubtedly affected the results.

**Results — Urea.** It requires about one minute of induction period before significant gas is evolved from urea. Between two and six minutes, the reaction is very rapid and the greatest quantity of gas is evolved during this period. The increase in volume is insignificant after 30 minutes. Care must be taken to prevent loss of material from the reaction vessel during heating or low results are obtained.

About 150 cc of gas per gram of urea can be expected in the first five minutes — a practical processing time. A plot of typical data for a temperature of 200°C is shown in Figure 3-41.

As the temperature of the reaction vessel changed from 200° to 250°C, the amount of gas collected increased to 280 cc/gm, and this was evolved in the shorter time of five minutes. After 30 minutes, the amount of gas in the burette had decreased to 180 cc/gm. This change occurred because ammonia, a definite reaction product (odor, litmus paper), dissolved in H<sub>2</sub>O, which was also a possible reaction product. Figure 3-42 illustrates the reaction. It is evident that at the higher temperature, a larger volume of gas is evolved in a shorter period of time. The volume of gas decreases after about five minutes, however, because of chemical recombination so that after 30 minutes the volumes of gas evolved in the decomposition are about the same per gram of reactant.

**Results — Oxalic Acid.** Oxalic acid was decomposed at 200°, 250°, and 300°C. Under the conditions of the experiment and in the apparatus provided, the amount of gas evolved at 200°C averaged out to 233 cc/gm. The range was from 190 to 300 cc/gm. This large range was caused by loss of material during the initial heating period. Some sublimed and deposited in cold parts of the apparatus such as the capillary tube or the sample bulb. The method of enclosing the sample in tinfoil also affects the time before substantial amounts escaped the reaction zone. Loose wrapping allowed too easy an escape, but tight wrapping

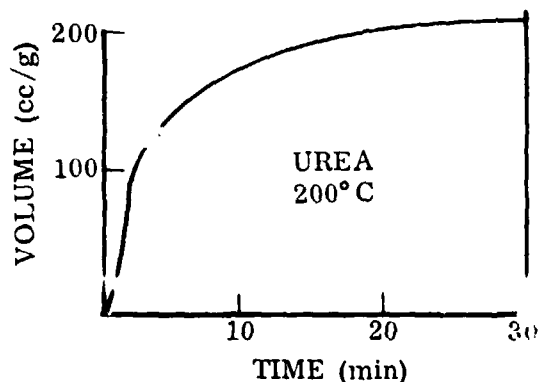


Figure 3-41. Gas Evolution of Urea at 200°C

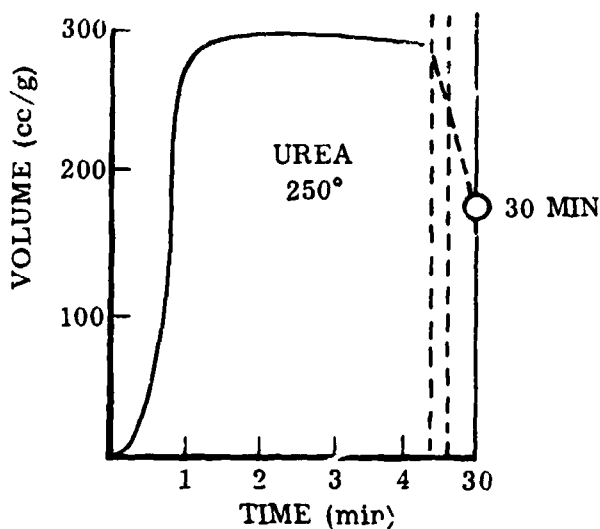


Figure 3-42. Gas Evolution of Urea at 250°C

caused the foil to rip open from gas pressure with the same low results. Hence, the yield range is 225 to 250 cc/gm at 200°C.

At 250°C the yield is not very different from the urea results. About the same total gas is evolved as at 200°C and most of it comes off in the first four minutes.

At 300°C the amount of gas evolved is considerably reduced because the higher temperature causes the salt to be lost by volatilization out of the reaction zone before it is decomposed. The amount of gas captured is about 25% less, but this is because reaction is incomplete. As before, however, the reaction is fast after about one minute of induction and is essentially complete in four minutes.

Results — Ammonium Oxalate. Ammonium oxalate at 300°C decomposed with a pattern similar to oxalic acid at the same temperature. The induction period, a heating-up time is about one minute. Reaction is essentially complete in two minutes and after four minutes, contraction caused by cooling of evolved gas and solution of ammonia gas in water is well underway. For preparations of foam that are complete in less than this time, the contraction is of no consequence.

Results — Hydrides. Calcium hydride is an inorganic salt and decomposes faster with rising temperature. The decomposition temperature was limited by the temperature capabilities of the flame — a Meker burner was used because the electrical heater lacked capacity. The following table presents the data for the decomposition.

Temperature		Time (Min)	Volume	
(°F)	(°C)		(cc)	(cc/gm)
480	249	0	0	0
520	271	1	0.5	5.3
700	371	2	6.0	64.0
950	510	3	10.0	107
1120	604	4	10.6	113
1280	693	5	11.3	121
1340	727	6	11.8	126
1355	735	7	12.2	130
Volume at 22°C			9.2	98.2

The volume of gas available from the total decomposition of  $\text{CaH}_2$  is 532 cc/gm at standard conditions. The low value confirmed visual observations that the material had deteriorated from age. The rapid decomposition occurred between 300° and 500°C with this salt.

Results -  $\text{KBH}_4$  and  $\text{NaBH}_4$ .  $\text{KBH}_4$  and  $\text{NaBH}_4$  behaved similarly to  $\text{CaH}_2$ . The induction period for  $\text{KBH}_4$  was three minutes before rapid gas evolution occurred. The temperature at which rapid decomposition begins is about  $600^\circ\text{C}$ . The total gas evolved was 600 cc/gm. Complete decomposition to  $\text{H}_2$  calls for 832 cc/gm. Therefore, 72% of the theoretical amount of gas was obtained.

$\text{NaBH}_4$  decomposes at a fairly steady rate as temperature increases. Its induction period is shorter and the end of decomposition was not apparent when the temperature reached the limit attainable with the burner.

The amount of gas obtained from  $\text{NaBH}_4$  averaged 252 cc/gm at room temperature. Theoretical is 1133 cc/gm - again confirming visual observations that the material had deteriorated.

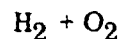
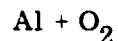
Results  $\text{TiH}_2$ . The  $\text{TiH}_2$  decomposition temperature is higher than that of the salts previously discussed. Side reactions and phenomena occur whose elucidation was beyond the scope of the present work. The hydrogen evolved could react with unstable oxides (such as  $\text{CuO}$ ) with contaminating oxygen gas or with metals. It could react reversibly on cooling and could diffuse readily through the connecting tubing. Decompositions performed in copper tubes resulted in negative pressures on standing because the  $\text{H}_2\text{O}$  formed and exhibited pressure during the heating cycle but later diffused out of the reaction zone and condensed in the cooler portions of the apparatus.  $\text{TiH}_2$  could also re-form when the apparatus cooled from high temperatures.

The apparatus and techniques described reduced but did not eliminate the errors. Procedures used were consistent with those that would be used in producing foam, but did not entail the meticulous attention to detail required for a kinetic study.

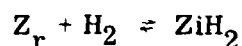
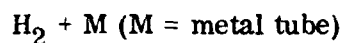
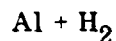
Under the previously stated conditions,  $\text{TiH}_2$  decomposition was found to begin at about  $600^\circ\text{C}$  and proceeded quite rapidly at  $650^\circ\text{C}$ . The amount of gas evolved ranged from 142 to 178 cc per gram or about 38% of the theoretical possible. The gas evolution proceeds steadily, and at a temperature of 650 to  $700^\circ\text{C}$  the decomposition is essentially complete within two minutes - although more gas comes off slowly as the temperature increases. The gas evolution profile is therefore similar to Figures 3-41 and 3-42 and will not be repeated.

Results -  $\text{ZrH}_2$ .  $\text{ZrH}_2$  decomposition is more regular than the  $\text{TiH}_2$  reaction; it did not exhibit as rapid an acceleration at the decomposition temperature. There was also a greater pressure drop on cooling, perhaps by a reversal of the decomposition. Aluminum capsules were used as containers at higher temperatures; consequently, the foil could possibly react with some of the evolved gas. In brief, the side reactions might be listed as

a. Oxygen reactions



b. Hydrogen reactions



c. Hydrogen diffusion

By using inert gas environment, clean tubes, small sample containers, careful manipulations, and tight seals for the rubber tubing, the known problems were minimized and the following data obtained.

The amount of gas evolved from  $\text{ZrH}_2$  varied from 42 to 102 cc/g. The average expected volume is 80 cc/g or 33% of the theoretical. The initial temperature of decomposition is 600 to 650°C as for  $\text{TiH}_2$  but the very rapid acceleration stage does not appear. As the temperature is increased more gas is evolved. This characteristic suggests it might be preferable for use with Fe and Ni rather than  $\text{TiH}_2$ .

For the majority of compounds it was not instructive to plot the volume of gas versus temperature for a programmed change of temperature because a rapid and essentially complete decomposition occurred in a very narrow temperature range.  $\text{ZrH}_2$  behaved differently as shown in Figure 3-43.

The curve shows that there is a temperature at which the decomposition accelerates — at about 600°C. The gas evolution rate decreases above 700°C and remains approximately steady until about 950°C. Note that the curve for volume is exaggerated because it represents measured gas and contains no correction to standard conditions for the high-temperature gas contained in the reaction zone. At about 950°C, the temperature rise rate begins to flatten out but the measured gas volume decreases at a steady rate. This temperature therefore represents the beginning of a reaction or process that removes  $\text{H}_2$ . It was not further investigated but could represent reaction with Al foil in the system or with the steel tube or diffusion into the steel or through a flaw or weld that sealed the end of the tube.

Summary of Results. The decomposition parameters sought were:

- a. Maximum volume of gas evolved.
- b. Volume of gas evolved per unit weight of salt.
- c. Volume of gas versus time at a given temperature.

REPRODUCIBILITY OF THE ORIGINAL PAGE IS POOR.

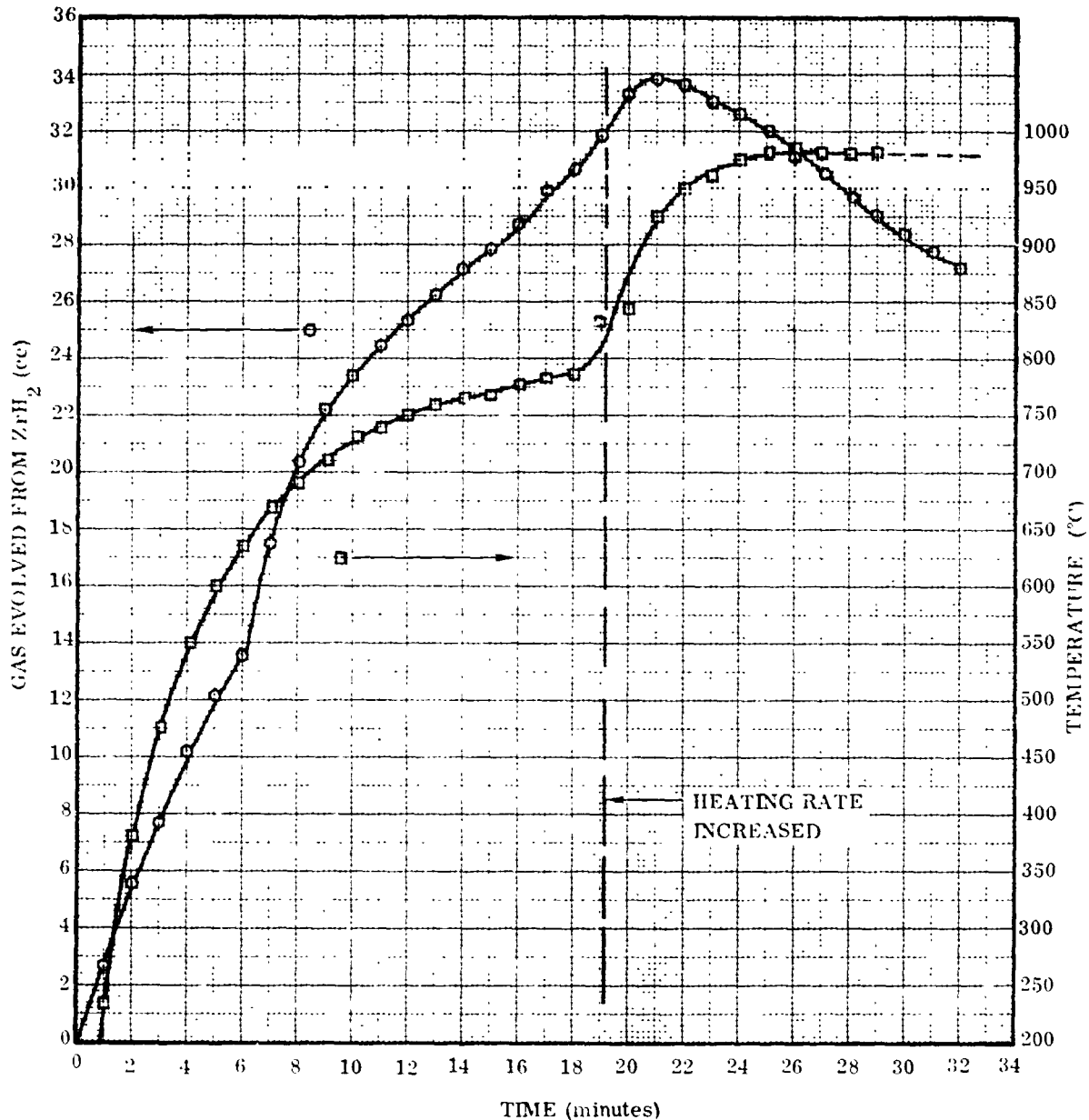


Figure 3-43.  $ZrH_2$  Decomposition Versus Time and Temperature

- d. Volume of gas at various given temperature levels.
- e. Volume of gas versus time as programmed temperature changed.
- f. Lowest temperature of evolution.

Because most of the compounds investigated decomposed rapidly at a given temperature, the only relevant parameters are a, b, and f. Parameter e was applicable to  $NaBH_4$  and  $ZrH_2$ , but the  $NaBH_4$  data is flawed because the sample had deteriorated. The parameter e is given for  $ZrH_2$  in the curve in Figure 3-43. The remaining results are summarized in the following table where parameters a and b are combined.

<u>Name</u>	<u>Volume (cc/g)</u>	<u>T<sub>min</sub> (°C)</u>
Urea	>150	200
Ammonium oxalate	187	<300
Oxalic acid	225	200
CaH <sub>2</sub>	98	450
KBH <sub>4</sub>	600	600
NaBH <sub>4</sub>	>>300	290
LiAlH <sub>4</sub>	—	130
TiH <sub>2</sub>	150	640
ZrH <sub>2</sub>	80	600

Accurate data for the moisture sensitive LiAlH<sub>4</sub>, CaH<sub>2</sub> and KBH<sub>4</sub> are not available because these salts were not fresh. The decomposition temperature of KBH<sub>4</sub> is much too high; the gas volume for CaH<sub>2</sub> is much too low and is not given at all for LiAlH<sub>4</sub> because the material is not representative.

Conclusions. The results of the measurements made on foaming materials shows that the preparation of metal foams is entirely feasible. Details of optimizing the process through selection of appropriate combinations of matrix materials, promoters, and gas formers remain to be worked out. Tests should be made to determine whether stirring in the foaming agents at zero-g will make good foams. In gravity, the stable foams are best prepared by sintering the materials, melting, and quickly quenching the product. It would be desirable to omit the sintering step.

The amount of salt required to generate sufficient gas for foaming is truly minute. Thus the volume of a ton of aluminum could be increased three-fold by a little over 6.3 lb of LiAlH<sub>4</sub>. Only 0.05% Li as a contaminant would be contained in the product if this occurred.

The choice of foaming agents and promoters is important for each product. The gas must normally be generated above the melting point of the matrix. If the temperature is too low, the gas escapes before bubbles can form. If the temperature is too high before gassing occurs, the melt becomes too liquid and the bubbles from the foaming agent quickly coalesce because of the low viscosity so that the product is inferior.

Another parameter that must be controlled is the size of the salt particles. These particles must be very finely powdered because each is the nucleus of a gas bubble. Course particles produce inferior foam containing large bubbles; they may also cause the coalescence of gas and disengagement of gas from the matrix. The foam, if formed, would then collapse.

Reinforcements can be added to foams for two reasons, to strengthen the matrix and to act as a promoter for enabling the foam to be produced.

In summary, foamed metals are entirely feasible as zero-g products. Bubbles can be generated in metals. These will be stable in zero-g. The factors that must be controlled to attain a successful product are the choice, amount, and size of gas former; choice, amount, and size of a promoter; process temperature; process time amount and kind of stirring; and processing by melting and by sintering.

### 3.3.7.3 Preparation Techniques

#### Procedures

The technique used to prepare a metal foam depends on the properties, physical state, and reactivity of the material. The important parameters are the melting point range of the metal matrix; its viscosity, surface tension, and density; and its compatibility with the foaming agent and with the promoter.

Pure metals alone do not foam, although a few bubbles can be trapped by rapid quenching. A more efficient way is to use an alloy with a wide pasty range and/or a high viscosity. The gas bubbles are then generated in place from gas-producing compounds. The foam structure is stabilized against collapse by additives or procedures that prevent the coalescence of bubbles and the drainage and thinning of the walls of the foam. The method might include any or all of the following:

- a. Lowering processing temperature to increase the melt viscosity.
- b. Selecting compositions with wide range of semiliquid phase.
- c. Adding "promoters" that
  1. Increase viscosity.
  2. Affect pasty range.
  3. Retard drainage from walls.
  4. Provide solid attachment points for the "bubbles."
- d. Sintering the metal/salt mix then melt.

Pb-Sn Alloys with a wide pasty range can be made to incorporate gas but the preparation is not very satisfactory.

Cerromatrix, a commercial alloy with a melting range of 98° to 277°C, is very useful for investigative purposes because it begins to fuse below the boiling point of water, has a wide semiliquid range, and can be used with organic gas formers that decompose at lower temperatures than necessary with more practical materials.

The size of the bubbles is greatly determined by the viscosity. Tests with synthetic foam showed that a liquid with a medium viscosity gave the best results and the most uniform bubbles. If the viscosity is too low, many bubbles are formed and they are large. They arise fast and quickly collapse. The size of bubbles is also regulated by the size of the gas-forming particles. Smaller bubbles are produced by finer particles. The surface tension, density, and chemical reactivity determine the quality of the product especially for reinforced foams. Reinforcements must be wet by the metal matrix — a function of surface tension and surface condition — but the wetting must not be so thorough that it leads to solubility or reaction.

Two general methods may be used to produce foam:

### I. Premelt Technique

Foaming by Submerging the Foaming Agent. Submerging a gas-forming salt beneath the surface of a molten metal alloy is ineffective because the gas evolves in bulk and is not dispersed into fine bubbles. Commercial foams have been made by vigorously stirring the foaming agent into the molten metal.

Submerging Foamer Plus a Promotor. A promotor is a material that:

- a. Can be wetted by the matrix metal.
- b. Has a melting point more than 100° C higher than the matrix metal.
- c. Is slightly or slowly soluble in the matrix metal.

It is most effective when added to the melt at the same time and place as the foaming agent. One may submerge a gas-forming salt containing a promotor beneath a molten metal such as Sn and quench rapidly as soon as the salt has reached the bottom of the melt. This technique showed foam could be prepared but the following was necessary:

- a. Better control of bubble size.
- b. Better control of bubble location.

Add Foamer and Promotor in a Foil of Matrix Material. One may add the salt former plus copper promotor in a tinfoil capsule to the melted tin. This attempt to control the heating and gas discharge rate does not greatly improve the gas distribution. Heating powders is not a good technique because 1) metal tends to ball because of surface tension, 2) foam gas blows out, 3) foam is a poor conductor (if the temperature gradient is large the foam will not be uniform), and 4) powder causes interconnecting porosity.

### II. Premix Technique

There are several variations to this approach. A sintering or compaction step precedes the heating as follows.

One may mix the powdered metal with the gas foamer or foaming agent and promotor; press, sinter, and heat to melting. This technique predisposes the foaming agent so that when the gas is evolved the bubbles are dispersed throughout. The powdered metal will normally be coated with oxide. The oxide forms an internal network that tends to stabilize the structure. Temperature control is also easier with this method.

Cerromatrix alloy produces a good foam when this technique is used. It has a wide melting range and incipient melting occurs just below the boiling point of water. The alloy is powdered, mixed with foaming agent, pressed and sintered in boiling water. This method allows good consolidation and easy temperature control below the decomposition temperature of the foaming agent. Because melting of the sintered compact could be completed at temperatures of 160° to 205°C, well above the decomposition temperature, good stable foams could be obtained. Suitable gas formers for use with this alloy are  $\text{LiAlH}_4$ , ammonium oxalate, oxalic acid, and urea.

Miscellaneous Procedures. Other techniques for producing stable foams involve adding reinforcement fibers to the compact prior to sintering. The sinter-body then contains powdered forms of matrix metal, foaming agent, promotor and reinforcing fibers. Copper-beryllium wires are suitable reinforcements, but any high tensile wire compatible with (wetted by) the matrix can be used.

### Results

A number of observations can be made from the foaming experiments. The resultant microstructures were similar regardless of the foaming agent used. Many large voids were present, probably not because of the agglomeration of bubbles but because of inadequate comminution and dispersion of the foaming agents (Figure 3-44). The thin walls between adjacent voids seen in Figure 3-45 show that the driving force for the voids to coalesce is not too great. The void shape changes with the foaming temperature used on the alloy (Figure 3-46). At the low end of the melting range the high proportion of solid phase restricts the spherical expansion of the gas bubbles and causes them to deform ( $T_1 - A$ ).

At higher temperatures ( $T_2 - A$ ) the voids are freer to expand and become more spherical but are still trapped in place by the solid phase. Near the liquidus temperature, because of lower viscosity, or more likely, the absence of a sufficient network of the solid phase, the gas will segregate out of the melt and the foam collapses ( $T_3 - A$ ).

A foam reinforced with Cd plated Be-copper shows a similar random void shape and distribution ( $T_1 - B$ , Figure 3-46, and Figure 3-47). At intermediate temperatures, when more movement is possible, the fibers and voids tend to join up where possible ( $T_2 - B$ ). Significantly, at the temperature ( $T_3$ ) when the unreinforced foam collapsed, the reinforced foam remained stable and well distributed ( $T_3 - B$ ). No signs of gravity segregation are evident.

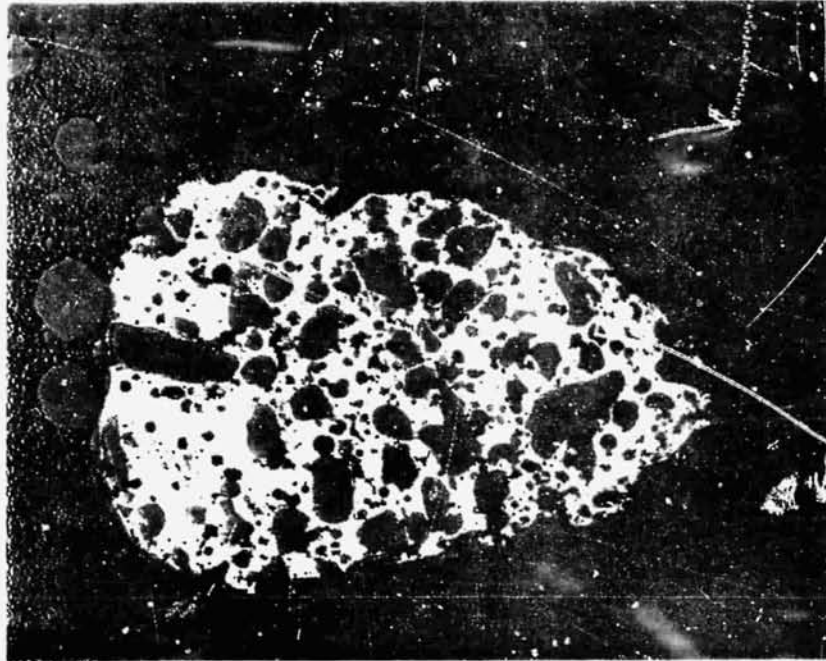


Figure 3-44. Foamed Cerrmatrix Sample (larger voids filled with resin to facilitate metallography)

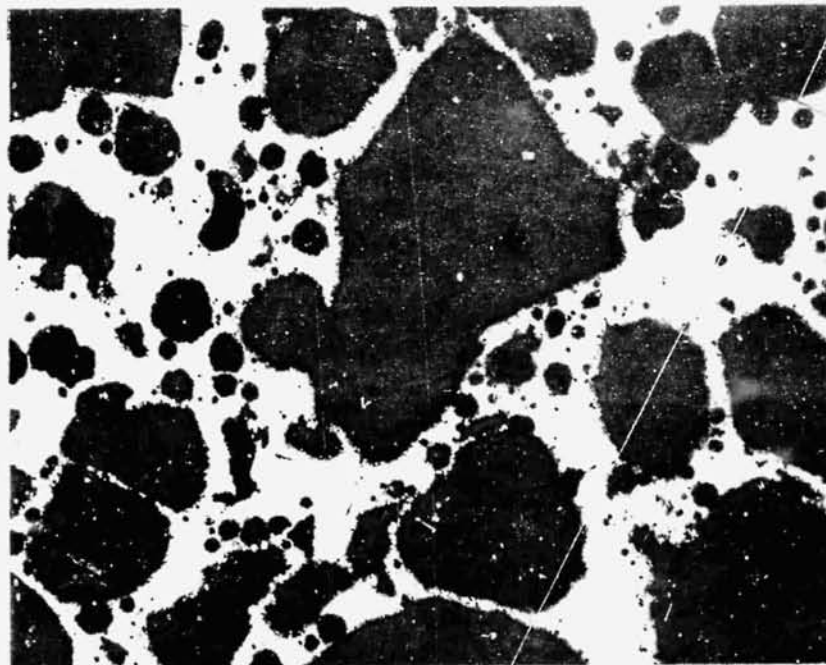


Figure 3-45. Thin Walls Between Voids (from Figure 3-44)

REPRODUCIBILITY OF THE ORIGINAL PAGE IS POOR.

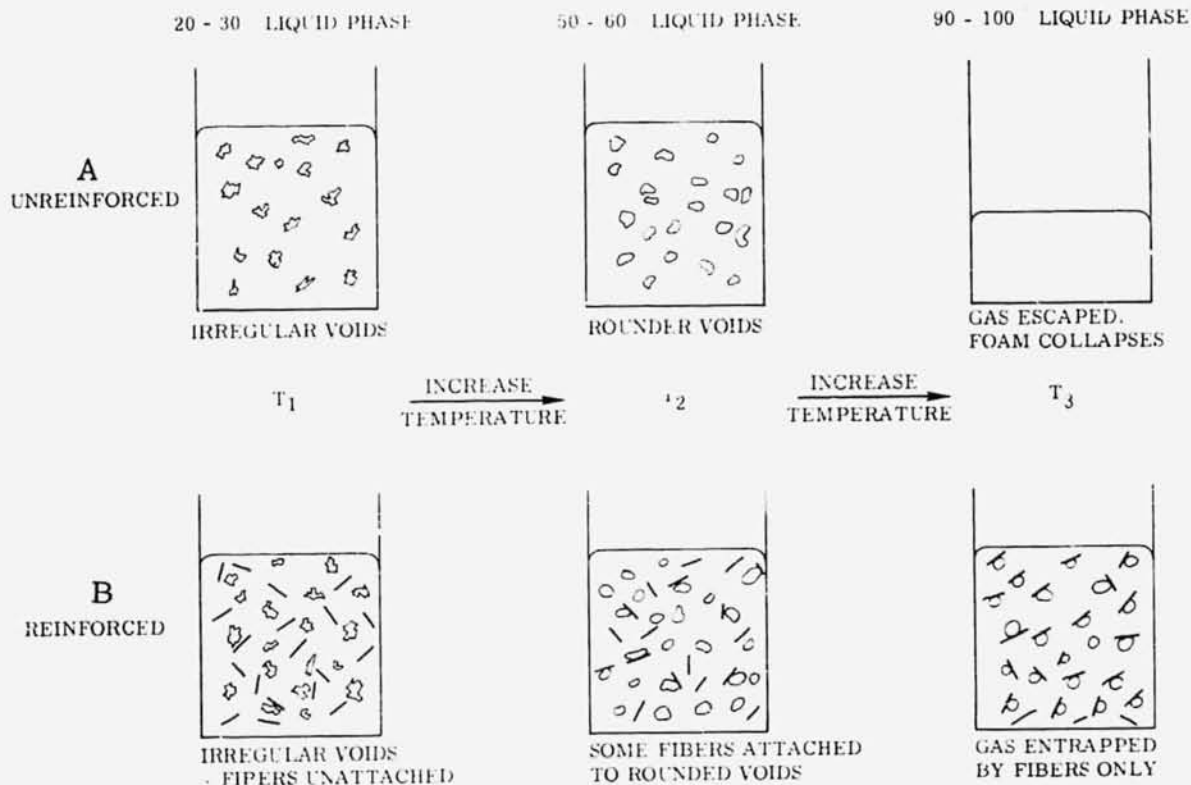


Figure 3-46. Effect of Temperature on Foamed Metal with Pasty Range

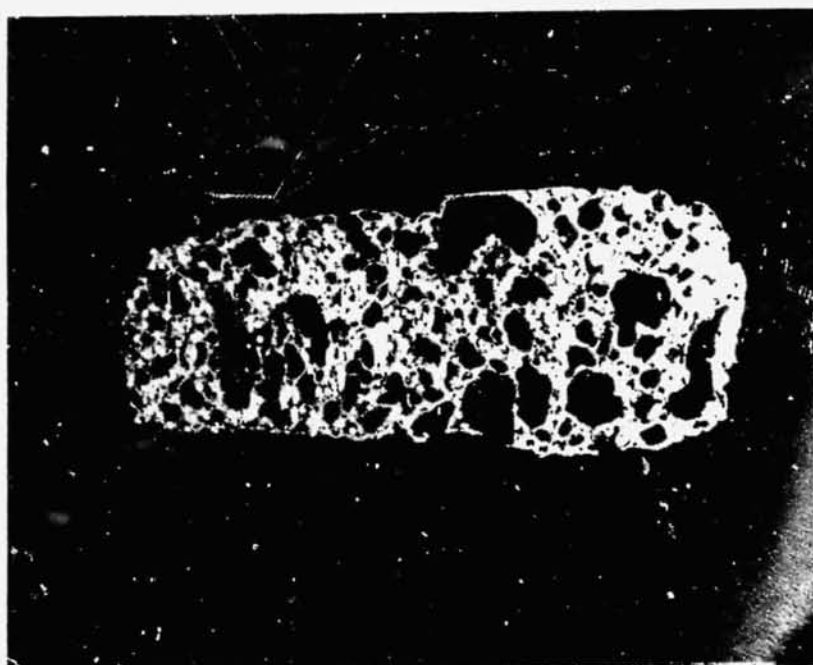


Figure 3-47. Cerromatrix Foam Reinforced with Copper Fibers

3.3.7.4 Foaming Experiments. Exploratory experiments on the generation of foams with decomposing additives were carried out, varying matrix materials, foaming agents, and processing techniques. The results and preliminary conclusions of the experimental investigations follow. The successful preparation of metal foams depends greatly on procedure and material selection. It will be suitable here to review the results of foaming experiment in the order of increasing melting point of the matrix. Plain and reinforced foam experiments are reviewed.

#### Plain Cerromatrix Foam

The earliest experiments were done with microspheres. These experiments have already been described. Other experiments were performed using the foaming agents  $\text{LiAlH}_4$ , urea, oxalic acid, and ammonium oxalate. The procedure used was to make filings of Cerromatrix alloy, mix with the foaming agent, press in a vise, and then heat. Using this technique the results were:

With  $\text{LiAlH}_4$ . Heated to  $103^\circ\text{C}$  then quenched in water. Porosity was evident. Much black powder formed from  $\text{LiAlH}_4$  decomposition. Samples quenched under water and in a glass container looked the same. Reactive material remained in the pores of the sample, which was quenched in glass. Adjacent bubbles exhibited thin walls (Figure 3-45).

With Urea. Used technique above. Some porosity was exhibited, but the  $130^\circ\text{C}$  maximum heating cycle was insufficient for this compound.

With Oxalic Acid. Used technique above. Some porosity was achieved, but the heating cycle to  $171^\circ\text{C}$  maximum was insufficient. Voids were large and irregular. A micro-photo of an unfoamed specimens showed that the salt agglomerated during mixing in a mortar.

With Ammonium Oxalate. Used same technique but heated to  $191^\circ\text{C}$ , which caused loss of salt by vaporization (white fumes) but gave a good foam with rounder bubbles because of the higher temperature. Much salt remained after the quench. When heated to  $210^\circ\text{C}$  at which the metal is virtually melted, the gas escapes and the foam collapses.

A second technique, in which ammonium oxalate was dissolved in water and mixed with Cerro-matrix powder, then the water evaporated, the mixture dried in a vacuum oven and heated to  $177^\circ\text{C}$ , resulted in a slight oozing of liquid. The porosity was distributed quite evenly but was interconnected and flat rather than bulbous. Ball milling would be a better method for comminution.

#### Reinforced Cerromatrix Foam

With Ammonium Oxalate. Cd-plated Be-Cu wires measuring 0.005 by 0.100 inch were mixed, pressed, and sintered at  $102^\circ\text{C}$ . The specimen was then heated in glass

at 210° C. Some gas escaped; foam and voids were present. The fibers were well distributed.

The same experiment performed with no reinforcements failed because all the gas escaped. This action emphasizes the fact that foam bubbles can be trapped by reinforcing fibers in a process which is doubly beneficial.

#### In/Bi Foam

With Urea. Urea was placed in In/Bi foil. The alloy was melted, and a fine wire screen was used to submerge the urea foaming agent. Gas was trapped by the screen and collected into large bubbles that escaped around the sides.

Most of the In/Bi work was done with microspheres reported in Section 3.3.6.

#### Plain Sn Foam

Preliminary studies were made on a glass slide.

A. Micro Experiment. Mixed 325 mesh Sn with 12 volume % urea and 12 volume % Cu powder. Placed between glass slides and heated.

Results: 1. Urea melts.  
2. Urea sublimates and decomposes to form gas.  
3. Sn melts and system is quenched fast.

A dispersion of gas in metal forms for a fleeting period of time. If the quenching is not quickly done, the gas escapes and the tin fuses into little balls of solid. This emphasizes the importance of programming the temperature. The Cu acts as the promotor.

B. Mixing experiments. Used 4.3 gm 325 mesh Sn, 0.015 gm urea and about 50 volume % 325 mesh Cu in foil. Added foil-wrapped urea-tin mixture to Sn at 238° C.

Results: 1. Bubbles are small.  
2. Gas evolution is controlled only fairly.  
3. Bubbles not well distributed - mostly at the top.  
4. Better mixing required.  
5. 325 mesh may be a poor choice. Even the pure material has voids when melted.  
6. If the temperature rises excessively, gas is evolved too fast and the foam package floats to the top.  
7. Grinding the components together before adding to molten Sn improved the preparation very little.  
8. Stirring during addition improved the preparation very little.  
9. Increasing the viscosity by using the alloy 25 Sn/75 Pb gave some porosity throughout the sample.

10. Ammonium oxalate results are the same as urea results.
11. Compacting the urea-Cu mix did not improve results.
12. The course of reaction in argon was the same as in air.
13. If too much Cu was added and mixing was poor, Cu was visible around voids.

Conclusions:

1. The bubble size must be reduced by optimizing the size of particles of foaming agent.
2. Bubble distribution must be improved by:
  - a. Precise temperature control.
  - b. Optimized agitation and stirring.

Reinforced Sn Foam

Procedure A: Compact the ammonium oxalate foaming agent with 325 mesh Cu promotor. Prepare a composite of 5- by 100-mil Cu wires in pure Sn. Remelt the composite and pour into a warm tube containing the foaming package.

Result: The Cu wires dissolved in the Sn.

Procedure B: Make a compact of Cu reinforcements with Sn powder, and ammonium oxalate powder with Cu promotor. Compact with and also without flux, then heat.

Result: 1. Gas tends to blow out powders  
2. Cu fibers do trap gas bubbles.

Plain Al Foam

With Urea. Aluminum was melted in a stainless steel tube. Ground urea powder in a smaller horizontal tube was submerged into the melt.

Result: Uncontrollable process.

With TiH<sub>2</sub>. Using the same procedure, the process was poor and gave large uncontrolled masses of gas.

From Compacts. In small apparatus of test tube size, mixing a foaming agent into a hot molten metal yields very poor foaming results. The gas evolution accelerates rapidly and is difficult to control. The large volumes of gas combine to produce bulk gas rather than bubbles. The preferred method for study purposes is therefore to use premixed compacts in which the components have been pressed together in predetermined ratios.

With TiH<sub>2</sub>. Mixed 0.64 gm of 2024 Al filings with 0.04 gm TiH<sub>2</sub> powder and 0.08 gm reduced Cu powder, compacted the mix in a Cu tube, and heated to temperature above the Al melting point.

- Results:
1. The Al did not melt even at temperatures as high as 880°C although it sintered.
  2. The compact should be made with a single press rather than many because the ejected material breaks up. There is no cohesion at the interfaces where the compression steps were made.
  3. Powder and filing mix poorly and tend to segregate. Therefore the mix must be made portionwise.
  4. The Al has an oxide coat that must be removed because it restricts the flow and wetting properties of the metal and interferes with the foaming process.
  5. Argon used to blanket the experiment was not effective. The fire system must be enclosed.

A typical result is shown in Figure 3-48. The sample was composed of 0.52 gm 2024 Al, 0.13 gm  $TiH_2$  and 0.05 gm Cu. The  $TiH_2$  was mixed, then added portionwise to the Al filings and compressed to 5000 psi. The sample was placed in a carbon susceptor located in a one-inch-diameter Vycor tube suspended inside the heating coil of an induction heater.

The induction coil was energized so that the temperature rose to 930°C in one minute. In 95 seconds the sample began to melt as shown by observation in a mirror set below the coil. The top of the compact expanded first then the bottom which was resting on the cooler surface of the Vycor tube, melted and the sample spread out. Argon gas blanketed the top of the 28 cm tube which was open to air. The heat cycle was stopped as soon as the sample melted.



Figure 3-48. Typical Result with  $TiH_2$

Discussion: The voids produced were not round, and many were interconnected. The strongest structure will have round, small, separate unconnected bubbles with thin walls. The most desirable foaming agent will be easily dispersed in Al and will decompose at a temperature just above its melting point. An iron or tungsten stirring spatula would help in attaining good bubble distribution.

#### Miscellaneous Al Foam Experiments

Experiments were performed with other alloys of aluminum and with  $ZrH_2$ . The objective was to find an aluminum alloy with flow properties conducive to forming foam at the melting point. The alloys contained Si, Mg, and Cu and were used in the form of filings, single rods, powder, and turnings.

Results: The aluminum foams produced contained about 25 to 30% voids. In most cases the product was hard and seemed to have reacted on the surface.

$ZrH_2$  does not change the course of the foaming reaction to any marked degree. It may provide a more controllable gas production rate because the decomposition temperature is not as sharply marked as the  $TiH_2$  decomposition temperature.

#### Reinforced Al Foam

A. Al Turnings and Cu Turnings. Mixed 2.2 gm Al alloy turnings and 2.1 gm Cu turnings together. Added 0.8 gm  $TiH_2$  portionwise to the Al-Cu mixture and compacted into a copper tube. Heated tube in a carbon susceptor located inside the coil of an induction furnace. When activity ceased (no fumes) the Cu tube was quenched in water and sawed in half.

Results: Some unalloyed fibers remained in the bottom of the tube, but most had been dissolved in the melt. The volume of the sample was almost doubled by the bubbles but the bubbles were large. The Al surface of the bubbles was black. Al-Cu fusion had occurred. Too much  $TiH_2$  was present. The Cu turning reinforcements were too thin so that they disappeared into solution at the reaction temperature.

B. Al Casting Alloy and Cu in a Stainless Steel Tube in Vacuum. Mixed 1.4 gm A-356 Al alloy, 3.3 gm Cu, 1.4 gm  $TiH_2$  portionwise, compacted and placed in tube. Placed tube in carbon susceptor in a Vycor chamber located in the coil of an induction heater. Evacuated the Vycor chamber to  $1 \times 10^{-5}$  mm Hg. Heated to the melting temperature and stirred with a tungsten rod passing through a vacuum fitting attached to the chamber. Relieve vacuum with argon.

Results: The alloy easily flowed through the crimped end of the stainless steel tube. The decomposition gases ejected much of the sample. The Al sintered and became hard. Much of the Cu did not wet.

C. Al Wire, Cu Wire, Stainless Steel Tube, Vacuum. Added 2.7 gm Al wire, 0.25 to 0.38 inch long; 3.4 gm of 0.04 by 0.20 Cu wire; and 1.4 gm Ti H<sub>2</sub> portionwise to a stainless steel tube. Heat to melting as in (B) and allowed to cool. Relieved vacuum with argon.

Results: Vacuum is not appropriate for foaming under the conditions used. Spattering and ejection occurs.

The product obtained is shown in Figure 3-49. The fibers were wetted but they were too large for the size of bubbles attained. Sections of increasing magnification are shown. Bubble distribution and size is quite random. Figure 3-50 shows the result when the experiment was repeated with components that had been pickled in dilute H<sub>2</sub>SO<sub>4</sub> and the heating was begun after the vacuum had been relieved with argon.

Finally, Figure 3-51 shows the product from the experiment performed with pickling, vacuum removal of oxygen, and heating under argon in a closed system using a tungsten rod as a stirrer. Some of the foam collapsed because it could not be quenched rapidly enough. The bubbles in the upper portion were large and irregular, but those in the lower section were smaller and rounder as well as more evenly distributed. The fibers are still too long for the foam but are well wetted.

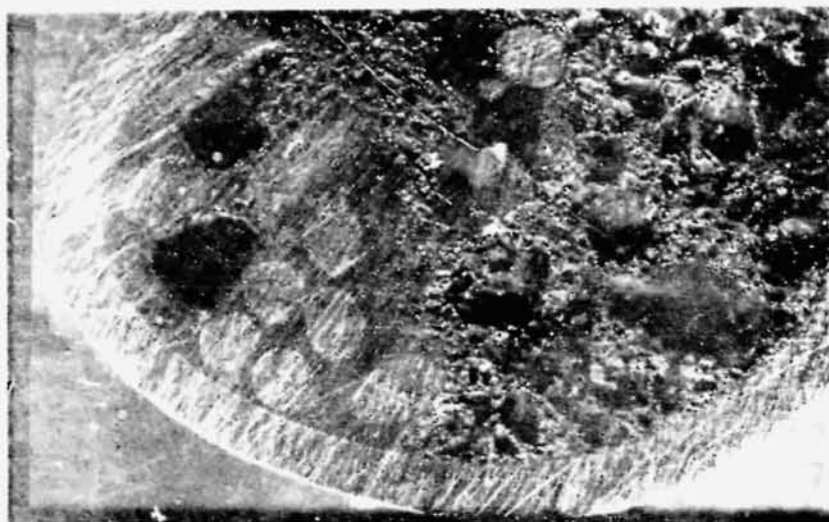
Conclusions: The ease of preparation as well as the quality of the foam improved as the melting point of the matrix metal increased. It now appears that it will be possible to obtain a good metal foam by compaction techniques. There remain problems of the size, shape, and distribution of the bubbles. Experiments have shown reinforced foam is easier to obtain than plain foam. It is also more desirable because the reinforcements rebuild some of the properties lost by making voids. This creates additional problems of fiber wetting, size, shape, and distribution, however.

3.3.7.5 Foam Simulation Experiments. The experiments with reinforcements in solid metals were difficult to interpret because the particles could not be visualized. Theory already provided information regarding the motion of fibers in liquids but a micrograph shows only a momentary status of the system and even then it is in the solidified state.

To document for study the effects associated with gas/matrix/fiber interface phenomena the system was simulated with a transparent matrix using Nylon fibers and a foaming solution

Two types of reinforced foam were simulated: 1) reinforced foam with dispersion controlled by bubbles - fibers had a small L/B ratio where L/B = ratio of fiber length to bubble diameter, and 2) reinforced foam with dispersion controlled by fibers - fibers had a large L/B ratio.

REPRODUCIBILITY OF THE ORIGINAL PAGE IS POOR.



8X



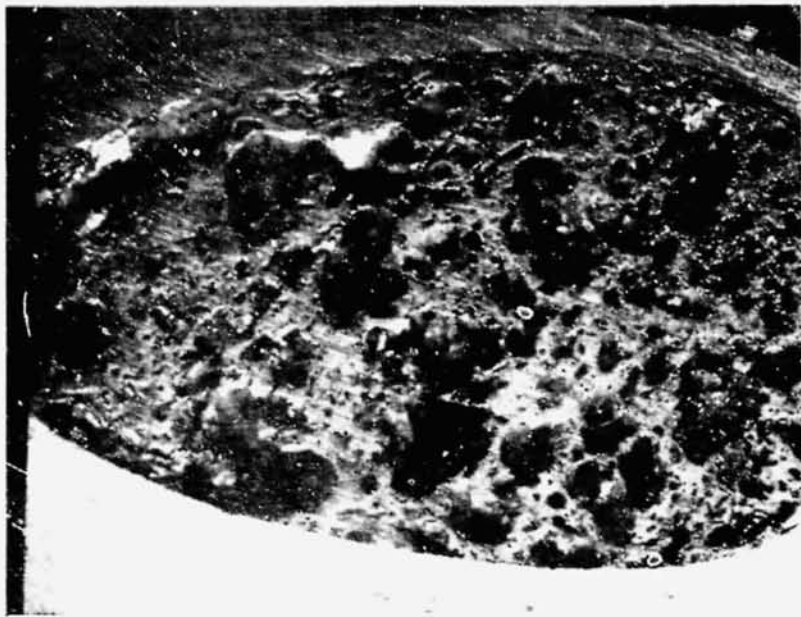
23X



78X

Figure 3-49. Product of Al Wire, Cu Wire in Stainless Steel Tube in Vacuum

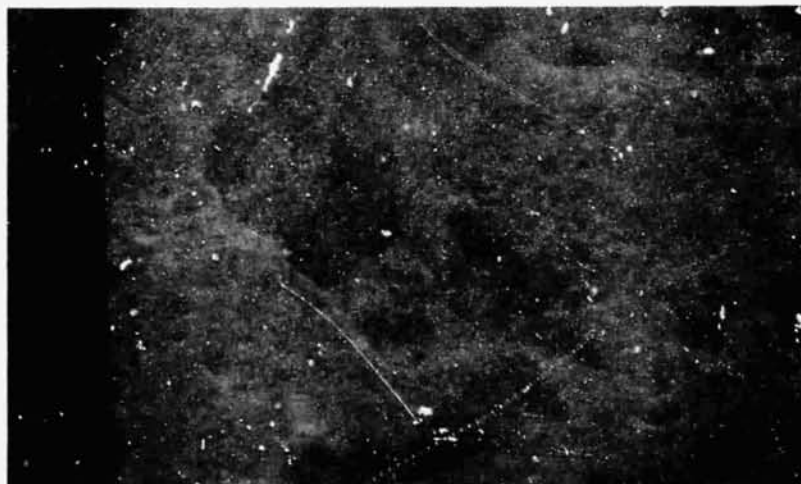
REPRODUCIBILITY OF THE ORIGINAL PAGE IS POOR.



5X



20X



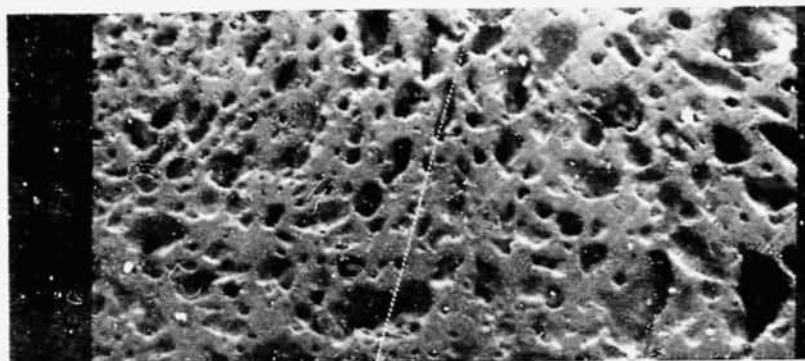
48X

Figure 3-50. Result of Experiment Repeated Under Changed Conditions

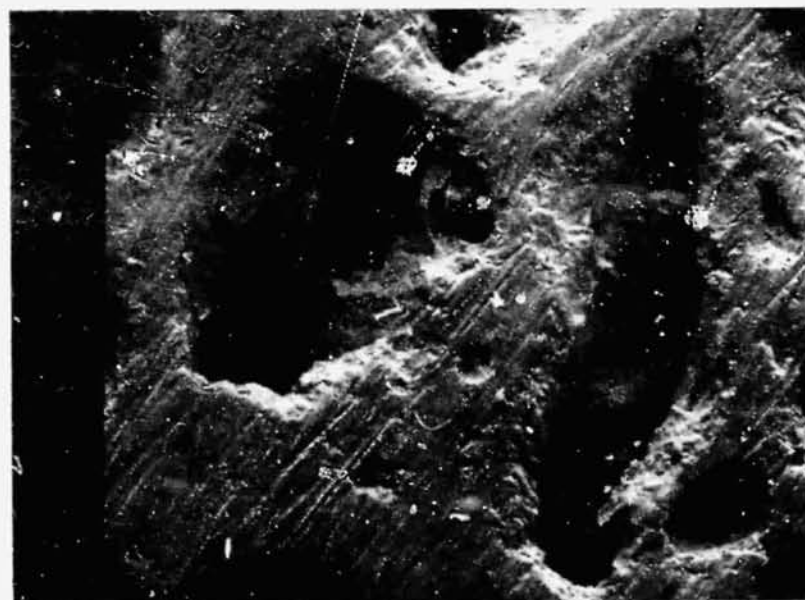
REPRODUCIBILITY OF THE ORIGINAL PAGE IS POOR.



8X



24X



200X

Figure 3-51. Result of Repeated Experiment Under Third Set of Conditions

## Materials

Fibers. The fibers consisted of Nylon cut to appropriate size to simulate long or short fibers. The filament was dyed black for better visibility in a photograph.

Foam. The foam solution was required to provide stable large and small bubbles. It was prepared as follows

Gum arabic	4%
Dove detergent	2%
Glycerine	25%
Water	69%

The detergent allowed the bubbles to form; the glycerine prevented the film from drying out in the heat of photographic lamps; the gum arabic increased the viscosity and stabilized the bubbles.

## Apparatus

The apparatus consisted of several Lucite containers, but chiefly one five inches square. A beaker of foaming agent rested on the bottom. An air tube reaching to the bottom of the beaker and terminating in various size nozzle tips produced bubbles of various sizes when air pressure was applied. Another one-inch-square container had a matted float of Nylon fibers suspended at the top of an almost equal density salt solution.

Pictures were taken with a still camera and with a motion picture camera.

## Procedure

Foam was produced by blowing air through the detergent solution. Nylon fibers with a large L/B and with a small L/B were sprinkled on the foam. Additional solution was poured over the fibers because the dry fibers usually caused the foam to collapse before they were sufficiently wetted. Bubbles were generated in the second container by placing 1/16-inch aluminum wires in the bottom of the one-inch-square container and adding dilute HCl to the liquid.

Results: It was very difficult to start with a solution containing fibers and then cause them to appear in foam produced by blowing air into the solution. The wetted fibers preferentially remain in the pure liquid, which wets them. It was therefore necessary to sprinkle the fibers into the foam to determine how they would move.

The dry fibers ruptured the bubbles as they passed through until they became wetted. Then two different effects were observed as expected.

In the first effect, small fibers always lined up at the intersection of two bubbles; they never rested on the surface of a bubble or intersected a surface. If the particles were caused to move by adding liquid on top of the bubbles, the fibers traveled in the downward direction with jerky movements as they abruptly changed directions where three bubbles met.

A fiber that touched the flat wall of the container never left the flat wall but any motion still followed the line of bubble intersections.

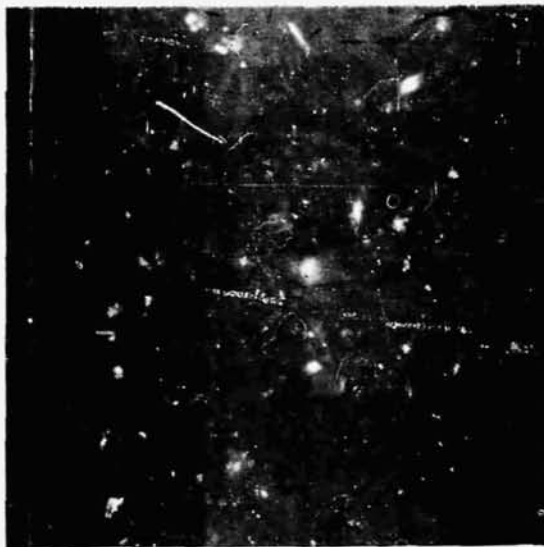


Figure 3-52. Small L/B Fibers in Foam

The photographs cannot depict the phenomenon in three dimensions adequately. Figure 3-52 shows the effect using a few fibers in a small container before the fibers reach a wall.

In the second effect, large fibers also moved along lines of bubble intersections as they traveled downward. However, since their length was enough to bridge more than one bubble diameter, the bubbles were displaced as the fibers descended. A fiber attached to a wall remained at the wall and, in the absence of any great liquid flow, firmly determined the movement of any bubbles attached to it. Figure 3-53 shows the phenomena with a few fibers none of which are attached to the wall. Much of the important detail is lost because of the short focal depth and the reproduction.

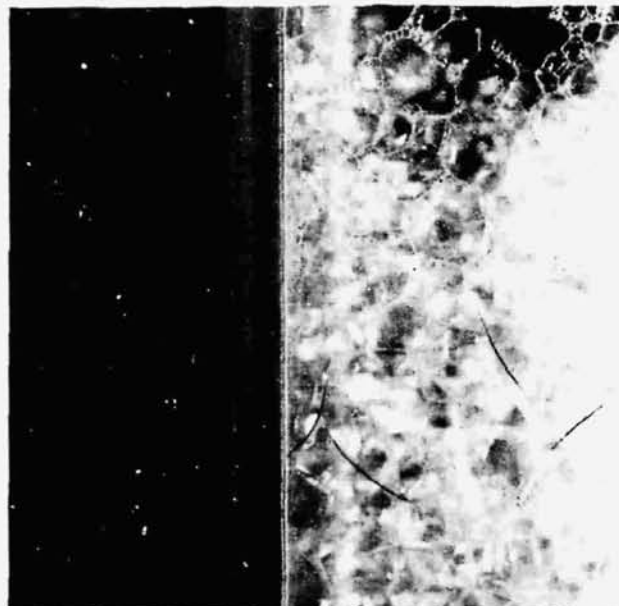


Figure 3-53. Long Fibers in Foam

Figure 3-54 shows the effect of fibers in controlling a foam environment. Bubbles rising from a source reach a network of Nylon fibers. Here they become enmeshed and trapped in place showing that fibers will increase the stability or perhaps in some cases enable the existence of foam.

Figure 3-55 further confirms this effect because not only are the bubbles enmeshed in the mat but many adhere to the surface of the fiber as well. These effects were discussed theoretically in a previous section. The next section summarizes some of the items that need to be better understood to place metal foaming processes on a solid foundation.

### 3.3.7.6 Summary of Major Subjects for Further Study and Lab Experiments

- Materials:      Definition of matrix and reinforcement materials  
                  Definition of gases for foaming by gas injection  
                  Definition of vapor-producing salts  
                  Gases/gas additives for surface stabilization  
                  Vapor pressures of metals  
                  Solubility of gases in metals
- Processing:     Bubble stability; criteria for coalescence  
                  Heating and cooling programs for various materials and masses  
                  Optimization of temperature  
                  Mechanism of bubble start and growth; effect of nucleation particles  
                  Methods of bubble size control  
                  Methods of bubble dispersion control  
                  Behavior of gas-filled microspheres during heating under matrix-constraint  
                  Behavior of liquid-gas and liquid-solid-gas mixtures under various agitation modes
- Techniques:    Dry mixing techniques  
                  Wet mixing techniques  
                  Agitation techniques  
                  Compacting of metal-salt and metal-microballoon composites  
                  Gas injection techniques  
                  Ultrasonic foaming and agitation techniques  
                  Finer distribution of salts  
                  More even distribution of salts

REPRODUCIBILITY OF THE ORIGINAL PAGE IS POOR.

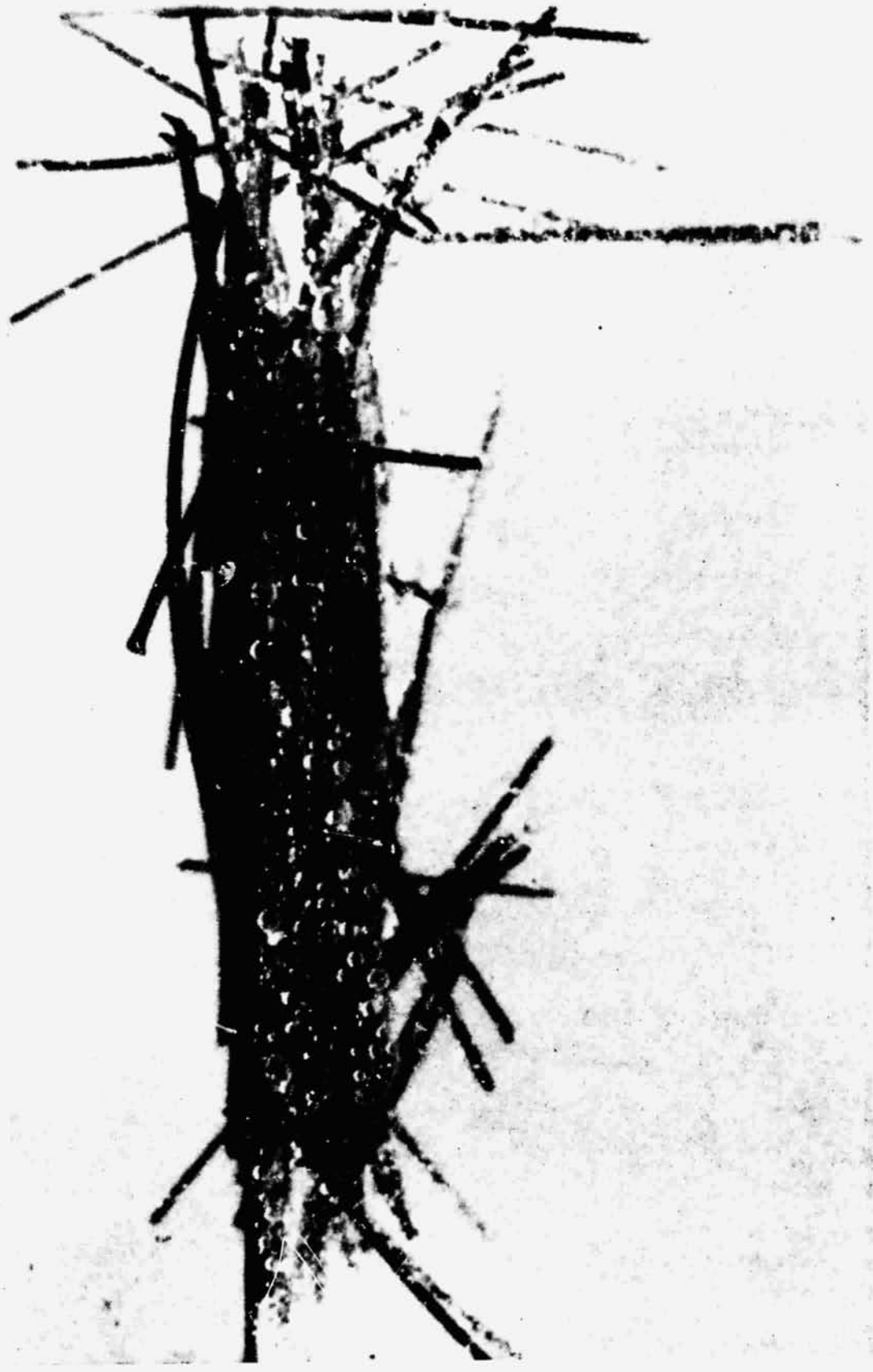


Figure 3-54. Effect of Fibers in Controlling a Foam Environment

REPRODUCIBILITY OF THE ORIGINAL PAGE IS POOR.



Figure 3-55. Bubble Trapped and Adsorbed by Fibers

3.3.8 GAS INJECTION FOAMING EXPERIMENTS AND RESULTS. This concept for foam generation involves a flowing stream of molten metal traveling through a tube, into which is injected a continuous flow of gas emitted from a nozzle. As the gas and metal move downstream, surface tension forces break up the column of gas into discrete bubbles. Laboratory experiments were performed to define engineering design parameters and demonstrate feasibility as a manufacturing process. For the experiments, which used water (representing molten metal), the effects of gravity were minimized by miniaturizing both the nozzle and tube; the most prominent effect being the coalescence of gas bubbles. The results of this work are being incorporated into a free fall experimental apparatus<sup>10</sup> that uses molten metal, and collects the solidified foam for evaluation.

### 3.4 UNIDIRECTIONAL EUTECTICS

The production of composites from Ta and Nb base eutectic alloys by unidirectional solidification is highly attractive for products that require high isotropic strength at extreme temperatures, such as gas turbine blades. The product properties attainable in zero-g processing are expected to be approximately twice as high as those obtained in 1-g due to the sensitivity of the formation of the intermetallic phase to g-induced phenomena.

3.4.1 PROCESS AND PRODUCT DEFINITION. Under conventional isotropic cooling and solidification the intermetallic phase of a eutectic alloy precipitates in randomly distributed globules or lamellae. If, instead, cooling is induced from one end of the melt, a discrete solidification front moves slowly away from the cooled end. In this progressive solidification, the intermetallic compound may precipitate in continuous, unidirectional rods or lamellae. The configuration of the intermetallic phase is primarily related to the alloy composition; small percentages of intermetallics precipitate preferably in the form of needles; as the percentage increases, rods, blades or lamellae are formed.

The formation of unidirectional intermetallics under gravity is very limited (downward cooling) since the heat of fusion released at the solidification front produces violent convection currents that disrupt the continuity and directionality of the compounds. It is expected that under zero-g, directional solidification can be achieved with practically any eutectic, provided that two basic requirements are met: 1) high alloy purity, and 2) extremely slow cooling rate, in the order of 1 cm/hr. The process is, however, limited to oblong shapes, such as wires, rods, or more complex oblong components, since the radial thermal gradient of large cross-sections interferes with the integrity of the axial (primary) thermal gradient.

<sup>10</sup> Contract NAS8-28056, Preparation and Evaluation of Free Fall Experiments, Convair Aerospace Division of General Dynamics, San Diego.

Prime product characteristics are anisotropic mechanical, thermal, or electrical properties. The strength in the direction of the intermetallic may differ from the random-oriented eutectic by a factor of 2 to 4, and the elastic modulus up to a factor of 2, depending on the specific alloy.

The spacing of the intermetallics over the cross-section is determined by the initial distribution at the start of solidification. In most cases, it is rather uniform; uniformity and spacing can, however, be controlled by a grid of nuclei at the cooling end. The process will, therefore, consist of the following mandatory and optional steps:

- a. Preparation of a high purity eutectic alloy.
- b. Melting.
- c. (Optional) Introduction of a grid of nuclei at end A.
- d. Cooling and progressive solidification from end A.

Whether several melting and solidification cycles (b, d) improve the desired characteristics of the end product is not established. In addition, it is rather impractical, as the process is very time consuming to begin with.

#### 3.4.2 SUMMARY OF RESULTS

1. The most promising eutectic alloys for unidirectional solidification and high isotropic strengths are Al-Al<sub>3</sub>Ni, Al-CuAl<sub>2</sub>, Nb-NbC, and Ta-Ta<sub>2</sub>C.
2. Unidirectionally solidified eutectics have composite characteristics and remain stable up to 99% of the matrix melting temperature.
3. The moderate strength gains obtained in 1-g processing - about half of the theoretically predicted values - are due to g-induced disturbances during solidification. In zero-g processing the strength is expected to approach the theoretical values.
4. Laboratory experiments indicated that highest alloy purity is the primary requirement for successful processing.
5. The optimum solidification (cooling progression) rate in zero-g is considerably lower than in 1-g. The exact determination of the optimum rate can only be accomplished in zero-g experiments.
6. For practical applications, the Ta and Nb base composites are most attractive; they require, however, processing temperature between 2400 and 2800° C. The Al-base composite may serve as experimental systems in view of their moderate temperature requirements (600° C).

3.4.3 MATERIALS AND PREDICTED PROPERTIES. A number of eutectic composites made by directional solidification have been prepared experimentally or suggested for structural, optical, electronic, and magnetic applications. The structural eutectics have received the most attention to date, in particular the  $Al_3Ni$ -Al,  $CuAl_2$ -Al,  $Ta_2C$ -Ta, and NbC-Nb systems, for which significant strength improvements have been demonstrated over the conventionally cast alloys. The theoretical and experimentally demonstrated ultimate tensile strength data for these systems are:

System	Theoretical (psi)	Experimental (psi)
$Al_3Ni - Al$	47,000	43 to 51,000
$CuAl_2 - Al$	75,000	35 to 43,000
$Ta_2C - Ta$	295,000	155,000
NbC - Nb	(475,000)*	156,000

Calculated from bend strength data of  $Nb_2C$  whiskers.

High-strength systems result when an intermetallic phase of the eutectic solidifies as high-aspect-ratio 'perfect' crystals (as rods (whiskers) or lamellae usually) dispersed in the ductile base metal phase. The strength of these intermetallics frequently exceeds one million psi, similar to the ceramic whiskers grown from the vapor phase. Growing the whiskers in situ obviates the usual problems of achieving perfect alignment, good dispersion, and good compatibility including wetting and interfacial bonding. Although the whiskers are precipitated from the melt, the microstructure remains stable up to about 99% of the melting point and is even retained after deformation of the eutectic. High strength and elastic modulus efficiencies are therefore retained at elevated temperatures.

3.4.4 SOLIDIFICATION EXPERIMENTS. Theoretical 'rule of mixtures' strengths can be readily attained with the  $Al_3Ni$ -Al system, which exhibits an ideal whisker dispersion. The whiskers can be very long, perfectly aligned and spaced, and free of defects such as branching or kinking. This system is well characterized. The effects of purity and solidification rate on strength, and microstructural aspects such as whisker size, shape and spacing are documented. Experimental work has shown that lower than ideal strengths have been obtained with the  $CuAl_2$ -Al and  $Ta_2C$ -Ta systems. The  $CuAl_2$  platelets tend to have a high density of faults, which can lead to chemical instability and lower strengths, and the  $Ta_2C$  rods tend to be too short (below the critical L/D ratio) for effective strengthening. Based on the  $Ta_2C$  whisker strength, the eutectic composite strength should be of the order of 295 ksi whereas 150 ksi is the practical value with this system. A zero-g environment may contribute to higher strengths by allowing longer whiskers to grow or by reducing faults that may be a result of thermal convection currents.

The effect of zero-g on the growth of these eutectics and perhaps single crystals is not known with certainty, but the elimination of convection currents has been suggested as a very desirable feature to aid in producing more near perfect crystals. However, currents due to the Marangoni effect may still be present.

The melting point of the  $Ta_2C - Ta$  system is too high for convenient experimentation; consequently, zero-g experiments are tentatively proposed using  $Al_3Ni - Al$  and  $CuAl_2 - Al$  with melting temperatures of  $640^\circ C$  and  $548^\circ C$  respectively.

3.4.5 ZERO-G EXPERIMENTS. By choosing at least two purity levels and two solidification rates for each system and comparing flight and ground samples, the overall beneficial effect of zero-g on crystal growth from the melt could be determined. These materials are selected because in 1g,  $Al_3Ni-Al$  may be considered as a 'perfect' system and  $CuAl_2-Al$  is subject to faulting in the lamellae.

The expected presence of the Marangoni effect, which may or may not be of sufficient magnitude to have the equivalent disrupting effect that thermal convection has in 1g, can be evaluated by its influence on microstructure and strength. The absence of any currents could also have an adverse effect. For instance, impurities built up just ahead of the solidification front can lead to constitutional supercooling and breakdown of the plane interface. Any internal stirring action, such as convection, normally helps to dilute this concentration if impurities exist below a critical level in the remaining melt; in its absence, dilution can take place only by a slower diffusion process. Growth rates would therefore need to be much slower in zero-g, or conversely, much higher purity materials would be required for a given growth speed than for 1g casting. The expense of the higher purity materials and lower production rates could well be justified, though, if worthwhile property improvements are attained.

By including a very slow growth rate experiment it may be determined that 'perfect' eutectics or crystals can be made, albeit very slowly, even if solute (impurity) diffusion is the only mechanism present in zero-g to maintain the necessary plane solid/liquid interface.

The impurity levels determine the maximum solidification rate. Therefore, if in zero-g, for a given purity and maximum 1g growth rate, lower strengths are experienced with the (ideal)  $Al_3Ni - Al$  system when compared to the ground sample, it indicates the effect of impurities negates any beneficial effect in zero-g. However, an improvement in the properties of  $CuAl_2 - Al$  system and perhaps a reduction of the number of faults in zero-g will show a definite directional trend for improving this and probably the other systems such as  $Ta_2C - Ta$ . Further work on this more difficult system would then be justified. The aim with the  $Ta_2C - Ta$  system would, of course, be to increase the length of the whiskers while maintaining their perfection which, in turn, is expected to bring the strength of the composite close to the theoretical value of 295,000 psi (ambient).

### 3.5 COMPILATION OF MATERIALS DATA

This section comprises a compilation of such materials data as are of significance for the design, processing, and product capabilities of the concerned types of composites. It was prepared primarily for use in the experimental and theoretical investigations of this study. At the same time, it may serve as a data source for further work on composites and for the evaluation of flight experiments. Moreover, the data on liquid materials will be useful in other zero-g processes as they all involve the liquid state of matter.

Most of the presented data have been obtained from a literature search. Wherever data were not available they were either determined experimentally or - tentatively - omitted. Incomplete data were encountered particularly on the properties of liquid metals. Two types of test apparatus for the determination of surface tension, wetting characteristics, and liquid state density were, therefore, set up, with a temperature capability up to 2000°C. Tests will be limited to a few select matrices, as the efforts for a complete program far exceed the scope and resources of this study. The facilities will, however, be maintained in operational condition so that any data requirements that may be encountered in the development or evaluation of zero-g experiments can be readily satisfied.

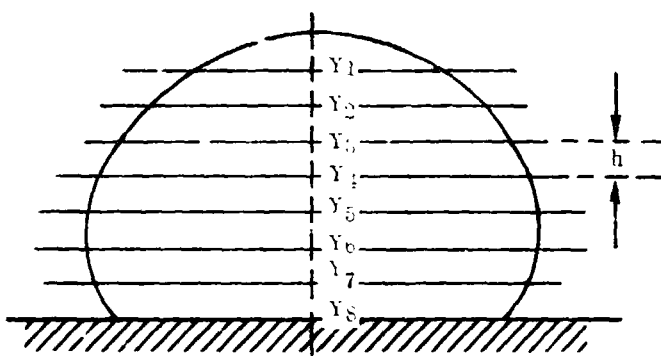
The data are presented for three material classes: simulated matrices (Section 3.5.2), molten metals (Section 3.5.3), and reinforcements (Section 3.5.4). The results of wettability experiments carried out on a variety of potentially applicable material combinations are presented separately.

**3.5.1 APPARATUS DESCRIPTION.** The density values for almost every material were obtainable from the literature or from manufacturers' data. During the course of the work some densities (such as foamed metals) were measured by immersing the material in a liquid of known density and using Archimedes' principle. Water is a satisfactory liquid to use with metals. The weighing pan of an analytical balance is bridged with a metal sheet that holds the container of water. When the weight of the material, suspended by a very fine wire is obtained in air,  $W_A$ , and then in the water,  $W_L$ , the difference gives the weight of the volume of water displaced, from which the volume of the sample may be calculated. The density of the sample is then given by the ratio of weight in air to volume. Corrections are made for buoyancy, wire volume, etc. for precision results.

When necessary, liquid densities at ambient temperature were obtained with a pycnometer and a flask of calibrated volume. At higher temperatures, some densities were calculated from literature data on  $d\rho/dT$  and an arbitrary correction for the volume change during the solid-liquid phase transformation. These data are in parentheses in Tables 3-5 and 3-6 in Sections 3.5.2 and 3.5.3.

Another approach to the liquid-state density problem was to determine the profile of a molten droplet of metal. The metal was melted by means of a 100-watt laser beam or in the coil of a Lepel induction heater. The samples were supported on a graphite table. Vitreous graphite is the best support material because of its inertness and lack of porosity. Figure 3-56 shows the apparatus using the laser for melting. The laser is on the right and an optical pyrometer for temperature measurements is on the left. A potentiometer for reading a thermocouple is resting in the foreground and the test apparatus with vacuum connections is to the left of the laser. Figure 3-57 shows the optical system for photographing the drop profile and Figure 3-58 shows the image being analyzed on a toolmaker's microscope.

The volume of the droplet is calculated by dividing the height of the image into eight equal parts,  $h$ . Then the volume,  $V$ , is given by



$$V = \frac{\pi h}{6} \left[ y_0^2 + 4y_2^2 + 2y_4^2 + 4y_6^2 + y_8^2 \right]$$

or

$$V = \frac{\pi h}{12} \left[ y_0^2 + 4y_1^2 + 2y_2^2 + 4y_3^2 + 2y_4^2 + 4y_5^2 + 2y_6^2 + 4y_7^2 + y_8^2 \right]$$

where  $y_0 = 0$

This equipment and procedure was useful for obtaining very approximate data. Precision data for high-temperature metals require extreme precautions against surface and impurity contamination. This necessitates very high vacua, careful manipulations, and special handling apparatus to assure clean surfaces.

Melting and boiling point data are entirely from the literature.

Surface tension data are from the literature. Laboratory data were obtained by the sessile drop method. These laboratory data also could be only approximate because of difficulties in obtaining pure uncontaminated molten droplets of metal. Even small amounts of gas such as  $O_2$ ,  $N_2$ , and  $CO_2$  may form oxides, nitrides or other contaminating films. Carbides may form at elevated temperatures. Also the drops are small so that corrections must be made for the curvature of the top of the molten drop. It was found, for example, that the measurement for the surface tension of water drops depended on their radius up to a radius of about 1 cm.

REPRODUCIBILITY OF THE ORIGINAL PAGE IS POOR.

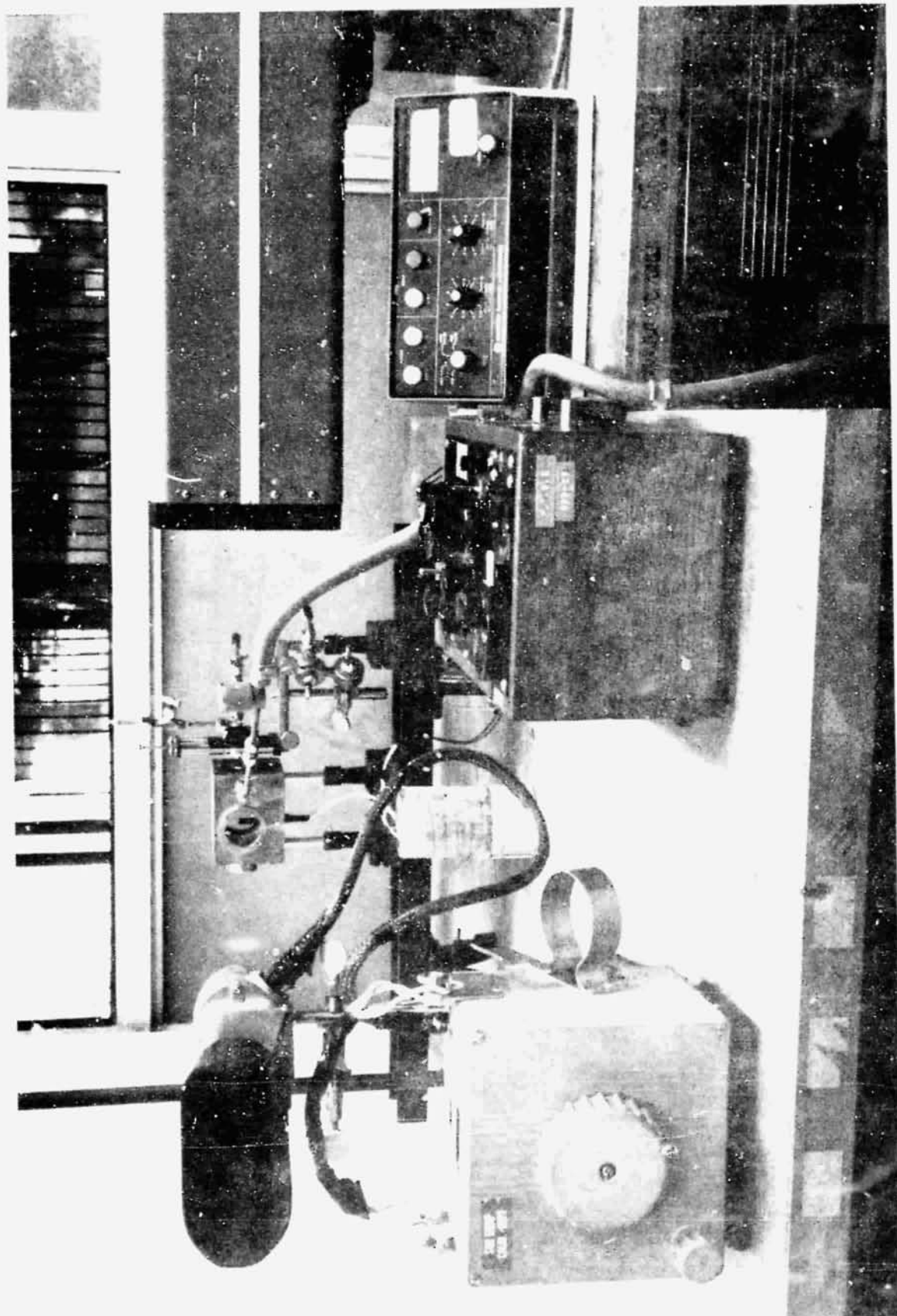


Figure 3-56. Droplet Melting Apparatus

REPRODUCIBILITY OF THE ORIGINAL PAGE IS POOR.

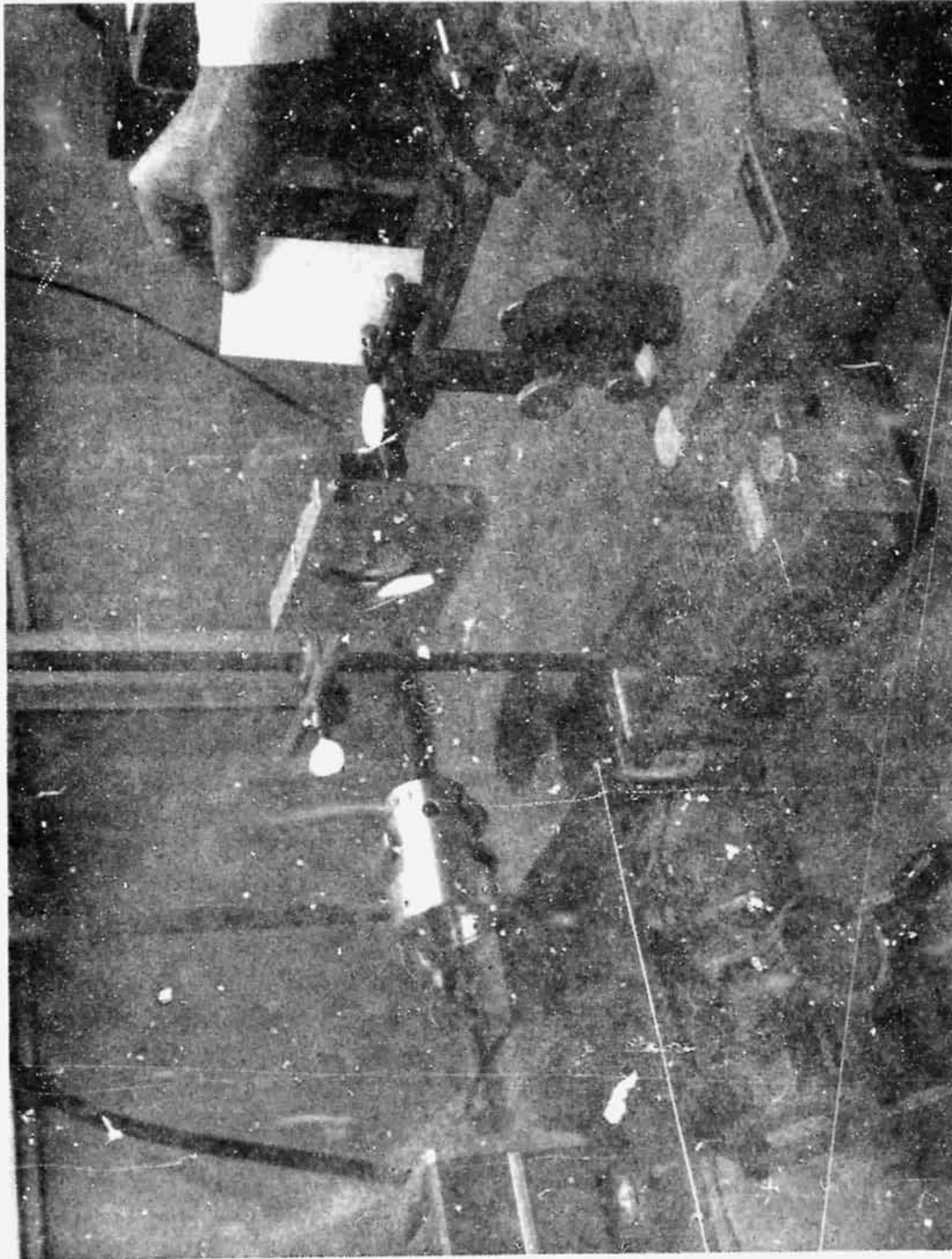


Figure 3-57. Optical System for Obtaining Droplet Profile

REPRODUCIBILITY OF THE ORIGINAL PAGE IS POOR.



Figure 3-58. Photographic Measurement System

In the accompanying sketch, the pressure  $p$  for a large drop is essentially the same at the apex within and outside the drop. Then one may write the equilibrium for a drop at rest

$$\gamma \left( \frac{1}{R_1} + \frac{1}{R_2} \right) = \rho gh$$

where

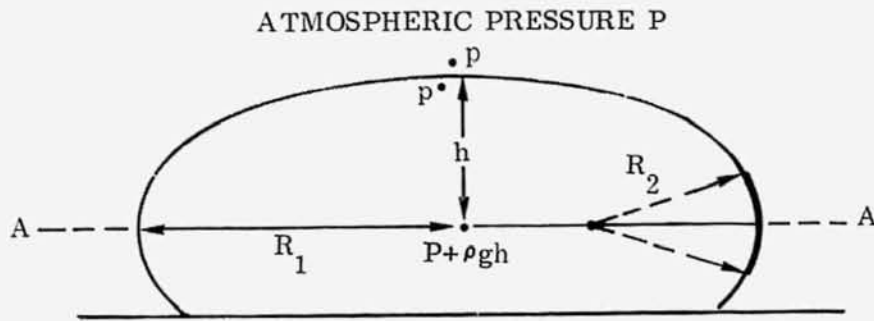
$h$  = height of drop above horizontal plane of maximum width A-A

$R_1$  = radius of drop at maximum width

$R_2$  = radius of drop at right angles to  $R_1$

$g$  = gravitational constant

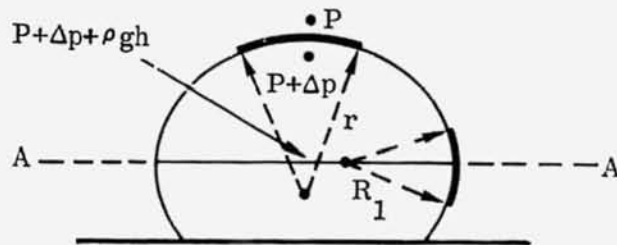
$\rho$  = density of liquid



There is an excess pressure in a small drop because of its curvature. This amounts to  $2\gamma/r$  as shown in the sketch.

$$\Delta p = \frac{2\gamma}{r}$$

$r$  = radius of apex



Hence, equating forces for the resting small drop

$$\gamma \left( \frac{1}{R_1} + \frac{1}{R_2} \right) = \rho gh + \frac{2\gamma}{r}$$

or

$$\gamma = \frac{\rho gh}{\frac{1}{R_1} + \frac{1}{R_2} - \frac{2}{r}}$$

for symmetrical drops. Many times, the contamination even on supposedly cleaned surfaces causes a surface film that destroys the symmetry and prevents the analysis. The initial specimen must also be reshaped so that it collapses on melting to provide an advancing contact angle that can be duplicated.

The surface tensions of simulated matrices were obtained conventionally by a commercially obtained DuNouy tensiometer as shown in Figure 3-59. Nested beakers provided temperature control of about  $\pm 1^\circ\text{C}$ . This apparatus measures the force required to detach a circular platinum ring of circular wire from a liquid surface. The size and diameter of the wire is chosen so that the results may be read on a scale directly.

The apparatus for viscosity measurements consisted of a Brookfield Viscometer (Figure 3-60). It measures the shear force generated by a cylinder spinning in the test liquid. The use of a scale and calculation factors gives results directly.

The experimental determination of heat capacity, latent heat of fusion, thermal conductivity, elastic modulus, and tensile strength were beyond the scope of this work. These data were obtained from the literature.

**3.5.2 PROPERTIES OF SIMULATED MATRICES.** Table 3-5 is a list of the properties of transparent matrices used in the course of experimentation. Manufacturers' literature values were used for common liquids. Values were determined independently for the liquids used in the laboratory experiments. Paraffin, sodium acetate, and Burtonite are solid at room temperature. Burtonite possesses the desirable property of being transparent at room temperature in the solid state. The viscosity of glycerine of various concentrations in water is tabulated in handbooks, but the values are open to question because of its tendency of absorbing water. The values given for glycerine are laboratory values.

The materials for the transparent matrix experiments were selected to represent an effective range of surface tension and viscosity. When viscosity alone was the variable studied, a wide variety of values was obtained with glycerine-water solutions. The selected materials further provided a variation of wetting characteristics with regard to the solids used in the experimental mixtures.

**3.5.3 PROPERTIES OF MOLTEN METALS.** A list of pure liquid metal properties is presented in Table 3-6. In some cases for which the liquid properties are not readily available, blanks are shown that will be filled in ultimately either from literature or from experiment. The data are mostly from the literature and have been compiled chiefly from the "Encyclopedia of the Chemical Elements" by Clifford H. Hampel. Comparisons with alternate sources such as the Metals Handbook and Smithell's Metals Reference Book reveal that the Hampel text is more recent, is very comprehensive, and displays a high measure of scholarly evaluation and authority. The order of listing is by solid density, although any order might have been taken. Melting and boiling points are given in both  $^\circ\text{C}$  and  $^\circ\text{F}$  and the metallurgical properties are in English units. The remaining properties are given in cgs units.

REPRODUCIBILITY OF THE ORIGINAL PAGE IS POOR.

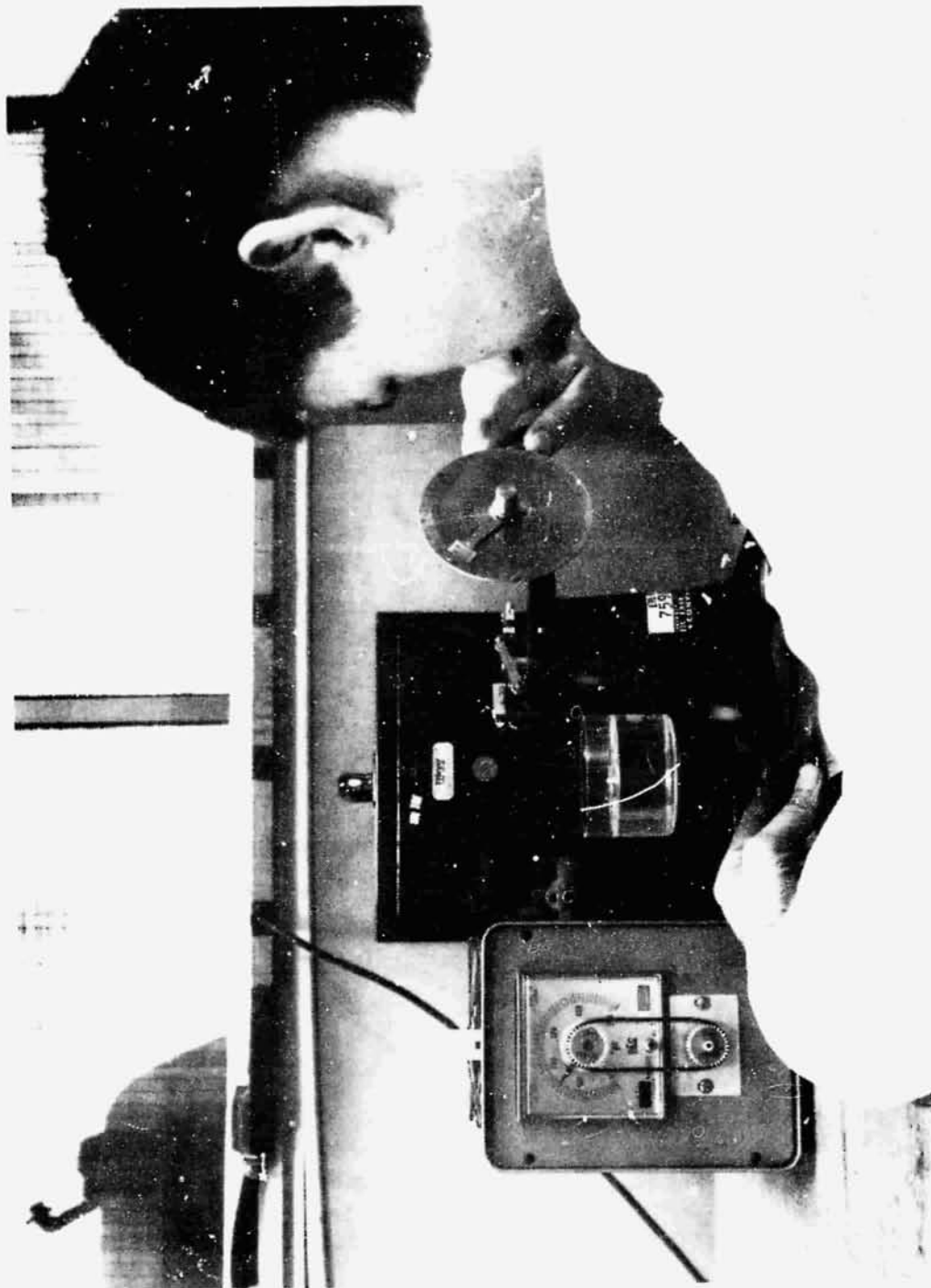


Figure 3-59. Measuring Surface Tension of Simulated Matrices

REPRODUCIBILITY OF THE ORIGINAL PAGE IS POOR.

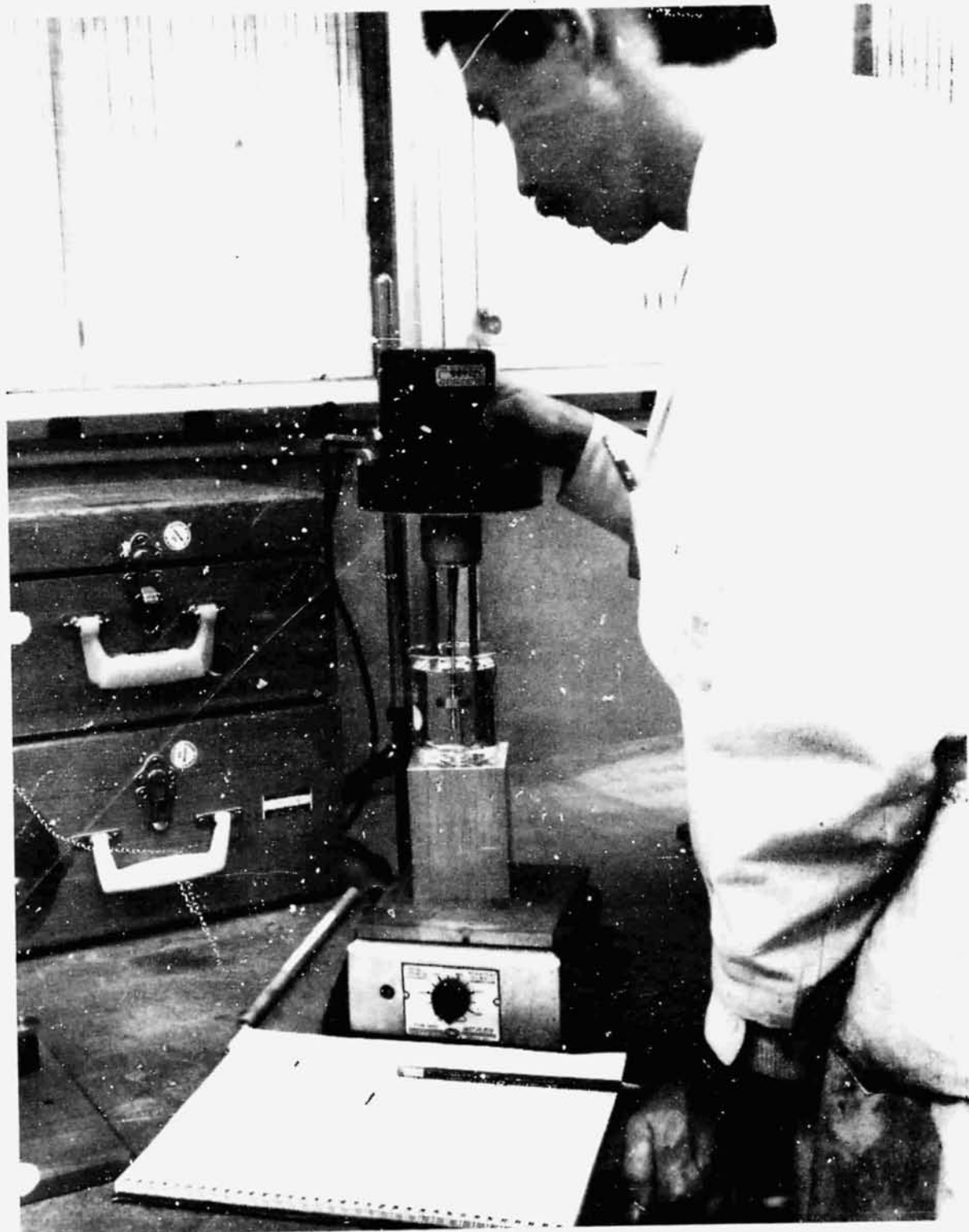


Figure 3-60. Measuring Viscosity

Table 3-5. Transparent Matrix Properties

Transparent Matrix	Density (gm/cc) 25°C	Surface Tension (dyne/cm)			Viscosity (centipoise)			Transparency * **	
		25°C	50°C	74°C	25°C	50°C	74°C	Liquid	Solid
Paraffin	0.87	(Solid)	25		Solid	Solid		0	X
Silicone 200 Fluid	(0.966)	(25.8)	(22.0)	(20.4)	(101)	(58.3)	(43.1)	0	X
Distilled Water	(1.005)	(73.5)	(63.2)		1.00	0.549	0.380	0	0
Burtonite 5/8%	1.02	(Solid)	(63.0)		Solid	(8.2)	(5.7)	0	0
Glycerin 10%	1.024	(52.3)	(53.5)		(3.5)	(3.0)	(2.6)	0	X
Glycerin 25%	(1.080)	(68.9)			(4.3)			0	X
Glycol	1.11	47			17.3			0	X
Diethyl Phthalate	1.12	37.5						0	X
Glycerin 50%	1.127	(51.4)	(47.8)		(14.9)	(7.8)	(5.9)	0	X
Methyl Salicylate	1.18	32						0	X
Glycerin 75%	(1.195)	(66.6)			(27.5)			0	X
Glycerin 100%	1.26	(56.1)	(51.2)	(45.2)	(627)	(72.4)	(27.0)	0	X
Fluorosilicone 1265 Fluid	1.28	(28.2)			(1380)	605	256	0	X
Sodium Acetate	1.44	59 (M. Pt)	Solid		Solid	Solid		0	X
Fluoroluöe FS-5	(1.900)	(29.8)	(26.5)	(22.5)	(30.6)	(16.2)	(11.9)		X

( ) Parenthesized values indicate laboratory measured data; all other data are from available literature.

\* By special treatments to remove air and nuclei, many organic compounds can be solidified to a clear glassy solid.

\*\* 0 = Transparent  
X = Translucent

**3.5.4 PROPERTIES OF REINFORCEMENT MATERIALS.** The properties of fibers, whiskers, and wires that have potential use as reinforcements for the zero-g processed composites are given in Table 3-7. They apply to processes 1 (fiber and particle composites), 2 (reinforced foams), and 3 (cemented compacts).

**3.5.5 WETTING DATA.** Series of tests were carried out with seven metal matrices and nine reinforcement materials to determine the wetting characteristics in the liquid matrix and the degree of adhesion after matrix solidification. Adequate wetting and adhesion between the fiber and the matrix is a mandatory requirement for any composite. In addition, it is desirable that a strong chemical or physical bond between the two components be formed in the final product. On the other hand, too much chemical reaction can produce an interface of a third phase that impairs the overall properties and reduces any advantage of reinforcement.

Table 3-8 lists the results of wetting and adherence experiments carried out with a number of candidate metal matrices and reinforcement materials.

Table 3-6. Liquid Metal Properties

Material	Solid Density, $\rho_s$ (gm/cc)	Liquid Density, $\rho_l$ (gm/cc)	Melting Point, M.P.		Boiling Point, B.P.		Tension, $\gamma$ (dynes/cm)	Viscosity, $\mu$ (centipoise)	Specific Heat, C <sub>p</sub> (cal/gm·°C)	Latent Heat of Fusion, $\Delta H_f$ (cal/gm)	Conductivity, $\kappa$		Elastic Modulus E <sub>s</sub> (10 <sup>6</sup> psi)	Ultimate Tensile Strength, $\sigma_{tens}$ (ksi)
			(°C)	(°F)	(°C)	(°F)					Liquid	Solid		
Ga	5.904	6.095	29.78	85.8	2403	4,357	735 <sup>30*</sup>	1.60 <sup>30*</sup>	0.0977 <sup>29*</sup>	19.19	0.65 <sup>30*</sup>			
Phosphorus	1.83	1.74	44.1	111.4	290.5	536	86	1.69	0.189	5.03				
Potassium	0.856	0.819	63.4	146.1	757	1,393	411	0.515	0.200 <sup>63*</sup>	14.87	0.10-3 <sup>200</sup>	0.272		
Sodium	0.967	0.927	97.8	208.0	882.9	1,621.2	192	0.690	0.130	27.06	0.285	0.205		
Sulphur	2.07	1.61	115.21	239.38	444.6	832.4	60.93	11.5	0.36	12.79	0.0003	0.0007		
Iridium	7.28	(6.97)	156.6	313.9	2075	3,767	586	1.69 <sup>200*</sup>	0.55	6.8	0.10	0.17	1.51	0.380
Lithium	0.53	0.507	179	354.2	1317	2,403	~400	0.592	1.01	103.2	0.109	0.17		
Selenium	4.79	(4.4)	217	422.6	894.9	1,265	72		0.075 <sup>25*</sup>	15.8				
Tin	7.29	6.97	231.9	449.4	2270	4,100	5.26	1.91	0.038	14.2	0.078	0.145 <sup>100*</sup>	~6	1.7
Bismuth	9.8	10.07	271.3	520.4	1560	2,840	376	1.63	0.034	12.5	0.041	0.020	4.6	1.3
Thallium	11.85	11.289	303	577	1457	2,655	401	2.116 <sup>441*</sup>	0.036	5.04	0.059	0.093	2.56	2.0
Lead	11.34	10.51	327	621	1377	3,159	442	3.17	0.037	5.89	0.039	0.083	10-20	
Zinc	7.13	6.62	419.5	787	907	1,664	785 <sup>510*</sup>	1.30	0.115	24.4	0.415	0.27		
Antimony	6.49	6.49	630.5	1167	1635	2,975	383	1.24	0.066	38.3	0.045	0.052	6.5	6.8-16.3
Magnesium	1.74	1.57	650	1202	1110	2,020	563	1.12	0.291	88	0.20	0.37		
Aluminum	2.69	2.368	660	1220	2467	4,471	865	1.12	0.23	94.1	0.20	0.82	9	
Barium	3.6	(3.2)	729	1344	1637	2,977	195		0.088 <sup>25*</sup>	13.3				
Silver	10.5	9.18	960.8	1762	2210	4,010	900	3.59	0.056 <sup>25*</sup>	25.04				
Gold	19.28	19.300*	1063	1945	2808	5,087	1128	3.78	0.0353 <sup>1100*</sup>	14.96		0.97	11	18-20 (Annealed)
Copper	8.91	8.03	1083	1961	2582	4,660	1104	3.41	0.118	48.95		0.34	11.2	32-37 (Annealed)
Beryllium	1.84	(1.6)	1283	2345	2970	5,378	1100		0.44 <sup>25*</sup>	250-275		0.911	17	46-78
Nickel	8.908	7.9	1453	2647	2740	4,946	1736		0.122 <sup>200*</sup>	73.8		0.44 <sup>07*</sup>	44.5	
Cobalt	8.90	(7.7)	1493	2720	3100	5,619	1405		0.111	62		0.198	30	40-160
Iron	7.873	7.00	1536.5	2738	3000	5,432	1835	4.45	0.172	65.5		0.195	30	40-160
Titanium	4.507	(4.0)	1668	3034	3260	5,900	1427		0.13 <sup>20*</sup>	10.4		0.2 <sup>07*</sup>	28.5	30
Chromium	7.19	(6.4)	1875	3407	2189	3,990			0.11 R.T.	61.5		0.041	13.5	34
Vanadium	6.11	(5.4)	1890	3434	3000	5,432			0.12 R.T.	78.5		0.16	~36	15-35
Boron	2.34	(2.0)	2300	4172	2550	4,622			0.30 <sup>2</sup> R.T.	~68.8		0.074 <sup>100*</sup>	18-19	28-74
Niobium	8.57	(7.6)	2468	4474	4927	8,901			0.064 R.T.			0.004		
Molybdenum	10.22	(8.8)	2710	4730	5560	10,040	2240		0.0133	69.8		0.125	15.1	40-85
Tantalum	16.654	(14.8)	2996	5426	5427	9,801			0.0334 R.F.	41.4		0.33	~46	
Tungsten	19.3	(17.1)	3410	6170	5930	10,710	2300		0.012 R.T.			0.13	27	30-60

Table 3-7. Reinforcement Properties

Fiber*	Material		Density (gm/cc)	Melting Point		Boiling Point		Young's Modulus (psi x 10 <sup>6</sup> )	Tensile (psi x 10 <sup>6</sup> )
	Whisker*	Wire		(°C)	(°F)	(°C)	(°F)		
Al <sub>2</sub> O <sub>3</sub>	AlN		3.4	2200	3990	Subl>2000	3,680	50	2-3
			3.15	2040	3700	2250	4,080	25	0.30
	Al <sub>2</sub> O <sub>3</sub>		3.96	2040	3700	2250	4,080	2	3.00
B			2.65	2300	4170	2550	4,620	55	0.40
B <sub>4</sub> C			2.36	2450	4440	3500	6,330	70	0.33
	B <sub>4</sub> C		2.52	2450	4440	3500	6,330	70	2.00
BN			1.90	2980	5400	5067	9,153	13	0.20
Be			1.83	1280	2340	2970	5,378	35	0.19
	BeO		2.85	2570	4660	~3900	~7,050	50	1.90
C			1.5	3650	6600	4200	7,590	30	0.35
	C		1.66	3650	6600	4200	7,590	102	2.85
	Cr		7.20	1890	3430	2199	3,990	35	1.29
	Cu		8.92	1083	1980	2582	4,680	18	0.427
Steel			7.74	1400	2550			29	0.60
	Fe		7.83	1540	2800	3000	5,482	29	1.90
Glass			2.19	1660	3020	2230	4,046	10.5	0.85
	MgO		3.6	2800	5070	3600	6,512	45	3.5
Mo			10.2	2620	4750	5560	10,040	52	0.32
	Ni		8.98	1455	2650	2730	4,940	31	0.56
René 41			8.26	1370	2460			24	0.29
SiC			4.09	2690	4870	Subl>2200	Subl>3,992	70	0.50
	SiC, α		3.15	2690	4870	Subl>2200	Subl>3,992	70	3-5
	SiC, β		3.15	2690	4870	Subl>2200	Subl>3,992	100-150	1-3
	Si <sub>3</sub> N <sub>4</sub>		3.18	1900	3450			55	2.00
TiB <sub>2</sub>			4.48	2980	5400			74	0.015
W			19.4	3400	6150	5930	10,710	59	0.58
ZrO <sub>2</sub>			4.84	2650	4800	4300	7,772	50	0.30
		Cu - 0.010 in.						17	0.050*
		Cu-Be-0.005 in.						19	0.190*
		Ni - Alloys						32	0.200*
		Ni - Spring						30	0.130*
		SS - 0.006 in.						28	0.313*
		Steel - 0.003 in.						29	0.377*
		E-glass - 0.00015 in.	2.54					10	0.500
		Quartz - 0.0004 in.	2.2					10	0.100-0.300
		Teflon - 0.00078 in.	2.3					0.4	0.0047

\* SAMPE, Vol. 10, p. B-1 (1966)

Wetting characteristics were determined by dipping of wires or sheet strips with various surface conditions in the liquid matrix and observation of the behavior of the liquid film after removal. Wettability was expressed as nonwetting (-), partially wetting (o) and fully wetting (●).

Samples that showed adequate wetting characteristics were slowly cooled; after solidification of the matrix film, adherence was tested by scraping with a cutting tool. Adhesion was classified as strong bond (●), weak bond (o) and no bond (-). Surface treatments were applied to the point where 100% wetting and adherence was obtained.

Table 3-8. Wetting and Adherence Experiments

		● = Fully-wetting	O = Non-wetting	◐ = Partially wetting	
MATRIX	SUBSTRATE	SUBSTRATE SURFACE CONDITION		WETTING ADHER	
Copper	Al <sub>2</sub> O <sub>3</sub>	DEGREASED	O	-	
		DEGREASED + FLUX	O	-	
	BORON	DISSOLVES	-	-	
		COPPER	DISSOLVES	-	-
	IRON	DILUTE HCL	●	●	
		DEGREASED + SS FLUX	●	●	
		DEGREASED	●	●	
	NICKEL	CONC. HNO <sub>3</sub>	O	-	
		DILUTE HCL	●	●	
		DILUTE HNO <sub>3</sub> (10%)	●	●	
		DEGREASED	◐	-	
	SILICON - CARBIDE	DEGREASED	O	-	
		DEGREASED + SS FLUX	O	-	
	AM 350 STEEL	DILUTE HCL	O	-	
		DILUTE HNO <sub>3</sub>	O	-	
		DEGREASED + SS FLUX	●	●	
		TUNGSTEN	DILUTE HCL	O	-
			DILUTE HNO <sub>3</sub>	O	-
		DEGREASED + SS FLUX	O	-	
	IN-BI	Al <sub>2</sub> O <sub>3</sub>	DEGREASED	O	-
DEGREASED + SS FLUX			O	-	
BORON		DEGREASED	O	-	
		DEGREASED + SS FLUX	O	-	
		HCL + NON-COR. FLUX	O	-	
COPPER		HCL	●	●	
		SS FLUX & NON-COR. FLUX	●	●	
		DILUTE HNO <sub>3</sub>	●	●	
		CONC. HNO <sub>3</sub>	O	-	
IRON		HCL	●	●	
		SS FLUX & NON-COR.	●	●	
		DEGREASED	◐	-	
NICKEL		DEGREASED	O	-	
		DEGREASED + SS FLUX	●	●	
		DEGREASED + NON-COR. FLUX	●	●	
		DILUTE HNO <sub>3</sub>	O	-	
		DILUTE HCL	●	-	
SILICON - CARBIDE		DEGREASED	O	-	
		DEGREASED + SS FLUX	O	-	

Table 3-8. Wetting and Adherence Experiments, Contd

	AM 350 STEEL	DEGREASED	O	-
		DILUTE HCL	O	-
		DILUTE HNO <sub>3</sub>	O	-
		DEGREASED + SS FLUX	●	●
	TUNGSTEN	DEGREASED	O	-
		DEGREASED + SS FLUX	O	-
		DILUTE HCL	O	-
		DILUTE HNO <sub>3</sub>	O	-
LEAD	AL <sub>2</sub> O <sub>3</sub>	DEGREASED	O	-
		DEGREASE + FLUX	O	-
	BORON	DEGREASED	O	-
		DEGREASED + SS FLUX	O	-
		HCL + NON-COR. FLUX	O	-
	COPPER	HCL	●	●
		SS FLUX & NON-COR. FLUX	●	●
		DILUTE HNO <sub>3</sub>	●	●
		CONC. HNO <sub>3</sub>	O	-
	IRON	HCL	●	●
		SS FLUX & NON-COR. FLUX	●	●
		DEGREASED	○	-
	NICKEL	DEGREASED	O	-
		DEGREASED + SS FLUX	●	●
		DEGREASED + NON-COR. FLUX	●	●
		DILUTE HCL	●	●
		DILUTE HNO <sub>3</sub>	O	-
	SILICON -	DEGREASED	O	-
	CARBIDE	DEGREASED + SS FLUX	O	-
	AM 350 STEEL	DEGREASED	O	-
		DILUTE HCL	O	-
		DILUTE HNO <sub>3</sub>	O	-
		DEGREASED + SS FLUX	○	-
	TUNGSTEN	DEGREASED	O	-
		DEGREASED + SS FLUX	O	-
		DILUTE HCL	O	-
		DILUTE HNO <sub>3</sub>	O	-
LINOTYPE	AL <sub>2</sub> O <sub>3</sub>	DEGREASED	O	-
		DEGREASED + SS FLUX	O	-
	BORON	DEGREASED	O	-
		DEGREASED + SS FLUX	O	-
		HCL + NON-COR. FLUX	O	-
	COPPER	HCL	●	●
		SS FLUX & NON-COR. FLUX	●	●
		DILUTE HNO <sub>3</sub>	O	-
		CONC. HNO <sub>3</sub>	O	-

Table 3-8. Wetting and Adherence Experiments, Contd

IRON	HCL	O	-
	SS FLUX & NON-COR. FLUX	●	●
NICKEL	DEGREASED	●	-
	DEGREASED	O	-
	DEGREASED + SS FLUX	●	●
SILICON - CARBIDE	DEGREASED + NON-COR. FLUX	●	●
	DILUTE HCL	●	●
	DILUTE HNO <sub>3</sub>	O	-
AM 350 STEEL	DEGREASED	O	-
	DILUTE HCL	O	-
	DILUTE HNO <sub>3</sub>	O	-
TUNGSTEN	DEGREASED + SS FLUX	●	●
	DEGREASED	O	-
	DEGREASED + SS FLUX	O	-
SILVER	DILUTE HCL	O	-
	DILUTE HNO <sub>3</sub>	O	-
	DEGREASED	O	-
AL <sub>2</sub> O <sub>3</sub>	DEGREASE + FLUX	O	-
	DEGREASED	●	-
BORON	DEGREASED + SS FLUX	O	-
	HCL + NON-COR. FLUX	O	-
COPPER	HCL		
	SS FLUX & NON-COR FLUX		
	DILUTE HNO <sub>3</sub>	DISSOLVES	
IRON	CONC. HNO <sub>3</sub>	AFTER WETTING	
	HCL	●	●
	SS FLUX & NON-COR. FLUX	●	●
NICKEL	DEGREASED	●	●
	DEGREASED + SS FLUX	●	●
	DEGREASED + NON-COR. FLUX	●	●
SILICON - CARBIDE	DILUTE HCL	●	●
	DILUTE HNO <sub>3</sub>	●	●
	DEGREASED	O	-
AM 350 STEEL	DEGREASED + SS FLUX	O	-
	DEGREASED	O	-
	DILUTE HCL	O	-
TUNGSTEN	DILUTE HNO <sub>3</sub>	O	-
	DEGREASED + SS FLUX	●	●
	DEGREASED	O	-
TUNGSTEN	DEGREASED + SS FLUX	O	-
	DILUTE HCL	O	-
	DILUTE HNO <sub>3</sub>	O	-

Table 3-8. Wetting and Adherence Experiments, Contd

TIN	AL <sub>2</sub> O <sub>3</sub>	DEGREASED	O	-
		DEGREASED + FLUX	O	-
	BORON	DEGREASED	O	-
		DEGREASED + SS FLUX	O	-
		HCL + NON-COR. FLUX	O	-
	COPPER	HCL	●	●
		SS FLUX & NON-COR. FLUX	●	●
		DILUTE HNO <sub>3</sub>	●	●
		CONC. HNO <sub>3</sub>	O	-
	IRON	HCL	O	-
		SS FLUX & NON-COR. FLUX	●	●
	NICKEL	DEGREASED	●	●
		DEGREASED	O	-
		DEGREASED + SS FLUX	●	●
		DEGREASED + NON-COR. FLUX	●	●
	SILICON - CARBIDE AM 350 STEEL	DILUTE HCL	●	●
		DILUTE HNO <sub>3</sub>	O	-
		DEGREASED	O	-
		DEGREASED + SS FLUX	O	-
		DEGREASED	O	-
		DILUTE HCL	O	-
	TUNGSTEN	DILUTE HNO <sub>3</sub>	O	-
		DEGREASED + SS FLUX	●	●
		DEGREASED	O	-
DEGREASED + SS FLUX		O	-	
DILUTE HCL		O	-	
DILUTE HNO <sub>3</sub>		O	-	
ZINC	AL <sub>2</sub> O <sub>3</sub>	DEGREASED	O	-
		DEGREASED + FLUX	O	-
	BORON	DEGREASED	O	-
		DEGREASED + SS FLUX	O	-
		HCL + NON-COR. FLUX	O	-
	COPPER	HCL	●	●
		SS FLUX & NON-COR. FLUX	●	●
		DILUTE HNO <sub>3</sub>	O	●
		CONC. HNO <sub>3</sub>	●	●
	IRON	HCL	●	●
		SS FLUX & NON-COR. FLUX	●	●
	NICKEL	DEGREASED	○	-
		DEGREASED	●	●
		DEGREASED + SS FLUX	●	●
		DILUTE HCL	●	●
		DILUTE HNO <sub>3</sub>	●	●

Table 3-8. Wetting and Adherence Experiments, Contd

SILICON - CARBIDE AM 350 STEEL	DEGREASED	O	-
	DEGREASED + SS FLUX	O	-
	DEGREASED	O	-
	DILUTE HCL	O	-
	DILUTE HNO <sub>3</sub>	O	-
TUNGSTEN	DEGREASED + SS FLUX	●	●
	DEGREASED	●	●
	DEGREASED + SS FLUX	●	●
	DILUTE HCL	●	●
	DILUTE HNO <sub>3</sub>	●	●

## SECTION 4

### ZERO-G EXPERIMENT REQUIREMENTS

This section defines, in conceptual terms, the major operational and equipment requirements of zero-g experiments which permit the performance of the complete process cycle and produce composite samples of sufficient size for the evaluation of mechanical properties. Two typical zero-g facilities have been selected for this discussion: (1) suborbital research rockets representing the minimum capability and (2) shuttle-based orbital laboratories as the ultimate capability within a foreseeable time frame.

#### 4.1 PROCESSING METHODS

Several processing methods for fiber/particle composites and for controlled density materials have been defined in this study, representing various combinations of ground and flight operations.

Three basic processing methods and sequences of operations for fiber and particle composites are illustrated in Figure 4-1. In compact method (A), the dispersion is established on the ground by dry-mixing of powdered matrix metal and reinforcements, followed by compaction into the final sample configuration. Zero-g processing consists of a matrix-melt and solidification cycle. In method (B) a pre-mixed ingot, containing the reinforcements in segregated condition, is prepared on the ground by casting; in this case, the dispersion is established by liquid-state mixing in zero-g. In method (C) all operations, except for the preparation of component materials, are carried out in zero-g.

The preparation of controlled density materials is confined to three methods whose feasibility has been established in this study (Figure 4-2). In method (A) the gas cells are dispersed on the ground by dry-mixing of gas-filled microspheres, reinforcements and powdered matrix, followed by compaction; zero-g processing consists merely of a matrix melt cycle. In the compact foaming method (B), the dispersion is likewise established on the ground by dry-mixing; however, the foam is generated in zero-g by the decomposition of the pre-dispersed foaming agents during the melt cycle. In the gas injection foaming method (C), all operations, except for the preparation of component materials, are carried out in zero-g. The ultrasonic and nucleate foaming methods are omitted pending further studies of feasibility and techniques.

The method for the preparation of unidirectional eutectics is not illustrated as it is straightforward: a high-purity alloy sample is cast on the ground; zero-g processing consists of remelting of the entire sample and progressive, unidirectional solidification at a specified cooling rate.

## 4.2 SUBORBITAL EXPERIMENT REQUIREMENTS

The discussion of suborbital experiments is limited to research rockets as they are by far the most economical and feasible device for the testing of composites and most other space manufacturing processes. Rockets presently in service, such as the Aerobee 170, provide zero-g times up to 10 minutes and payload capabilities of 150 Kg. This capability is fully adequate for complete processing of composites with moderate melting temperatures including aluminum alloys. In advanced rocket versions, which can be adapted to the specific requirements of zero-g experiments, the zero-g time can be increased to accommodate tests with materials of higher melting temperature, such as Ni, Co or Fe.

The minimum sample size is determined by mechanical test requirements and is in the order of 1.5 cm diameter x 7 cm length, or a volume of 12 cm<sup>3</sup>. For aluminum-base composites, the major operational requirements for the simultaneous processing of four samples in tandem arrangement are:

Heating time	5 minutes
Processing time	2 minutes
Cooling time	0.5 minutes
Net heat input, samples	32,000 cal
Total experiment heat input	160,000 cal
Power input, heating	170 wh
Power input, processing	30 wh
Total power requirements	0.2 KWh
Maximum power rate	2 kW
Total coolant weight	12 Kg
Battery weight, approximate	4 Kg

For controlled density metal experiments, the apparatus would accept only 3 samples due to expansion requirements. This does not affect the above data significantly, as most of the energy is absorbed by the apparatus.

A preliminary design of the experiment payload assembly is shown in Figure 4-3. It consists of two major subassemblies: (1) the basic experiment equipment module, comprising all experiment support components, such power supply controls and recording equipment and (2) the experiment apparatus which, in this design, includes the coolant supply.

A typical experiment programming diagram, identifying the timing of major processing operations and events, is shown in Figure 4-4.

### 4.3 ORBITAL EXPERIMENT REQUIREMENTS

The sustained zero-g environment of orbital vehicles is particularly attractive for composite materials, as the ultimate applications, such as the casting of structural components, involve substantial material quantities and, consequently, processing times in terms of hours. The objective of orbital experiments is, therefore, the processing of larger material quantities and/or high temperature materials, including the development of zero-g casting techniques.

Orbital facilities comprise manned (Skylab, RAM) and unmanned systems (automated satellites). For the definition of processing requirements for composites, the shuttle-based orbital laboratory has been selected, since it represents the first step toward the ultimate goal, the production of commercial products in orbital factories. During the initial shuttle period emphasis will be placed on sortie missions. Space manufacturing experiments are particularly compatible with sortie missions since they do not require continuous operation over long periods of time. The performance of experiments in sortie missions further eliminates the space station requirement of a separate logistics system for raw material supply and product return.

4.3.1 MISSION DEFINITION. The discussion of requirements is based on the 7-day shuttle sortie mission and limited to the equipment and operations for composite experiments, even though other experiments may be carried concurrently in the same payload vehicle. The 7-day sortie mission provides a total experiment payload capability in the order of 6,000 kg, and a total time for experiment operations of 150 hours. It is assumed that the payload vehicle is equipped with all basic support and operational systems, not peculiar of specific experiments, such as central instrumentation and data transmission facilities or life support systems.

Experiment programming studies for the 7-day mission have been carried out with numerical trade-offs of the number of experiments, material mass, processing temperature, experiment time and the resulting requirements as to power, heat dissipation, apparatus size, equipment weights and crew time. These studies showed that an optimum utilization of the 7-day mission for composite experiments is obtained with a total of 12 experiments and an average material mass of 3 kg.

4.3.2 EXPERIMENT APPARATUS. The experiment-peculiar equipment consists of two groups: 1) the experiment apparatus and 2) direct-support equipment.

The variety of composite types and processing methods calls for a high adaptability of the apparatus to different processing requirements. This is achieved most effectively by a design similar to the one shown in Figure 4-5. It consists of the

basic apparatus assembly and a number of interchangeable processing attachments.

The basic apparatus assembly consists of the processing chamber, a subassembly for the attachment of various processing devices, a pressurizing system and a control and measuring system with a panel for observation and manual control.

The processing chamber provides atmosphere control for the experimental materials and for high-temperature processing components. At the same time it serves as a protective envelope for the crew. It can be opened for the exchange of experiment materials and internal processing attachments, and for cleaning and/or refurbishment. The stationary section of the chamber includes the multiple-attachment head with a standardized interface for the attachment of various internal processing components. Internal attachments comprise furnaces, cooling devices and molds.

The multiple-attachment head is connected with the subassembly for the attachment of external processing devices, such as mixing system, foaming system, reinforcement feeding system or the base-material melting chamber with a liquid metal feeding system.

**4.3.3 SUPPORT SYSTEMS.** The major experiment-peculiar support requirements are: 1) power supply, 2) power conditioning and distribution system, 3) cooling system, 4) atmosphere control system and 5) central controls. The functional layout of these systems as related to the experiment apparatus is illustrated in Figure 4-6.

**1. Power supply:** Composite experiments call for high power peaks over relatively short periods; the input rate, in the order of 8 KW, far exceeds the spacecraft supply and a separate power source with high storage capacity is required. The most effective source is a medium-size, rechargeable battery (Ni-Cd-35 Kg/KWh) in connection with a fuel cell power generator. An alternate source is a large non-rechargeable battery (Ag-Zn-15Kg/KWh) dimensioned for the total mission power consumption; while this is feasible for the 7-day mission, it is considerably heavier than the fuel cell-battery system (see data in 4.3.5 below).

**2. Power conditioning:** While for most operations the power can be taken directly from the battery, power conditioning is required for specific processing methods, such as induction heating. The conditioning system consists of a solid-state inverter, a transformer and a solid-state rectifier. It permits a choice of DC or AC and a wide range of voltage-current combinations.

**3. Cooling system:** A special cooling system is required (a) for solidification control and (b) for spacecraft environment control since the high energy inputs far exceed

the capacity of the life support system. For the 7-day mission the total energy (in the order of 70,000 kcal) can be absorbed by a single-cycle heat sink system; weight-wise more effective is a two-cycle water/ice (-100° C) system; the lightest system is a two-cycle water system with a vaporizer (see data in 4.3.5 below).

4. Some composite experiments require high-purity argon, either for oxidation control or for pressurization (liquid metal feeding system, casting). The atmosphere control system consists of gas supply containers and pressure/flow rate control devices.

5. For effective experiment operation the controls for all support systems are integrated in a control center, located closely to the experiment control panel.

#### 4.3.4 EXPERIMENT PERFORMANCE

Depending on the individual experiment objectives and processing methods, the experiments may be carried out in two basic ways:

1. Complete in-chamber processing: The mold, filled with material on the ground, is installed together with all processing devices in the chamber; all processing operations are activated by remote control, either manually or from a taped program.
2. External processing: In this case, only the mold is installed in the processing chamber. A supply of base metal is liquidized in the external melting chamber and fed through the applicable external processing devices to the mold. This process permits the casting of several samples from the same material supply; the composition of each casting or specific processing parameters can be varied by manual setting of the external processing attachments.

4.3.5 OPERATIONAL REQUIREMENTS. The major operational requirements and the pertinent data for composite experiments in a 7-day sortie mission are as follows:

Experiment Data	
Average Material Volume	600 cm <sup>3</sup>
Average Material Weight	3 Kg
Power requirements	7 KWh
Maximum power input	8 KW
Heat input/cooling	6,000 Kcal
Duration (incl. cooling)	8 hrs
Crew time	4 hrs

#### 7-Day Sortie Mission Data

Number of experiments	12
Total experiment time	96 hrs
Total crew time (including attachment exchange)	64 hrs
Total power requirement	84 KWh
Heat generation/dissipation	72,000 Kcal

#### Sortie Payload Weights

Apparatus including attachments	110 Kg
Experiment material and molds	30 Kg
Support system (experiment peculiar)	300 Kg
Expendable battery (Ag-Zn)	(1,300 Kg)
Fuel cell system	560 Kg
Ni-Cd battery - 12 KWh	420 Kg
Fuel cells with fuels	140 Kg
Power conditioning system	200 Kg
Heat-sink cooling system	(1,150 Kg)
Two-cycle cooling system	620 Kg
Cooling system with vaporizer	(330 Kg)
Total Payload Weight	1,820 Kg
(Experiment peculiar only)	

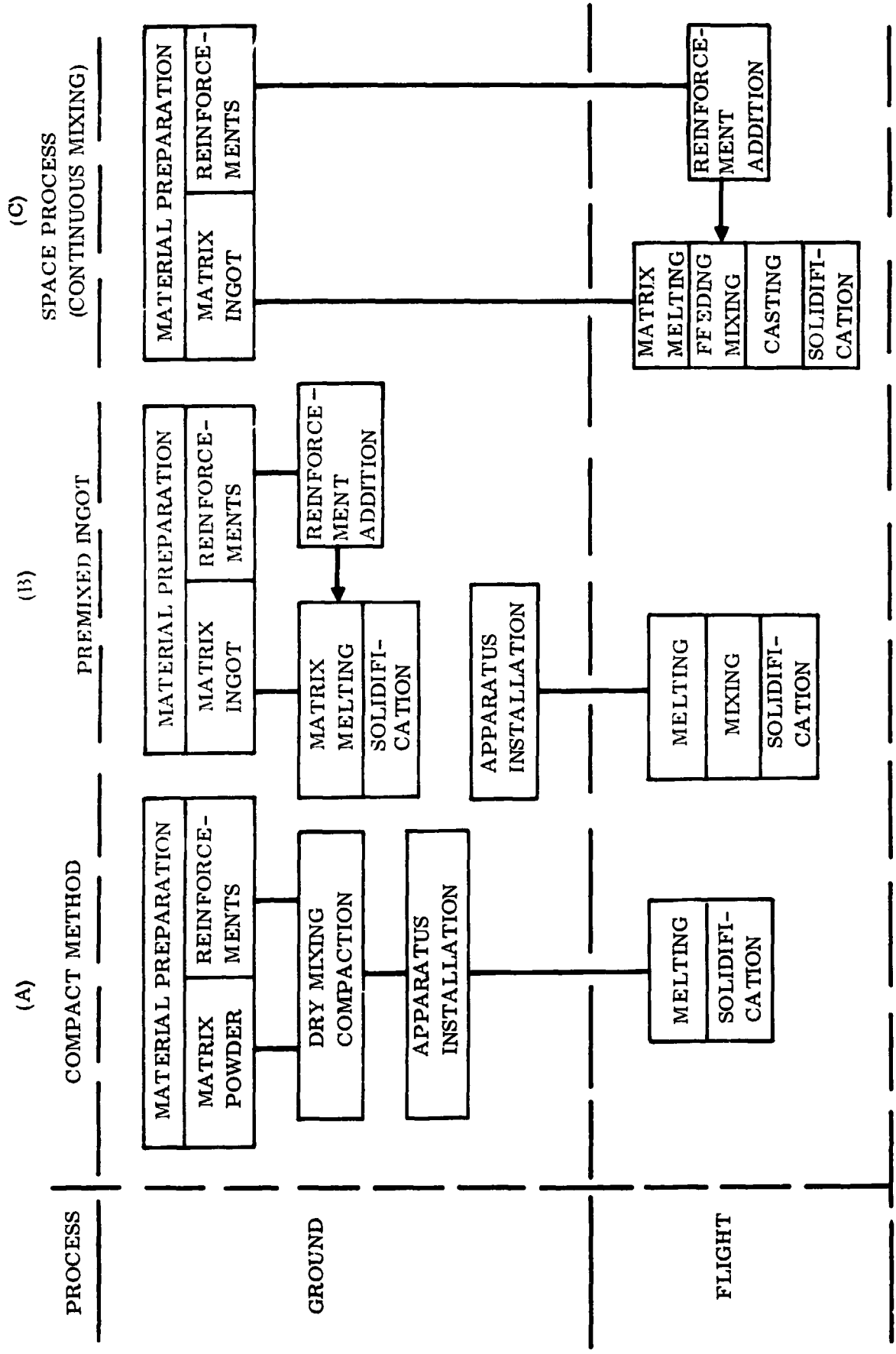


Figure 4-1. Processing Methods for Fiber and Particle Composites

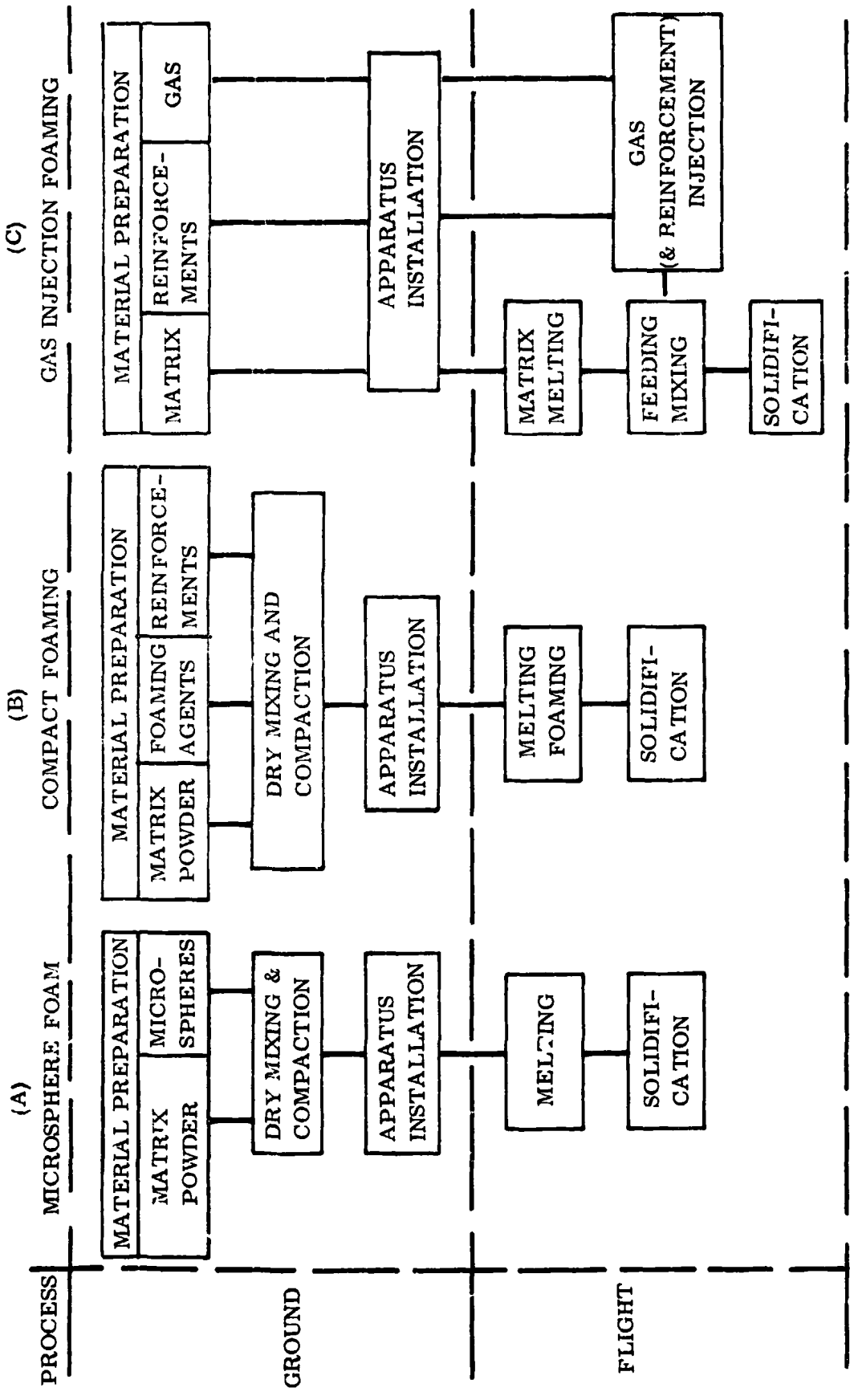
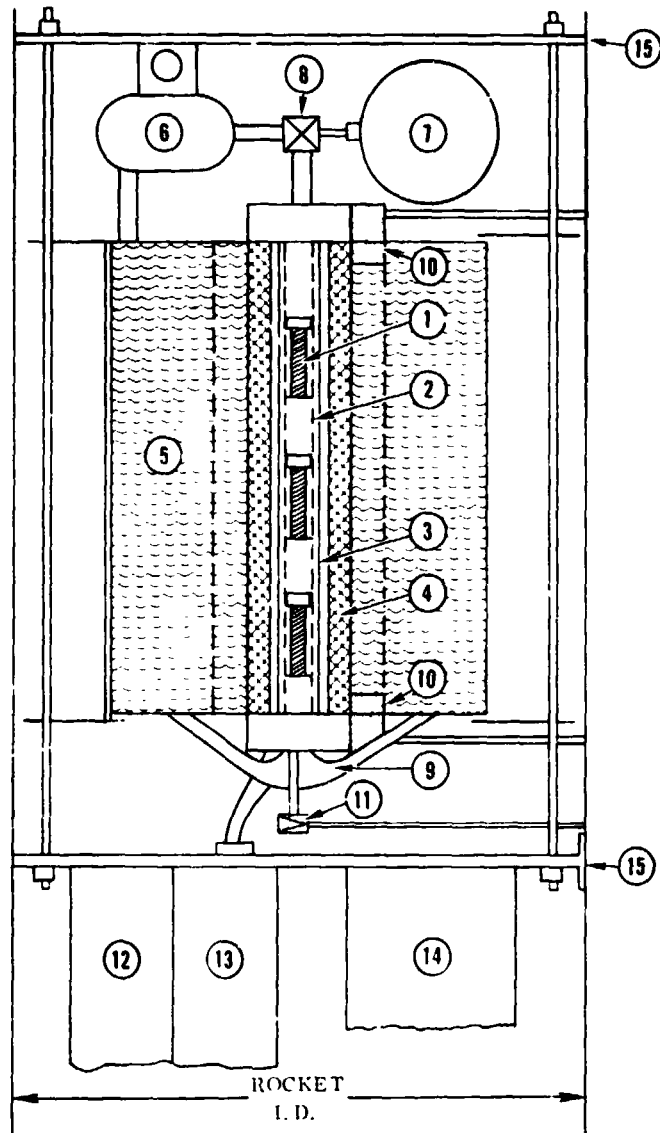


Figure 4-2. Processing Methods for Controlled Density Materials



1. EXPANDABLE FOAMING SAMPLES WITH ARRESTING HEADS
2. SAMPLE EXPANSION/ARRESTING GUIDES
3. TUBULAR HEATING ELEMENT (SPLIT)
4. INSULATION
5. WATER SUPPLY
6. WATER CIRCULATION PUMP
7. ARGON SUPPLY
8. 3-WAY VALVE
9. WATER/STEAM RETURN (ROTATES WATER IN 5)
10. STEAM SEPARATOR WITH CHECK VALVE AND VENT
11. ARGON VENT VALVE
12. BATTERY (AG-ZN)
13. POWER CONDITIONING SYSTEM
14. CONTROLS AND RECORDING
15. BASE PLATES

Figure 4-3. Rocket Experiment Apparatus (for Compact Foaming and Fiber/Particle Composite Experiments)

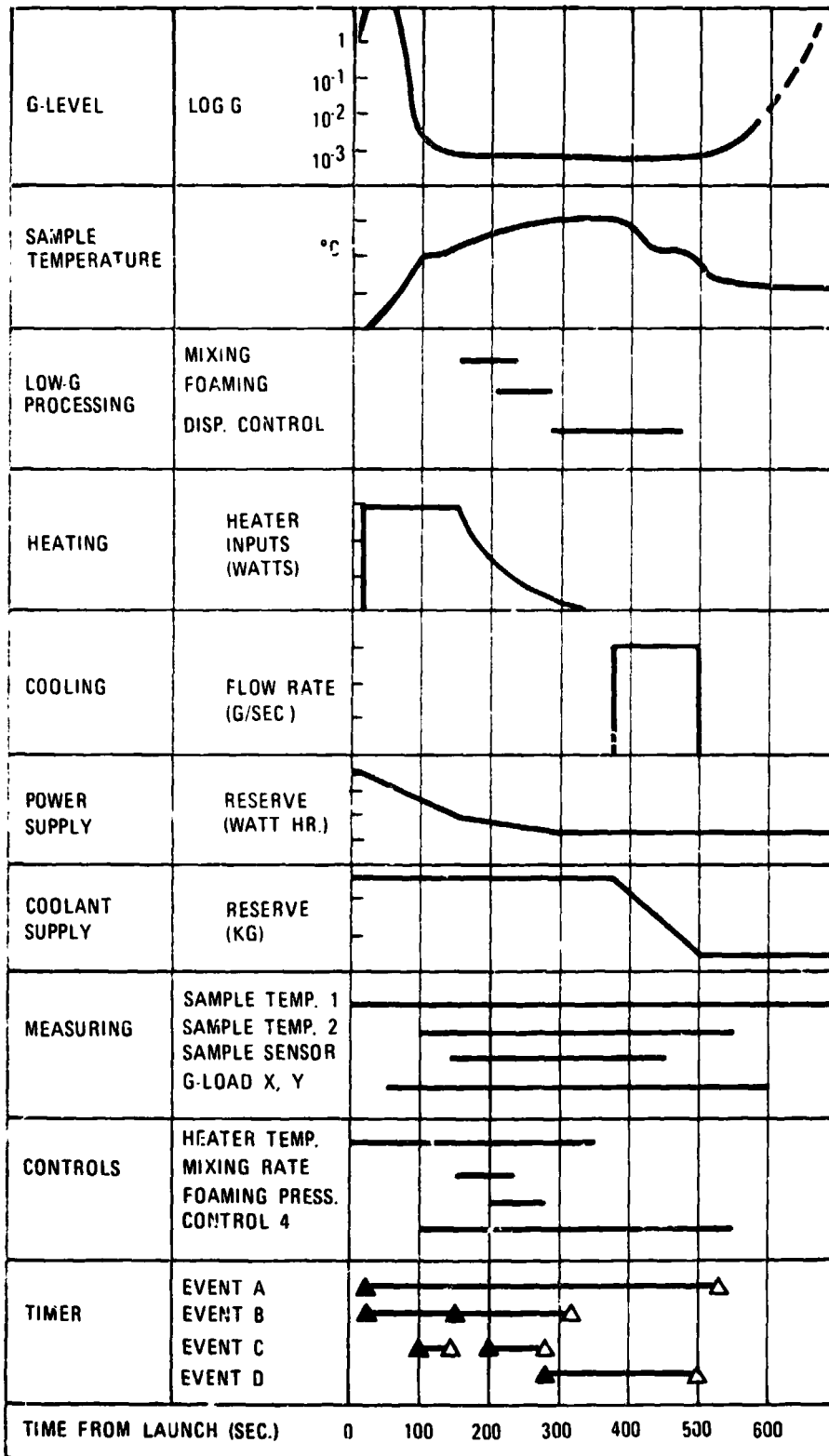
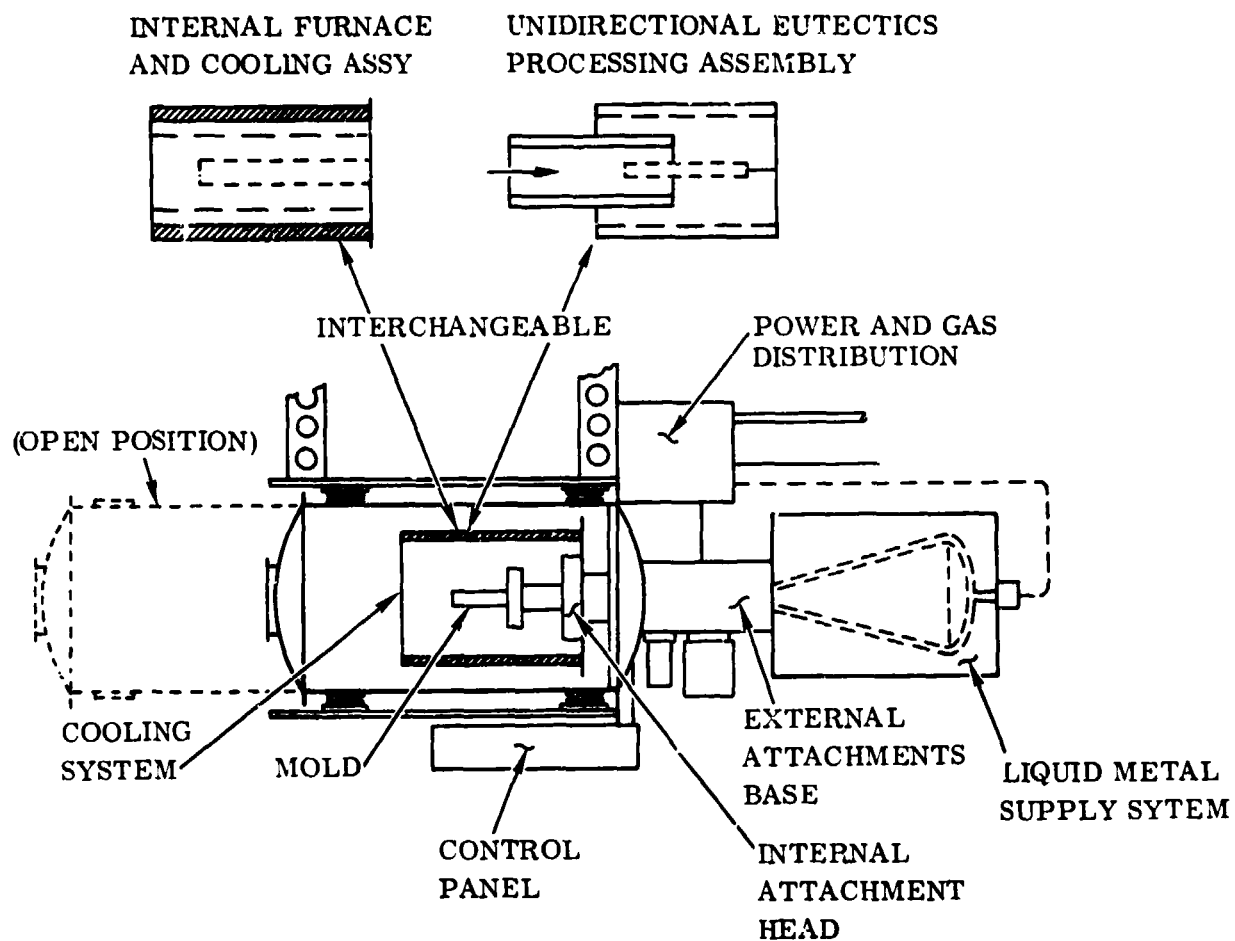


Figure 4-4. Typical Rocket Experiment Program



(Apparatus assembled for multiple castings using external melting chamber, feeding system and processing attachments. For individual experiments, internal attachments as shown at top are installed in processing chamber.)

Figure 4-5. Composite Processing Apparatus for Manned Orbital Laboratories

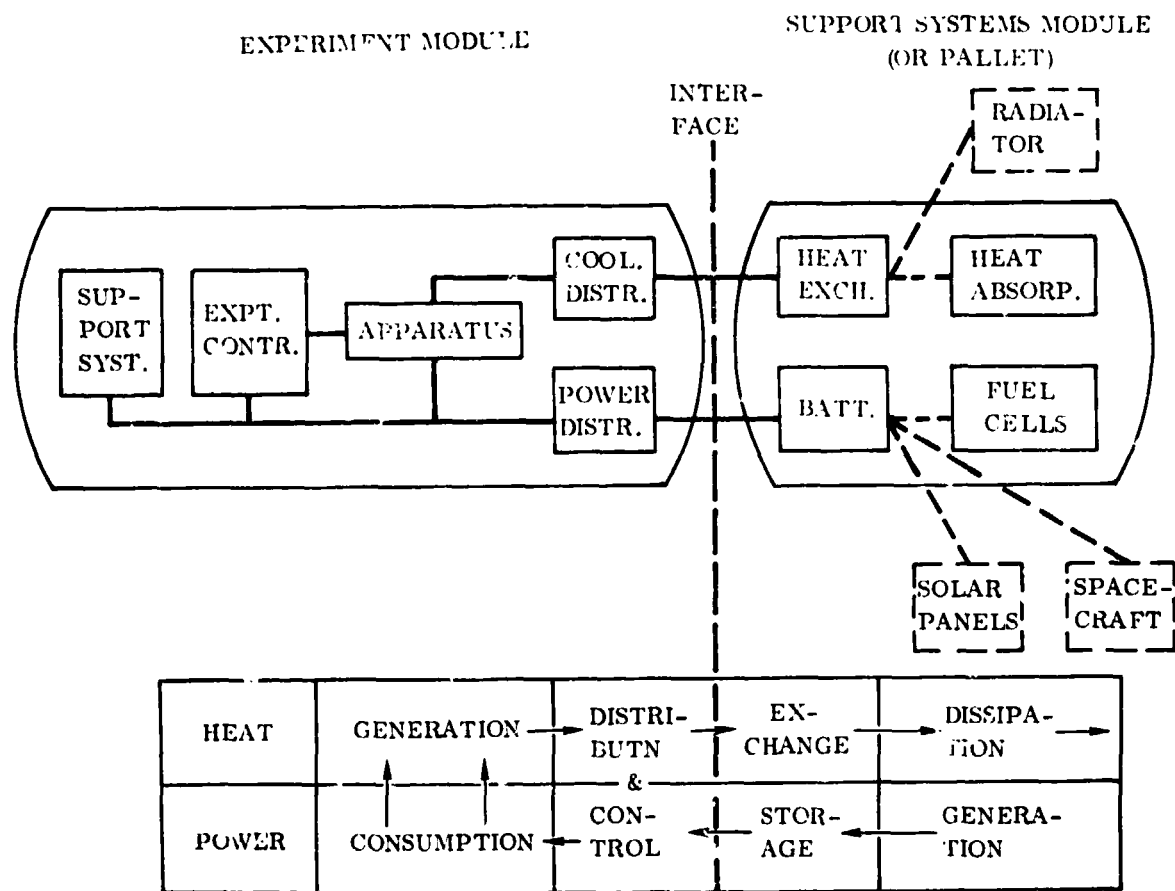


Figure 4-6. Functional Equipment Layout for Sortie Missions (1978)

## SECTION 5

### CONCLUSIONS

#### 5.1 GENERAL CONCLUSIONS

1. The preparation of composites by liquid-state processing is unfeasible in the terrestrial environment due to prohibitive segregation. It is, therefore, unique to orbital gravity environments. This implies further, that capability data can only be obtained by the processing of samples in zero- or low-g and that an early activation of facilities for extended low-g testing is mandatory.
2. Liquid-state processing of composites is a new field of technology that is faced with a complete absence of fundamental and technological information. The generation of such information, including data for liquid metals, is a prerequisite for an effective and minimum-effort development of such composites and the related zero-g processes.
3. Due to the complexity of interactions between molten metals and solid or gaseous dispersions, material treatments and processing techniques have to be developed specifically for each material combination. The magnitude of the involved efforts call for an initial concentration on a limited number of base materials and processing methods.
4. Zero-g produced composites promise properties and, particularly, unique combinations of properties which cannot be achieved in terrestrial production.

#### 5.2 FIBER AND PARTICLE COMPOSITES

1. The preparation of fiber - and particle composites by liquid state processing is unique to zero- or low-g. Experimental measurements of segregation rates as related to density difference, matrix viscosity and reinforcement configuration showed that even at a density difference as low as  $0.1 \text{ g/cm}^3$  prohibitive segregation is encountered in 1-g. For this reason it is impossible to prepare measurable laboratory samples. The properties of composites can only be derived from low-g experiments, and earliest activation of facilities for extended low-g testing are indicated.
2. The production of composites in zero gravity may be accomplished by either of three basic techniques: 1) Pre-dispersion of component materials by dry-mixing and compacting in 1-g, followed by a matrix-melting cycle in zero-g.

- 2) Casting of segregated mixture of component materials in 1-g, followed by melting, mixing and solidification in zero-g. 3) Performance of all processing phases in zero-g with the exception of reinforcement coatings and treatments which can be carried out in 1-g.
3. A mandatory requirement for reinforcement dispersion is high wetting characteristics. All effective reinforcement materials have been found to be non-wetting with regard to all defined matrix materials. Chemically stable coatings and the related coating techniques have to be developed specifically for each matrix - reinforcement combination.
  4. In view of the high sensitivity wetting characteristics to surface contamination and oxidation, the preparation of component materials and the assembly of test samples have to be carried out in high-purity inert gas or in high vacuum.
  5. A second reinforcement requirement is physical and chemical stability at the liquid matrix temperature and in contact with the liquid matrix. All reinforcements are physically and chemically compatible with molten Al and Mg. For base metals of higher melting temperature, only  $Al_2O_3$  reinforcements are fully compatible with Ni, Co and Fe; all other reinforcements are either physically or chemically unstable. Reinforcements which exhibit strength degradation, such as B or BN are unfit for high temperature composites. For all others, barrier coatings have to be developed which prevent chemical reaction with the molten matrix.
  6. The dynamic characteristics of liquid/solid mixtures in zero-g, such as the mobility of reinforcements in molten metals, the response of reinforcements to induced liquid motion modes and the sensitivity to specific low-g levels can be accurately predicted. Applicable relationships have been established by theoretical fluid mechanics studies and laboratory experiments.
  7. For the concerned random-reinforced composites, the maximum content for particles is 60% and for high L/D fibers 14%. The fiber content limitation permits only moderate strength improvements. However, substantial improvements can be achieved by the combined dispersion of fibers and particles. Further, the prime attractiveness of zero-g produced fiber and particle composites is their anisotropy of properties, the castability of end-product shapes and the potential of unique property combinations.
  8. Material preparation techniques and processing parameters have to be developed and specified individually for each matrix/reinforcement material combination. In view of the substantial efforts involved in each case, it is indicated to concentrate near-term efforts on one base material, such as aluminum, including the determination of composite properties in low-g experiments.

### 5.3 CONTROLLED DENSITY MATERIALS

1. In view of the low viscosity of liquid metals, a stable dispersion of discrete gas bubbles in a molten metal, necessary for the preparation of metal foams, can only be achieved at very low g-levels. This places a severe limitation on laboratory investigations. Capabilities of metal foams and the related liquid-state processing parameters can only be verified in zero-g experiments.
2. On the basis of capability assessments and applications studies, three types of promising controlled density metals have been identified: (a) plain (non-reinforced) metal foams; (b) short-fiber reinforced foams (ratio of fiber length to bubble diameter  $< 1$ ); (c) long-fiber reinforced foams (ratio  $> 1$ ).
3. Promising methods of foam generation are (a) dispersion of gas-filled microspheres, (b) gas generation by pre-dispersed additives ("compact foaming"); (c) gas injection foaming; (d) ultrasonic foaming and (e) nucleate foaming. For near-term development and zero-g experiments, the compact foaming method is most effective with regard to relative simplicity, demonstrated successfulness and adaptability to the limitations of suborbital experiments.
4. The behavior of individual gas bubbles and their interaction with reinforcements during liquid-state processing, such as the sensitivity to g-forces and to thermal gradients, can be predicted; initial fluid-mechanics relationships have been established.
5. The prime problem of foam generation is bubble coalescence. This may be prevented or minimized by any or combinations of the following means: (a) stationary mixture (as in the case of compact foaming), (b) trapping of the gas bubbles in a fiber network (long-fiber reinforced foam); (c) use of a slightly oxidizing gas (gas injection foaming), (d) matrix alloys which exhibit a high-viscosity melting range.
6. For reinforced foams, fibers have to exhibit high wettability in order to be retained in the matrix.
7. Successful foaming agents for base-metals of intermediate melting temperature, such as Al or Mg, are  $TiH_2$  and oxalates.
8. For plain and short-fiber reinforced foams, the achievement of gas contents in the order of 50% is reasonably assured; higher gas contents are feasible. The selection of gas and reinforcement content depends on specific product applications.

9. Promising applications are: (a) for plain foams, underwater high-buoyancy components. (b) For reinforced foams, components of high stiffness to density ratio, lightweight armor or structures of low thermal conductivity. Selected combinations of these properties are particularly attractive for air, surface and deep-sea weapon systems.
10. The investigations indicate clearly that specific foaming methods, specific material treatments and specific processing parameters have to be defined individually for each base metal and reinforcement combination. The most effective approach, technically and economically, is, therefore, a concentration of efforts on one base material and one foaming method with the objective to obtain product capability data from processing experiments in suborbital low-g test facilities. The obtained results will provide a reliable basis for the selection of other base materials, the development of other foaming methods and the definition of product applications.

#### 5.4 UNIDIRECTIONAL EUTECTICS

1. The feasibility of achieving high unidirectional properties in certain eutectic alloys by discrete and unidirectional formation of the intermetallic phase has been demonstrated. Properties obtained in 1-g are, however, far from the theoretically expected values due to gravity-induced disturbances. It is expected that substantially higher properties are obtained by processing in zero-g.
2. The essential processing requirements are (a) exact definition of the solidification (progressive cooling) rate which will be lower in zero-g and (b) highest purity of the alloys. The definition of the solidification rate can only be obtained in zero-g experiments.
3. Since the process is of a metallurgical nature and does not involve dynamic effects, zero-g experiments and equipment requirements are comparatively simple and similar to those required for single-crystal experiments.
4. Due to the high processing time and temperature requirements, suborbital experiments are limited to small samples of Al-base eutectics and metallurgical evaluation. Exact processing data and product capabilities can only be obtained in orbital experiments. They should be carried out with practical high-temperature materials, such as Nb-C and Ta-C alloys, producing Nb-NbC and Ta-Ta<sub>2</sub>C alloys, producing Nb-NbC and Ta-Ta<sub>2</sub>C composites of substantial size.

## SECTION 6

### RECOMMENDATIONS

#### 6.1 GENERAL RECOMMENDATIONS

For near-term developmental efforts with the objective of generating experimental data on composite capabilities, the following approach is recommended:

- a. Initial concentration of efforts on one effective base material and on processing method for each composite class. Specifically, to use aluminum alloys as base materials for all composite classes, and the compact method for fiber/particle composites and controlled density metals.
- b. All efforts should be directed at the preparation of zero-g experiment samples of sufficient size to permit evaluation of mechanical properties.
- d. Earliest activation of a flight test program with suborbital rockets and preparation of flight apparatus for the processing of composite samples.
- e. On the basis of the results of initial zero-g experiments, extension of the composite program to other base metals and other processing methods.

#### 6.2 SPECIFIC RECOMMENDATIONS

For an effective implementation of the recommended general approach, the following tasks should be accomplished, initially for the selected single base material and processing method, and later for other materials and methods:

- (1) In-depth investigation of wetting characteristics and chemical effects between reinforcements and the molten matrix.
- (2) Bond strength between reinforcements and matrix after solidification and potential improvements by diffusion treatment.
- (3) Definition of coatings or treatments and related techniques which fulfill all requirements of (1) and (2).
- (4) Development of mixing modes and techniques to achieve random dispersion of reinforcements and/or gases.

- (5) Definition of optimum composite compositions with regard to expected composite properties and matrix microstructure.
- (6) Definition of gases for specific matrices which suppress bubble coalescence by surface stabilization.
- (7) Preparation of optimized gas-forming additives for compact foaming.
- (8) Establishment of detailed processing specifications for low-g experiments.
- (9) Establishment of techniques and facilities for the preparation of flight samples.
- (10) Definition of methods for flight sample evaluation.
- (11) Correlation of predicted and experimental composite properties and definition of means for improvement.
- (12) Assessment of product applications on the basis of zero-g experiment results.

### 6.3 RECOMMENDED SUPPORTING EFFORTS

For an effective accomplishment of the technological efforts defined in 6.2, the performance of the following supporting studies is indicated:

- (1) Fundamental studies and experiments on the fluid mechanics of liquid metals and mixtures with solids and/or gases in zero-g, with emphasis on effective mixing modes and the achievement of perfect dispersion.
- (2) Effect of liquid metal properties, such as surface tension, viscosity and wetting characteristics upon dispersion and mixture stability.
- (3) Theoretical correlation of intermolecular forces and surface energies with the properties of liquid metals; application to the characteristics of liquid/solid and liquid/gas interfaces.
- (4) Experimental establishment of data for liquid metals, not available in the literature.
- (5) Assessment of the effect of small g-forces and thermal gradients upon composites during liquid-state processing and correlation with the results of zero-g experiments.

- (6) Establishment of analytical methods for the prediction of the bulk properties of random-reinforced composites and controlled density metals.
- (7) Analysis of the deformation mechanism and the limiting criteria of plain foams and fiber-reinforced composites under various loading modes; assessment of the performance of composites in specific product applications.
- (8) Definition of other than mechanical properties attainable in the concerned composites; definition of unique property combinations and promising product applications.
- (9) Investigation of individual processing parameters and zero-g phenomena, such as interface or solidification effects, in drop tower experiments.

#### 6.4 RECOMMENDED EXPERIMENTAL PROGRAM

It has been clearly established in this study that a conclusive verification of composite capabilities and the pertinent processes can be obtained only in experiments under zero- or low-g conditions. Orbital experiments involve high cost and long lead times. Consequently, an experimental program is recommended that provides for an early generation of urgently needed data and a gradual build-up of capabilities at minimum cost. It consists of the following sequence of experiment phases:

- a. Laboratory experiments for the exact specification of zero-g experiments.
- b. Experiments in drop towers and the KC-135 in support of (a).
- c. Extended low-g time experiments in research rockets to produce samples that can be tested for composite properties.
- d. Experiments in automated satellites to accommodate larger material quantities and higher processing temperatures, as well as for the evaluation of product casting techniques.
- e. Experiments in shuttle-based orbital laboratories for the production of prototype products.

An overview of the recommended experiment program is presented in the form of a master plan, Figure 6-1.

**6.4.1 LABORATORY EXPERIMENTS.** The prime purpose of laboratory experimentation is the definition of zero-g experiments in terms of materials and process

specifications. It is recommended to devote laboratory work during the first half of CY 73 exclusively to the exact specification of Al-base rocket experiments, specifically the definition of composite compositions, sample configurations, processing specifications, and in-flight measurements, as well as techniques and procedures for sample preparation and evaluation. During the second half of 73, laboratory experiments on other matrix materials and on advanced processing methods should be started, which would continue through the following years as required. Laboratory work during the latter period would also include experiments in support of the evaluation of flight samples.

6.4.2 DROP TOWER AND KC-135 EXPERIMENTS. Short-time low-g experiments have two objectives: 1) evaluation of individual phenomena and processing details; 2) preparation of small feasibility demonstration samples. During the first half of CY 73 it is recommended to continue the bubble interface and the gas injection foaming experiments started in CY 72, and to prepare small (flat) foam samples by the compact foaming method with several low-melting alloys. During the second half of CY 73, experiments may be carried out on the metallurgical effect of various particle and fiber mixtures and on the effect of various mixing modes upon dispersion of reinforcements. Drop tower and/or KC-135 experiments in support of composite development and fundamental studies may be continued through the following years as indicated.

6.4.3 RESEARCH ROCKET EXPERIMENTS. It is strongly recommended to activate a research rocket program at the earliest possible time since it is a comparatively inexpensive means to obtain a conclusive feasibility and capability verification for composites, as well as for other space manufacturing processes. Assuming that flight opportunities become available in CY 73, work should be started immediately on apparatus design and fabrication, as outlined in Section 4.1, so that experiments can be carried out in the second part of CY 73. A minimum of three flights are recommended for CY 73 with Al-base fiber/particle composites and controlled density materials, which can be carried out in the same apparatus and would yield 10 samples. One flight is recommended for Al-base unidirectional eutectics, which may be combined with single-crystal experiments.

During the second half of CY 73, apparatus modifications should be defined and prepared to facilitate experiments with base metals of higher melting temperature and other processing methods. A high-frequency rocket test program is recommended for CY 74 (FY 74) to optimize composite compositions and to generate the data necessary for the definition of specific product applications. Rocket experiments may be continued throughout the subsequent years for the evaluation of new space manufacturing concepts that will undoubtedly evolve from present efforts.

6.4.4 AUTOMATED SATELLITES. It is recommended to program experiments on automated (unmanned) satellites for the 1975 - 1977 period. The long zero-g times of such vehicles that can be deployed with existing launch systems permit large material quantities, high processing temperatures, and verification of casting techniques representative of specific product requirements. Preliminary experiment definitions for the purpose of specifying equipment requirements should be made early in CY 73, followed by equipment design studies in the second half of CY 73. The definition of a detailed experiment program and the preparation of equipment hardware should be carried out in CY 74 to permit the start of the flight test program in CY 75.

6.4.5 SHUTTLE-BASED LABORATORIES. The prime objective of experiments in shuttle-based laboratories, preferably carried out in sortie missions, is the production of prototype components for subsequent ground testing under practical service conditions. They further permit the manned control and observation of processes. It is, however, recommended to postpone the development of processing equipment until reliable requirements can be defined on the basis of the results of the rocket test program as they will become available in the later part of CY 74. Experiment definition and equipment design studies may then be scheduled for CY 75/76 and hardware fabrication and checkout for CY 77, to meet the presently planned initiation of sortie missions in CY 78.

	Cy 1973	74	75	76	77	78	79	80
<u>LABORATORY EXPERIMENTS</u> Al-Composite Expt. Definition Al-Sample Preparation & Evaluation Advanced Composites Development	██████████	██████████	██████████	██████████				
<u>TOWER &amp; KC-135 EXPERIMENTS</u> Fundamental Experiments Gas Injection Foaming Experiments Compact Foaming & Metallurgical Expts.	██████████	██████████	██████████	██████████				
<u>RESEARCH ROCKET EXPERIMENTS</u> Al-Composite Apparatus Preparation Al-Composite Experiments Advanced Apparatus Preparation Advanced Composite Experiments	██████████	██████████	██████████		██████████			
<u>PRE-SHUTTLE ORBITAL EXPERIMENTS</u> Experiments Definition Apparatus Design & Fabrication Experiment Operations	██████████	██████████	██████████	██████████	██████████	██████████		
<u>SHUTTLE-SORTIE EXPERIMENTS</u> Experiments Definition Equipment Design & Fabrication Experiment Operations		██████████	██████████	██████████	██████████	██████████	██████████	██████████

Figure 6-1. Equipment Program Master Plan 1973 - 1980

## APPENDIX A

### RELAXATION OF VISCOUS FLUID MOTION IN A CYLINDRICAL CONTAINER

To obtain quantitative estimates on the process of decay of viscous fluid motion, we consider an incompressible fluid contained in an infinite circular cylinder. We set the velocity component parallel to the axis of the cylinder equal to zero. Thus the motion remains confined to planes perpendicular to the cylinder axis. For reasons of symmetry we further require the tangential velocity  $q$  to remain constant along concentric circles about the axis, i. e.,  $q = q(r, t)$ , where  $r$  and  $t$  are the radial distance and time, respectively. We then find that the radial velocity component must be zero everywhere (in view of the continuity equation together with the requirement of vanishing radial velocity at the cylinder wall).

The fluid pressure  $p$  may, again for symmetry reasons, be assumed constant along concentric circles. The only remaining pressure gradient will then be perpendicular to the streamlines so as to balance the centrifugal force on the fluid particles. Hence,

$$\frac{\partial p}{\partial r} = \frac{\rho q^2}{r} \quad (\text{A1})$$

where  $\rho$  is the fluid density (which is assumed constant throughout).

Under the foregoing simplifications the Navier-Stokes equation of motion in tangential direction becomes,

$$\frac{1}{\nu} \frac{\partial q}{\partial t} = \frac{\partial^2 q}{\partial r^2} + \frac{1}{r} \frac{\partial q}{\partial r} - \frac{q}{r^2} \quad (\text{A2})$$

the nonlinear inertia terms being identically zero.  $\nu$  is the kinematic viscosity of the fluid.

If the container is at rest, the no-slip condition at the wall requires  $q(a, t) = 0$ ,  $a$  being the cylinder radius. Furthermore,  $q(0, t)$  must be finite.

Equation A2 being linear, complete solutions for arbitrary initial conditions (at  $t = 0$ ) can be obtained through superposition of elementary solutions. The latter are readily derived by substituting,

$$q(r, t) = e^{-k^2 \nu t} f(r)$$

where  $k$  is an as yet undetermined constant. Equation A2 now becomes

$$r^2 f'' + r f' + (k^2 r^2 - 1) f = 0$$

The solutions are the Bessel functions of the first and second kind of order unity:

$$f = J_1(kr), Y_1(kr)$$

Because  $Y_1(0) = -\infty$ , we must reject the second solution in view of the condition that the velocity be finite at the axis. The solution to Equation A2 then becomes

$$q(r,t) = A_n e^{-k^2 \nu t} J_1(kr) \quad (A3)$$

Where  $A_n$  is an undetermined constant. The admissible values of  $k$  can now be determined from the wall condition

$$J_1(ka) = 0$$

Let the zeros of  $J_1(z)$  be given by  $z = \alpha_n$  ( $n = 1, 2, 3, \dots$ ;  $\alpha_0 = 0$  giving the trivial solution  $q \equiv 0$ ). The possible values of  $k$  are then found to be

$$k = \frac{\alpha_n}{a} \quad ; n = 1, 2, 3, \dots$$

so that the possible velocity distributions are, according to Equation A3,

$$q_n(r,t) = A_n e^{-\alpha_n^2 \frac{\nu t}{a^2}} J_1\left(\alpha_n \frac{r}{a}\right) ; n = 1, 2, 3, \dots \quad (A4)$$

The first three zeros of  $J_1$  are  $\alpha_1 = 3.83$ ,  $\alpha_2 = 7.02$ ,  $\alpha_3 = 10.2$ , and the corresponding velocity distributions are sketched in Figure A-1.

Because none of the solutions of Equation A4 will, in general, satisfy the specified initial distribution at time zero, we must form the most general solution through linear superposition

$$q(r,t) = \sum_{n=1}^{\infty} q_n(r,t) = \sum_{n=1}^{\infty} A_n e^{-\alpha_n^2 \frac{\nu t}{a^2}} J_1\left(\alpha_n \frac{r}{a}\right) \quad (A5)$$

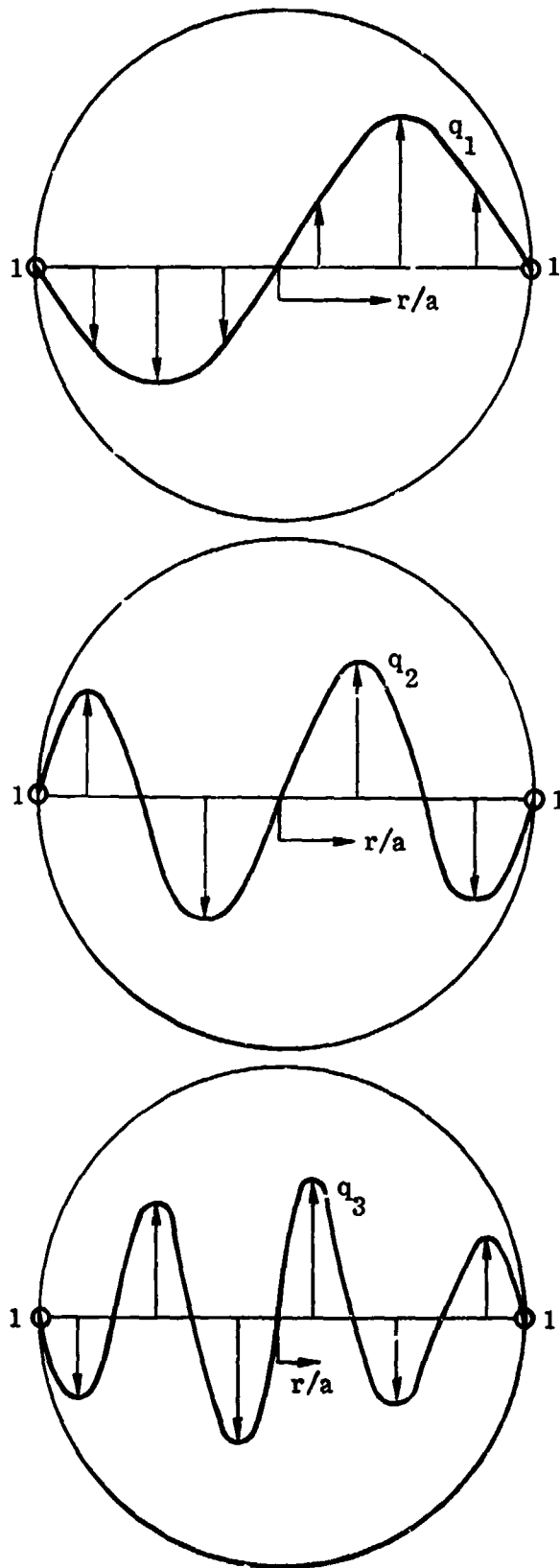


Figure A-1. Admissible Velocity Distributions  $q_1$ ,  $q_2$ ,  $q_3$  in Cylindrical Container

Equation A5 will satisfy the initial condition if we set the coefficients  $A_n$  equal to those of the Fourier-Bessel expansion of the initial velocity distribution, i. e.,

$$q(r, 0) = \sum_{n=1}^{\infty} A_n J_1\left(\alpha_n \frac{r}{a}\right) \quad (\text{A6})$$

Because at this stage we are especially interested in the decay of the fluid motion, it suffices to restrict attention to the mode with the slowest decay, i. e., the first term on the right-hand side of Equation A5, which contains the smallest value of  $\alpha_n$ . The (absolute) values of the coefficients  $A_n$  will moreover form a decreasing sequence.

If we define the relaxation time  $\tau$  of the fluid motion (somewhat arbitrarily) as the time required for the velocity distribution to drop off to 10% of its initial level, we find

$$e^{-\alpha_1^2 \frac{\nu \tau}{a^2}} = 0.1$$

so that, substituting  $\alpha_1 = 3.83$ ,

$$\tau = 0.16 \frac{a^2}{\nu} \quad (\text{A7})$$

As indicated before, the subsequent velocity modes in Equation A5 will exhibit a faster decay (the second and third mode requiring  $\tau = 0.047 a^2/\nu$  and  $0.022 a^2/\nu$  respectively).

Of course, the foregoing results are strictly valid for a cylinder of infinite height. In reality, the fluid motion in a container of finite height will decay faster because of the additional friction exerted by the endwalls. To obtain an estimate of such end effects on the relaxation time, we now let the tangential velocity  $q$  depend on the axial coordinate  $z$  also. In that case the equation of motion, Equation A2, must be re-written as

$$\frac{1}{\nu} \frac{\partial q}{\partial t} = \frac{\partial^2 q}{\partial z^2} + \frac{\partial^2 q}{\partial r^2} + \frac{1}{r} \frac{\partial q}{\partial r} - \frac{q}{r^2} \quad (\text{A8})$$

Assuming the fluid to be enclosed in a cylinder of height  $2h$ , the simplest possible mode satisfying Equation A8 and the no-slip condition at the end plates is obtained by substituting

$$q(r, z, t) = \cos\left(\frac{\pi z}{2h}\right) e^{-k^2 \nu t} f(r)$$

We then find

$$r^2 f'' + r f' + \left[ \left( k^2 - \frac{\pi^2}{4h^2} \right) r^2 - 1 \right] f = 0$$

with admissible solution

$$f = J_1 \left( \sqrt{k^2 - \frac{\pi^2}{4h^2}} r \right)$$

Selecting the first root  $\alpha_1 = 3.83$  in the satisfaction of the wall condition  $q = 0$  at  $r = a$ , we find

$$k^2 = \frac{\alpha_1^2}{a^2} + \frac{\pi^2}{4h^2}$$

and our solution for the flow field becomes

$$q(r, z, t) = A_1 \cos\left(\frac{\pi z}{2h}\right) e^{-\left[1 + \left(\frac{\pi a}{2\alpha_1 h}\right)^2\right] \alpha_1^2 \frac{\nu t}{a^2}} J_1\left(\alpha_1 \frac{r}{a}\right)$$

The previously defined relaxation time is now found to be

$$\tau = \frac{\tau_\infty}{1 + \left(\frac{\pi a}{2\alpha_1 h}\right)^2} = \frac{\tau_\infty}{1 + 0.17 \left(\frac{a}{h}\right)^2} \quad (\text{A9})$$

where  $\tau_\infty$  represents the relaxation time for the infinite cylinder. Equation A9 indicates that, unless the cylinder is very short, the relaxation time is not significantly reduced by the presence of the endplates. For a cylinder with a slenderness ratio  $h/a = 1$ , the reduction amounts to 15%. In fact, in the latter example one would not expect the relaxation time to be substantially different from that of a fluid contained in a spherical vessel of the same radius (which we will analyze in Appendix B). The complete solution for the fluid motion in a suddenly stopped cylinder is readily obtained as follows. If the initial velocity distribution in the cylinder is given by  $q(r, 0) = g(r/a)$ , then the coefficients of the Fourier-Bessel expansion, Equation A6, are found, according to standard procedure, to be

$$A_n = \frac{2}{J_2^2(\alpha_n)} \int_0^1 \frac{r}{a} g\left(\frac{r}{a}\right) J_1\left(\alpha_n \frac{r}{a}\right) d\left(\frac{r}{a}\right) \quad (\text{A10})$$

Now let the cylinder and the fluid initially rotate as a solid body with tangential wall velocity  $q_w$ . At  $t = 0$  the cylinder is suddenly stopped. Substituting  $g = q_w r/a$  into Equation A10, we then find

$$A_n = \frac{2 q_w}{J_2^2(\alpha_n)} \int_0^1 \left(\frac{r}{a}\right)^2 J_1\left(\alpha_n \frac{r}{a}\right) d\left(\frac{r}{a}\right) = \frac{2 q_w}{\alpha_n J_2(\alpha_n)}$$

After the cylinder has been stopped, the velocity distribution in the fluid is thus found to be

$$q(r, t) = q_w \sum_{n=1}^{\infty} \frac{2 e^{-\alpha_n^2 \frac{\nu t}{a^2}} J_1\left(\alpha_n \frac{r}{a}\right)}{\alpha_n J_2(\alpha_n)}$$

From the foregoing solution for the suddenly stopped cylinder the solution for the suddenly accelerated cylinder is immediately found to be

$$q(r, t) = q_w \left[ \frac{r}{a} - \sum_{n=1}^{\infty} \frac{2 e^{-\alpha_n^2 \frac{\nu t}{a^2}} J_1\left(\alpha_n \frac{r}{a}\right)}{\alpha_n J_2(\alpha_n)} \right]$$

which satisfies Equation A2 and the conditions  $q(a, t) = q_w$ ,  $q(0, t) = 0$ ,  $q(r, 0) = 0$  and yields  $q(r, \infty) = q_w r/a$ . The time required by the fluid motion to build up to a near-steady pattern is again determined by the relaxation time of the first mode. The velocity profiles for decelerated and accelerated motion are depicted in Figures A-2 and A-3.

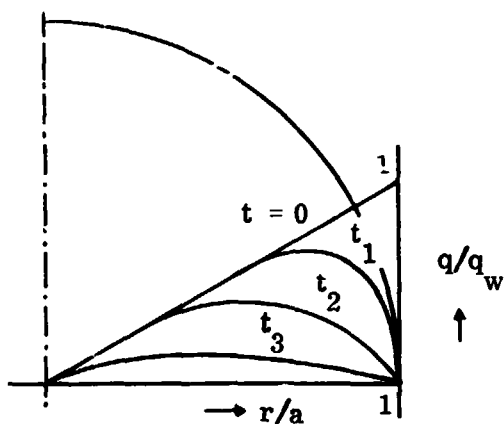


Figure A-2. Velocity Profile in Suddenly Stopped Cylinder

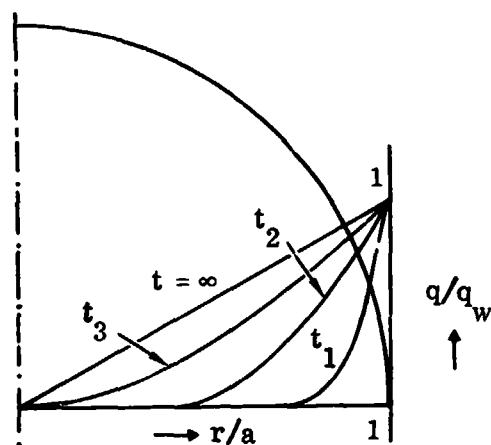


Figure A-3. Velocity Profile in Suddenly Accelerated Cylinder

## APPENDIX B

### RELAXATION OF VISCOUS FLUID MOTION IN A SPHERICAL CONTAINER

Let us now consider the time-dependent fluid motion in a spherical container of radius  $a$ . We assume that all fluid particles in a spherical shell, concentric with the container, move with the same angular velocity  $\Omega(r, t)$ . In that case the fluid velocity will everywhere be perpendicular to the plane through the axis of rotation. Its magnitude is given by  $q = \Omega r \sin \theta = q_1(r, t) \sin \theta$ , where  $\theta$  is the angle between the axis of rotation and the radius  $r$  measured from the center of the sphere to the fluid particle. For reasons of symmetry the fluid pressure may be assumed constant along streamlines. Under the foregoing simplifications the Navier-Stokes equation of motion along streamlines reduces to

$$\frac{1}{\nu} \frac{\partial q_1}{\partial t} = \frac{\partial^2 q_1}{\partial r^2} + \frac{2}{r} \frac{\partial q_1}{\partial r} - \frac{2 q_1}{r^2} \quad (\text{B1})$$

the nonlinear inertia terms again being zero. If the container is at rest, the wall condition is  $q_1(a, t) = 0$ . Furthermore, an initial velocity distribution at time zero must be prescribed. The velocity field can be solved in terms of elementary solutions similar to the development in Appendix A. Substitution of

$$q_1(r, t) = e^{-k^2 \nu t} f(r)$$

into Equation B1 yields

$$r^2 f'' + 2r f' + (k^2 r^2 - 2) f = 0$$

The solutions are the spherical Bessel functions of the first and second kind of order unity:

$$j_1(kr) = \sqrt{\frac{\pi}{2kr}} J_{3/2}(kr), \quad y_1(kr) = \sqrt{\frac{\pi}{2kr}} Y_{3/2}(z)$$

Because  $y_1(\infty) = -\infty$  we must reject the second solution so that

$$q_1(r, t) = B_n e^{-k^2 \nu t} j_1(kr) \quad (\text{B2})$$

The admissible values of  $k$  are again determined from the wall condition

$$j_1(k a) = 0$$

Thus

$$k = \frac{\alpha_n}{a} ; n = 1, 2, 3, \dots$$

Where  $\alpha_1 = 4.49$ ,  $\alpha_2 = 7.73$ ,  $\alpha_3 = 10.9$ , etc. are the zeros\* of  $j_1$  ( $\alpha_0 = 0$  giving again the trivial solution). The general solution then becomes

$$q_1(r, t) = \sum_{n=1}^{\infty} B_n e^{-\alpha_n^2 \frac{\nu t}{a^2}} j_1\left(\alpha_n \frac{r}{a}\right) \quad (B3)$$

The successive velocity modes are qualitatively the same as those depicted in Figure A-1. The relaxation time (again defined as the time required for the velocity distribution to drop off to 10% of the initial level) of the first three modes is  $\tau = 0.11 a^2/\nu$ ,  $0.039 a^2/\nu$ , and  $0.019 a^2/\nu$  respectively.

As might have been anticipated, these relaxation times are of the same order as those found in Appendix A for the fluid motion in a circular cylinder. Once more, the decay of the fluid motion as a whole is determined by the relaxation time of the first mode as it exhibits the slowest decay.

The complete solution for the fluid motion in a suddenly stopped sphere is obtained as follows.

At time zero, Equation B3 becomes

$$q_1(r, 0) = \sum_{n=1}^{\infty} B_n j_1\left(\alpha_n \frac{r}{a}\right) \quad (B4)$$

---

\*)  $j_1(z)$  can be expressed in terms of elementary functions as follows:

$$j_1(z) = \frac{\sin z}{z} - \frac{\cos z}{z^2}$$

Hence, the zeros of  $j_1(z)$  are determined by

$$\tan z = z$$

If the initial distribution of  $q_1$  is given by  $g(r/a)$ , then the coefficients of the Fourier-Bessel expansion, Equation B4, are found, by standard means, to be

$$B_n = \frac{2}{j_2^2(\alpha_n)} \int_0^1 \left(\frac{r}{a}\right)^2 g\left(\frac{r}{a}\right) j_1\left(\alpha_n \frac{r}{a}\right) d\left(\frac{r}{a}\right) \quad (\text{B5})$$

We now let the sphere and the fluid initially rotate as a solid body with angular velocity  $\Omega_0$ . At  $t = 0$  the sphere is suddenly stopped. Substituting  $g = \Omega_0 r$  into Equation B5, we then find

$$B_n = \frac{2a\Omega_0}{j_2^2(\alpha_n)} \int_0^1 \left(\frac{r}{a}\right)^3 j_1\left(\alpha_n \frac{r}{a}\right) d\left(\frac{r}{a}\right) = \frac{2a\Omega_0}{\alpha_n j_2(\alpha_n)}$$

After the sphere has been stopped, the angular velocity of the fluid particles is thus found to be

$$\Omega(r, t) = \Omega_0 \sum_{n=1}^{\infty} \frac{2a}{r} \frac{e^{-\alpha_n^2 \frac{\nu t}{a^2}} j_1\left(\alpha_n \frac{r}{a}\right)}{\alpha_n j_2(\alpha_n)}$$

It follows immediately for the solution of the suddenly accelerated sphere that

$$\Omega(r, t) = \Omega_0 \left[ 1 - \sum_{n=1}^{\infty} \frac{2a}{r} \frac{e^{-\alpha_n^2 \frac{\nu t}{a^2}} j_1\left(\alpha_n \frac{r}{a}\right)}{\alpha_n j_2(\alpha_n)} \right]$$

The velocity profiles for decelerated and accelerated motion are qualitatively the same as those depicted in Figures A-2 and A-3.

## APPENDIX C

### OSCILLATORY FLUID MOTION IN CYLINDRICAL CONTAINER

In this appendix we consider the fluid motion in an infinite circular cylinder, which is in oscillatory motion about its axis with angular frequency  $\omega_0$ . Just as in Appendix A the motion will be governed by

$$\frac{1}{\nu} \frac{\partial q}{\partial t} = \frac{\partial^2 q}{\partial r^2} + \frac{1}{r} \frac{\partial q}{\partial r} - \frac{q}{r^2} \quad (C1)$$

However, in view of the periodicity of the motion, we now seek a solution of the form

$$q(r, t) = e^{i\omega_0 t} f(r) \quad (C2)$$

where, as usual, either the real or the imaginary part must be considered. Substitution into Equation C1 yields

$$r^2 f'' + r f' - (m^2 r^2 + 1) f = 0$$

where  $m = \sqrt{i\omega_0 / \nu}$ . The solutions are the modified Bessel functions of the first and second kind of order unity

$$I_1(mr) \quad , \quad K_1(mr)$$

The second solution tends to infinity as  $r$  tends to zero and must therefore be rejected. Thus, our solution for the velocity field becomes

$$q(r, t) = C e^{i\omega_0 t} I_1(mr)$$

where the constant  $C$  must be determined from the no-slip condition at the wall of the container. Let the cylinder rotate with wall velocity

$$q(a, t) = q_0 e^{i\omega_0 t}$$

where it is again understood that either the real or the imaginary part is being considered. We then find  $C = q_0 / I_1(ma)$  and the solution becomes

$$q(r, t) = q_0 e^{i\omega_0 t} \frac{I_1(r/r_0)}{I_1(ma)} = q_0 e^{i\omega_0 t} \frac{I_1\left[\frac{(i+1)M}{a} r\right]}{I_1\left[\frac{(i+1)M}{a} a\right]} \quad (C3)$$

where we have substituted  $\sqrt{i} = (i+1)/\sqrt{2}$  and where

$$M = \sqrt{\frac{\omega_0^2 a^2}{2\nu}}$$

More insight into the properties of the solution is gained if we employ the following integral representation of the Bessel function

$$I_1(Z) = \frac{1}{\pi} \int_0^\pi e^{Z \cos \theta} \cos \theta d\theta \quad (C4)$$

Our solution, Equation C3, can then be rewritten as

$$q(r, t) = \frac{q_0}{\pi I_1\left[\frac{(i+1)M}{a} a\right]} \int_0^\pi e^{M \frac{r}{a} \cos \theta} e^{i\left(M \frac{r}{a} \cos \theta + \omega_0 t\right)} \cos \theta d\theta \quad (C5)$$

We recall that a simple traveling wave with amplitude  $A$ , wave length  $\lambda$  and angular frequency  $\omega_0$  may, in complex notation, be represented by

$$q = A e^{i\left(\frac{2\pi r}{\lambda} - \omega_0 t\right)}$$

The wave velocity  $c$  is obtained by setting the exponent equal to a constant, giving  $c = dr/dt = \omega_0 \lambda / 2\pi$ .

Thus the velocity field in the cylinder, as represented by Equation C5 may be interpreted as a system of infinitesimal waves (the amplitude being proportional to  $\exp\left(M \frac{r}{a} \cos \theta\right) (\cos \theta d\theta)$ ) with wave velocity

$$c = - \frac{\sqrt{2\nu\omega_0}}{\cos \theta}$$

Half of the velocity waves are running radially inward ( $\cos \theta > 0$ ); the other half (being generated at the opposite wall) are running radially outward ( $\cos \theta < 0$ ). At the center of the cylinder the two systems of opposite-running waves interfere destructively to produce zero net velocity. The wave amplitude drops off exponentially away from the generating wall.

It is of interest to consider the following limiting cases:

(i) Flow fields with small M

In this case we may expand the Bessel function, defined in Equation C4, for small values of its argument. Thus,

$$I_1(z) = \frac{1}{\pi} \int_0^{\pi} (1 + z \cos \theta + \dots) \cos \theta d\theta = \frac{z}{\pi} \int_0^{\pi} \cos^2 \theta d\theta + \dots = \frac{z}{2}$$

According to Equation C3 the solution for the velocity field then becomes

$$q(r, t) = q_0 e^{i\omega_0 t} \frac{r}{a}$$

Thus for small values of M (slow oscillations, slender cylinders or large viscosity the fluid will rotate as a solid with the cylinder.

(ii) Flow fields with large M

In this case we evaluate the integral expression of Equation C4 for large values of the argument. We restrict our attention to the flow near the wall so that  $r/a$  remains of order unity. We may neglect the contribution to the integral arising from negative values of  $\cos \theta$  (physically this implies that the wave damping is so strong that we may neglect the waves emanating from the opposite wall). Thus

$$I_1(z) \sim \frac{1}{\pi} \int_0^{\pi/2} e^{z \cos \theta} \cos \theta d\theta = \frac{1}{\pi} \int_0^1 e^{z \sqrt{1-x^2}} dx$$

Furthermore, to arrive at an asymptotic expression it suffices to consider only the contribution near the lower limit where the integrand attains its largest values (i. e., we are considering the waves with the largest amplitude only). We then find

$$\begin{aligned}
 I_1(z) &\sim \frac{1}{\pi} \int_0^1 e^{z(1 - \frac{1}{2}x^2)} dx = \frac{e^z}{\pi} \int_0^1 e^{-\frac{1}{2}zx^2} dx \\
 &= \sqrt{\frac{2}{z}} \frac{e^z}{\pi} \int_0^{\sqrt{z/2}} e^{-\xi^2} d\xi \sim \sqrt{\frac{2}{z}} \frac{e^z}{\pi} \int_0^{\infty} e^{-\xi^2} d\xi = \frac{e^z}{\sqrt{2\pi z}}
 \end{aligned}$$

The solution, Equation C3, now becomes

$$q(r, t) = q_0 e^{i\omega_0 t} \sqrt{\frac{a}{r}} e^{(i+1)M(\frac{r}{a} - 1)} = q_0 \sqrt{\frac{a}{r}} e^{-M\frac{y}{a}} e^{i(\omega_0 t - M\frac{y}{a})} \quad (C6)$$

where  $y = a - r$  is the distance from the wall. If we take for instance the real part of the solution, we find that near the wall ( $r/a \rightarrow 1$ )

$$q(r, t) = q_0 e^{-M\frac{y}{a}} \cos(\omega_0 t - M\frac{y}{a})$$

Thus, the fluid motion becomes identical with that generated by an oscillating infinite flat plate (Stokes' second problem<sup>1</sup>). The wave length  $\lambda$  is given by

$$\frac{\lambda}{a} = \frac{2\pi}{M}$$

Over a distance of one wave length the amplitude drops off by a factor  $\exp(-2\pi) = 0.0019$ . Thus, for large values of  $M$  (fast oscillations, large cylinders, or small viscosity) the oscillatory fluid motion remains confined to a thin layer adjacent to the wall, the inner core of the fluid being at rest.

Figure C-1 depicts the phase lag of the fluid layers with respect to the motion of the wall.

<sup>1</sup>Schlichting, H., Boundary Layer Theory, p. 85, McGraw-Hill, 6th Edition, 1968.

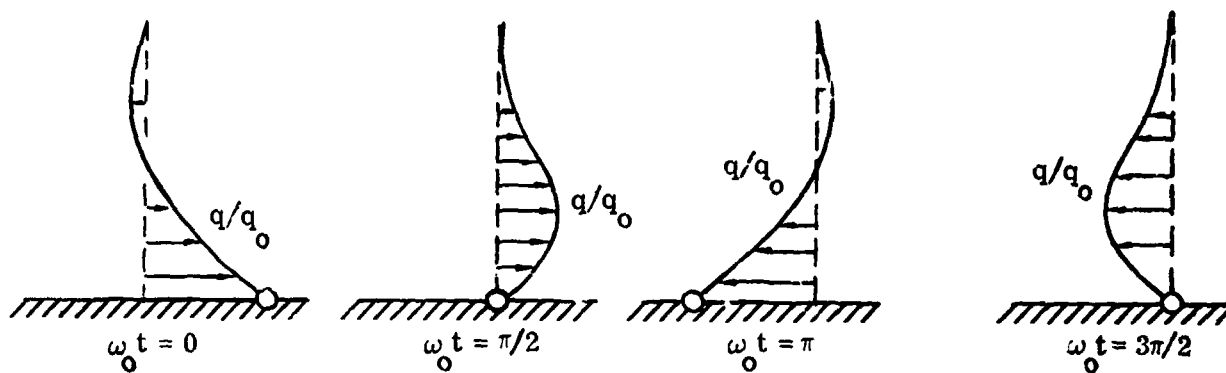


Figure C-1. Oscillatory Flow Near Container Wall ( $M \gg 1$ ).

When  $M$  is of the order of unity, the entire fluid is in motion according to a rather complicated system of waves. The complete solution can be obtained by separating Equation C3 into real and imaginary parts, which can be accomplished for instance through the use of Whitehead functions<sup>2</sup>. However, in view of the rather cumbersome algebra and limited application, these calculations are omitted.

<sup>2</sup> Watson, G. N., A Treatise on the Theory of Bessel Functions, Cambridge Univ. Press, 2nd Edition, 1962.

## APPENDIX D

### OSCILLATORY FLUID MOTION IN SPHERICAL CONTAINER

The analysis of the fluid motion in a sphere, which oscillates about an axis through its center, proceeds quite similar to that of Appendix C. Just as in Appendix B, the governing equation is,

$$\frac{1}{\nu} \frac{\partial q_1}{\partial t} = \frac{\partial^2 q_1}{\partial r^2} + \frac{2}{r} \frac{\partial q_1}{\partial r} - \frac{2q_1}{r^2}$$

Substituting the periodic solution,

$$q_1(r, t) = e^{i\omega_0 t} f(r)$$

We find,

$$r^2 f'' + 2rf' - (m^2 r^2 + 2) f = 0 \quad (D1)$$

where  $m$  is defined the same as in the previous section. The solutions of Equation D1 are the modified spherical Bessel functions of the first and second kind of order unity:

$$i_1(mr) = \sqrt{\frac{\pi}{2mr}} I_{3/2}(mr), \quad k_1(mr) = \sqrt{\frac{\pi}{2mr}} K_{3/2}(mr)$$

The second solution tends to infinity as  $r$  tends to zero and must therefore be rejected. Our solution then becomes,

$$q_1(r, t) = D e^{i\omega_0 t} i_1(mr)$$

Let the spherical container rotate with angular velocity  $\Omega_0 \exp(i\omega_0 t)$ . The no-slip condition at the wall then yields  $D = a \Omega_0 / i_1(ma)$  and our solution becomes,

$$q_1(r, t) = a \Omega_0 e^{i\omega_0 t} \frac{i_1(mr)}{i_1(ma)} = a \Omega_0 e^{i\omega_0 t} \frac{i_1\left[\frac{(i+1)M r}{a}\right]}{i_1\left[\frac{(i+1)M}{a}\right]} \quad (D2)$$

where  $M$  is defined as before.

As previously shown, more insight is gained if the Bessel function is expressed as an integral (although in this case the integral is readily calculated in closed form).

We have,

$$\begin{aligned}
 i_1(z) &= \frac{1}{2} \int_{-1}^{+1} e^{zt} t dt = \frac{1}{2z} (e^z + e^{-z}) - \frac{1}{2z^2} (e^z - e^{-z}) \\
 &= \frac{1}{z} \cosh(z) - \frac{1}{z^2} \sinh(z) \qquad (D3)
 \end{aligned}$$

Just as for the case of the cylinder we may interpret the solution as an infinite system of infinitesimal waves, one half moving radially inward and the other half (being generated at the opposite wall) moving radially outward. The parameter  $M$  determines again the nature of the flow field with the following two limiting solutions. As  $z \rightarrow 0$ , Equation D3 gives  $i_1(z) \approx z/3$ . It then follows from Equation D2 for the angular velocity  $\Omega$ , as  $M \rightarrow 0$ ,

$$\Omega(r, t) = \frac{q_1(r, t)}{r} = \Omega_0 e^{i\omega_0 t}$$

Thus for small values of  $M$  the fluid will rotate as a solid with the sphere.

As  $z \rightarrow \infty$ , Equation D3 yields  $i_1(z) \approx (1/2z)e^z$ . It then follows from Equation D2 for the fluid velocity near the wall, as  $M \rightarrow \infty$ ,

$$q(\theta, r, t) = q_0 e^{i\omega_0 t} \frac{a}{r} e^{(i+1)M(\frac{r}{a}-1)}$$

Where  $q_0(\theta, a, t) = \sin \theta a \Omega_0$  is the local wall velocity. Thus, similar to the case of the cylinder, for large values of  $M$  the fluid motion near the wall becomes identical with the flow pattern generated by an oscillating infinite flat plate.

The complete solution in the intermediate regime, governed by values of  $M$  of the order of unity, involves the separation of Equation D2 into real and imaginary parts. Although in the present case these calculations can be carried out in terms of elementary functions, the final results, being somewhat unwieldy, will not be needed and are therefore omitted.